Mixed Quantum-Classical Dynamics in Cavity Quantum Electrodynamics

Dissertation zur Erlangung des Doktorgrades
an der Fakultät für Mathematik, Informatik und
Naturwissenschaften, Fachbereich Physik,
der Universität Hamburg

vorgelegt von:

Norah M. Hoffmann

Hamburg
2020

Gutachter/innen der Dissertation:	Prof. Dr. Angel Rubio Prof. Dr. Ludwig Mathey
Zusammensetzung der Prüfungskommission:	Prof. Dr. Angel Rubio Prof. Dr. Ludwig Mathey Prof. Dr. Neepa T. Maitra Dr. Heiko Appel Prof. Dr. Michael A. Rübhausen
Vorsitzende/r der Prüfungskommission:	Prof. Dr. Michael A. Rübhausen
Datum der Disputation:	02.06.2020
Vorsitzender Fach-Promotionsausschusses Physik:	Prof. Dr. Günter Hans Walter Sigl
Leiter des Fachbereichs Physik:	Prof. Dr. Wolfgang Hansen
Dekan der Fakultät MIN:	Prof. Dr. Heinrich Graener

"Sometimes science is more art than science, Morty. Lot of people don't get that."

— **Rick Sanchez**, Rick And Morty (Season 1, Episode 6)

ABSTRACT

Considering the ultimate limit of molecules interacting with a few photons, the classical description of the electromagnetic field does not suffice anymore and the quantum nature of light needs to be taken into account. Moreover, to describe chemical processes mediated by quantum light, an accurate, flexible and computationally efficient treatment of light-matter interactions is required. Therefore the present work focuses on the theoretical approaches of light-matter interaction in cavity quantum electrodynamics. In particular, we investigate the extension of mixed-quantum classical trajectory methods as well as the concept of time-dependent potential energy surfaces, both traditionally introduced for electron-nuclear problems, to the photonic degrees of freedom. The goal is to pave the way for a full *ab initio* and computationally feasible description of quantum effects in strongly correlated light-matter systems. We find, that classical Wigner dynamics for photons can be used to describe quantum effects such as spontaneous emission, correlation functions, bound photon states and cavity-induced suppression of proton-coupled electron transfer by properly accounting for the quantum statistics of the vacuum field while using classical/semi-classical trajectories to describe the time-evolution. Additionally, this classical Wigner treatment for the photons allows us to go beyond the usual single-mode picture, and to include the many photon modes supported in most realistic cavities, in a numerically efficient way. Here, we find that as more photon modes are included, cavity-modified phenomena can significantly change and the self-polarization, which is often neglected, has an increasingly crucial impact on the dynamics and even more so presents a potential new tool to control and change chemical reactions. To this end, we introduce the concept of self-polarization-modified Born-Oppenheimer surfaces as an instructive tool for analysis. Furthermore, in order to gain a fundamental understanding of the dynamics obtained by the mixed-quantum classical methods, we investigate the time-dependent potential energy surfaces within the exact factorization framework. Here we find on the one hand that the corresponding time-dependent potential energy surfaces for photons show significant differences to the harmonic potentials used in conventional approaches. On the other hand, analyzing the time-dependent potential energy surface driving the proton motion of a cavity-induced chemical suppression, we show how its features directly correlate to the proton dynamics, in contrast to the polaritonic surfaces. Particularly, within the mixed-quantum classical methods for photons we identify a promising route towards describing quantum effects in realistic correlated light-matter systems. Especially, combining the introduced methods with an existing *ab initio* electronic structure methods such as time-dependent density functional theory would provide an *ab initio* computationally feasible way to simulate photon-field fluctuations and correlations in realistic three-dimensional systems.

ZUSAMMENFASSUNG

Zur Analyse der Wechselwirkung von Molekülen mit nur wenigen Photonen, ist die klassische Beschreibung des elektromagnetischen Feldes unzureichend und die Quanteneigenschaften des Lichts müssen berücksichtigt werden. Darüber hinaus erfordert die Simulaton chemischer Prozesse mit starker Quantenlicht-Wechselwirkung eine genaue, flexible und rechnerisch effiziente Beschreibung von Licht-Materie-Wechselwirkung. Die vorliegende Arbeit untersucht daher Theorien der Licht-Matrie-Wechselwirkung für Resonatorquantenelektrodynamik an der Schnittstelle von Quantenoptik und Quantenchemie. Insbesondere betrachten wir die Erweiterung der gemischt quanten-klassischen Trajektorienmethoden, sowie das Konzept der zeitabhängigen Potentialenergieflächen, beides ursprünglich für Elektron-Kern Systeme entwickelt, auf die photonischen Freiheitsgrade. Wir stellen fest, dass die klassische Wigner-Dynamik für Photonen gut geeignet ist, um Quanteneffekte wie spontane Emission, Korrelationsfunktionen, gebundene Photonenzustände und resonatorinduzierte chemische Suppression des Proton-Elektron gekoppelten Ladungstransfers zu beschreiben. Hierbei berücksichtigen wir einerseits die Quantenstatistik des Vakuumfeldes und verwenden andererseits klassische/semi-klassische Trajektorien zur Beschreibung der Zeitevolution. Geht man außerdem über die üblicherweise verwendete Kopplung zu nur einer Photonenmode hinaus, verändern sich die beobachteten resonatormodifizierten Phänomene erheblich und die oft vernachlässigte Selbstpolarisation hat einen immer wichtigeren Einfluss auf die Dynamik und stellt darüber hinaus ein potenzielles neues Werkzeug zur Kontrolle und Veränderung chemischer Reaktionen dar. Zu diesem Zweck stellen wir das Konzept der selbstpolarisationsmodifizierten Born-Oppenheimer-Potentialenergieflächen als instruktives Analysewerkzeug vor. Um ein grundlegendes Verständnis der simulierten Dynamik innerhalb der gemischt quanten-klassischen Trajektorienmethoden zu erhalten, untersuchen wir weiterhin die zeitabhängigen Potentialenergieflächen. Wir stellen fest, dass sich diese für Photonen signifikant von dem üblicherweise verwendeten harmonischen Bild unterscheiden. Darüber hinaus analysieren wir die zeitabhängige Potentialenergiefläche, die die Protonenbewegung einer resonator-induzierten chemischen Suppression des Proton-Elektron gekoppelten Ladungstransfers antreibt, und zeigen wie ihre Charakteristik, im Gegensatz zu polaritonischen Potentialenergieflächen, direkt mit der Protonendynamik zusammenhängen. Wir kommen zu dem Schluss, dass die gemischt quanten-klassischen Methoden für Photonen ein vielversprechender Weg zur Beschreibung von Quanteneffekten in realistischen korrelierten Licht-Materie-Systemen darstellen. Insbesondere die Kombination der vorgestellten Methoden mit einer schon bestehenden *ab initio* elektronischen Strukturmethode, wie zum Beispiel der zeitabhängigen Dichtefunktionaltheorie, eröffnet die Möglichkeit sowohl Photonenfeldschwankungen als auch Photonkorrelationen in realistischen dreidimensionalen Systemen zu simulieren.

PREFACE

This cumulative dissertation is based on the publications [O1–O5]. In these papers we investigate theoretical approaches for light-matter interaction in cavity quantum electrodynamics at the interface of quantum optics and quantum chemistry. In particular, we focus on extending mixed quantum-classical trajectory methods as well as the concept of time-dependent potential energy surfaces, traditionally introduced for electron-nuclear problems, to the photonic degrees of freedom, in order to develop *ab initio* and computational feasible descriptions of cavity modified chemical systems and processes. In Chapter 1 we first provide an introduction to the field of cavity quantum electrodynamics and the current theoretical state of the art. Furthermore, we include an outline and brief discussion of our scientific contribution i.e. the extension of the methods to the photonic degrees of freedom and the main findings. The corresponding research papers can be found in Chapter 2 and 3. A conclusion and brief outlook on future work is provided in Chapter 4. Furthermore, when referring to the scientific contributions throughout this thesis the reference index of the corresponding publication is used as below.

LIST OF PUBLICATIONS

[O1] Norah M Hoffmann, Christian Schäfer, Angel Rubio, Aaron Kelly, and Heiko Appel. "Capturing vacuum fluctuations and photon correlations in cavity quantum electrodynamics with multitrajectory Ehrenfest dynamics." In: *Physical Review A* 99.6 (2019), p. 063819. DOI: 10.1103/PhysRevA.99.063819.

[O2] Norah M Hoffmann, Heiko Appel, Angel Rubio, and Neepa T Maitra. "Light-matter interactions via the exact factorization approach." In: *The European Physical Journal B* 91.8 (2018), p. 180. DOI: 10.1140/epjb/e2018-90177-6.

[O3] Norah M Hoffmann, Christian Schäfer, Niko Säkkinen, Angel Rubio, Heiko Appel, and Aaron Kelly. "Benchmarking semiclassical and perturbative methods for real-time simulations of cavity-bound emission and interference." In: *The Journal of Chemical Physics* 151.24 (2019), p. 244113. DOI: 10.1063/1.5128076.

[O4] Lionel Lacombe, Norah M Hoffmann, and Neepa T Maitra. "Exact Potential Energy Surface for Molecules in Cavities." In: *Physical Review Letters* 123.8 (2019), p. 083201. DOI: 10.1103/PhysRevLett.123.083201.

[O5] Norah M Hoffmann, Lionel Lacombe, Angel Rubio, and Neepa T Maitra. "Effect of Many Modes on Self-Polarization and Photochemical Suppression in Cavities." In: *ArXiv* (2020). arXiv: 2001.07330.

CONTENTS

Part I

INTRODUCTION

1

THEORETICAL BACKGROUND AND CONTRIBUTION

This thesis is about fundamental research in quantum physics. Therefore, let us first answer the question: What does *quantum* mean? In general, quantum mechanics can be roughly thought of as the study of systems on small (atomic) length scales. Early work setting the foundations of quantum theory e.g. [1–3], already showed that the continuous and deterministic picture of physical processes does not hold for atomic length scales. But what does this mean exactly? On the one hand, non-continuous refers to quantities that can only take discrete values and also motivates the name *quantum*, which means *how much*. On the other hand, non-deterministic means that observables in quantum mechanics are only given by their probability. More precisely, in classical mechanics, we can consider a particle at a given position and time. Once we obtained this information we can directly determine the velocity, momentum, energy or other dynamical variables of interest by applying Newton's second law. Quantum mechanics, in contrast, treats these problems quite differently. Here, in order to determine the dynamics of the particle, one has to solve the Schrödinger equation [4], where its position is now deduced by a wave function. This means that the position of the particle is not localized but spread over the space according to its wave function. Therefore, in order to determine the actual position of the particle (or as it is called in quantum mechanics, the state of the particle) we have to calculate its probability at a given position and time [5].

Although the Schrödinger equation might in itself be a simple equation, it is unfortunately exceedingly difficult to solve for more than a few particles [6]. For example, assume we want to calculate, disregarding spin and time, the groundstate wave function of an oxygen atom. And, in order to solve this problem, we use a rather moderate grid of ten grid-points for each direction in three dimensions and, since the oxygen atom has eight electrons, we will need to store 10^{24} numbers to calculate the full goundstate wave function. Now, assuming each number requires one byte of physical memory and a typical workstation has a hard-drive storage of around one Terabyte, we will need the incredibly large number of one Trillion hard-drives just to store the groundstate wave function. Therefore, including even more degrees of freedom such as spins, larger grid sizes, full molecules or even time dynamics will make this problem impossible to solve. However, this problem is already very well known as the so-called exponential wall of the quantum many-body problem [7] and is the reason why in the past much effort has been invested into solving the Schrödinger equation. Moreover, it is important to note that the full wave function also contains far more information than one could possibly need or even want. Therefore, indeed, in many instances a fully quantum mechanical treatment is probably unnecessary, and numerous approximate quantum theories such as Density Functional Theory (DFT) [8], Time-Dependent Density Functional Theory (TDDFT) [9], Cou-

pled Cluster [10] or Quantum Monte Carlo [11] to name a few, have allowed deep insights into a broad range of physical and chemical problems.

One trajectory-based approach that allows a treatment of a large number of atoms is the Molecular Dynamics method [12, 13]. It leverages two underlying approximations. First, the Born-Oppenheimer (BO) approximation [14], which exploits the fact that the nuclei and the electrons have disparate masses and allows the separation of the coupled electron-nuclei motion and, thus, reduces the dynamics of the nuclei to a single adiabatic Potential Energy Surface (PES). Second, the nuclei motion is treated by classical mechanics. However, there are a lot of applications that require either more PESs with transitions among them (break-down of BO approximation), or quantized vibrational levels (break-down of the classical treatment). Therefore, Mixed-Quantum Classical (MQC) methods were developed to overcome these problems by bringing in non-adiabatic effects with treating only a few crucial degrees of freedom quantum mechanically while still applying a multi-dimensional classical treatment for most of the system [15, 16]. The crucial point within these methods is self-consistency. On the one hand, the quantum mechanical degrees of freedom must evolve correctly under the influence of the surrounding classical motions, whereas, in turn, the classical degrees of freedom must respond correctly to quantum transitions.

Available techniques in the family of the trajectory-based MQC approaches are, for example, Ehrenfest mean field dynamics [15, 17–19], fully linearized and partially linearized path integral methods [20–26], forward-backward trajectory methods [24, 25, 27], and trajectory surface-hopping algorithms [28–34]. All these techniques have some ability to describe essential quantum mechanical effects, such as tunnelling, interference, and zero-point energy conservation. Further, they typically do not exhibit the exponential scaling with respect to the nuclear degrees of freedom, as all trajectories are treated independently, and, thus, allow to reduce the computational effort via parallelization. Finally, these methods provide an intuitive qualitative understanding of nonadiabatic molecular dynamics and their applicability has been demonstrated for a wide range of physical phenomena and parameter regimes.

In addition to their valuable properties for practical calculations, trajectory-based methods provide much intuition through their central concept of PESs. One of the rigorous PES approaches is the so called Exact Factorization (EF), which is formally exact and, moreover, introduces time dependency via Time-Dependent Potential Energy Surface (TDPES). Therefore, a single TDPES replaces the manifold of static PESs, represents the exact potential in which the nuclear wave packet evolves, and exactly contains the effects of electron coupling [35, 36]. Thus, the TDPES allows to obtain fundamental and valuable information for adiabatic and nonadiabatic molecular dynamics. Furthermore, for calculations of complex realistic systems, a well-defined single classical force obtained by the TDPES is highly desirable and, thus, a TDPES-based MQC method [37–39] paved the way to determine nonadiabatic dynamics in such systems.

Both the MQC method and the EF approach were traditionally introduced for molecular dynamics, i.e. pure electron-nuclear interaction. Considering the wide range of photoinduced phenomena, the interaction of the particles with electro-

magnetic fields needs to be taken into account, too. The latter interaction, is, if at all, commonly described by the coupling of the matter to the Maxwell's equation, i.e. an interaction of the matter with classical light fields. However, with respect to the ultimate limit of single molecules interacting with a few photons, as it is the case in cavity Quantum Electrodynamics (QED) [40], the classical description of the electromagnetic field does not suffice anymore. In this case, the quantum nature of the electromagnetic field has to be taken into account.

Therefore, in the present thesis we face the question, *whether and to what extent does the analysis and simulation of photoinduced processes change by going beyond the classical Maxwell description?*

Objectives of this thesis

We generalize the idea of the trajectory-based MQC methods, traditionally introduced for electron-nuclear problems, to electron-nuclei-photon correlated systems by incorporating the quantized light fields explicitly and highlighting the possibilities and theoretical challenges of these methods. Furthermore, we extend the EF approach, also traditionally introduced for electron-nuclei interaction, to the electron-nuclei-photon case for further analysis of the MQC approach. Our work and findings include:

(i) We find that the Multi-Trajectory Ehrenfest (MTEF) approach can be used to describe quantum effects in correlated light-matter systems (here an electron-photon correlated system) by properly accounting for the quantum statistics of the vacuum field while using mean field trajectories to describe the time-evolution [O1].

(ii) We extend the EF approach to the photonic degrees of freedom and show that the TDPES for photons exhibits significant differences to the common harmonic approaches, especially for strong coupling [O2].

(iii) We benchmark a selection of MQC methods and perturbative dynamic techniques in its applicability to strong light-matter interaction (here an electron-photon correlated system) [O3].

(iv) We analyze the exact TDPES driving the proton motion of a cavity-induced chemical suppression of Proton-Coupled Electron Transfer (PCET) and show how its features directly correlate to the proton dynamics, in contrast to the polaritonic surfaces, and discuss cavity-modifications of its structure responsible for the suppression [O4].

(v) We extend the introduced MTEF approach to the full electron-nuclei-photon system and analyze the process of cavity-induced chemical suppression of PCET. Here, we find that cavity-modified phenomena and self-polarization effects can significantly change as more photon modes are included and introduce the new tool of self-polarization-modified Born-Oppenheimer (spBO)-surfaces [O5].

In summary, our work is concerned with the extension of two methods: On the one hand, we extent the MQC methods to the photonic degrees of freedom in order to enable *ab initio* calculations in complex realistic systems. On the other hand, we investigate the TDPES in the EF approach in order to obtain a fundamental understanding of the results found in the MQC methods and to set a starting point for the development of new MQC methods. While the first three cases (i)–(iii) explore these methods for electron-photon coupled systems, the latter two (iv)–(v) focus on the full electron-nuclei-photon correlated system.

The remainder of this chapter is structured as follows. In Sec. 1.1 we briefly review the realm of light-matter interaction in cavity QED, provide an overview on the quantum chemical and quantum optical paradigms and introduce the full QED Hamiltonian and our model systems. We then outline the methodological extension to the photonic degrees of freedom for the MQC methods in Sec. 1.2 and the EF approach in Sec. 1.3. In Sec. 1.4 we recapitulate our contribution and discuss it relative to the existing state of the art research.

In the subsequent chapters we provide the papers corresponding to the scientific contributions, where Chap. 2 collects the work on electron-photon correlated systems [O1–O3], and Chap. 3 the work on the full electron-nuclei-photon system [O4, O5]. Chap. 4 concludes and gives an outlook on future work.

1.1 CAVITY QUANTUM ELECTRODYNAMICS

Recently, rapid experimental and theoretical advances have drawn attention to fascinating phenomena that depend on the quantization of the light field and its interaction with matter. This includes few-photon coherent nonlinear optics with single molecules [40], direct experimental sampling of electric-field vacuum fluctuations [41, 42], multiple Rabi splittings under ultrastrong vibrational coupling [43], exciton-polariton condensates [44, 45], polaritonically enhanced superconductivity in cavities [46], and frustrated polaritons [47], among others. Therefore, we first consider the question, what the quantization of the light field, i.e. few photon limit, means exactly and how it can be achieved.

1.1.1 *Towards Quantized Light Fields*

MAXWELL FIELD EQUATIONS In general, the propagation of classical light fields is described by the well-known Maxwell's equations [48]:

$$\boldsymbol{\nabla} \cdot \mathbf{E}(\mathbf{r}, t) = \frac{\boldsymbol{\rho}(\mathbf{r}, t)}{\epsilon_0} \tag{1}$$

$$\boldsymbol{\nabla} \cdot \mathbf{B}(\mathbf{r}, t) = 0 \tag{2}$$

$$\boldsymbol{\nabla} \times \mathbf{E}(\mathbf{r}, t) = -\frac{\partial \mathbf{B}(\mathbf{r}, t)}{\partial t} \tag{3}$$

$$\boldsymbol{\nabla} \times \mathbf{B}(\mathbf{r}, t) = \epsilon_0 \mu_0 \frac{\partial \mathbf{E}(\mathbf{r}, t)}{\partial t} + \mu_0 \mathbf{j}(\mathbf{r}, t), \tag{4}$$

where $\mathbf{E}(\mathbf{r}, t)$ is the electric field, $\mathbf{B}(\mathbf{r}, t)$ the magnetic field, $\mathbf{r}$ the three-dimensional position vector, t the time and $\boldsymbol{\rho}(\mathbf{r}, t)$ and $\mathbf{j}(\mathbf{r}, t)$ the electronic charge density and current density, respectively. Furthermore, μ_0 describes the magnetic permeability and ϵ_0 the vacuum permittivity with $\epsilon_0\mu_0 = \frac{1}{c^2}$, where c denotes the speed of light.

RIEMANN-SILBERSTEIN VECTOR Besides the standard representation, the propagation of the classical electromagnetic field can also be rewritten in terms of the Riemann-Silberstein vector $\mathbf{F}(\mathbf{r}, t)$ [49, 50]:

$$\mathbf{F}(\mathbf{r}, t) = \sqrt{\frac{\epsilon_0}{2}}\mathbf{E}(\mathbf{r}, t) + i\sqrt{\frac{1}{2\mu_0}}\mathbf{B}(\mathbf{r}, t). \tag{5}$$

Consisting only of the electric and magnetic field components, this notation has the advantage of being gauge independent. More precisely, the two Gauss Laws, Eqs. (1), (2), can be rewritten in terms of $\mathbf{F}$ such that

$$\boldsymbol{\nabla} \cdot \mathbf{F}(\mathbf{r}, t) = \frac{1}{\sqrt{2\epsilon_0}}\boldsymbol{\rho}(\mathbf{r}, t). \tag{6}$$

Furthermore, re-arranging Faraday's Law, Eq. (3), and Ampere's Law, Eq. (4), in Riemann-Silberstein form yields

$$i\partial_t \mathbf{F}(\mathbf{r}, t) = \pm c_0 \boldsymbol{\nabla} \times \mathbf{F}(\mathbf{r}, t) - \frac{i}{\sqrt{2\epsilon_0}}\mathbf{j}(\mathbf{r}, t). \tag{7}$$

Finally, multiplying Eq (6) and Eq. (7) with $\hbar$ and rewriting the curl operator in Eq. (7) in terms of spin-1 matrices $\mathbf{S}$ for photons (see detailed derivation in [51]) then yields a Schrödinger-like expression for the Maxwell's equation

$$i\hbar\partial_t \ \mathbf{F}(\mathbf{r}, t) = c_0 \frac{\hbar}{i}\Big(\mathbf{S} \cdot \boldsymbol{\nabla}\Big)\mathbf{F}(\mathbf{r}, t) - \frac{i\hbar}{\sqrt{2\epsilon_0}}\mathbf{j}(\mathbf{r}, t). \tag{8}$$

Successful implementations using this formulation for real-time solutions of coupled Ehrenfest-Maxwell-Pauli-Kohn-Sham equations were done in [51]. Note that we discuss a connection of this application with the multi-trajectory approach for photons introduced in Chap. 4 to outline possible future extensions.

COULOMB GAUGE Generally, the electric and magnetic field may be expressed in terms of a scalar potential $\Phi(\mathbf{r}, t)$ and vector potential $\mathbf{A}(\mathbf{r}, t)$, which yields

$$\mathbf{E}(\mathbf{r}, t) = -\boldsymbol{\nabla}\Phi(\mathbf{r}, t) - \frac{\partial \mathbf{A}(\mathbf{r}, t)}{\partial t} \tag{9}$$

$$\mathbf{B}(\mathbf{r}, t) = \boldsymbol{\nabla} \times \mathbf{A}(\mathbf{r}, t). \tag{10}$$

The potentials $\Phi(\mathbf{r}, t)$ and $\mathbf{A}(\mathbf{r}, t)$ define the gauge freedom [52, 53]. More precisely, these potentials are, in contrast to the electric and magnetic field, non-measurable and also unphysical, since two different pairs of vector and scalar

potentials can yield identical electric and magnetic fields. However, fixing the gauge removes all unphysical degrees of freedom and yields a unique vector potential. Throughout this thesis we apply the Coulomb gauge

$$\boldsymbol{\nabla} \cdot \mathbf{A} = 0. \tag{11}$$

Now, assuming no sources of radiation and charges, the Maxwell's equations in terms of the vector potential can be written as

$$\boldsymbol{\nabla}^2 \mathbf{A} - \frac{1}{c^2} \frac{\partial^2 \mathbf{A}}{\partial t} = 0, \tag{12}$$

which satisfies the wave equation.

QUANTIZATION OF LIGHT FIELDS Let us now turn our attention to the main question, how to quantize light fields. Technically, the quantization of the light field can be achieved by optical cavities, an arrangement of mirrors, which develops standing light waves. These standing waves are called modes and appear in a discrete, though infinite, set and yield the quantization of the electromagnetic field [54]. Assuming a cubic cavity with length L and perfectly reflecting mirrors, one can impose periodic boundary conditions

$$\mathbf{k} = \frac{2\pi}{L}(n_x, n_y, n_z), \tag{13}$$

where $n_{x,y,z}$ defines the normal mode of the field, with the total number of modes given as

$$N = 2\left(\frac{L}{2\pi}\right)^3 \Delta k_x \Delta k_y \Delta k_z, \tag{14}$$

with $\Delta k_{x,y,z}$ characterizing the k-space intervals. Furthermore, the magnitude of k is related to the frequency $\omega_k = kc$ [52, 53]. The quantization of the light field can be achieved by associating each mode $\mathbf{k}s$, depending on two independent polarizations $s = \{1, 2\}$, with a quantum mechanical harmonic oscillator and demanding the canonical variables to satisfy the commutation relations

$$[\hat{a}_{\mathbf{k}s}, \hat{a}_{\mathbf{k}'s'}] = 0 = [\hat{a}^+_{\mathbf{k}s}, \hat{a}^+_{\mathbf{k}'s'}] \tag{15}$$

$$[\hat{a}_{\mathbf{k}s}, \hat{a}^+_{\mathbf{k}'s'}] = \delta_{\mathbf{k}\mathbf{k}'}\delta_{ss'}, \tag{16}$$

where $\hat{a}^+_{\mathbf{k}s}$ denotes the creation operator of the radiation field and $\hat{a}_{\mathbf{k}s}$ the annihilation operator. As a result, the field amplitudes also become operators and have the form

$$\hat{A}_{\mathbf{k}s} = \left(\frac{\hbar}{2\omega_k \epsilon_0 V}\right)^{\frac{1}{2}} \hat{a}_{\mathbf{k}s}. \tag{17}$$

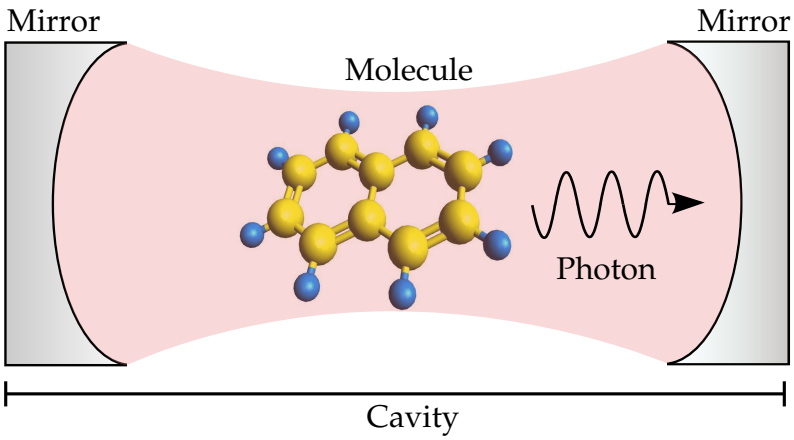

Figure 1: A Naphthalene molecule trapped in a cavity.

Furthermore, the energy of the field becomes a Hamiltonian operator

$$\hat{H} = \epsilon_0 V \sum_{\mathbf{ks}} \omega_k^2 \hat{A}_{\mathbf{ks}} \hat{A}^*_{\mathbf{ks}} = \sum_{\mathbf{ks}} \hbar\omega_k (\hat{a}^+_{\mathbf{ks}} \hat{a}_{\mathbf{ks}} + \frac{1}{2}), \tag{18}$$

where $E_0 = \frac{1}{2}\sum_{\mathbf{ks}} \hbar\omega_{\mathbf{k}}$ is denoted the zero-point or vacuum energy, which is a real property of the quantum electromagnetic field and does not have a classical analog. This term becomes especially important for the work presented in this thesis, when considering the initial state sampling and normal ordering within the MQC approach for photons. Finally, the vector field, electric field and magnetic field also take an operator form and are given by

$$\hat{\mathbf{A}}(\mathbf{r}, t) = \sum_{\mathbf{ks}} \left(\frac{\hbar}{2\omega_k \epsilon_0 V}\right)^{\frac{1}{2}} \mathbf{e}_{\mathbf{ks}} \left[\hat{a}_{\mathbf{ks}} e^{i(\mathbf{k}\cdot\mathbf{r})-\omega_k t} + \hat{a}^+_{\mathbf{ks}} e^{-i(\mathbf{k}\cdot\mathbf{r})-\omega_k t}\right] \tag{19}$$

$$\hat{\mathbf{E}}(\mathbf{r}, t) = i \sum_{\mathbf{ks}} \left(\frac{\hbar\omega_k}{2\epsilon_0 V}\right)^{\frac{1}{2}} \mathbf{e}_{\mathbf{ks}} \left[\hat{a}_{\mathbf{ks}} e^{i(\mathbf{k}\cdot\mathbf{r})-\omega_k t} - \hat{a}^+_{\mathbf{ks}} e^{-i(\mathbf{k}\cdot\mathbf{r})-\omega_k t}\right] \tag{20}$$

$$\hat{\mathbf{B}}(\mathbf{r}, t) = \frac{i}{c} \sum_{\mathbf{ks}} (\kappa \times \mathbf{e}_{\mathbf{ks}}) \left(\frac{\hbar\omega_k}{2\epsilon_0 V}\right)^{\frac{1}{2}} \mathbf{e}_{\mathbf{ks}} \left[\hat{a}_{\mathbf{ks}} e^{i(\mathbf{k}\cdot\mathbf{r})-\omega_k t} - \hat{a}^+_{\mathbf{ks}} e^{-i(\mathbf{k}\cdot\mathbf{r})-\omega_k t}\right], \tag{21}$$

respectively, where $V = (L)^3$ is the quantization volume, $\mathbf{e}_{\mathbf{ks}}$ denotes the polarization vector and $\kappa = \frac{\mathbf{k}}{|\mathbf{k}|}$.

ZERO-BOUNDARY CONDITIONS Considering the cavity QED set-ups investigated throughout this thesis, we impose the so-called zero-boundary conditions [55, 56] such that Eq. (13) changes to

$$\mathbf{k} = \frac{\pi}{L}(n_x, n_y, n_z), \tag{22}$$

where by introducing the normalized mode function as

$$S(\mathbf{k}\cdot\mathbf{r}) = \left(\frac{2}{L}\right)^{3/2}\prod_{i=1}^{3}\sin(k_i r_i), \tag{23}$$

the vector field operator yields

$$\hat{\mathbf{A}}(\mathbf{r},t) = \sum_{\mathbf{k}s}\left(\frac{\hbar}{2\omega_k\epsilon_0 V}\right)^{\frac{1}{2}}\mathbf{e}_{\mathbf{k}s}\left[\hat{a}_{\mathbf{k}s}+\hat{a}^{+}_{\mathbf{k}s}\right]S(\mathbf{k}\cdot\mathbf{r}). \tag{24}$$

Furthermore, with the matter-photon coupling strength $\lambda \propto S(\mathbf{k}\cdot\mathbf{r})$, one remarkable advantage of cavity QED is the possibility of tuning the interaction strength just by changing the quantization volume V via the mirror distances. Thus, a cavity set-up allows to control and measure a quantum system simply by coupling it to a finite volume (cavity) defined by walls (mirrors) instead of using complex and expensive external laser set-ups. A schematic of such a cavity set-up is depict in Fig. 1 exemplary for a trapped Naphthalene molecule. This set-up is commonly referred to as microcavity, i.e. photonic crystals [57, 58] or other semiconductor structures [59, 60], where the coupling to the outside mode is mediated by mirrors and cavity-length scales are in the micrometer regime. Alternatively, there are also nanocavities, i.e. plasmonic cavities [61–64], which have a reduced spatial dimension in the nanometer regime. Due to the reduced size, these types of cavities allow higher confinement and, thus, are especially important for single-molecule strong-coupling [65]. However, the consideration of losses is substantial in these cases and therefore in this work we, for now, only focus on microcavity-like set-ups with no losses.

1.1.2 *Bridging Quantum Chemistry and Quantum Optics*

The interaction between photons and quantum systems is the foundation of an incredibly wide spectrum of phenomena, ranging from spontaneous emission to quantum sensing and quantum communication [66]. Although the forefront of the rapidly expanding domain of cavity-modified chemistry has been strongly driven by experiments, recent theoretical investigations have revealed complementary insights [67–71]. The description of chemical processes that are strongly correlated with quantum light [72–74], requires an accurate and flexible, and computationally efficient, treatment of the light-matter interactions. Thus, to develop an *ab initio* theoretical description of cavity modified chemical systems, extensions to the traditional theoretical tool-kits of quantum optics and quantum chemistry are required.

In Fig. 2 we schematically illustrate the relation between quantum chemsitry and quantum optics over the level of matter system complexity and the quantumness of the light field. Quantum chemistry (green area in Fig. 2), is able to handle realistic and large quantum systems, i.e. multi-molecular systems and solids, by using well known methods like Hartree-Fock, DFT and Coupled Clus-

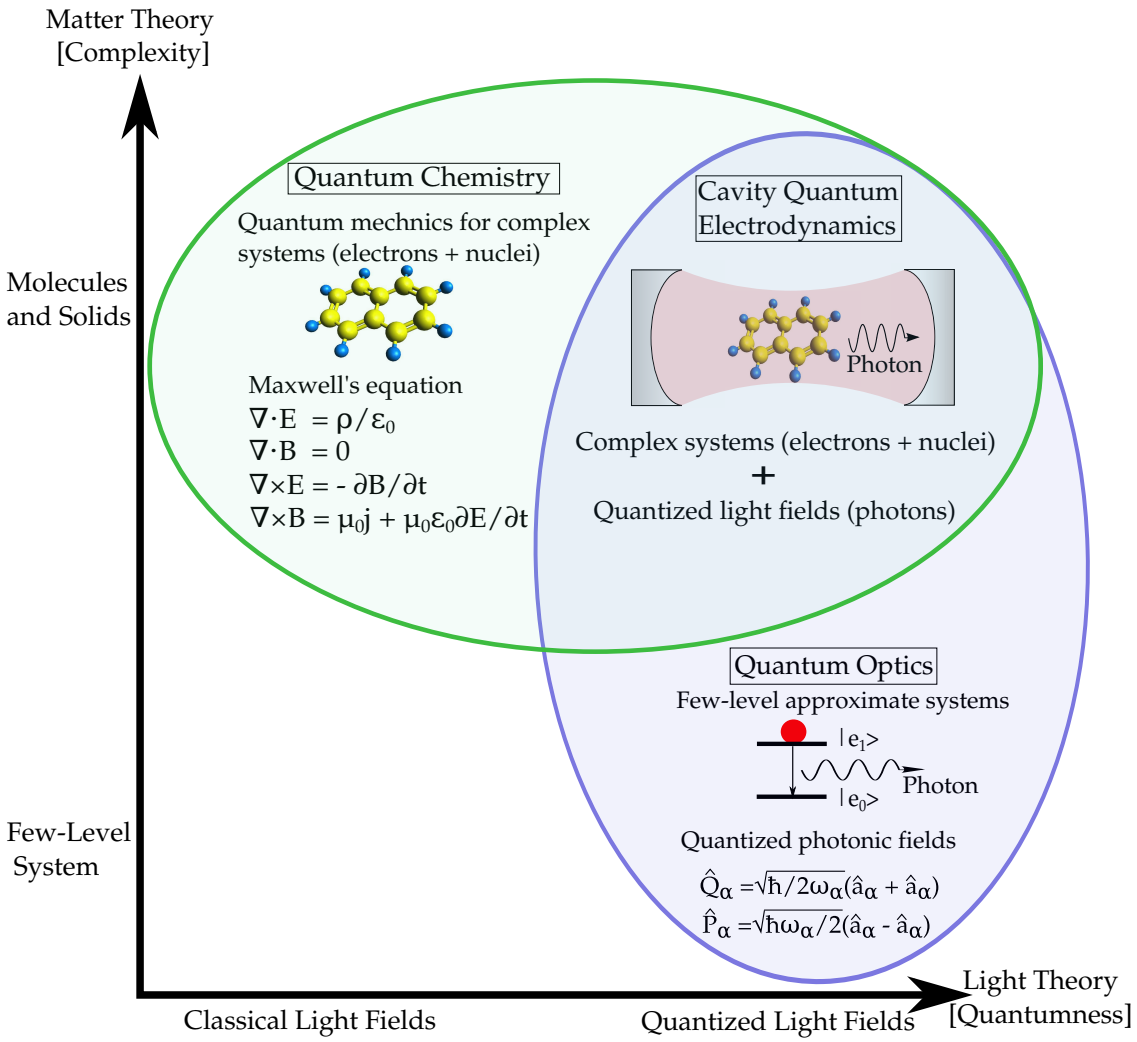

Figure 2: A schematic overview of the relation between quantum chemsitry and quantum optics over the level of matter system complexity and the quantumness of the light field. The green area characterizes theory-levels, which can treat complex matter systems. The blue area contains theory-levels which are able to take the quantum nature of the light into account. The overlap of both areas renders the field of interest of this thesis.

ter Theory. However, these methods, if at all, take classical light fields into account via Maxwell's equation. Quantum optics (blue area in Fig. 2), on the other hand, captures the quantum nature of light in great detail. However, quantum optical models of the matter system are typically over-simplified (few-level) and therefore break down for realistic systems. Thus, we have to face the question: Is there a way to bridge quantum chemistry and quantum optics (green-blue intercept in Fig. 2) in order to treat realistic systems, ideally *ab initio*, but retain the quantum nature of light?

Due to the similarity of electron-photon and electron-nuclear problems, simulation methods that are established in the quantum chemistry community, such as MQC methods and the EF approach, may offer an interesting lead towards finding a feasible intercept between quantum chemistry and quantum optics. Recall that MQC methods treat only a few crucial degrees of freedom quantum

mechanically and apply a classical treatment to the rest of the system. Typically, the electronic system is treated quantum mechanically, e.g. via Hartree-Fock or TDDFT, and the nuclei system classically, e.g. via Wigner-dynamics. This builds on the assumption of the nuclei moving slow compared to the electrons, which allows the negligence of the nuclear kinetic-energy contribution. However, this assumption can not be made for an electron-photon system, as photons move, by far, faster than electrons. Yet, considering that the photonic Hamiltonian in a matter-free system is a sum over harmonic Hamiltonians for each mode, a classical Wigner treatment of the photonic system is reasonable and a potential route to introduce quantized light fields to MQC methods. In the following, we show how to extend traditional MQC methods to the photonic degrees of freedom, i.e. quantized light fields. For further analysis, we also extend and investigate the corresponding exact TDPES within the EF approach for the applied systems.

1.1.3 *Hamiltonian and Model Systems*

Before we proceed with a discussion of the extension of MQC methods and the TDPES, we first turn our attention to the Hamiltonian and model systems used in these approaches. The starting point for our full QED Hamiltonian is the non-relativistic Pauli-Fierz Hamiltonian in minimal coupling [56, 75]

$$\begin{aligned}\hat{H}_{PF} = &\sum_{l=1}^{N_e} \frac{1}{2m_e}\left[\boldsymbol{\sigma}_l \cdot \left(-i\hbar\nabla_{\mathbf{r}_l} + \frac{|e|}{c}\hat{\mathbf{A}}_{tot}(\mathbf{r}_l, t)\right)\right]^2 \\ &+ \sum_{l=1}^{N_n} \frac{1}{2M_l}\left[\mathbf{S}_l^{\frac{n_l}{2}} \cdot \left(-i\hbar\nabla_{\mathbf{R}_l} + \frac{Z|e|}{c}\hat{\mathbf{A}}_{tot}(\mathbf{R}_l, t)\right)\right]^2 \\ &+ \frac{1}{2}\sum_{l\neq m}^{N_e} w(|\mathbf{r}_l - \mathbf{r}_m|) + \frac{1}{2}\sum_{l\neq m}^{N_n} Z_l Z_m w(|\mathbf{R}_l - \mathbf{R}_m|) \\ &+ \sum_{l=1}^{N_e}\sum_{m=1}^{N_n} Z_m(|\mathbf{r}_l - \mathbf{R}_m|) + \sum_{\mathbf{k},s} \hbar\omega_k \hat{a}^+_{\mathbf{k},s}\hat{a}_{\mathbf{k},s},\end{aligned} \tag{25}$$

where $\mathbf{R}$, eZ, M, $\mathbf{S}^{n_l/2}$ denote the nuclear, and $\mathbf{r}$, e, m_e, $\boldsymbol{\sigma}_l$ the electronic coordinates, charge, mass and spin, respectively. Here, $\mathbf{S}^{n_l/2}$ characterizes a vector of spin $n_l/2$ matrices reflecting the $n_l/2$-value of the spin of the l-th nucleus. The internal transversal and classical external vector potentials are aggregated in $\hat{\mathbf{A}}_{tot}$.

The minimal coupling in QED is introduced in order to take into account the influence of charged particles on the electromagnetic field and vice versa. Therefore, within the minimal coupling $\hat{\mathbf{p}}_l \to \hat{\mathbf{p}}_l - e\hat{\mathbf{A}}(\mathbf{r}_l)$ the charge current becomes the source of the electromagnetic field, while simultaneously modifying it, where $\hat{\mathbf{p}}$ denotes the momentum operator. This and the analogous formulation for the nuclei gives rise to the structure of the first and second term in Eq. (25). However, it is known that this coupling causes local photon-matter interactions, which, even in a perturbative regime, diverges beyond first order approximation

and leads to unphysical results [76]. To overcome this issue we assume an energy cut-off [77] well below 1 MeV [75], which is reasonable for the processes investigated in this thesis, and also neglect the creation of electron pairs, i.e. the non-relativistic limit. Furthermore, it is also sufficient to assume that the nuclei can be approximated by positive point charges with spin, since in the low energy regime only the nuclear motion and not the internal structure (proton, neutrons) is relevant.

Moreover, as already introduced in Sec. 1.1, we consider the Coulomb gauge, i.e. the photons only have transversal polarizations $s = \{1, 2\}$, for all calculations. This gives rise to the Coulomb interaction $w(|\mathbf{r} - \mathbf{r}'|) = \frac{e^2}{4\pi\epsilon_0}|\mathbf{r} - \mathbf{r}'|$ (analogously for the nuclei) among particles, i.e. the interaction of the charge-density operator and the longitudinal part of the field.

Furthermore, we consider the dipole approximation, where the wavelength of the electromagnetic field is assumed to be much larger than the spatial extension of the matter system. As a result, we can treat the mode functions as constant and expect only the total dipole element of the matter and the uniform electric field to contribute to the coupling.

Next, instead of describing the free photonic field in terms of creation and annihilation operators we rewrite the last term of Eq. (25) in terms of displacement $\hat{q}$ and momentum $\hat{p}$ operators via

$$\hat{q}_{\mathbf{k}s} = \sqrt{\frac{\hbar}{2\omega_k}}(\hat{a}^+_{\mathbf{k}s} + \hat{a}_{\mathbf{k}s}) \tag{26}$$

$$\hat{p}_{\mathbf{k}s} = i\sqrt{\frac{\hbar\omega_k}{2}}(\hat{a}^+_{\mathbf{k}s} - \hat{a}_{\mathbf{k}s}). \tag{27}$$

Finally, with the assumption of no classical external fields and no spin-coupling, the non-relativistic Hamiltonian in dipole approximation and Coulomb gauge for N_e electrons, N_n nuclei, and N_p quantized photon modes is defined as [53, 56, 70, 75, 78–82]:

$$\hat{H}(q, r, R) = \hat{H}_p + \hat{H}_e + \hat{H}_n + \hat{H}_{en} + \hat{H}_{np} + \hat{H}_{ep} + \hat{H}_{pen}. \tag{28}$$

The first term of Eq. (28) is the free photonic field and characterizes the cavity-photon Hamiltonian

$$\hat{H}_p = \frac{1}{2}\left(\sum_{\alpha=1}^{2N_p} \hat{p}^2_\alpha + \omega^2_\alpha \hat{q}^2_\alpha\right) = \hat{T}_p + \hat{V}_p, \tag{29}$$

where α denotes the photon mode and $\alpha = \{1, ..., 2N_p\}$ due to the two polarization possibilities. The second term of Eq. (28) denotes the electronic Hamiltonian given as

$$\hat{H}_e = \sum_{i=1}^{N_e} \frac{\hat{\mathbf{p}}^2_i}{2m_e} + \frac{e^2}{4\pi\epsilon_0}\sum_{i>j}^{N_e} \frac{1}{|\mathbf{r}_i - \mathbf{r}_j|} = \hat{T}_e + \hat{V}_{ee}. \tag{30}$$

Similarly structured, the third term of Eq. (28) describes the nuclear Hamiltonian given as

$$\hat{H}_n = \sum_{I=1}^{N_n} \frac{\hat{\mathbf{P}}_I^2}{2M_I} + \frac{e^2}{4\pi\epsilon_0} \sum_{i>j}^{N_n} \frac{Z_I Z_J}{|\mathbf{R}_I - \mathbf{R}_J|} = \hat{T}_n + \hat{V}_{nn}. \tag{31}$$

The remaining terms of Eq. (28) denote the couplings between the subsystems. Specifically, the electron-nuclear coupling, in the Coulombic interaction, is given as

$$\hat{H}_{en} = -\sum_{i=1}^{N_e} \sum_{J=1}^{N_n} \frac{e^2 Z}{|\mathbf{r}_i - \mathbf{R}_J|}, \tag{32}$$

the nuclear-photon coupling, in dipole approximation, is given as

$$\hat{H}_{np} = \sum_{\alpha=1}^{2N_p} \omega_\alpha \hat{q}_\alpha \lambda_\alpha \cdot \sum_{I=1}^{N_n} e Z_I \mathbf{R}_I, \tag{33}$$

and the electron-photon coupling, in dipole approximation, is given as

$$\hat{H}_{ep} = -\sum_{\alpha=1}^{2N_p} \omega_\alpha \hat{q}_\alpha \lambda_\alpha \cdot \sum_{i=1}^{N_e} e\mathbf{r}_i. \tag{34}$$

with the matter-photon coupling strength given as

$$\lambda_\alpha = \sqrt{4\pi} S_\alpha (\mathbf{k}_\alpha \cdot \mathbf{X}) e_\alpha, \tag{35}$$

where S_α denotes the mode function, e.g. a product of sine-functions for the case of a cubic cavity [56, 79], $\mathbf{k}_\alpha$ the wavevector, and $\mathbf{X}$ the total dipole of the system. In particular, these mode functions introduce a dependence of the coupling constants on the quantization volume of the electromagnetic field. Finally, the last term of Eq. (28) represents the self-polarization of the matter in the radiation field given as

$$\hat{H}_{pen} = \frac{1}{2} \sum_{\alpha=1}^{2N_p} \left(\lambda_\alpha \cdot \left(\sum_{I}^{N_n} Z_I \mathbf{R}_I - \sum_{i}^{N_e} e\mathbf{r}_i \right) \right)^2, \tag{36}$$

which is essential for a mathematically well-defined light-matter interaction. Without $\hat{H}_{pen}$ the Hamiltonian is unbounded from below, and, additionally, looses its translational invariance [83, 84]. In Sec. 3.2, we further emphasize its increasing significance on chemical reactions the more photon modes are included.

To evaluate qualitative and quantitative properties and potential theoretical challenges of the MQC methods and the EF approach, we require credible benchmarks. However, benchmarking both extended methods, demands an exact reference solution and, thus, at first, restricts the applicable Hilbert-space of interest.

To focus on the evolution of the photonic degrees of freedom, we start by restricting our matter part to a two and three level atomic system, as detailed in [O1–O3] and, then, extend this to a full molecular model system, i.e. the Shin-Metiu model [85], as presented in [O4, O5]. The following paragraphs explain the applied model systems more detailed. Note that the following equations are given in atomic units ($\hbar = e^2 = m_e = 1$).

COUPLED ELECTRON-PHOTON MODEL SYSTEM The work in [O1–O3], see Chap. 2, investigates correlated electron-photon systems by considering an one-dimensional model of a cavity in which a few-level (two and three levels) system interacts with either one [O2] or 400 [O1, O3] cavity modes in dipole approximation [70, 86]. Fig. 3 shows a schematic of the applied model.

The Hamiltonian for this model system is given as

$$\begin{aligned}\hat{H} = &\sum_{k=1}^{m} \epsilon_k |k\rangle\langle k| + \frac{1}{2}\sum_{\alpha}^{2N_p}\left(\hat{p}_\alpha^2 + \omega_\alpha^2 \hat{q}_\alpha^2\right) \\ &+ \sum_{\alpha}^{2N}\sum_{k,l=1}^{m} \mu_{kl}\omega_\alpha \lambda_\alpha(r_A)\hat{q}_\alpha |k\rangle\langle l|,\end{aligned} \tag{37}$$

where μ_{kl} denotes the transition moment, λ_α the coupling strength, ω_α the mode frequency, r_A the atomic position and m the number of atomic energy levels. Furthermore, with the coupling of a 1D-cavity given as

$$\lambda_\alpha = \sqrt{\frac{2}{\epsilon_0 L}}\sin(k_\alpha r_A), \tag{38}$$

with $k_\alpha = \frac{\omega_\alpha}{c} = \frac{\alpha\pi}{L}$ and the atomic position fixed at $r_A = \frac{L}{2}$, where L is the cavity length, only half of the cavity modes (only the odd modes) couple to the atomic system by symmetry $\lambda_\alpha = \sqrt{\frac{2}{\epsilon_0 L}}\sin(\alpha\frac{\pi}{2})$. For more details on the precise parameter choice we refer to Chap. 2.

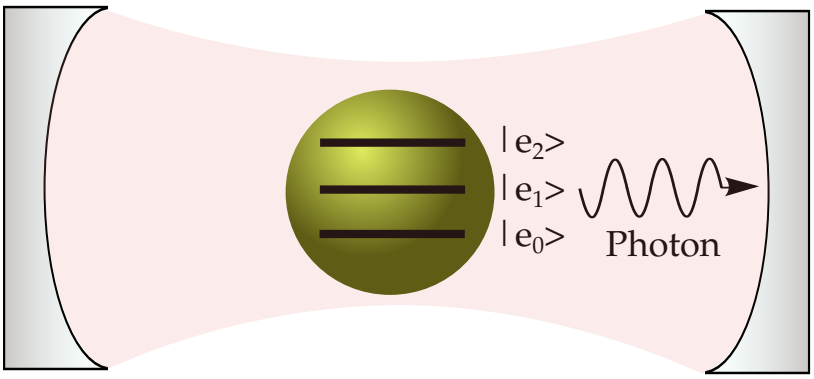

Figure 3: A schematic of a few-level atomic system (green) trapped in a cavity. Here $|e_0\rangle$ denotes the electronic groundstate, $|e_1\rangle$ the electronic first excited state and $|e_2\rangle$ the electronic second excited state.

COUPLED ELECTRON-NUCLEI-PHOTON MODEL SYSTEM To approach more realistic systems, we replace the few-level system from above with a molecular model system and include the nuclei degrees of freedom. Hence, we employ the minimal model of Shin and Metiu [85, 87, 88], which consists of three ions and a single electron, where two ions are fixed at a distance of L_I and the third ion and the electron can move between the two fixed ions. This model has been proven to be remarkably instructive for studying adiabatic and nonadiabatic effects in cavity-free cases [87–90] as well as in-cavity cases [82, 91]. Fig. 4 depicts a schematic of this model system. We study nonadiabatic effects of PCET within a cavity set-up by coupling the Shin-Metiu minimal model to the photonic degrees of freedom. The non-relativistic photon-matter Hamiltonian in the dipole approximation in the Coulomb gauge [56, 75, 78, 82], thus, takes the from

$$\begin{aligned}\hat{H} = &-\frac{1}{2M}\frac{\partial^2}{\partial R^2} + -\frac{1}{2}\frac{\partial^2}{\partial r^2} + \frac{1}{2}\sum_\alpha \left(\hat{p}_\alpha^2 + \omega_\alpha^2 \hat{q}_\alpha^2\right) \\ &+ \sum_\alpha \omega_\alpha \lambda_\alpha \hat{q}_\alpha \left(ZR - r\right) + \hat{V}_m + \hat{V}_{sp},\end{aligned} \tag{39}$$

with $\hat{V}_m$ the molecular potential given as

$$\hat{V}_m = \sum_{\sigma=\pm 1}\left(\frac{1}{|R + \frac{\sigma L_I}{2}|} - \frac{\operatorname{erf}\left(\frac{|r+\frac{\sigma L_I}{2}}{a_\sigma}\right)}{|r + \frac{\sigma L_I}{2}|}\right) - \frac{\operatorname{erf}\left(\frac{|R-r|}{a_f}\right)}{|R-r|}, \tag{40}$$

and $\hat{V}_{sp}$ the self-polarization term given as

$$\hat{V}_{sp} = \frac{1}{2}\sum_\alpha \left(\lambda_\alpha \cdot (ZR - r)\right)^2. \tag{41}$$

Note that in the single-mode coupling investigated in [O4] this term has a negligible effect and therefore can be discarded. In contrast, considering the multimode coupling studied in [O5] this term has an significant impact and neglecting it does not only yield quantitative differences of the results but also qualitatively changes the physics tremendously. Furthermore, the electron-photon coupling strength λ_α generally depends on the mode function of the cavity. However, for both cases we will take it as a constant, assuming that the cavity is much longer than the spatial range of the molecular dynamics. For the EF approach [O4] we couple the molecule to one single photon mode, whereas in the MTEF approach [O5] we first investigate dynamics with coupling to one photon mode, in comparison to an exact reference solution, and then, with the exact reference solution out of reach, extend the coupling up to 440 photon modes. Again, with the position of the molecule fixed at L/2, only half of the cavity modes couple by symmetry. For more details about the precise parameter choice we refer to Chap. 3.

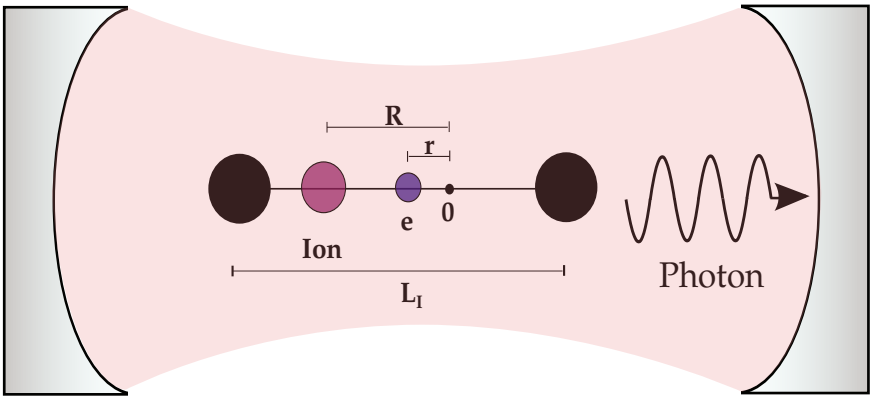

Figure 4: A schematic of the molecular Shin-Metiu model system trapped in a cavity. This model includes two fixed ions (black) in a distance L_I. The third ion (magenta) and the single electron (purple) given at a distance R and r can move in between these fixed ions.

1.2 MIXED-QUANTUM CLASSICAL MEHTODS FOR PHOTONS

In this section we outline the extension of the MQC methods, traditionally introduced to electron-nuclear systems, to coupled light-matter systems. With the intention not to exceed the scope of this introduction, we do not elaborate on the traditional electron-nuclei MQC theory in detail. We refer the interested reader to the following references for more information and technical background on

- the MTEF method [15, 17–19],
- fewest switch surface hopping algorithms [29–34],
- semiclassical mapping methods [20–26].

Furthermore, Sec. 2.3 gives an overview of the different methods within the light-matter framework. However, note that this thesis is mainly concerned with the extension of the MTEF method to light-matter interaction, see Sec. 2.1 and 3.2. Thus, the following paragraphs present the central concepts of MQC methods for photons, i.e. photonic initial state sampling, operator normal ordering and spBO-surfaces. The section is concluded by an overview on the numerical implementation, see Fig. 7.

1.2.1 *Wigner Transformation for Photons*

In quantum mechanics the concept of phase-space is obstructed by the quantities being described by their probability and, moreover, obeying the uncertainty principle [92]. For example, considering a classical particle, which has a phase-

space distribution $P_{cl}(q,p)$, where q and p denote its position and momentum respectively, the average of some arbitrary function $A(q,p)$ can be calculated as

$$\langle A_{cl}\rangle = \int dq \int dp A(q,p) P_{cl}(q,p). \tag{42}$$

In contrast, in quantum mechanics the particle is defined by its density matrix $\hat{\rho}$ and the corresponding average (expectation value) of an arbitrary quantum operator $\hat{A}(\hat{q},\hat{p})$, where $\hat{q}$ and $\hat{p}$ are now operators, can be calculated by

$$\langle \hat{A}\rangle_{qm} = Tr\,\langle \hat{A}\hat{\rho}\rangle\,. \tag{43}$$

Therefore, in order to obtain a phase-space representation of the quantum state, a connection between Eq. (42) and Eq. (43) is required. However, it is known that for a given classical $A(q,p)$ the corresponding quantum operator $\hat{A}(\hat{q},\hat{p})$ is not uniquely defined [92]. Nonetheless, this problem can be overcome by defining a so-called quasi-distribution $P_Q(q,p)$ and using well defined correspondence rules such that

$$\langle \hat{A}\rangle_{qm} = \int dq \int dp\ A(q,p) P_Q(q,p). \tag{44}$$

One well-known quasi distribution was introduced by Wigner [93] in order to find quantum corrections to classical mechanics. This quasi-distribution has been studied extensively [92, 94–99] and renders a central concept for classical and semiclassical ensemble-trajectory methods. More precisely, the Wigner distribution is given by [100]

$$W(q,p) = \frac{1}{2\pi\hbar}\int e^{\frac{-ipy}{\hbar}} \psi(q+\frac{y}{2})\psi(q-\frac{y}{2})dy, \tag{45}$$

where ψ denotes the wavefunction of the particle. The expectation value of the quantum operator $\hat{A}$ is defined as

$$\langle \hat{A}\rangle = \int\int W(q,p)\widetilde{A}(q,p)dqdp, \tag{46}$$

where $\widetilde{A}$ denotes the Weyl-transform [101, 102] and is given as

$$\widetilde{A}(q,p) = \int e^{\frac{-ipy}{\hbar}} \left\langle q+\frac{y}{2}\right| \hat{A} \left|q-\frac{y}{2}\right\rangle dy. \tag{47}$$

Integrating the Wigner function over p yields $\int W(q,p)dp = \psi^*(q)\psi(q)$ by applying the relation $\int \exp\left[\frac{ipq}{\hbar}\right] dp = 2\hbar\delta(q)$. The analogous integration for q yields $\int W(q,p)dq = \phi^*(p)\phi(p)$, where $\Psi(q)$, $\phi(p)$ denote the probability density in position and momentum space respectively. With the projection of $W(q,p)$ on q defining the probability distribution in q and the projection of $W(q,p)$ defining the probability distribution in p, the Wigner function characterizes a phase-space distribution represented by the wavefunction $\Psi(q)$. In other words, the Wigner

function introduces a quantum correction to classical statistical mechanics by transforming the wavefunction to a quasi-probability in phase-space.

The Wigner function is also a central and important concept for the extension of the MQC methods to photonic degrees of freedom, i.e. the sampling of the initial photon state. Even though the photonic degrees of freedom are defined classically, quantum effects can be introduced via the initial state obtained from the Wigner distribution. Note that this corresponds to properly accounting for the quantum statistics of the initial vacuum field. In the studied MQC method for photons, see Secs. 2.1, 2.3 and 3.2, we consider a vacuum in the cavity at time zero, i.e. no photon, and, thus, the Wigner transform of this groundstate yields a Gaussian phase-space distribution. More precisely, the free photonic field Hamiltonian is given by an harmonic oscillator structure as

$$\hat{H}_p = \frac{1}{2}\left(\sum_\alpha \hat{p}_\alpha^2 + \omega^2 \hat{q}_\alpha^2\right) \tag{48}$$

and the corresponding groundstate wavefunction is

$$\Psi_0(q) = \sum_\alpha \left(\frac{\omega_\alpha}{\pi\hbar}\right)^{\frac{1}{4}} \exp\left[-\frac{\omega_\alpha \hat{q}_\alpha^2}{2\hbar}\right]. \tag{49}$$

Inserting $\Psi_0(q)$ into the Wigner transform of Eq. (45) then yields a Wigner distribution

$$W_0(q,p) = \prod_\alpha \frac{1}{\pi\hbar} \exp\left[-\frac{p_\alpha^2}{\omega_\alpha} - \frac{\omega_\alpha q_\alpha^2}{\hbar}\right], \tag{50}$$

where Eq. (50) defines the distribution for the photonic initial state sampling. Here α, again, denotes the photon mode. Note that, although not investigated in this work, the Wigner transform could also be applied for excited photonic states. We briefly discuss this possible future extension in Chap. 4.

1.2.2 *Vacuum Fluctuation and Normal Ordering*

Quantum mechanical operators underlie commutation relations, which makes the order in which the operators occur crucial [103]. More precisely, quantum mechanical particles, such as photons (or alternatively phonons), obey the Bose-Einstein statistics and therefore satisfy the following commutation relation

$$[\hat{a}, \hat{a}^+] = 1 \rightarrow \hat{a}\hat{a}^+ - \hat{a}^+\hat{a} = 1, \tag{51}$$

where $\hat{a}^+$, $\hat{a}$ compactly denote the creation and annihilation operator, respectively. The resulting non-commutativity $\hat{a}^+\hat{a} \neq \hat{a}\hat{a}^+$ incurs the so-called ordering problem of the operators and plays an important role in the construction of quantum operators and the calculation of their expectation values. If all annihilation operators are on the right hand side, i.e. for calculations of number or coherent state expectation values, the ordering is called normal ordering, denoted as $:\hat{O}:$

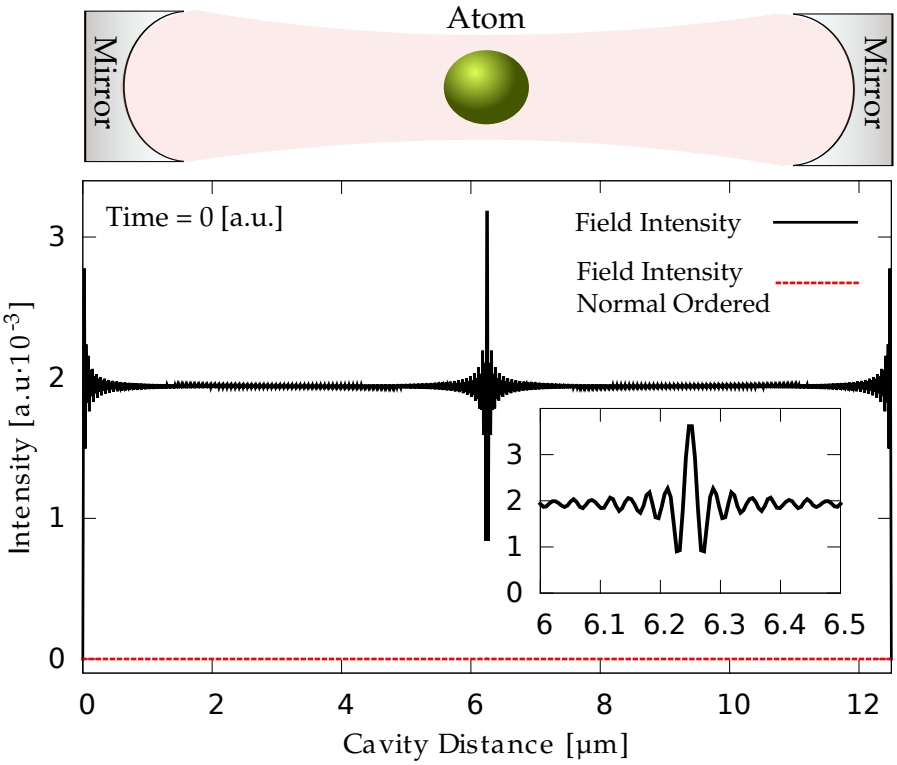

Figure 5: An example of the difference between normal ordered photonic field intensity (red) and not normal ordered photonic field intensity (black) at the initial time. The inset depicts a zoom-in of the peak at the atomic position. Figure adapted from [O1].

for an arbitrary operator $\hat{O}$. This normal ordering is especially important within the MQC approach for photons, because non-normal ordered operators yield results that include the vacuum fluctuation. Although being essential, the vacuum fluctuation is a typically non-measurable effect in experiments [104, 105] and therefore needs to be removed from the results, i.e. by normal ordering. In other words, for the calculation of the electric field and the field intensity it has to be ensured that both observables are zero when in the vacuum state, irrespective of the number of photon modes in the cavity field (note that all observables in the following are given in atomic units). The effect of this operator ordering is particularly evident for the photon number operator

$$:\hat{N}_{pt}:=\frac{1}{2}\sum_{\alpha}\left(\frac{\hat{p}_{\alpha}^{2}}{\omega_{\alpha}}+\omega_{\alpha}\hat{q}_{\alpha}^{2}-1\right). \tag{52}$$

Here the normal ordering produces a constant shift due to the zero-point energy term, i.e. $-\frac{2N}{2}=-N$, where 2N is the maximum mode number. However, this offset can become rather complex, e.g for the quantized field intensity operator,

or, even more so, for correlation functions. Fig. 5 shows this effect by plotting the normal ordered electric field intensity given as

$$: \hat{E}^2(r,t) :=: \hat{I}(r,t) := 2\sum_{\alpha} \omega_\alpha \zeta_\alpha^2(r)\hat{q}_\alpha^2(t) - \sum_{\alpha} \zeta_\alpha^2(r), \tag{53}$$

where

$$\zeta_\alpha(r) = \sqrt{\frac{\omega_\alpha}{\epsilon_0 L}} \sin\left(\frac{\alpha\pi}{L} r\right), \tag{54}$$

against its canonical counterpart. In addition to the constant shift, the normal ordering also eliminates oscillations observed in the canonical field intensity near boundaries and matter position. Note that the canonical field intensity shown in Fig. 5 exactly corresponds to the vacuum fluctuation of the system.

This shift gets even more complex when the second order correlation function g^2 for the photon field is considered. This function is frequently used in quantum optics to discriminate between classical light ($g^2 = 1$) and non-classical light that exhibits photon bunching ($g^2 > 1$) or photon anti-bunching ($g^2 < 1$) [106]. More precisely, in the case of a spatial second order correlation function given at time t as

$$\hat{g}^2(r_1, r_2, t) = \frac{\langle \hat{E}^+(r_1,t)\hat{E}^+(r_2,t)\hat{E}(r_2,t)\hat{E}(r_1,t)\rangle}{\langle \hat{I}(r_1,t)\rangle \quad \langle : \hat{I}(r_2,t)\rangle}, \tag{55}$$

the numerator of g^2, also referred to as $G^2(r_1, r_2, t)$, takes the complex normal-ordered form of

$$\begin{aligned} : \hat{G}^2(r_1, r_2, t) :=& 4\sum_{\alpha} \omega_\alpha^2 \zeta_\alpha(r_1)\zeta_\alpha(r_2)\zeta_\alpha(r_2)\zeta_\alpha(r_1)\hat{q}_\alpha^4(t) \\ &- \sum_{\alpha\beta} \Big(4\zeta_\beta(r_1)\zeta_\beta(r_2)\zeta_\alpha(r_1)\zeta_\alpha(r_2) + \zeta_\beta^2(r_2)\zeta_\alpha^2(r_1) \\ &+ \zeta_\beta^2(r_1)\zeta_\alpha^2(r_2)\Big) \cdot 2\omega_\alpha \hat{q}_\alpha^2(t). \end{aligned} \tag{56}$$

Considering the time-correlation function the commutation operators are additionally time dependent, thus further increasing the complexity of the normal ordering. For the frequently assumed case of $\Delta\tau = 0$, with $t_2 = t_1 + \Delta\tau$, the time-correlation function at position r for a single photon mode is given as

$$\hat{g}^2(r,t) = \frac{\langle \hat{N}_{pt}(t)\left(\hat{N}_{pt}(t) - 1\right)\rangle}{\langle \hat{N}_{pt}(t)^2\rangle}, \tag{57}$$

and $: G^2(r,t) :$ takes the normal ordered form of

$$: \hat{G}^2(r,t) := \frac{1}{4}\left(\frac{\hat{p}(t)}{\omega^2} + \hat{p}(t)^2\hat{q}(t)^2 + \hat{q}(t)^2\hat{p}(t)^2 - \frac{4\hat{p}(t)^2}{\omega} - \omega\hat{q}(t)^2 + 3 + \frac{\omega^2\hat{q}(t)^4}{4}\right). \tag{58}$$

However, the remaining momentum and displacement operator multiplications $(\hat{p}^2\hat{q}^2 + \hat{q}^2\hat{p}^2)$ in Eq. (58) additionally require a Weyl transform [21, 101, 102]. Complementary to the Wigner transform, which guarantees the correct phase-space representation for the wavefunction, the Weyl transform ensures the correct phase-space representation of the operators corresponding to physical observables. More precisely, applying the Weyl transform (indicated by the $\sim$ operator) as [100]

$$\widetilde{\hat{q}^2\hat{p}^2} + \widetilde{\hat{p}^2\hat{q}^2} = 2q^2p^2 - 1, \tag{59}$$

produces a constant shift (-1) and therefore yields

$$:G^2(r,t) := \frac{1}{4}\left(\frac{p(t)}{\omega^2} + 2q(t)^2p(t)^2 - \frac{4p(t)^2}{\omega} - \omega q(t)^2 + 2 + \frac{\omega^2 q(t)^4}{4}\right), \tag{60}$$

for the classical limit of the time-correlation function. Note that a classical limit without Weyl ordering, on the other hand, would yield $2p^2q^2$ (without a shift).

1.2.3 *Self-Polarization-Modified Born-Oppenheimer Surfaces*

The concept of PESs plays a central role for the simulation and analysis of MQC methods e.g., (cavity) BO-surfaces [14, 82], polaritonic surfaces [107, 108] or TDPES [35, 36] for the analyses of coupled dynamics. However, the contribution of the self-polarization term, see Eq. (36), has so far been neglected for PESs in cavities. This is reasonable in many cases, especially within the commonly applied single (resonant) photon mode coupling. Also, for the systems investigated in [O1–O4] the self-polarization provably has no impact on the dynamics and surfaces. Nonetheless, recent publications emphasize the overall importance of this term [83, 84], particularly when assuming the ultra-strong coupling regime, even within single-mode coupling [71]. In line with these publications, we find that, the closer we get to modeling realistic systems, i.e. full electron-nuclei-photon systems coupled to multiple photon modes, this term can become highly significant [O5].

To analyze the impact of the self-polarization term, we define the spBO-surface

$$\hat{H}^{sp}_{BO}\Phi^{sp}_{BO} = \epsilon^{sp}_{BO}(R)\Phi^{sp}_{R,BO}, \tag{61}$$

where H^{sp}_{BO} defines the traditional BO-Hamiltonian plus the self-polarization term, $\hat{H}^{sp}_{BO} = \hat{T}_e + \hat{V}_m + \hat{V}^{sp}$ with $\hat{T}_e$ the electronic kinetic term, $\hat{V}_m$ the molecular potential and $\hat{V}_{sp}$ the self-polarization term. See Sec. 3.2 for a more comprehensive description. Fig. 6 shows the ground and first excited surfaces (black curves) of the molecular model system investigated in [O5] exemplary for a single photon mode and 10, 40, 200, 440 photon modes. For the single-mode case in Fig. 6(a) the BO-surfaces and the spBO-surfaces are essentially identical. However, the more photon modes are accounted for, these surfaces show an increasing difference from the original form with significant changes in the overall slope

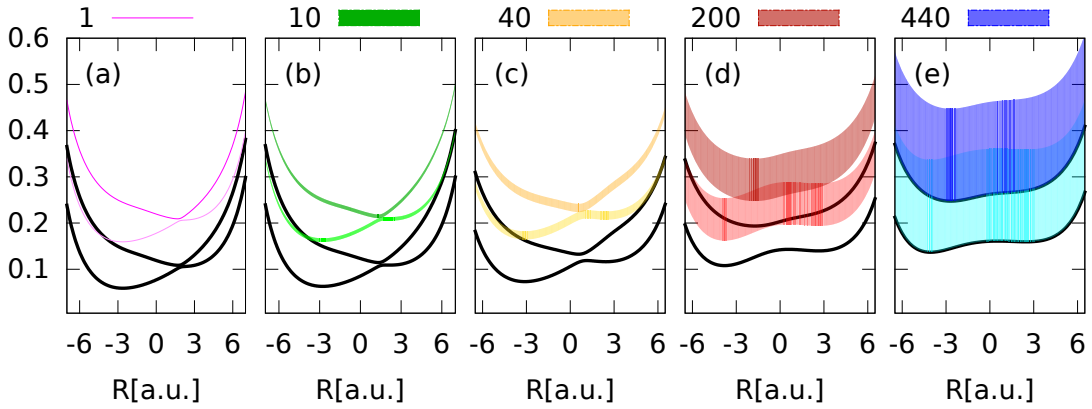

Figure 6: The self-polarization-modified BO surfaces for 1 (a), 10 (b), 40 (c), 200 (d) and 440 (e) photon-mode coupling depict for the ground and first excited surface within the model investigated in [O5], where R denotes the nuclear coordinate. Figure adapted from [O5]

as well as the size and position of the avoided crossing Fig. 6(d–e). This clearly shows the impact of the self-polarization term on the resulting dynamics.

We now additionally define the 1-photon spBO-surface by shifting the spBO-surface uniformly by the energy of the photon $\hbar\omega_\alpha$. For a single photon mode coupling this shift yields well separated surfaces, see Fig. 6(a). However, the more photon modes are accounted for, these surfaces develop band-like structures indicated by the colored areas in Fig. 6(b–e). These areas represent parallel surfaces separated by the mode spacing. Specifically, the frequencies chosen to generate Fig. 6 are given by $\omega_\alpha = 0.1 + \frac{\alpha\pi c}{L}$ where 0.1 is the initial resonant frequency and $\alpha = \{-\frac{N}{2} \cdots \frac{N}{2}\}$. Here L denotes the cavity length and N the number of modes ranging from 0 (single mode) to 10, 40, 200, 440. Therefore, by accounting for more photon modes, also the overlap of the band-like surfaces increases, as shown in Fig. 6(c–e), and suggests that a nuclear wavepacket, evolving between excited state and groundstate, will encounter an increasing number of avoided crossings.

Subsequently, we have two microscopic mechanisms that are fundamentally responsible for differences in the corresponding dynamics compared to single mode simulations: First, the self-polarization term grows in significance with more modes with the effect that spBO-surfaces are distorted significantly away from their cavity-free shape (compare pink to blue surfaces). Second, the 1-photon-spBO-bands become wider and increasingly overlapping, yielding a very mixed electronic character and continual exchange between surfaces. Again, see Sec. 3.2 for a more detailed discussion. Note that these changes of the PES occur without changing the matter-photon coupling strength and therefore could yield a new way to control and change chemical reactions via the self-polarization without the need to explicitly change the light-matter coupling strength itself.

1.2.4 *Numerical Implementation*

This section outlines the numerical implementation of the MQC dynamics methods for photons. Recall that we aim to treat the electronic degrees of freedom quantum mechanically and the nuclei and photonic degrees of freedom via classical Wigner dynamics, see Sec. 1.1.2. For the correlated electron-photon system this implies a classical treatment of the photons, see Secs. 2.1 and 2.3. For the full electron-photon-nuclei system, on the other hand, we explore the classical treatment of both photons and nuclei, see Sec. 3.2. Therefore, the numerical implementation presented below focuses on the latter case, as it is the most general.

Fig. 7 shows a schematic of the algorithm for the resulting full electron-photon-nuclei system. To obtain the initial state distribution, we first calculate the Wigner transformation of the photonic and nuclear initial density operators $\hat{\rho}_{0,W_p}(q_\alpha, p_\alpha)$ and $\hat{\rho}_{0,W_n}(R_\beta, P_\beta)$, respectively. Again α denotes the photonic modes and, additionally, β the nuclear degrees of freedom. Note that as we consider no photon to be in the cavity at time zero, i.e. vacuum state at zero temperature, for all calculations performed in this work, the Wigner transform yields a Gaussian distribution with frequency-depending variance. Furthermore, we also choose the nuclear initial distribution to be Gaussian. Thus, to obtain a set of initial conditions $(q_\alpha^j(0), p_\alpha^j(0))$, $(R_\beta^j(0), P_\beta^j(0))$ for the trajectory ensemble, we perform a Monte Carlo sampling from the photonic and nuclear Wigner transforms for each trajectory j. Furthermore, as the electronic degrees of freedom are treated quantum mechanically, we choose the initial electronic state to be excited. We then generate an ensemble of trajectories, by independently evolving each initial condition $|I_{total}^j\rangle$, as shown in Fig. 7, according to the MTEF electron-photon-nuclei correlated equations of motion. The corresponding equations of motion for multiple photon modes α, a single nuclear degree of freedom and two BOPESs are given as

$$\ddot{q}_\alpha^j(t) = -\omega_\alpha^2 q_\alpha^j - \omega_\alpha \lambda_\alpha (Z\langle R\rangle^j - \langle r\rangle^j) \tag{62}$$

$$M\ddot{R}^j(t) = -\langle \partial_R \epsilon_{BO}(R^j)\rangle - \sum_\alpha \omega_\alpha \lambda_\alpha q_\alpha^j + \sum_\alpha \left(\lambda_\alpha^2 \cdot (Z\langle R\rangle^j - \langle r\rangle^j)\right) \tag{63}$$

$$i\partial_t \begin{pmatrix} C_1(t) \\ C_2(t) \end{pmatrix} = \begin{pmatrix} h_{11} & h_{12} \\ h_{21} & h_{22} \end{pmatrix} \begin{pmatrix} C_1(t) \\ C_2(t) \end{pmatrix}, \tag{64}$$

with the diagonal matrix elements given as

$$\begin{aligned} h_{kk} =& \epsilon_{BO}^k(R^j) + \sum_\alpha \omega_\alpha \lambda_\alpha q_\alpha^j (ZR^j - r_{kk}(R^j)) \\ &+ \frac{1}{2}\sum_\alpha \lambda_\alpha^2 \cdot \left((ZR^j)^2 - 2ZR^j r_{kk}(R^j) + r_{kk}^{(2)}(R^j)\right), \end{aligned} \tag{65}$$

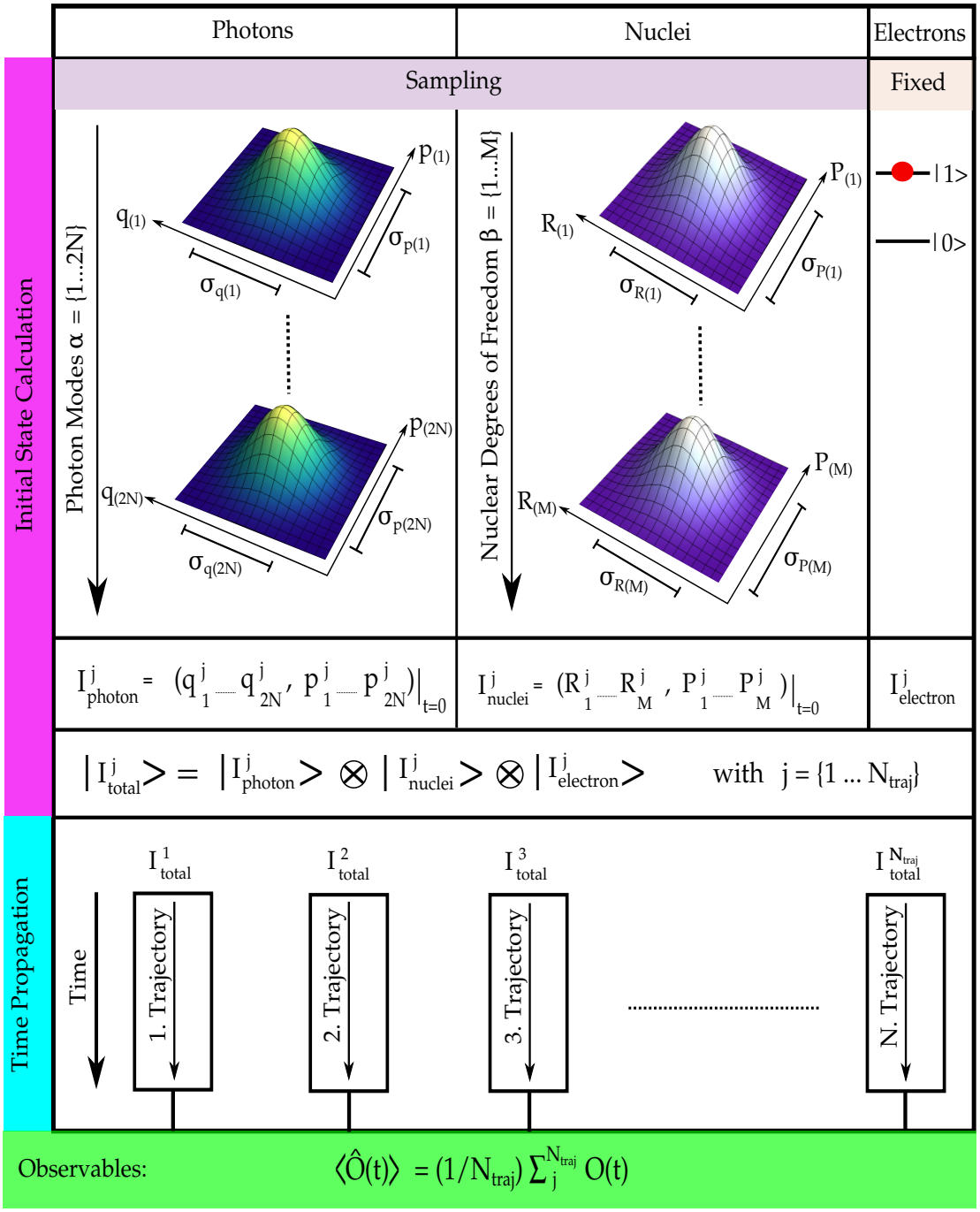

Figure 7: Overview of the numerical implementation of the MQC dynamics for the full electron-nuclei-photon correlated system with a quantum-classical-classical treatment, respectively. The upper panels (magenta) show the initial state calculation, i.e. Wigner sampling for the photons and nuclei and the choice of an excited electronic state. Then, the evolution of each initial condition is performed independently according to the applied electron-photon-nuclei correlated equations of motion (cyan) of Eqs. (62), (63), (64). The average values of an arbitrary observable $\hat{O}$ are constructed by summation over the entire trajectory ensemble and normalizing the result with respect to the total number of trajectories N_{traj} (green), see also Eq. (68).

and the off-diagonal matrix elements given as

$$\begin{aligned} h_{kl} =& i\left(\frac{P^j}{M} d_{kl}(R^j)\right) - \sum_\alpha \omega_\alpha \lambda_\alpha q_\alpha^j r_{kl}(R^j) \\ &+ \frac{1}{2}\sum_\alpha \lambda_\alpha^2 \cdot \left(-2ZR^j r_{kl}(R^j) + r_{kl}^{(2)}(R)\right) \end{aligned} \tag{66}$$

$$\begin{aligned} h_{lk} =& -i\left(\frac{P^j}{M} d_{lk}(R^j)\right) - \sum_\alpha \omega_\alpha \lambda_\alpha q_\alpha^j r_{lk}(R^j) \\ &+ \frac{1}{2}\sum_\alpha \lambda_\alpha^2 \cdot \left(-2ZR^j r_{lk}(R^j) + r_{lk}^{(2)}(R^j)\right). \end{aligned} \tag{67}$$

Eqs. (62), (63), (64) give the equations of motion for the photons, nuclei and electrons respectively. Furthermore, $d_{kl}(R) = \langle \Phi_{R,k}^{BO} | \partial_R \Phi_{R,l}^{BO} \rangle$ denotes the nonadiabatic coupling term and $r_{kl}^{(n)} = \langle \Phi_{R,k}^{BO} | r^n | \Phi_{R,l}^{BO} \rangle$ the electronic transition dipole moment. The coefficients $C_k(t)$ are the expansion coefficients of the electronic wavefunction in the BO basis. Finally, we construct the average values of an arbitrary observable $\hat{O}$ by summation over the entire trajectory ensemble and normalizing the result with respect to the total number of trajectories in the ensemble N_{traj}

$$\langle \hat{O}(t) \rangle = \frac{1}{N_{traj}} \sum_j^{N_{traj}} O^j(t). \tag{68}$$

1.3 TIME-DEPENDENT POTENTIAL ENERGY SURFACE

We now move to the concept of TDPES within the EF approach and its extension to the photonic degrees of freedom. The concepts of PES and, even more so, TDPES allow to obtain an intuitive understanding of both adiabatic and nonadiabatic molecular dynamics. Furthermore, besides corroborating the analysis of the results found within the MQC methods, they also provide a rigorous starting point for new approximate MQC methods. Again, with the intention not to exceed the scope of this introduction, we do not elaborate on the traditional electron-nuclei EF approach in detail. For more information and technical background we refer the interested reader to [35, 36, 109–112]. Furthermore, more details on the derivation of the equations in light-matter systems can also be found in Secs. 2.2 and 3.1.

1.3.1 *Traditional Exact Factorization Approach*

In general, the dynamics of coupled systems is given by the solution of the time-dependent Schrödinger equation, where the full wavefunction contains the complete information of the coupled system. On the one hand, this high-dimensional wavefunction is very difficult to interpret intuitively and, on the other hand,

in many cases only one of the subsystems is of interest. For electron-nuclear correlated systems a popular approximation to investigate and understand subsystems is the BO approximation. However, as this approximation assumes that the electronic system remains always in the instantaneous eigenstate associated with the nuclear configuration, it misses the physics associated with nonadiabatic effects, including wavepacket branching and decoherence. One approach that overcomes these caveats is the EF approach (alternatively this could also be approached via the conditional wavefunction approach [113]). Although the form of the EF approach is similar to the BO approximation, EF includes all these effects exactly in the coupling terms. More precisely, the EF approach may be viewed as a reformulation of the quantum mechanics of interacting coupled systems, where the full molecular wavefunction (electronic and ionic) can be factorized as

$$\Psi(\mathbf{r}, \mathbf{R}, t) = \chi(\mathbf{R}, t)\Phi_{\mathbf{R}}(\mathbf{r}, t) \tag{69}$$

and $\chi(\mathbf{R}, t)$ characterizes the marginal amplitude and $\Phi_{\mathbf{R}}(\mathbf{r}, t)$ the conditional amplitude [35, 36, 109, 110]. This factorization is unique, provided that $\Phi_{\mathbf{R}}$ satisfies the Partial Normalization Condition (PNC) $\int d\mathbf{r}|\Phi_{\mathbf{R}}(\mathbf{r}, t)|^2 = 1$, up to a gauge-like transformation. The equation for the nuclear amplitude χ has a time-dependent Schödinger-like form [35, 36, 111, 112] with a time-dependent vector potential and a time-dependent scalar potential, which include all effects of coupling to the electronic system and external fields. The latter potential plays an analogous role as the BO-PES, but now time-dependent and exact, and is denoted as TDPES.

More precisely, in the absence of a time dependent external field the electron-nuclear Hamiltonian can be written as [89]

$$\hat{H} = \hat{H}_{BO}(\mathbf{r}, \mathbf{R}) + \hat{T}_n(\mathbf{R}), \tag{70}$$

where $\mathbf{R}$ and $\mathbf{r}$ denote the nuclear and electronic coordinates, respectively, $\hat{H}_{BO}(\mathbf{r}, \mathbf{R})$ characterizes the traditional BO electronic Hamiltonian and $T_n(\mathbf{R})$ the nuclear kinetic energy. Furthermore, the exact electronic wave function satisfies

$$\left(\hat{H}_{el} - \epsilon(\mathbf{R}, t)\right) \Phi_{\mathbf{R}}(\mathbf{r}, t) = i\partial_t \Phi_{\mathbf{R}}(\mathbf{r}, t), \tag{71}$$

where the electronic Hamiltonian is given by

$$\hat{H}_{el}(\mathbf{r}, \mathbf{R}, t) = \hat{H}_{BO}(\mathbf{r}, \mathbf{R}) + \hat{U}_{en}[\Phi_{\mathbf{R}}, \chi], \tag{72}$$

with

$$\begin{aligned}\hat{U}_{en}[\Phi_{\mathbf{R}}, \chi] = \sum_{\nu=1}^{N_n} \frac{1}{M_\nu} \Bigg[&\frac{(-i\nabla_\nu - \mathbf{A}_\nu(\mathbf{R}, t))^2}{2} \\ &+ \left(\frac{-i\nabla_\nu \chi(\mathbf{R}, t)}{\chi(\mathbf{R}, t)} + \mathbf{A}_\nu(\mathbf{R}, t)\right) (-i\nabla_\nu - \mathbf{A}_\nu(\mathbf{R}, t)) \Bigg].\end{aligned} \tag{73}$$

Here, M_ν denotes the nuclear mass, N_n the number of nuclei accounted for in the system and $\mathbf{A}_\nu(\mathbf{R},t)$ the vector potential. The time evolution of the nuclear wave function is governed by the Schrödinger equation

$$\left(\sum_{\nu=1}^{N_n}\frac{(-i\nabla_\nu+\mathbf{A}_\nu(\mathbf{R},t))^2}{2M_\nu}+\epsilon(\mathbf{R},t)\right)\chi(\mathbf{R},t)=i\partial_t\chi(\mathbf{R},t), \tag{74}$$

where $\epsilon(\mathbf{R},t)$ now defines the TDPES given by

$$\epsilon(\mathbf{R},t)=\langle\Phi_{\mathbf{R}}(t)|\,\hat{H}_{el}(\mathbf{r},\mathbf{R},t)-i\partial_t\,|\Phi_{\mathbf{R}}(t)\rangle_{\mathbf{r}} \tag{75}$$

and the vector potential given as

$$\mathbf{A}_\nu(\mathbf{R},t)=\langle\Phi_{\mathbf{R}}(t)|-i\nabla_\nu\,|\Phi_{\mathbf{R}}(t)\rangle_{\mathbf{r}}\,. \tag{76}$$

The factorization in Eq. (69) is unique up to a gauge-like transformation, provided the PNC is satisfied. More precisely, Eqs. (71), (74–76) are form-invariant under phase transformation

$$\Phi_{\mathbf{R}}(\mathbf{r},t)=e^{i\Theta(\mathbf{R},t)}\Phi_{\mathbf{R}}(\mathbf{r},t), \tag{77}$$
$$\chi_{\mathbf{R}}(\mathbf{r},t)=e^{-i\Theta(\mathbf{R},t)}\chi_{\mathbf{R}}(\mathbf{r},t), \tag{78}$$

with the potentials undergoing a gauge-like transformation

$$\mathbf{A}_\nu(\mathbf{R},t)=\mathbf{A}_\nu(\mathbf{R},t)+\nabla_\nu\Theta(\mathbf{R},t), \tag{79}$$
$$\epsilon_\nu(\mathbf{R},t)=\epsilon_\nu(\mathbf{R},t)+\partial_t\Theta(\mathbf{R},t). \tag{80}$$

In practice, to calculate the TDPES, we have to perform an inversion [36] by first solving the time-dependent Schrödinger equation $\Psi(\mathbf{r},\mathbf{R},t)$ on a grid and then extract

$$\chi(\mathbf{R},t)=|\chi(\mathbf{R},t)|e^{iS(\mathbf{R},t)}, \tag{81}$$

by using the relation

$$|\chi(\mathbf{R},t)|=\sqrt{\int d\mathbf{r}|\Psi(\mathbf{R},\mathbf{r},t)|^2}, \tag{82}$$

and

$$S(\mathbf{R},t)=\int^{R}\left(\frac{\mathrm{Im}\int d\mathbf{r}\Psi(\mathbf{r},\mathbf{R}',t)\frac{d\Psi(\mathbf{r},\mathbf{R}',t)}{d\mathbf{R}'}}{|\chi(\mathbf{R}',t)|^2}\right)d\mathbf{R}'. \tag{83}$$

After inserting Eq. (81) in

$$\Phi_{\mathbf{R}}(\mathbf{r},t)=\frac{\Psi(\mathbf{r},\mathbf{R},t)}{\chi(\mathbf{R},t)}, \tag{84}$$

we obtain the final TDPES from combining Eq. (84) and Eq. (75).

It is important to note that, in contrast to the BO approximation, there is no assumption on different timescales in the EF approach and therefore neither in the calculation of the TDPES. This makes it particularly appealing for systems that include photonic degrees of freedom as, for example, the assumption that photons are slower than electrons is invalid. Therefore, now considering the full matter-photon system involving electrons, photons and nuclei, there are three possibilities for such a factorization and we expect each to be useful in different contexts. The derivation of the TDPES for these matter-photon coupled systems proceeds quite analogously to [35, 36, 111] and the following section shows these factorization and their corresponding TDPES.

1.3.2 *Exact Factorization Approach for Photons in Cavities*

The first factorization possibility, explored in detail in Sec. 2.2, chooses the photonic system as the marginal, such that:

$$\Psi(\mathbf{q}, \mathbf{r}, \mathbf{R}, t) = \chi(\mathbf{q}, t)\Phi_{\mathbf{q}}(\mathbf{r}, \mathbf{R}, t). \tag{85}$$

This yields a time-dependent Schrödinger equation for the photonic system with the PNC $\int d\mathbf{r}d\mathbf{R}|\Phi_{\mathbf{q}}(\mathbf{r}, \mathbf{R}, t)|^2 = 1$ for each field-coordinate $\mathbf{q}$ and all times t. Within this factorization form, the scalar potential and vector potential contain the feedback of the matter-system on the photonic field. In free space, the potential acting on the photons is quadratic, as follows from the free photon field Hamiltonian in Eq. (29). However, in the presence of matter, the potential determining the photonic state deviates from its harmonic form due to interactions with the matter. This deviation was also introduced and demonstrated within the cavity-BO approximation [82] and the Born-Huang expansion [114]. However, the EF now renders this concept exact, time-dependent, and beyond any adiabatic assumptions.

Considering the full matter-photon Hamiltonian, we can define

$$\hat{H}_m(\mathbf{r}, \mathbf{R}, \mathbf{q}, t) = \hat{H}_{qBO}(\mathbf{r}, \mathbf{R}, \mathbf{q}) + \hat{U}_{ep}[\Phi_{\mathbf{q}}, \chi], \tag{86}$$

where additionally to the nuclear and electronic coordinates $\mathbf{q}$ denotes the photonic displacement coordinates. Furthermore, H_{qBO} characterizes the BO Hamiltonian for the photonic system defined as

$$\hat{H}_{qBO} = \hat{H}_e + \hat{H}_n + \hat{H}_{en} + \hat{H}_{pen} + \hat{H}_{ep} + \hat{H}_{np} + \frac{1}{2}\sum_{\alpha=1}^{2N_p} \omega_\alpha \hat{q}_\alpha^2 \tag{87}$$

and $\hat{U}_{en}$ is given as

$$\hat{U}_{en}[\Phi_{\mathbf{q}}, \chi] = \sum_{\alpha=1}^{2N_p} \Bigg[\frac{(-i\partial_{\mathbf{q}_\alpha} - \mathbf{A}_\alpha(\mathbf{q}, t))^2}{2} + \left(\frac{-i\partial_\alpha \chi(\mathbf{q}, t)}{\chi(\mathbf{q}, t)} + \mathbf{A}_\alpha(\mathbf{q}, t) \right) (-i\partial_\alpha - \mathbf{A}_\alpha(\mathbf{q}, t)) \Bigg]. \tag{88}$$

In analogy to the traditional EF we obtain the factorization equations

$$\left(\hat{H}_m - \epsilon(\mathbf{q}, t)\right) \Phi_{\mathbf{q}}(\mathbf{r}, \mathbf{R}, t) = i\partial_t \Phi_{\mathbf{q}}(\mathbf{r}, \mathbf{R}, t), \tag{89}$$

and

$$\left(\sum_{\alpha=1}^{2N_p} \frac{(-i\partial_{\mathbf{q}_\alpha} + \mathbf{A}_\alpha(\mathbf{q}, t))^2}{2} + \epsilon(\mathbf{q}, t) \right) \chi(\mathbf{q}, t) = i\partial_t \chi(\mathbf{q}, t), \tag{90}$$

with the TDPES given as

$$\epsilon(\mathbf{q}, t) = \left\langle \Phi_{\mathbf{q}}(t) \right| \hat{H}_m(\mathbf{q}, \mathbf{r}, \mathbf{R}, t) - i\partial_t \left| \Phi_{\mathbf{q}}(t) \right\rangle_{\mathbf{r},\mathbf{R}}, \tag{91}$$

and the vector potential defined by

$$\mathbf{A}_\alpha(\mathbf{q}, t) = \left\langle \Phi_{\mathbf{q}}(t) \right| - i\partial_{\mathbf{q}_\alpha} \left| \Phi_{\mathbf{q}}(t) \right\rangle_{\mathbf{r},\mathbf{R}}. \tag{92}$$

Further, in analogy to Eqs. (77–80), Eqs. (89–92) are also form-invariant under phase transform with the potentials undergoing the gauge-like transformation. However, in contrast to the traditional EF approach $\chi(\mathbf{q}, t)$ now characterizes the displacement field density and reproduces the full wave function with the relation given by

$$|\chi(\mathbf{q}, t)| = \sqrt{\int d\mathbf{r} d\mathbf{R} |\Psi(\mathbf{q}, \mathbf{r}, \mathbf{R}, t)|^2}. \tag{93}$$

Therefore, observables associated with the multiplication of $\mathbf{q}$, e.g. the electric field, can be directly calculated from $\chi(\mathbf{q}, t)$ such that

$$\mathbf{E}(\mathbf{r}, t) = \sum_\alpha \omega_\alpha \boldsymbol{\lambda}_\alpha(\mathbf{r}, t) \int d\mathbf{q} q_\alpha |\chi(\mathbf{q}, t)|^2. \tag{94}$$

Finally, the TDPES for the photonic degrees of freedom can be obtained analogously to the inversion process introduced for traditional EF. In particular, con-

sidering the one-dimensional two-level system investigated in Sec. 2.2 within the introduced EF approach for photons, the TDPES takes the form

$$\epsilon(q,t) = \epsilon_{BO}(q,t) + \epsilon_{kin}(q,t) + \epsilon_{GD}(q,t) \tag{95}$$

$$\epsilon_{qBO}(q,t) = \langle \Phi_q(t)| \hat{H}_{qBO}(q,r,t) |\Phi_q(t)\rangle_r \tag{96}$$

$$\epsilon_{kin}(q,t) = \langle \Phi_q(t)| \sum_{\alpha}^{2N_p} \frac{\partial_\alpha^2}{2} |\Phi_q(t)\rangle_r \tag{97}$$

$$\epsilon_{GD}(q,t) = \langle \Phi_q(t)| -i\partial_t |\Phi_q(t)\rangle_r , \tag{98}$$

where the total TDPES $\epsilon(q,t)$ is decomposed into the weighted photonic BO (qBO), kinetic (kin), and gauge-dependent (GD) components. Note, that in general there is also a vector potential acting on the photons, which needs to be considered. However, as for all calculations within the EF approach we consider the one-dimensional nature of each photon-displacement mode, the vector potential can be chosen to be zero. In other words, one can always transform to a gauge in which the TDPES is the only potential driving the photonic dynamics.

1.3.3 *Exact Factorization Approach for Nuclei in Cavities*

Another possibility, which is perhaps the most natural extension of the traditional exact factorization is explored in detail in Sec. 3.1. Here the nuclear system is chosen as marginal and the photons are included in in the conditional amplitude, such that

$$\Psi(\mathbf{q},\mathbf{r},\mathbf{R},t) = \chi(\mathbf{R},t)\Phi_{\mathbf{R}}(\mathbf{q},\mathbf{r},t). \tag{99}$$

Here the PNC $\int d\mathbf{q}d\mathbf{r}|\Phi_{\mathbf{R}}(\mathbf{q},\mathbf{r},t)|^2 = 1$ for every nuclear configuration $\mathbf{R}$ at each time t. This, again, yields a time-dependent Schrödinger equation for the nuclear system. The time-dependent vector and scalar potential now include the effects on the nuclei of coupling both to the electrons and photons. This factorization is particularly useful for studying light-induced nonadiabatic chemical dynamics phenomena, when the quantum nature of light is expected to play a role, e.g cavity-induced suppression of proton-coupled electron-transfer. This phenomena was already introduced by an approximation based on the normal BO approximation for the electron-ion dynamics in the strong coupling regime [115]. However, again, the EF approach now renders this concept exact, time-dependent and beyond any adiabatic assumptions.

Note that due to the similarity of the equations of this EF approach and the traditional EF approach, we only discuss the most essential equations here. Considering the full matter-photon Hamiltonian, with the nuclear system being the marginal, the factorization equations are

$$\left(\hat{H}_{BO} + \hat{H}_p + \hat{V}_{pm} + \hat{V}_{sp} + \hat{U}_{ep-n} - \epsilon(\mathbf{R},t)\right)\Phi_{\mathbf{R}}(\mathbf{r},\mathbf{q},t) = i\partial_t\Phi_{\mathbf{R}}(\mathbf{r},\mathbf{q},t), \tag{100}$$

where $\hat{H}_{BO}$ denotes the BO Hamiltonian, $\hat{H}_p$ the free photonic field, $\hat{V}_{pm}$ the matter-photon interaction and $\hat{V}_{sp}$ the self-polarization. For the coupling to a single photon mode the equation for $\chi(\mathbf{R}, t)$ and U_{ep-n} take the same form as in Eq. (74) and Eq. (73), respectively, with the vector potential now given as

$$\mathbf{A}_\nu(\mathbf{R}, t) = \langle \Phi_{\mathbf{R}}(t)| - i\nabla_\nu |\Phi_{\mathbf{R}}(t)\rangle_{\mathbf{r},\mathbf{q}} \,. \tag{101}$$

Finally, the TDPES is defined as

$$\epsilon(\mathbf{R}, t) = \langle \Phi_{\mathbf{R}}(t)| \hat{H}_{BO} + \hat{H}_p + \hat{V}_{pm} + \hat{V}_{sp} + \hat{U}_{ep-n} - i\partial_t |\Phi_{\mathbf{R}}(t)\rangle_{\mathbf{r},\mathbf{q}} \,, \tag{102}$$

where we obtain $\Phi_{\mathbf{R}}(t)$ by inversion. Specifically, considering the Shin-Metiu minimal model coupled to a single photon mode, studied in detail in Sec. 3.1, the TDPES takes the form

$$\epsilon(R, t) = \epsilon_{wpol}(R, t) + \epsilon_{kin}(R, t) + \epsilon_{GD}(R, t) \tag{103}$$

$$\epsilon_{wpol}(R, t) = \langle \Phi_R(t)|\hat{H}_{BO} + \hat{H}_p + \hat{V}_{pm}|\Phi_R(t)\rangle_{r,q} \tag{104}$$

$$\epsilon_{kin}(R, t) = \frac{1}{2M}\langle \Phi_R(t)| - \nabla_R^2 \Phi_R(t)\rangle_{r,q} \tag{105}$$

$$\epsilon_{GD}(R, t) = \langle \Phi_R(t)| - i\partial_t \Phi_R(t)\rangle_{r,q}, \tag{106}$$

where the total TDPES $\epsilon(R, t)$ is considered against the backdrop of polaritonic surfaces and, thus, is decomposed into the weighted polaritonic (wpol), kinetic (kin), and gauge-dependent (GD) components.

Furthermore, we note that there is also a third factorization possibility, which is the natural extension of the reverse factorization [116], where the electronic system is the marginal amplitude and yields a TDPES for the electrons. Although not discussed within this work, this factorization could be particularly interesting for studying, for example, the impact of vacuum field on electrical conductivity in a molecule or semiconductor.

1.4 CONNECTING THE WORK OF THIS THESIS

This section outlines the findings of the scientific contributions comprising this thesis and connects them to each other. Fig. 8 sketches the connection and main messages of the research and its outlook. For clarity, let us first, briefly, reiterate the main motivation of our work:

1. Rapid experimental and theoretical advances have drawn attention to fascinating phenomena of quantized light fields interacting with matter, opening up a new field of research.

2. The investigation of physical effects in this field, however, involves multiple degrees of freedom such as systems with multi-molecules or multi-photon modes accounted for. Therefore, approximate methods (ideally *ab initio*) to solve the Schrödinger equation are required. We explore and extend the concept of MQC methods for photons in detail, which, due to their simplic-

ity, efficiency, and, especially, scalability, presents an interesting alternative or extension to existing quantum theory approximations. Specifically, as the trajectories are not coupled during their time evolution, the corresponding algorithms can be implemented in a highly parallel manner to reduce the total run-time.

3. In order to further analyze the results found within the MQC framework more fundamentally and also to set a starting point for the development of potential new MQC methods, we extend and explore the EF approach for the investigated systems. Although being similar to the BO approach, it allows to study the exact TDPES beyond any adiabatic and timescale assumptions, which is particularly useful for systems that include explicit photonic degrees of freedom.

1.4.1 *Outline of Scientific Contributions*

The work presented in [O1] employs the MTEF theory, traditionally developed for electron-nuclear problems, to simulate the spontaneous emission and photon-field correlation in a model QED cavity-bound atomic system (two and three energy levels). More precisely, we analyze observables such as atomic population, photon number, photon field intensity, and two-dimensional spatial correlation functions within the one and two photon emission process. We find, by correctly accounting for the vacuum fluctuation, that this MQC method is able to qualitatively characterize the correct dynamics and, even more so, can capture quantum mechanical features such as bound photon states and second order photon correlations.

Although accurate, the MTEF dynamics do suffer from some quantitative drawbacks. However, reference [118] suggests that in cases where the free photonic field is harmonic and the coupling to the matter is treated linearly, classical Wigner dynamics should yield exact results. Looking at the electron-photon coupled Hamiltonian in Eq. (37), one might assume that this is the case. However, with the photonic field reacting onto the matter system, but also the matter system reacting back to the photon field, the seemingly linear coupling turns out to be not linear at all. This nonlinearity further implies that the true potential driving the photonic motion is, in fact, not harmonic.

Therefore, the main focus of the work presented in [O2] is the investigation of this deviation from the typically assumed harmonic potential throughout the dynamics of spontaneous emission. Here we extend and illustrate the EF formalism and its TDPES for the electron-photon coupled system. More precisely, we investigate the TDPES for a two-level system, either coupled to an infinite number of photon modes in the Wigner-Weisskopf approximation, or to a single mode, both with various coupling strengths throughout the dynamics. We find significant differences to the potential used in conventional approaches, especially for strong-couplings and, thus, can corroborate the results in found [O1].

A natural extension to [O1] is presented in [O3]. With the intention of improving the results found in [O1], we benchmark a selection of MQC methods

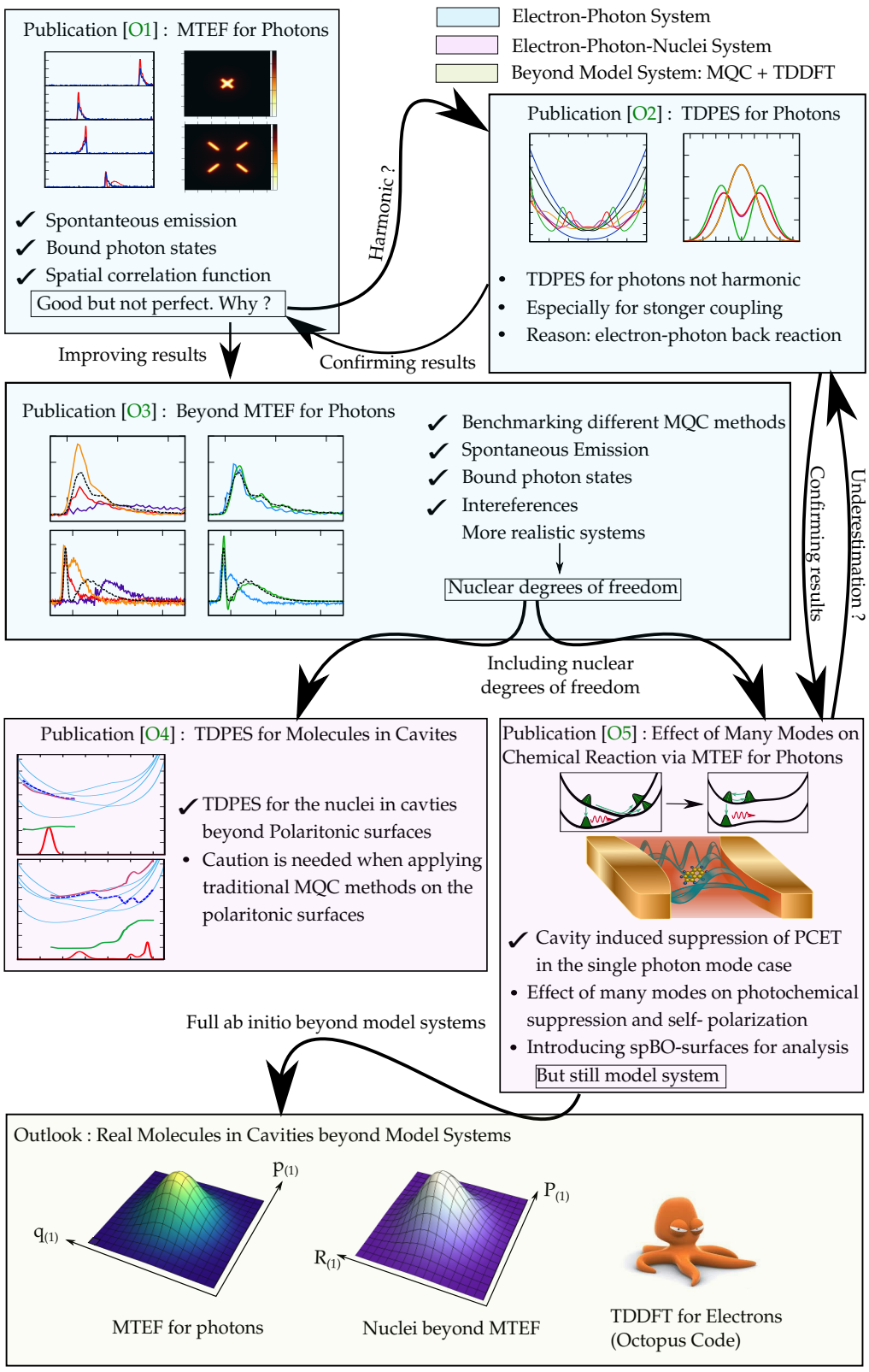

Figure 8: Connection of the different scientific contributions. The areas with blue background show the work within electron-photon correlated systems, the areas with pink background the work within electron-photon-nuclei correlated systems and the area with yellow background gives a short outlook on a possible future step such as connecting the MQC approach with an advanced TDDFT electron-structure code i.e. the open source Octopus code [117] .

and perturbative dynamics techniques. Here we investigate the same electron-photon correlated model system as in [O1] featuring spontaneous emission, interference, and strong coupling behaviour and compare the performance of different MQC methods, i.e. the fewest switches surface hopping, MTEF, linearized, and partially linearized semiclassical dynamics methods. We also investigate self-consistent perturbative methods by applying the Bogoliubov-Born-Green-Kirkwood-Yvon (BBGKY) hierarchy in the second Born approximation. We find that, with the exception of fewest switches surface hopping, all methods provide a reasonable level of accuracy for the correlated light-matter dynamics. Additionally, the path-integral methods were able to capture some level of interference effects, which were only seen as broadening of the wave packet within the MTEF method. Furthermore, the perturbative method performed exceptionally well, yet shows an exponential scaling with the degrees of freedom and therefore, in contrast to the MQC methods, is not suitable for realistic systems.

Next, we extend and investigate the EF approach and the MTEF method to the full matter-photon system (electron-photon-nuclei correlated system i.e. Shin-Metiu model [85] coupled to a cavity) to enable eventual applications to realistic systems. Here we analyze the TDPES as well as the performance of the MTEF within the effect of cavity-induced suppression of PCET.

More precisely, in the work presented in [O4] we simulate and analyze the exact TDPES driving the proton motion throughout the cavity-induced suppression of PCET. By examining the features of the TDPES in detail we find that this surface can, indeed, predict the suppression induced by the cavity. Furthermore, we observe that the pure polaritonic surfaces alone, although providing a useful backdrop, are not able to predict the dynamics. Further, we suggest that caution is needed when using polaritonic surfaces in order to perform MQC calculations, as even when their couplings are accounted for, the proliferation of avoided crossings will result in inaccuracies from over-coherence issues of usual MQC methods.

Finally, we extend the MTEF method to a full electron-photon-nuclei system. Based on [O4], we focus on the performance of MTEF within the process of cavity-induced suppression of PCET. With realistic systems in mind, but, on the other hand, requiring rigorous benchmarks of the MTEF-performance, we step-wise decrease the quantum treatment of the different components coupled to a single photon mode, i.e. full quantum treatment (quantum electron, photons, nuclei), MTEF treatment for the photons only (quantum electrons, nuclei) and MTEF treatment of both nuclei and photons (quantum electrons). In the single mode case we find that MTEF is, indeed, able to describe the suppression of PCET, but tends to underestimate these results, which we explain in detail by referring to [O2]. With the exact reference solution out of reach, we then couple the matter system to up to 440 photon modes. Here we find that, as more photon modes are included, chemical reactions can change significantly and self-polarization effects have an increasingly crucial impact on the dynamics. More precisely, we observe, that by including more photon modes a full photochemical suppression of the PCET can be induced via the self-polarization only, without changing the cou-

pling strength itself. To this end, we introduce the concept of spBO-surfaces as an instructive tool for analysis.

We conclude, that the MQC methods shown here, indeed, constitute a promising route to simulate realistic correlated quantum mechanical light-matter systems. These methods, besides enabling multi-photon mode simulations, are able to capture quantum mechanical effects, i.e. spontaneous emission, bound photon states, and photon field correlations and suppression of PCET, yet do not exhibit the exponential scaling. In particular, connecting the MQC approach to electronic structure calculations, i.e. TDDFT, in future work, provides a computational feasible *ab initio* path towards simulations of realistic correlated light-matter systems.

1.4.2 *Connecting to the State of the Art Research*

Research on quantized light fields interacting with matter is a rapidly expanding domain. Therefore, in this section we position our contribution relative to the emerging theoretical state of the art research. Here, the main difference of the approaches lies in how the photonic degrees of freedom are included in the calculations.

One possibility is to include the photonic degrees of freedom directly through the PES, which gave rise to the field of polaritonic chemistry. Here fascinating phenomena such as cavity-induced modifications of molecular structure [115], suppression of photochemical reactions [107], many-molecule reaction triggered by a single photon [119] up to new reactivities enabled by polariton photochemistry [120], and many more [108, 121–126] are found and described. However, those simulations are performed within model systems and it has been shown in recent publications [43, 71, 79, 114, 127] that such model systems, especially few-level approximations, have fundamental limitations. One prominent example is the superradiance phase transition due to the Dicke Model [128], where the physical implications of the few-level model is debated [75]. In such cases a treatment beyond model systems and towards *ab initio* calculations is required.

One promising *ab initio* route is the Quantum Electrodynamical Density Functional Theory (QEDFT) approach. Here the well known TDDFT approach is generalized to the photonic degrees of freedom, where the photons are included in the exchange-correlation functional [56, 78]. Furthermore, to extend this theory towards more realistic systems, a practical exchange-correlation functional [79], and an extension to the nuclear motion (by including a single Ehrenfest trajectory) [129], was recently introduced. However, the accuracy and scalability of this method solely depends on the choice of the exchange-correlation functional and, thus, can exhibit a wide range of problems [130, 131]. Therefore, obtaining a rigorous functional is analytically and numerically by far not a trivial task.

Therefore, due to the simplicity, efficiency, and especially scalability the extension of MQC methods to the photonic degrees of freedom is an interesting alternative or extension to approaches like QEDFT or polaritonic chemistry. In particular, combining the introduced MQC approach with an existing *ab initio* electronic structure method, such as TDDFT, could provide a computationally feasible way to simulate photon-field fluctuations and correlations in realistic

three-dimensional systems. Within this framework, besides the work presented in this thesis, an adjusted Ehrenfest theory based method was developed to investigate light-matter interactions. This method, by construction, can recover spontaneous emission, while also distinguishing between electromagnetic fluctuations and coherent emission [132–134]. However, besides being *ad-hoc*, this approach focuses on the interaction with classical light while our work targets quantized light fields.

REMARK First successful applications based on our Wigner approach for photons were just recently published in [135], where the Meyer-Miller-Stock-Thoss dynamics [20, 136] is applied in order to investigate superradiance and subradiance.[1]

1 Note that [135] only includes one-photon states in the exact reference simulation and therefore does not see any appearance of the polariton peak at the atomic position. However, in our simulations of this model, we have found that this peak appears due to contributions from two-photon states in the full configuration interaction expansion of the system and cavity field wavefunction (details about this can be found in Fig. 6 of [O3]). This error has been acknowledged by the authors of [135] and will be corrected in future versions of their paper.

Part II

SCIENTIFIC CONTRIBUTION

2

ELECTRON-PHOTON CORRELATED SYSTEMS

2.1 MULTI-TRAJECTORY EHRENFEST FOR PHOTONS

"Capturing Vacuum Fluctuations and Photon Correlations in Cavity Quantum Electrodynamics with Multitrajectory Ehrenfest dynamics"

NM Hoffmann, C Schäfer, A Rubio, A Kelly, H Appel

Physical Review A (2019), 99 (6), 063819

MOTIVATION Profound changes in the physical and chemical properties of material systems can be found in situations where the quantum nature of light plays an important role in the interaction with the system [67–69]. These exciting developments have been strongly driven by experimental efforts, thus exposing the immediate need for the development and improvement of theoretical approaches, especially beyond model systems [71, 79, 114, 127], that can bridge the gap between quantum optics and quantum chemistry [75]. Due to the similarity of the electron-photon and the electron-nuclear problems, simulation methods that have traditionally been of use in the quantum chemistry community, such as semiclassical and MQC methods, offer a potentially interesting avenue to bridge this gap. In particular, these techniques typically do not exhibit the pernicious exponential scaling of computational effort inherent in grid-based quantum calculations [136].

STATE OF THE ART One promising route beyond model systems towards *ab initio* calculations is the QEDFT approach. However, the accuracy and scalability of this method solely depends on the choice of the exchange-correlation functional and, thus, can exhibit a wide range of problems [130, 131] and obtaining a rigorous functional is analytically and numerically by far not a trivial task. Therefore, due to the simplicity, efficiency, and especially scalability the extension of MQC methods to the photonic degrees of freedom is an interesting alternative or extension to approaches like QEDFT. Available techniques in the family of exact and approximate MQC approaches (for nuclear-electron systems) are MTEF dynamics [15, 17–19], fully linearized and partially linearized path-integral methods, forward-backward trajectory methods [20–27], and trajectory surface-hopping algorithms [29–34]. All these techniques have some ability to describe essential quantum mechanical effects such as tunneling, interference, and zero-point energy conservation. Recently, an adjusted Ehrenfest theory-based method [132–134] was used to simulate the spontaneous emission of classical light. How-

ever, in contrast to these works, we target the description of quantized light fields.

CONTRIBUTION AND MAIN FINDINGS In the present work, we focus on the Ehrenfest mean-field approach and employ the MTEF implementation, traditionally developed for electron-nuclear problems, to simulate the spontaneous emission of radiation in a model quantum electrodynamical cavity-bound atomic system. More precisely, by properly accounting for the quantum statistics of the vacuum field i.e. employing the Wigner transform for photons, while using MQC (mean-field) trajectories to describe the evolution. We investigate the performance of this approach in capturing the dynamics of spontaneous emission from the perspective of both the atomic system and the cavity photon field through a detailed comparison with exact benchmark quantum mechanical observables and correlation functions. We find that MTEF dynamics are able to qualitatively characterize the correct dynamics for one-and two-photon spontaneous-emission processes in a QED cavity. However, MTEF dynamics does suffer from some quantitative drawbacks. Furthermore, we also observed that MTEF dynamics simulations can, in fact, capture quantum mechanical features such as bound polariton states and second-order photon correlations.

OUTLOOK Trajectory-based quantum classical algorithms emerge as a promising route towards treating more complex and realistic systems. In particular, as the equations of motion for the photonic system presented in this work can be seen as a one-dimensional Maxwell's equation, one possible route to extend the MTEF approach to realistic systems is the combination of our multi-trajectory approach with the recently presented work in [51]. This work presents an *ab initio* light-matter coupling methodology, which treats coupled classical light, electrons, and nuclei by solving the Ehrenfest-Maxwell-Pauli-Kohn-Sham equations in quantum electrodynamics and is ideally suited for applications in nano-optics and nanoplasmonics. Therefore, combining the MTEF approach with the methodology of [51] provides a computationally feasible way to simulate photon-field fluctuations and correlations in realistic three-dimensional systems.

However, before extending the MTEF to realistic systems, we first need to answer the following question:

(i) Why does the MTEF approach suffer from qualitative drawbacks and what are their causes? Investigated in [O2].

(ii) Can we improve the results found within the MTEF by using more advanced methods? Investigated in [O3].

(iii) In order to approach more realistic systems, how can we include the nuclei degrees of freedom into the MTEF approach for photons? Investigated in [O5].

PHYSICAL REVIEW A **99**, 063819 (2019)

Capturing vacuum fluctuations and photon correlations in cavity quantum electrodynamics with multitrajectory Ehrenfest dynamics

Norah M. Hoffmann,[1] Christian Schäfer,[1] Angel Rubio,[1,2] Aaron Kelly,[1,3,*] and Heiko Appel[1,†]

[1]*Max Planck Institute for the Structure and Dynamics of Matter and Center for Free-Electron Laser Science, 22761 Hamburg, Germany*

[2]*Center for Computational Quantum Physics (CCQ), Flatiron Institute, 162 Fifth Avenue, New York, New York 10010, USA*

[3]*Department of Chemistry, Dalhousie University, Halifax, Canada B3H 4R2*

(Received 29 January 2019; published 17 June 2019)

We describe vacuum fluctuations and photon-field correlations in interacting quantum mechanical light-matter systems by generalizing the application of mixed quantum classical dynamics techniques. We employ the multitrajectory implementation of Ehrenfest mean-field theory, traditionally developed for electron-nuclear problems, to simulate the spontaneous emission of radiation in a model quantum electrodynamical cavity-bound atomic system. We investigate the performance of this approach in capturing the dynamics of spontaneous emission from the perspective of both the atomic system and the cavity photon field through a detailed comparison with exact benchmark quantum mechanical observables and correlation functions. By properly accounting for the quantum statistics of the vacuum field, while using mixed quantum classical (mean-field) trajectories to describe the evolution, we identify a surprisingly accurate and promising route towards describing quantum effects in realistic correlated light-matter systems.

DOI: 10.1103/PhysRevA.99.063819

I. INTRODUCTION

Profound changes in the physical and chemical properties of material systems can be produced in situations where the quantum nature of light plays an important role in the interaction with the system [1–3]. A few notable recent examples of such effects are few-photon coherent nonlinear optics with single molecules [4], direct experimental sampling of electric-field vacuum fluctuations [5,6], multiple Rabi splittings under ultrastrong vibrational coupling [7], exciton-polariton condensates [8,9], and frustrated polaritons [10]. These exciting developments have been strongly driven by experimental efforts, thus exposing the immediate need for the development and improvement of theoretical approaches that can bridge the gap between quantum optics and quantum chemistry [11].

Due to the similarity of the electron-photon and the electron-nuclear problems, simulation methods that have traditionally been of use in the quantum chemistry community, such as semiclassical and mixed quantum classical methods, offer a potentially interesting avenue to bridge this gap. In particular, the family of trajectory-based quantum classical methods has the advantage of providing a very intuitive, qualitative understanding of nonadiabatic molecular dynamics. Further, these techniques typically do not exhibit the pernicious exponential scaling of computational effort inherent in grid-based quantum calculations [12]. Available techniques in this family of exact and approximate approaches are Ehrenfest mean-field dynamics, fully linearized and partially linearized path-integral methods, forward-backward trajectory methods [13–15], and trajectory surface-hopping algorithms [16]. All these techniques have some ability to describe essential quantum mechanical effects such as tunneling, interference, and zero-point energy conservation.

Recently, Subotnik and co-workers performed investigations of light-matter interactions where an adjusted Ehrenfest-theory-based method was used to simulate the spontaneous emission of classical light [17–19]. Here, in contrast with these works, we focus on the description of quantized light fields. We then generalize the well-established multitrajectory Ehrenfest method to treat quantum mechanical light-matter interactions. We highlight the possibilities and theoretical challenges of this method in comparison to the exact treatment of the quantum system by applying this approach to investigate spontaneous emission for a model atom in an optical cavity. Furthermore we point out that in contrast to many previous studies of atomic processes in quantum electrodynamical (QED) cavities that use an open quantum systems approach [20–22], in this work we treat the cavity bound atomic system as a closed quantum system where all the degrees of freedom of the atom and the cavity field are treated explicitly.

The remainder of this work is divided into three sections: in Sec. II, we briefly review general interacting light-matter systems and the multitrajectory Ehrenfest dynamics method. In this framework, we then introduce a one-dimensional (1D) model system comprising a single (two- or three-level) atomic system coupled to a multimode QED cavity. In Sec. III, we investigate the performance of multitrajectory Ehrenfest (MTEF) dynamics in describing the process of spontaneous emission. We conclude our results in Sec. IV and discuss some prospects for future work.

*aaron.kelly@dal.ca

†heiko.appel@mpsd.mpg.de

II. THEORY

A. Quantum mechanical light-matter interactions

To begin, we describe a general coupled field-matter system using Coulomb gauge and the dipole approximation [23,24]. The total Hamiltonian for the system is [25–29]

$$\hat{H} = \hat{H}_A + \hat{H}_F + \hat{H}_{AF}. \tag{1}$$

The first term $\hat{H}_A$ is the atomic Hamiltonian, which may be generally expressed in the spectral representation,

$$\hat{H}_A = \sum_k \varepsilon_k |k\rangle\langle k|. \tag{2}$$

Here, $\{\varepsilon_k, |k\rangle\}$ are the atomic energies and stationary states of the atomic system in the absence of coupling to the cavity. The second term is the Hamiltonian of the uncoupled cavity field $\hat{H}_F$,

$$\hat{H}_F = \frac{1}{2}\sum_{\alpha=1}^{2N}\left(\hat{P}_\alpha^2 + \omega_\alpha^2 \hat{Q}_\alpha^2\right). \tag{3}$$

The photon-field operators $\hat{Q}_\alpha$ and $\hat{P}_\alpha$ obey the canonical commutation relation $[\hat{Q}_\alpha, \hat{P}_{\alpha'}] = \imath\hbar\delta_{\alpha,\alpha'}$, and can be expressed using creation and annihilation operators for each mode of the cavity field,

$$\hat{Q}_\alpha = \sqrt{\frac{\hbar}{2\omega_\alpha}}(\hat{a}_\alpha^\dagger + \hat{a}_\alpha), \tag{4}$$

$$\hat{P}_\alpha = i\sqrt{\frac{\hbar\omega_\alpha}{2}}(\hat{a}_\alpha^\dagger - \hat{a}_\alpha), \tag{5}$$

where $\hat{a}_\alpha^\dagger$ and $\hat{a}_\alpha$ denote the usual photon-creation and -annihilation operators for photon mode α. The coordinatelike operators $\hat{Q}_\alpha$ are directly proportional to the electric displacement operator, while the conjugate momentalike operators $\hat{P}_\alpha$ are related to the magnetic field [27,28]. The upper limit of the sum in Eq. (3) is $2N$, as there are (in principle) two independent polarization degrees of freedom for each photon mode; however, in the 1D cavity models presented here, only a single polarization will be considered.

The final term in Eq. (1) represents the coupling between the atom and the cavity field,

$$\hat{H}_{AF} = \sum_{\alpha=1}^{2N}\left[\omega_\alpha \hat{Q}_\alpha(\lambda_\alpha\cdot\hat{\mu}) + \frac{1}{2}(\lambda_\alpha\cdot\hat{\mu})^2\right], \tag{6}$$

where we denote $\hat{\mu}$ as the electronic dipole moment vector of the atomic system, and λ_α as the electron-photon coupling vector [25,28]. In the case of a two-level electronic system, the quadratic term in the atom-field coupling Hamiltonian simply results in a constant energy shift and hence has no effect on observables [30], and we neglect this term in the case of the three-level model system. Furthermore, we note that this Hamiltonian can easily be extended to include nuclear degrees of freedom; however, this has been omitted in the present work.

B. Multitrajectory Ehrenfest dynamics

In this section, we apply the well-known multitrajectory Ehrenfest method, traditionally introduced to study electron-nuclear systems [31–33], to coupled light-matter systems [24,33,34].

A particularly simple and instructive route to derive the MTEF mean-field theory is via the quantum classical Liouville (QCL) equation [35]. This equation of motion for the density matrix is formally exact for an arbitrary quantum mechanical system that is bilinearly coupled to a harmonic environment, as is the case in the atom-field Hamiltonian studied here. The QCL equation can be written in a compact form as

$$\frac{\partial}{\partial t}\hat{\rho}_W(X,t) = -i\mathcal{L}\hat{\rho}_W(X,t). \tag{7}$$

It describes the time evolution of $\hat{\rho}_W(X,t)$, which is the partial Wigner transform of the density operator taken over the photon-field coordinates, which are thus represented by continuous phase-space variables, $X = (Q,P) = (Q_1, Q_2, \ldots, Q_{2N}, P_1, P_2, \ldots, P_{2N})$. The partial Wigner transform of the density operator, $\hat{\rho}$, is defined as

$$\hat{\rho}_W(Q,P) = \frac{1}{(2\pi\hbar)^{2N}}\int dZ e^{iP\cdot Z}\left\langle Q - \frac{Z}{2}|\hat{\rho}|Q + \frac{Z}{2}\right\rangle. \tag{8}$$

The QCL operator is defined as

$$i\mathcal{L}\cdot = \frac{i}{\hbar}[\hat{H}_W, \cdot] - \frac{1}{2}(\{\hat{H}_W, \cdot\} - \{\cdot, \hat{H}_W\}), \tag{9}$$

where $\hat{H}_W$ denotes the Wigner transform of $\hat{H}$, $[\cdot,\cdot]$ is the commutator, and $\{\cdot,\cdot\}$ is the Poisson bracket in the phase space of the environmental variables.

At this point, one may arrive at MTEF equations by assuming that the total density of the system can be written as an uncorrelated product of the atomic and photonic reduced densities at all times,

$$\hat{\rho}_W(X,t) = \hat{\rho}_A(t)\rho_{F,W}(X,t), \tag{10}$$

where the reduced density matrix of the atomic system is

$$\hat{\rho}_A(t) = \mathrm{Tr}_F[\hat{\rho}(t)] = \int dX\,\hat{\rho}_W(X,t), \tag{11}$$

and the Wigner function of the cavity field is $\rho_{F,W}(X,t) = \mathrm{Tr}_A[\hat{\rho}_W(X,t)]$. If one seeks solutions to the QCL equation of this form, the Ehrenfest mean-field equations of motion for the atomic system are obtained,

$$\frac{\partial}{\partial t}\hat{\rho}_A(t) = -\frac{i}{\hbar}\left[\hat{H}_A + \hat{H}_{AF,W}(X(t)), \hat{\rho}_A(t)\right], \tag{12}$$

where $\hat{H}_{AF,W}$ denotes the Wigner transform of $\hat{H}_{AF}$. The evolution of the Wigner function of the photon field can be represented as a statistical ensemble of independent trajectories, with weights w^j,

$$\rho_{F,W}(X,t) = \sum_j^{N_{\mathrm{traj}}} w^j \delta[X - X^j(t)], \tag{13}$$

that evolve according to Hamilton's equations of motion,

$$\frac{\partial Q_\alpha}{\partial t} = \frac{\partial H_{F,W}^{Eff}}{\partial P_\alpha}, \quad \frac{\partial P_\alpha}{\partial t} = -\frac{\partial H_{F,W}^{Eff}}{\partial Q_\alpha}. \tag{14}$$

The effective photon-field Hamiltonian is

$$H_{F,W}^{Eff} = \frac{1}{2}\sum_{\alpha}\left[P_{\alpha}^{2} + \omega_{\alpha}^{2}Q_{\alpha}^{2} + 2\omega_{\alpha}\lambda_{\alpha}Q_{\alpha}\mu(t)\right], \tag{15}$$

where $\mu(t) = \mathrm{Tr}_A[\hat{\rho}_A(0)\hat{\mu}(t)]$.

The exact expression for the average value of any observable, $\langle O(t)\rangle$, can be written as

$$\langle O(t)\rangle = \mathrm{Tr}_A \int dX \hat{O}_W(X,t)\hat{\rho}_W(X,t=0). \tag{16}$$

We note here that for this class of systems, the Ehrenfest equations of motion for the photon-field coordinates correspond to a mode-resolved form of Maxwell's equations. In applying the MTEF dynamics method numerically, we use the above expressions in the following manner:

(i) We first perform Monte Carlo sampling from the Wigner transform of the initial density operator of the photon field $\hat{\rho}_{F,W}(X,0)$ to generate an ensemble of initial conditions, for the trajectory ensemble $(Q_{\alpha}^{j}(0), P_{\alpha}^{j}(0))$. In this work, we used uniform weights $w^{j} = \frac{1}{N_{\mathrm{traj}}}$; however, other importance sampling schemes could be employed as the only requirement is that the sum of the weights is normalized, $\sum_j w^j = 1$.

(ii) We evolve each initial condition independently according to the Ehrenfest equations of motion, producing a trajectory. In the following, we refer to such a solution as an ensemble of independent trajectories.

(iii) Average values are constructed by summing over the entire trajectory ensemble and normalizing the result with respect to N_{traj}, the total number of trajectories in the ensemble, $\langle O(t)\rangle = \sum_{j}^{N_{\mathrm{traj}}} \mathrm{Tr}_A[\hat{O}_W(Q^j, P^j, t)\hat{\rho}_A(0)]/N_{\mathrm{traj}}$.

Here, $\rho_{F,W}(X,0)$ is the Wigner transform of the zero-temperature vacuum state,

$$\rho_{F,W}(X,0) = \prod_{\alpha}\frac{1}{\pi}\exp\left[-\frac{P_{\alpha}^{2}}{\hbar\omega_{\alpha}} - \frac{\omega_{\alpha}Q_{\alpha}^{2}}{\hbar}\right]. \tag{17}$$

C. Observables and normal ordering

Before we proceed with a discussion of our simulation results, we must note that the Wick normal-ordered form for operators (denoted $:\hat{O}:$ for some operator $\hat{O}$) is used when calculating the average values in this study. The reason for using the normal-ordered form, in practice, is to remove the effect of vacuum fluctuations from the results, which ensures that both $\langle E\rangle = 0$ and $\langle I\rangle = 0$, irrespective of the number of photon modes in the cavity field, when the field is in the vacuum state. The effect of this operator ordering is particularly evident for the photon-number operator,

$$:\hat{N}_{pt}: = \frac{1}{2}\sum_{\alpha}\left(\frac{\hat{P}_{\alpha}^{2}}{\hbar\omega_{\alpha}} + \frac{\omega_{\alpha}\hat{Q}_{\alpha}^{2}}{\hbar} - 1\right), \tag{18}$$

where normal ordering produces a constant shift due to the zero-point energy term.

The quantized electric-field operator is defined as

$$\hat{E}(r,t) = \sum_{\alpha}\sqrt{2\omega_{\alpha}}\zeta_{\alpha}(r)\hat{Q}_{\alpha}(t), \tag{19}$$

with

$$\zeta_{\alpha}(r) = \sqrt{\frac{\hbar\omega_{\alpha}}{\epsilon_0 L}}\sin\left(\frac{\alpha\pi}{L}r\right). \tag{20}$$

The corresponding normal-ordered electric-field intensity operator is given by

$$:\hat{E}^{2}(r,t): =: \hat{I}(r,t) := 2\sum_{\alpha}\omega_{\alpha}\zeta_{\alpha}^{2}(r)\hat{Q}_{\alpha}^{2}(t) - \sum_{\alpha}\zeta_{\alpha}^{2}(r). \tag{21}$$

The effect of normal ordering on this quantity is shown in Fig. 2, where the intensity of the electric field is plotted in both its canonical and normal-ordered forms. In addition to a constant shift with respect to the normal-ordered quantity, which is identically zero, the canonical average field intensity also displays additional oscillations near the boundaries and the atomic position, corresponding to the vacuum fluctuations for this system.

We also consider the second-order correlation function for the photon field [36],

$$:g^{2}(r_1,r_2,t): = \frac{\langle:\hat{E}^{\dagger}(r_1,t)\hat{E}^{\dagger}(r_2,t)\hat{E}(r_2,t)\hat{E}(r_1,t):\rangle}{\langle:\hat{I}(r_1,t):\rangle\quad\langle:\hat{I}(r_2,t):\rangle}. \tag{22}$$

This function is frequently used in quantum optics to discriminate between classical light and nonclassical states of the photon field that exhibit photon bunching ($g^2 > 1$) or photon antibunching ($g^2 < 1$). The normal-ordered form of the numerator in g^2, also referred to as $G^2(r_1,r_2,t)$, is

$$\begin{aligned}:G^{2}(r_1,r_2,t): = {}& 4\sum_{\alpha}\omega_{\alpha}^{2}\zeta_{\alpha}(r_1)\zeta_{\alpha}(r_2)\zeta_{\alpha}(r_2)\zeta_{\alpha}(r_1)\hat{Q}_{\alpha}^{4}(t)\\ &-\sum_{\alpha\beta}\left[4\zeta_{\beta}(r_1)\zeta_{\beta}(r_2)\zeta_{\alpha}(r_1)\zeta_{\alpha}(r_2)\right.\\ &\left.+\zeta_{\beta}^{2}(r_2)\zeta_{\alpha}^{2}(r_1)+\zeta_{\beta}^{2}(r_1)\zeta_{\alpha}^{2}(r_2)\right]2\omega_{\alpha}\hat{Q}_{\alpha}^{2}(t).\end{aligned} \tag{23}$$

The partial Wigner transforms of the polynomial functions of the bath-coordinate operators are simply polynomial functions of the continuous bath coordinates, $[\hat{Q}_{\alpha}^{n}(t)]_W = [Q_{\alpha}(t)]^n$ [37]. The same is also true for the corresponding momenta and thus the average values of the preceding operators can be easily calculated using mean-field trajectories.

D. Model system

Following previous work [26,38], we investigate a model atomic system in a one-dimensional electromagnetic cavity, as depicted in Fig. 1:

$$\begin{aligned}\hat{H} = {}&\sum_{k=1}^{m}\epsilon_k|k\rangle\langle k| + \frac{1}{2}\sum_{\alpha}^{2N}\left(\hat{P}_{\alpha}^{2} + \omega_{\alpha}^{2}\hat{Q}_{\alpha}^{2}\right)\\ &+\sum_{\alpha}^{2N}\sum_{k,l=1}^{m}\mu_{kl}\omega_{\alpha}\lambda_{\alpha}(r_A)\hat{Q}_{\alpha}|k\rangle\langle l|,\end{aligned} \tag{24}$$

where the upper limit of the first and last summation m denotes the number of atomic energy levels. In the case

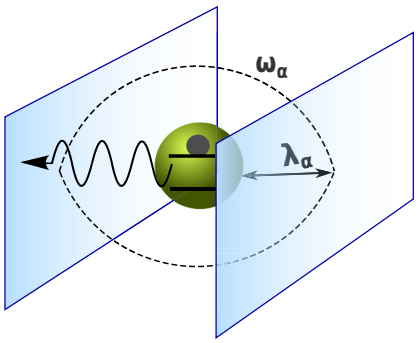

FIG. 1. Model atomic system in an electromagnetic cavity. The atom (green) is trapped between two mirrorlike surfaces of the cavity, supporting $2N$ photon modes with frequencies $\omega_\alpha = \frac{\pi c \alpha}{L}$, where $\alpha = \{1, 2, \ldots, 2N\}$ and L is the distance between the mirrors. The strength of the interactions between each mode of the cavity field and the atomic system is λ_α.

of a two-level atomic system, this corresponds to a special case of the spin-boson model. With the position of the atom fixed at $r_A = \frac{L}{2}$ in this study, half of the $2N$ cavity modes decouple from the atomic system by symmetry. We adopt the same parameters as in Refs. [26,39], which are based on a 1D hydrogen atom with a soft Coulomb potential (in atomic units): $\{\varepsilon_1, \varepsilon_2\} = \{-0.6738, -0.2798\}$, $\lambda_\alpha(\frac{L}{2}) = 0.0103(-1)^\alpha$, $L = 2.362 \times 10^5$, and $\mu_{12} = 1.034$. For the three-level atom, we adopt all the same parameters for the field and the atom-field coupling as for the two-level case. The atomic energies for the three-level model are $\{\varepsilon_1, \varepsilon_2, \varepsilon_3\} = \{-0.6738, -0.2798, -0.1547\}$ and, as before, the numerical parameters are based on the 1D soft-Coulomb hydrogen atom. The dipole moment operator only couples adjacent states, such that the only nonzero matrix elements are $\{\mu_{12}, \mu_{23}\} = \{1.034, -2.536\}$ and their conjugates.

Furthermore, with $\frac{g_{2,1}}{\epsilon_2 - \epsilon_1} = 1.2 \times 10^{-2}$ for the two-level system and $\frac{g_{3,2}}{\epsilon_3 - \epsilon_2} = 2.1 \times 10^{-2}$ for the three-level system, where $g_{i,j} = \mu_{k,l}\sqrt{\frac{\epsilon_i - \epsilon_j}{2}}\lambda$ is the coupling strength for the resonant mode, our system is beyond the weak coupling regime, specifically for the three level case. This can also be explicitly seen later in the results by the appearances of the polariton peaks in the intensity, which are strong coupling features and are beyond the description of the well-known analytic Wigner-Weisskopf solution for weak coupling.

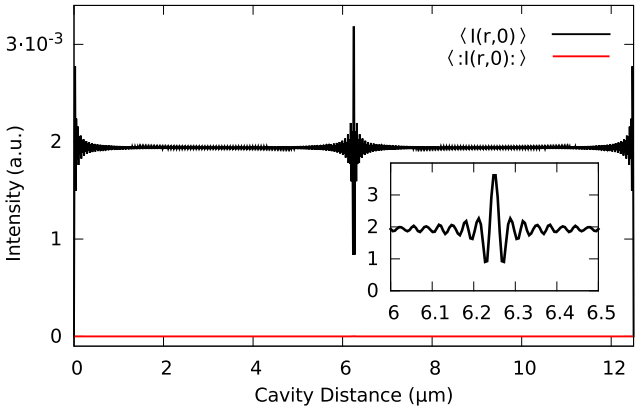

FIG. 2. Average value of the cavity electric-field intensity. Wick normal ordering has been applied to the operator in the case of the red dashed line, whereas the solid black line corresponds to the original operator. The cavity field is prepared in the vacuum state, at zero temperature.

III. RESULTS AND DISCUSSION

We now investigate the performance of the MTEF method in the context of cavity-bound spontaneous emission. In all calculations shown below, we use 400 photon modes to represent the cavity field. We choose the atom to be initially in the excited state, and the cavity field is in the vacuum state at zero temperature. In all simulations reported here, we use an ensemble of $N_{\text{traj}} = 10^4$ independent trajectories, sampled from the Wigner transform of the initial field density operator given in the previous section. This level of sampling is sufficient to converge the atomic observables to graphical accuracy; however, observables and correlations functions of the photon field would require a slightly larger trajectory ensemble for graphical convergence. All observables shown below correspond to their normal-ordered forms. For our benchmark numerical treatment, we solved the time-dependent Schrödinger equation by using a truncated configuration-interaction (CI) expansion. More precisely, the photon-field state space is truncated at two photons, whereas for the atomic system, a two- and three-state discrete variable representation is used in each case [26]. Numerical convergence is checked to ensure that the CI basis that we employ is complete for the models and parameter regimes studied in this work.

A. Two-level atom: One-photon emission process

In Fig. 3, we show the intensity of the cavity field along the axis of the cavity, at four different times. As the

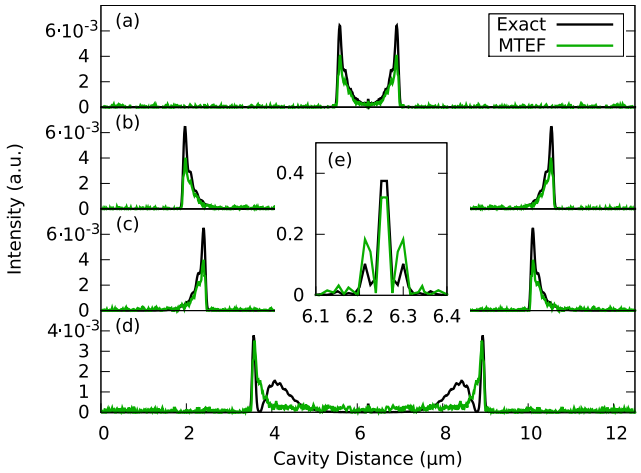

FIG. 3. Time evolution of the average field intensity for the one-photon emission process, at four different time snapshots: (a) $t = 100$, (b) $t = 600$, (c) $t = 1200$, (d) $t = 2100$ a.u. (e) Zoom-in of the polariton peak at the atomic position. Exact simulation results (black) and MTEF dynamics (green).

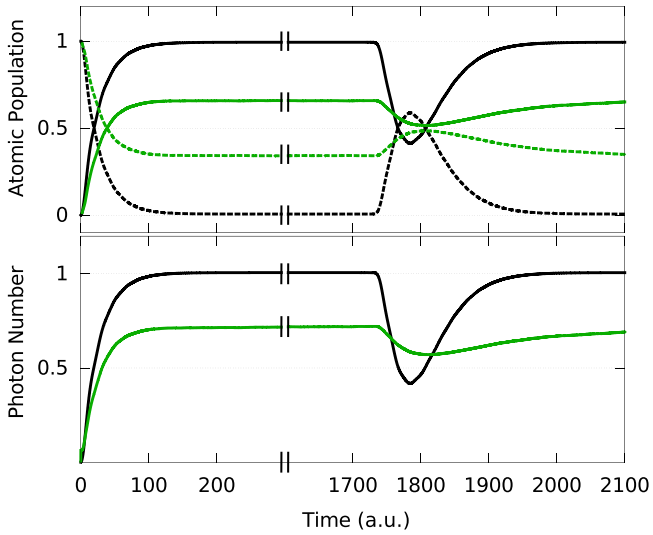

FIG. 4. Time evolution of the atomic-state populations (top panel) and the total photon number (bottom panel). Top panel: Solid lines represent the atomic ground state and dashed lines represent the excited state. Both panels: Exact simulation results (black) and MTEF (green).

spontaneous-emission process proceeds, a photon wave packet with a sharp front is emitted from the atom and travels toward the boundaries where it is reflected, and then travels back to the atom [e.g., Fig. 3(c)]. The emitted photon is then absorbed and reemitted by the atom, which results in the emergence of interference phenomena in the electric field. This produces a photonic wave packet with a more complex shape [Fig. 3(d)]. We observe that the MTEF simulations capture the qualitative character of the spontaneous-emission process extremely accurately, as well as the wave-packet propagation through the cavity. However, MTEF dynamics fails to reproduce the interference phenomena in the field due to reemission. We do note, however, that the MTEF simulations are capable of describing the remaining field intensity at the atomic position [Fig. 3(e)]. This feature corresponds to a bound electron-photon state, or polariton, which is an emergent hybrid state of the correlated light-matter system.

We also plot the excited-state population of the atomic system, and the average value of the photon number for the field, in Fig. 4. Again, MTEF is able to capture the qualitative behavior of both of these quantities very nicely. However, it fails to quantitatively reproduce the correct values for the emitted photon number and atomic population transfer, as these quantities are underestimated. Furthermore, as a result of this loss in accuracy, only a part of the subsequent reexcitation and reemission processes is captured.

In Fig. 5, we investigate the normalized second-order correlation function, $g^2(r_1, r_2, t)$, for the cavity photon field. The unperturbed vacuum state, which is coherent, corresponds to $g^2(r_1, r_2, t) = 1$, given by the black background seen in Fig. 5. The vacuum state is disturbed by the emitted wave packet, corresponding to antibunched light with $g^2(r_1, r_2, t) < 1$. The simplicity of the one-dimensional, one-photon process is quite clear in Fig. 6, where we show the associated

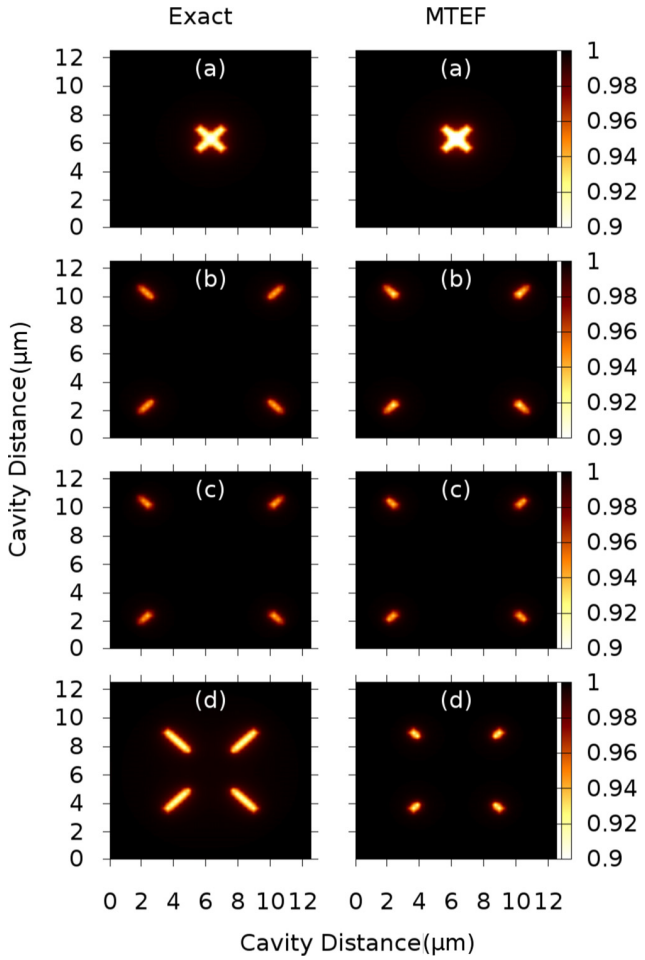

FIG. 5. Second-order correlation function for the photon field, $g^2(r_1, r_2, t)$, for the two-level model, plotted at four time snapshots: (a) $t = 100$, (b) $t = 600$, (c) $t = 1200$, (d) $t = 2100$ a.u. Exact simulation results (left panels) and MTEF (right panels).

one-dimensional cuts of g^2, along with projections of $g^2(r_1, r_2, t)$ along the positive and negative diagonals, $r_\pm = (r_1 \pm r_2)/\sqrt{2}$. Here we find, similar to the intensity, a nice qualitative agreement between MTEF and the exact result for the first three time snapshots. However, for the last time snapshot, the exact solution shows a broader correlation than MTEF, which corresponds to the fact that MTEF is not able to accurately capture reemission. Furthermore, as we only consider a one-photon process in this case, the correlation is symmetric in r_+ and r_-.

B. Three-level atom: Two-photon emission process

We now investigate the three-level system for the same observables as the previous section. The initial state for the atomic system is now the second-excited state. The photonic initial state remains the zero-temperature vacuum state.

In Fig. 7, we show the intensity of the cavity field during the two-photon emission process. Similar dynamics are observed compared with the two-level case. However, due to the additional intermediate atomic state, we now observe

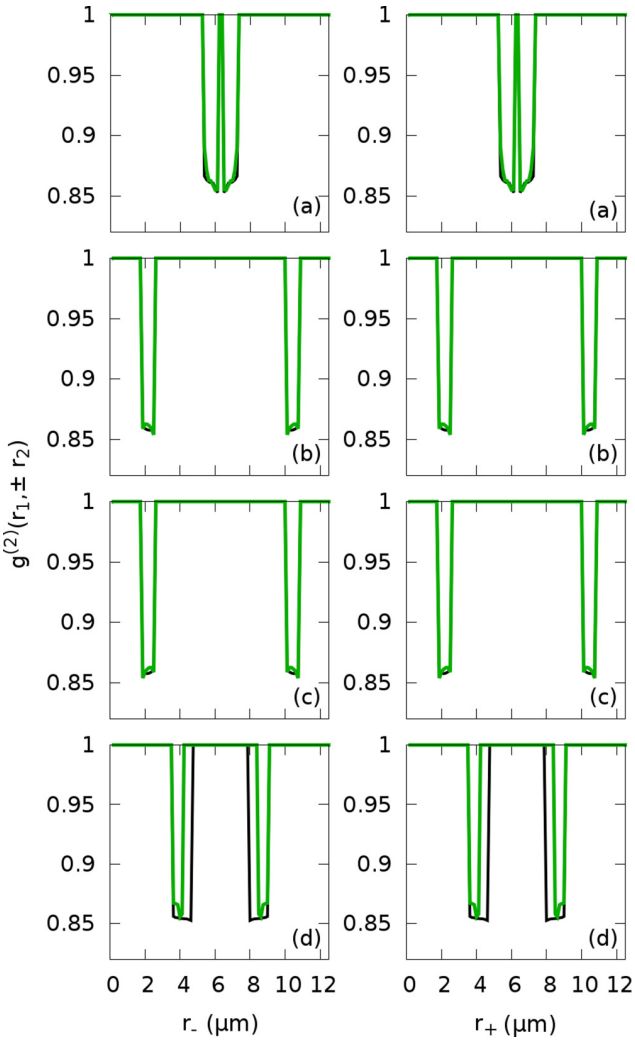

FIG. 6. Associated one-dimensional diagonal cuts $g^2(r_\pm, t)$ of the second-order correlation function, exact (black) and MTEF (green), plotted at four time snapshots: (a) $t = 100$, (b) $t = 600$, (c) $t = 1200$, (d) $t = 2100$ a.u.

a double-peak feature in the emitted photonic wave packet. This feature corresponds to the emission of two photons, as the excited atom initially drops to the first-excited state emitting one photon, and then further relaxes to the ground state, emitting a second photon. The polariton peak (the central feature in the field intensity profile) is overestimated in the MTEF simulations. This overestimation is due to the incomplete relaxation of the second-excited state within the Ehrenfest description.

In Fig. 8, we show the time evolution of the atomic-state populations and total photon number. Again, the emitted photonic wave packet moves through the cavity, is reflected at the mirrors, and returns to the atom. The first- and second-excited states are then repopulated due to stimulated absorption. A second spontaneous-emission process ensues and the emitted field again takes on a more complex profile due to interference. For the intensity, as well as the atomic population and photon number, we observe that MTEF displays qualitatively correct short-time dynamics. However, it fails to describe the

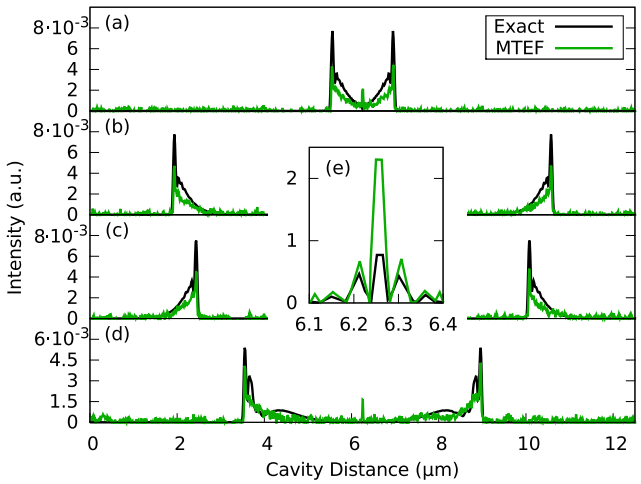

FIG. 7. Time evolution of the average field intensity for the two-photon emission process, at four different time snapshots: (a) $t = 100$, (b) $t = 600$, (c) $t = 1200$, (d) $t = 2100$ a.u. (e) Zoom-in of the polariton peak at the atomic position. Exact simulation results (black) and MTEF (green).

correct spatial structure of the (re)emitted two-photon wave packet, as well as the correct amplitude for the observables, in accordance with what was observed previously in the two-level case.

In Fig. 9, we show $g^2(r_1, r_2, t)$ for the two-photon emission process. The energy-level spacing in the three-level truncation of the 1D soft-Coulomb hydrogen atom is uneven, such that the two emitted photons are of different frequencies. Hence, in contrast to the one-photon process, we expect to observe asymmetric features in the second-order correlation function. In the exact result, we observe that the vacuum state is locally disturbed by a structured, antibunched photon wave packet.

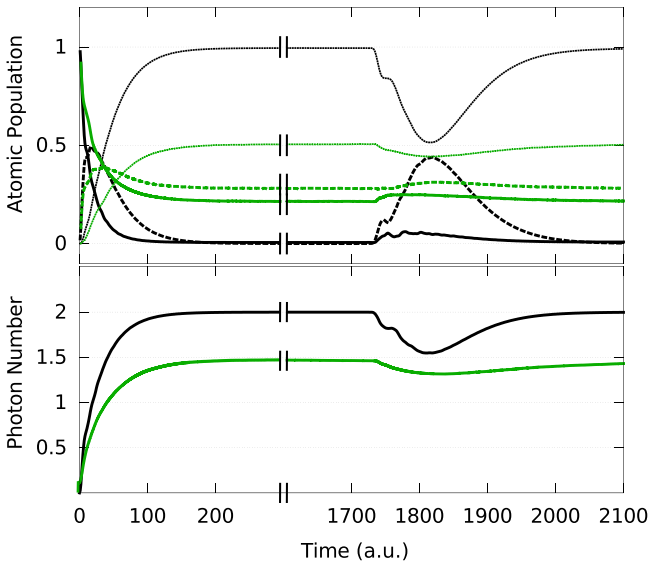

FIG. 8. Top panel: Time evolution of the atomic-state populations; solid line ($m = 3$), dashed lines ($m = 2$), and dotted line ($m = 1$). Bottom panel: Total photon number as a function of time. Exact simulation results (black) and MTEF (green).

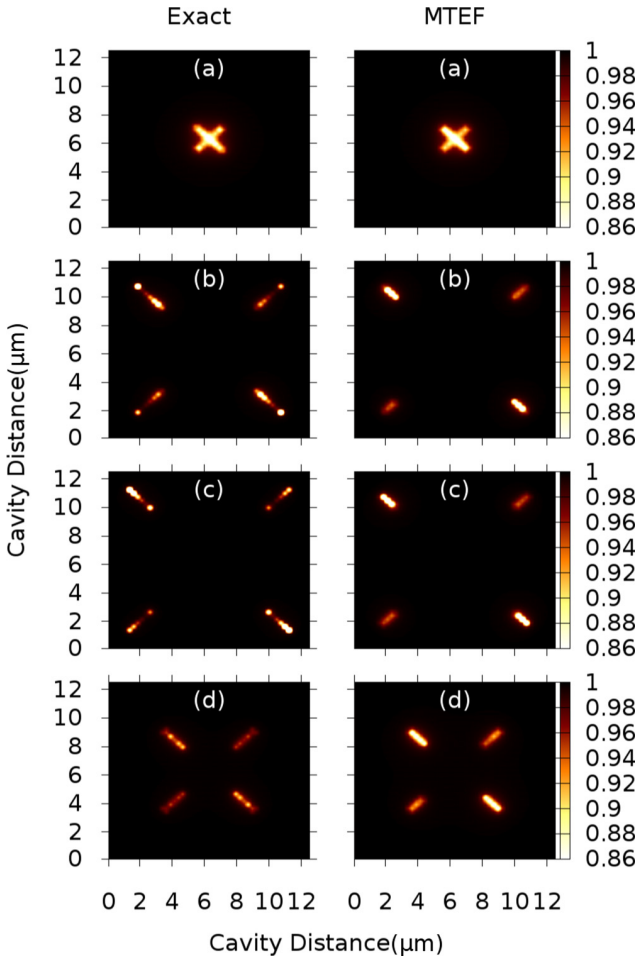

FIG. 9. Second-order correlation function for the photon field, $g^2(r_1, r_2, t)$, for the three-level model, plotted at four time snapshots: (a) $t = 100$, (b) $t = 600$, (c) $t = 1200$, (d) $t = 2100$ a.u. Exact simulation results (left panels) and MTEF (right panels).

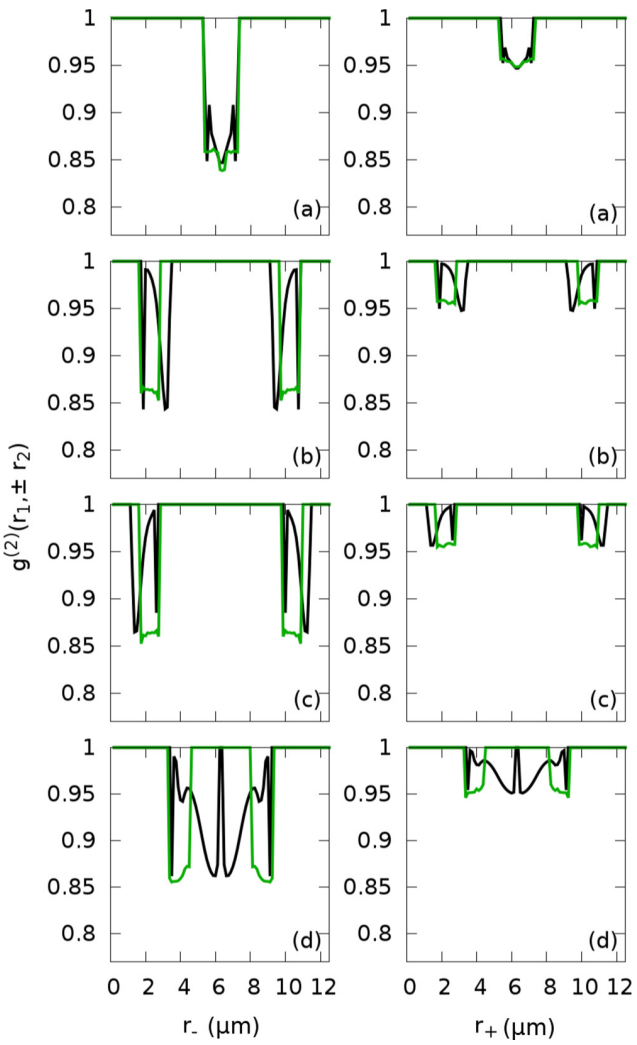

FIG. 10. Associated one-dimensional diagonal cuts $g^2(r_\pm, t)$ of the second-order correlation function, exact (black) and MTEF (green), plotted at four time snapshots: (a) $t = 100$, (b) $t = 600$, (c) $t = 1200$, (d) $t = 2100$ a.u.

The fine, multilobed spatial structure of the photon wave packet is blurred into a single, rather narrow feature in the MTEF result. However, MTEF dynamics indeed show the correct spatial asymmetry that is expected in $g^2(r_1, r_2, t)$. In the corresponding one-dimensional cuts of $g^2(r_1, r_2, t)$, shown in Fig. 10, we show in further detail the comparison of MTEF dynamics and the exact results in this more complex two-photon case.

IV. SUMMARY AND OUTLOOK

In this work, we have adapted the multitrajectory Ehrenfest (MTEF) method to simulate correlated quantum mechanical light-matter systems. We applied this mixed quantum classical dynamics method, which is traditionally applied to electron-nuclear dynamics problems, to two- and three-level model QED cavity-bound atomic systems, and in order to simulate observables and correlation functions for both the atomic system and the photon field. We find that MTEF dynamics is able to qualitatively characterize the correct dynamics for one- and two-photon spontaneous-emission processes in a QED cavity. However, MTEF dynamics does suffer from some quantitative drawbacks. Furthermore, we also observed that MTEF dynamics simulations can, in fact, capture some quantum mechanical features such as bound polariton states and second-order photon correlations. Moreover, as experimental advances drive the need for realistic descriptions of light-matter coupled systems, trajectory-based quantum classical algorithms emerge as a promising route towards treating more complex and realistic systems. In particular, as the equations of motion for the photonic system presented in this work can be seen as a one-dimensional Maxwell's equation, one possible route to extend the MTEF approach to realistic systems is the combination of our multitrajectory approach with the recently presented work of Jestädt *et al.* [40]. This work presents an *ab initio* light-matter coupling methodology, which treats coupled classical light, electrons, and nuclei by solving the Ehrenfest-Maxwell-Pauli-Kohn-Sham equations in quantum electrodynamics and is ideally suited for applications in nano-optics and nanoplasmonics. Therefore, combining the multitrajectory approach from the

present work with the methodology of Jestädt *et al*. provides a computationally feasible way to simulate photon-field fluctuations and correlations in realistic three-dimensional systems. Furthermore, by also including a sampling for the nuclei, this extension allows a fully quantized treatment of electrons, photons, and nuclei in such systems. Work along these lines is already in progress. Furthermore, an alternative to the independent trajectory-based approach employed here is the conditional wave-function approach, which allows one to address nonadiabatic dynamics problems in complex systems with higher accuracy than MTEF dynamics [41], and opens up an interesting potential route for mixed quantum classical methods in correlated light-matter systems.

ACKNOWLEDGMENTS

We would like to thank N. Säkkinen and J. Flick for insightful discussions and acknowledge financial support from the European Research Council (Grant No. ERC-2015-AdG-694097). A.K. acknowledges support from the National Sciences and Engineering Research Council (NSERC) of Canada.

[1] J. Feist and F. J. Garcia-Vidal, Extraordinary Exciton Conductance Induced by Strong Coupling, Phys. Rev. Lett. **114**, 196402 (2015).

[2] J. Schachenmayer, C. Genes, E. Tignone, and G. Pupillo, Cavity-Enhanced Transport of Excitons, Phys. Rev. Lett. **114**, 196403 (2015).

[3] M. Cirio, S. De Liberato, N. Lambert, and F. Nori, Ground State Electroluminescence, Phys. Rev. Lett. **116**, 113601 (2016).

[4] A. Maser, B. Gmeiner, T. Utikal, S. Götzinger, and V. Sandoghdar, Few-photon coherent nonlinear optics with a single molecule, Nat. Photon. **10**, 450 (2016).

[5] C. Riek, D. V. Seletskiy, A. S. Moskalenko, J. F. Schmidt, P. Krauspe, S. Eckart, S. Eggert, G. Burkard, and A. Leitenstorfer, Direct sampling of electric-field vacuum fluctuations, Science **350**, 420 (2015).

[6] A. S. Moskalenko, C. Riek, D. V. Seletskiy, G. Burkard, and A. Leitenstorfer, Paraxial Theory of Direct Electro-Optic Sampling of the Quantum Vacuum, Phys. Rev. Lett. **115**, 263601 (2015).

[7] J. George, T. Chervy, A. Shalabney, E. Devaux, H. Hiura, C. Genet, and T. W. Ebbesen, Multiple Rabi Splittings under Ultrastrong Vibrational Coupling, Phys. Rev. Lett. **117**, 153601 (2016).

[8] T. Byrnes, N. Young Kim, and Y. Yamamoto, Exciton-polariton condensates, Nat. Phys. **10**, 803 (2014).

[9] J. Kasprzak, M. Richard, S. Kundermann, A. Baas, P. Jeambrun, J. M. J. Keeling, F. M. Marchetti, M. H. Szymańska, R. Andre, J. L. Staehli *et al.*, Bose-Einstein condensation of exciton polaritons, Nature (London) **443**, 409 (2006).

[10] S. Schmidt, Frustrated polaritons, Phys. Scr. **91**, 073006 (2016).

[11] M. Ruggenthaler, N. Tancogne-Dejean, J. Flick, H. Appel, and A. Rubio, From a quantum-electrodynamical light-matter description to novel spectroscopies, Nat. Rev. Chem. **2**, 0118 (2018).

[12] M. Thoss and H. Wang, Semiclassical description of molecular dynamics based on initial-value representation methods, Annu. Rev. Phys. Chem. **55**, 299 (2004).

[13] C.-Y. Hsieh and R. Kapral, Nonadiabatic dynamics in open quantum-classical systems: Forward-backward trajectory solution, J. Chem. Phys. **137**, 22A507 (2012).

[14] C.-Y. Hsieh and R. Kapral, Analysis of the forward-backward trajectory solution for the mixed quantum-classical Liouville equation, J. Chem. Phys. **138**, 134110 (2013).

[15] S. A. Sato, A. Kelly, and A. Rubio, Coupled forward-backward trajectory approach for nonequilibrium electron-ion dynamics, Phys. Rev. B **97**, 134308 (2018).

[16] A. Kelly and T. E. Markland, Efficient and accurate surface hopping for long time nonadiabatic quantum dynamics, J. Chem. Phys. **139**, 014104 (2013).

[17] H.-T. Chen, T. E. Li, M. Sukharev, A. Nitzan, and J. E. Subotnik, Ehrenfest+R dynamics II: A semiclassical QED framework for Raman scattering, J. Chem. Phys. **150**, 044103 (2019).

[18] H.-T. Chen, T. E. Li, M. Sukharev, A. Nitzan, and J. E. Subotnik, Ehrenfest+R dynamics: A mixed quantum-classical electrodynamics simulation of spontaneous emission, J. Chem. Phys. **150**, 044102 (2019).

[19] T. E. Li, A. Nitzan, M. Sukharev, T. Martinez, H.-T. Chen, and J. E. Subotnik, Mixed quantum-classical electrodynamics: Understanding spontaneous decay and zero-point energy, Phys. Rev. A **97**, 032105 (2018).

[20] H. Eleuch and I. Rotter, Open quantum systems and dicke superradiance, Eur. Phys. J. D **68**, 74 (2014).

[21] H. Eleuch and I. Rotter, Resonances in open quantum systems, Phys. Rev. A **95**, 022117 (2017).

[22] H. Carmichael, Quantum jumps revisited: An overview of quantum trajectory theory, *Quantum Future From Volta and Como to the Present and Beyond*, Lecture Notes in Physics Vol. 517 (Springer, Berlin, Heidelberg, 2007), p. 15.

[23] F. H. Faisal, *Theory of Multiphoton Processes* (Springer, Berlin, 1987).

[24] J. Flick, H. Appel, M. Ruggenthaler, and A. Rubio, Cavity Born-Oppenheimer approximation for correlated electron-nuclear-photon systems, J. Chem. Theory Comput. **13**, 1616 (2017).

[25] I. V. Tokatly, Time-Dependent Density Functional Theory for Many-Electron Systems Interacting with Cavity Photons, Phys. Rev. Lett. **110**, 233001 (2013).

[26] J. Flick, M. Ruggenthaler, H. Appel, and A. Rubio, Atoms and molecules in cavities, from weak to strong coupling in quantum-electrodynamics (QED) chemistry, Proc. Natl. Acad. Sci. USA **114**, 3026 (2017).

[27] C. Pellegrini, J. Flick, I. V. Tokatly, H. Appel, and A. Rubio, Optimized Effective Potential for Quantum Electrodynamical Time-Dependent Density Functional Theory, Phys. Rev. Lett. **115**, 093001 (2015).

[28] J. Flick, M. Ruggenthaler, A. Heiko, and R. Angel, Kohn-Sham approach to quantum electrodynamical density-functional theory: Exact time-dependent effective potentials in real space, Proc. Natl. Acad. Sci. USA **112**, 15285 (2015).

[29] D. P. Craig and T. Thirunamachandran, *Molecular Quantum Electrodynamics: An Introduction to Radiation-molecule Interactions* (Dover, New York, 1998).

[30] C. Schäfer, M. Ruggenthaler, and A. Rubio, *Ab initio* nonrelativistic quantum electrodynamics: Bridging quantum chemistry and quantum optics from weak to strong coupling, Phys. Rev. A **98**, 043801 (2018).

[31] P. Ehrenfest, Bemerkungen über die angenäherte Gültigkeit der klassischen Mechanik innerhalb der Quantenmechanik, Z. Phys. **45**, 455 (1927).

[32] M. Makri and W. H. Miller, Time-dependent self-consistent field approximation for a reaction coordinate coupled to a harmonic bath: single and multiple configuration treatments, J. Chem. Phys. **87**, 5781 (1987).

[33] J. C. Tully, Mixed quantum-classical dynamics, Faraday Discuss. **110**, 407 (1998).

[34] A. D. McLachlan, A variational solution of the time-dependent Schrödinger equation, Mol. Phys. **8**, 39 (1964).

[35] R. Grunwald, A. Kelly, and R. Kapral, *Quantum Dynamics in Almost Classical Environments* (Springer, Berlin, 2009), pp. 383–413.

[36] R. J. Glauber, Photon Correlations, Phys. Rev. Lett. **10**, 84 (1963).

[37] M. Hillery, R. F. O'Connell, M. O. Scully, and E. P. Wigner, Distribution Functions in Physics: Fundamentals, Phys. Rep. **106**, 121 (1984).

[38] V. Bužek, G. Drobný, M. G. Kim, M. Havukainen, and P. L. Knight, Numerical simulations of atomic decay in cavities and material media, Phys. Rev. A **60**, 582 (1999).

[39] Q. Su and J. H. Eberly, Model atom for multiphoton physics, Phys. Rev. A **44**, 5997 (1991).

[40] R. Jestädt, M. Ruggenthaler, M. J. T. Oliveira, A. Rubio, and H. Appel, Real-time solutions of coupled Ehrenfest-Maxwell-Pauli-Kohn-Sham equations: Fundamentals, implementation, and nano-optical applications, arXiv:1812.05049 .

[41] G. Albareda, A. Kelly, and A. Rubio, Nonadiabatic ab initio quantum dynamics without potential energy surfaces, Phys. Rev. Materials **3**, 023803 (2019).

2.2 TIME-DEPENDENT POTENTIAL ENERGY SURFACE FOR PHOTONS

"Light-Matter Interactions via the Exact Factorization Approach"

NM Hoffmann, H Appel, A Rubio, NT Maitra

The European Physical Journal B (2018), 91 (8), 180

MOTIVATION The interaction of light with matter involves the correlated dynamics of photons, electrons, and nuclei. Even at a non-relativistic level the solution of Schrödinger's equation for the coupled subsystems is a daunting computation. In a given situation however, one is often measuring properties of only one of these subsystems, where the observable of interest involves one of the subsystems alone. Yet, to capture the dynamics of the relevant subsystem, clearly the effects of all subsystems are needed. The question then arises: can we write a Schrödinger equation for one of the subsystems alone, such that the solution yields the wavefunction of that subsystem? Note that the potential appearing in the equation would have to incorporate the couplings to the other subsystems as well as to any externally applied fields. More precisely, in order to analyze the finding of [O1] in more detail, the question can be specified as: Can we find the exact potential driving the photon motion and fully incorporating the effects of the matter system on the photonic dynamics?

STATE OF THE ART One possible way to answer this question is via the EF approach [35, 36, 109, 110], which was introduced for the case of coupled electronic and nuclear subsystems in the presence of a classical light field neglecting the magnetic field contribution. Here, it was shown that one can exactly factorize the complete molecular (electron-ion) wavefunction into a wavefunction describing the nuclear system, and a wavefunction describing the electronic system that is conditionally dependent on the nuclear subsystem: $\Psi(\mathbf{r},\mathbf{R},t) = \chi(\mathbf{R},t)\Phi_{\mathbf{R}}(\mathbf{r},t)$, where $\chi(\mathbf{R},t)$ characterizes the marginal amplitude and $\Phi_{\mathbf{R}}(\mathbf{r},t)$ the conditional amplitude with $\mathbf{r}$, $\mathbf{R}$ denoting the electronic and nuclear coordinates, respectively. The equation for the nuclear subsystem has a Schrödinger form, with scalar $\epsilon(\mathbf{R},t)$ and vector $\mathbf{A}(\mathbf{r},t)$ potentials that completely account for the coupling to the electronic system.

CONTRIBUTION AND MAIN FINDINGS We extend the EF approach to light-matter interactions $\Psi(\mathbf{q},\mathbf{r},\mathbf{R},t) = \chi(\mathbf{q},t)\Phi_{\mathbf{q}}(\mathbf{r},\mathbf{R},t)$, which yields a time-dependent Schrödinger equation for the photonic system, where $\mathbf{q}$ denotes the photonic

displacement vector. This choice is particularly relevant when one is primarily interested in the state of the radiation field. We illustrate the formalism and potential for a two-level system representing the matter coupled to an infinite number of photon modes in the Wigner-Weisskopf approximation, as well as to a single mode with various coupling strengths. Our main findings include, significant differences from convetional approaches in the potential that drives the photonic dynamics, due to large deviations from the harmonic form of the free-photon field. These deviations completely incorporate the effect of the matter system on the photonic dynamics. We also study the effect of beginning in an initially purely factorized light-matter state, compared to a photonic BO initial state, finding significant differences for larger coupling strengths in the ensuing dynamics, implying that in modelling these problems a careful consideration of the initial state is needed.

OUTLOOK Besides analyzing the TDPES for photons, in order to gain more indside to the results found in [O1], one can also use the EF approach as a guideline to develop semiclassical trajectory methods for efficient simulations of realistic light-matter dynamics. However, approximations will be needed, since solving the EF equations is at least as computationally expensive as solving the Schrödinger equation for the fully coupled system. It has been shown recently that mixed quantum-classical trajectory methods that are derived from the EF approach can correctly capture decoherence effects [37–39]. Since photons are intrinsically non-interacting and therefore even simpler to treat than nuclei, we expect in analogy to the electron-nuclear case that semiclassical trajectory methods derived from systematic and controlled approximations to the full EF of the light-matter wavefunction will be able to capture decoherence effects beyond the Ehrenfest limit for light-matter coupling.

Eur. Phys. J. B (2018) 91: 180
https://doi.org/10.1140/epjb/e2018-90177-6

THE EUROPEAN PHYSICAL JOURNAL B

Regular Article

Light-matter interactions via the exact factorization approach*

Norah M. Hoffmann[1,2,a], Heiko Appel[1,b], Angel Rubio[1,4,c], and Neepa T. Maitra[2,3,d]

[1] Max Planck Institute for the Structure and Dynamics of Matter and Center for Free-Electron Laser Science and Department of Physics, Luruper Chaussee 149, 22761 Hamburg, Germany
[2] Department of Physics and Astronomy, Hunter College of the City University of New York, 695 Park Avenue, New York, NY 10065, USA
[3] The Physics Program and the Chemistry Program of the Graduate Center of the City University of New York, New York, NY 10065, USA
[4] Center for Computational Quantum Physics, Flatiron Institute, 162 5th Avenue, New York, NY 10010, USA

Received 16 March 2018 / Received in final form 1 June 2018
Published online 6 August 2018

Abstract. The exact factorization approach, originally developed for electron-nuclear dynamics, is extended to light-matter interactions within the dipole approximation. This allows for a Schrödinger equation for the photonic wavefunction, in which the potential contains exactly the effects on the photon field of its coupling to matter. We illustrate the formalism and potential for a two-level system representing the matter, coupled to an infinite number of photon modes in the Wigner–Weisskopf approximation, as well as to a single mode with various coupling strengths. Significant differences are found with the potential used in conventional approaches, especially for strong couplings. We discuss how our exact factorization approach for light-matter interactions can be used as a guideline to develop semiclassical trajectory methods for efficient simulations of light-matter dynamics.

1 Introduction

The interaction of light with matter involves the correlated dynamics of photons, electrons, and nuclei. Even at a non-relativistic level the solution of Schrödinger's equation for the coupled subsystems is a daunting computation. In a given situation however, one is often measuring properties of only one of these subsystems. For example, one might be wanting to know how the electrical conductivity of a molecule is affected by the photons, as in the recent experiment showing the increased conductivity of organic semiconductors due to hybridization with the vacuum field [1]. On the other hand, one might want to understand how molecular dissociation after electronic excitation is affected in the presence of light, as in the recent study of light-induced versus intrinsic nonadiabatic dynamics in diatomics [2]. Or, one might want to measure the superradiance from a collection of atoms [3]. In each of these three cases, the observable of interest involves one of the subsystems alone, electronic, nuclear, and photonic, respectively, yet to capture the dynamics of the relevant subsystem, clearly the effects of all subsystems are needed. The question then arises: can we write a Schrödinger equation for one of the subsystems alone, such that the solution yields the wavefunction of that subsystem? The potential appearing in the equation would have to incorporate the couplings to the other subsystems as well as to any externally applied fields.

Hardy Gross, with co-workers, in fact already answered exactly these questions [4–6] for the case of coupled electronic and nuclear subsystems in the presence of a *classical* light field neglecting the magnetic field contribution. That is, for systems of electrons and nuclei, interacting with each other via a scalar potential (usually taken as Coulomb), and in the presence of an externally applied scalar potential, such as the electric field of light, it was shown that one can exactly factorize the complete molecular wavefunction into a wavefunction describing the nuclear system, and a wavefunction describing the electronic system that is conditionally dependent on the nuclear subsystem [4–7]: $\Psi(\underline{\underline{\mathbf{r}}}, \underline{\underline{\mathbf{R}}}, t) = \chi(\underline{\underline{\mathbf{r}}}, t)\Phi_{\underline{\underline{\mathbf{R}}}}(\underline{\underline{\mathbf{r}}}, t)$, where $\underline{\underline{\mathbf{r}}} = \mathbf{r}_1, \ldots, \mathbf{r}_{N_e}$ and $\underline{\underline{\mathbf{R}}} = \mathbf{R}_1, \ldots, \mathbf{R}_{N_n}$ represent all electronic and nuclear coordinates respectively. The equation for the nuclear subsystem has a Schrödinger form, with scalar and vector potentials that completely account for the coupling to the electronic system. One can reverse the roles of the electronic and nuclear subsystems, to instead get a Schrödinger equation for the

* Contribution to the Topical Issue "Special issue in honor of Hardy Gross", edited by C.A. Ullrich, F.M.S. Nogueira, A. Rubio, and M.A.L. Marques.

[a] e-mail: Norah-Magdalena.Hoffmann@mpsd.mpg.de
[b] e-mail: heiko.appel@mpsd.mpg.de
[c] e-mail: angel.rubio@mpsd.mpg.de
[d] e-mail: nmaitra@hunter.cuny.edu

electronic system, which is particularly useful when one is most interested in the electronic properties [8], e.g. in field-induced molecular ionization.

Recently rapid experimental and theoretical advances have however drawn attention to fascinating phenomena that depend on the quantization of the light field in its interaction with matter. This includes few-photon coherent nonlinear optics with single molecules [9], direct experimental sampling of electric-field vacuum fluctuations [10,11], multiple Rabi splittings under ultrastrong vibrational coupling [12], exciton-polariton condensates [13,14], polaritonically enhanced superconductivity in cavities [15], or frustrated polaritons [16] among others. Optical cavities can be used to tune the effective strength of the light-matter interaction, and, in the strong-coupling regime in particular, one finds for example non-radiative energy transfer well beyond the Förster limit between spatially separated donors and acceptors [17], strong coupling between chlorosomes of photosynthetic bacteria and confined optical cavity modes [18], photochemical reactions can be suppressed with cavity modes [19], the position of conical intersections can be shifted or they can be removed [2,20], or state-selective chemistry at room temperature can be achieved by strong vacuum-matter coupling [21]. Strong vacuum-coupling can change chemical reactions, such as photoisomerization or a prototypical deprotection reaction of alkynylsilane [21,22]. This has given rise to the burgeoning field now sometimes called "polaritonic chemistry" [20,23–27]. In addition, novel spectroscopies have been proposed which explicitly exploit correlated states of the photon field. For example the use of entangled photon pairs enables one to go beyond the classical Fourier limit [28,29], or correlated photons can be used to imprint correlation onto matter [20,27,30,31].

In this paper, we extend the exact factorization approach to non-relativistic coupled photon-matter systems within the dipole approximation. We focus particularly on finding the potential driving the photonic system in the present study. One motivation is towards developing mixed quantum-classical methods for the light-matter system. The observation that in a matter-free system, the photonic Hamiltonian is a sum over harmonic Hamiltonians for each mode of the radiation field suggests that a classical treatment of the photonic system would be accurate: if the system begins in a Gaussian wavepacket, classical Wigner dynamics exactly describes the motion [32]. Coupling to matter within the dipole approximation where the coupling operator is linear in the photonic variable preserves the quadratic nature of the Hamiltonian, and one might then think that again a classical Wigner treatment would be exact. However, although accurate, it is not exact. This implies that the true potential driving the photonic motion is in fact not quadratic. The exact factorization approach defines exactly what this potential should be. In this paper we explain the formalism and give some examples of this potential, that clearly show deviations from harmonic behaviour throughout the dynamics.

The theory is described in Section 2, presenting the Hamiltonian that we will consider, and the formalism of the factorization approach. Section 3 demonstrates the approach on two examples, that we choose as the simplest cases for this initial study. The matter system is described by a two-level system while the photonic system is chosen to either be an infinite number of modes treated within the Wigner–Weisskopf approximation, or a single cavity mode chosen to be resonant with the spacing of the two levels, explored over a range of coupling strengths. We find and interpret the potential driving the photonic system, which depends significantly on whether the initial state of the system is chosen correlated or fully factorized. Finally in Section 4 we summarize and discuss the relevance of this approach for future investigations of light-matter dynamics.

2 Theory

2.1 QED-Hamiltonian

In this work, we consider the non-relativistic limit of a system of N_e electrons, N_n nuclei, and N_p quantized photon modes, treated within the dipole approximation in Coulomb gauge [27,33,34]. For now, we do not consider any classical external fields, and neglect spin-coupling. The Hamiltonian of this coupled system is then defined by [20,35–38]

$$\hat{H}(\underline{\underline{\mathbf{q}}},\underline{\mathbf{r}},\underline{\underline{\mathbf{R}}}) = \hat{H}_p + \hat{H}_e + \hat{H}_n + \hat{H}_{\mathrm{ep}} + \hat{H}_{np} + \hat{H}_{\mathrm{en}} + \hat{H}_{\mathrm{pen}}, \tag{1}$$

which operates in the space of: $\underline{\mathbf{r}} = \{\mathbf{r}_1..\mathbf{r}_i..\mathbf{r}_{N_e}\}$ representing all electronic spatial coordinates, $\underline{\underline{\mathbf{R}}} = \{\mathbf{R}_1..\mathbf{R}_I..\mathbf{R}_{N_n}\}$ representing all nuclear coordinates, and $\underline{\underline{\mathbf{q}}} = \{q_1..q_\alpha..q_{N_p}\}$ representing all photonic displacement coordinates. The first term characterizes the cavity-photon Hamiltonian

$$\hat{H}_p(\underline{\underline{\mathbf{q}}}) = \frac{1}{2}\left(\sum_{\alpha=1}^{2N_p} \hat{p}_\alpha^2 + \omega_\alpha^2 \hat{q}_\alpha^2\right) = \hat{T}_p(\underline{\underline{\mathbf{q}}}) + \hat{V}_p(\underline{\underline{\mathbf{q}}}). \tag{2}$$

Here $\hat{q}_\alpha = \sum_\alpha \sqrt{\frac{\hbar}{2\omega_\alpha}}(\hat{a}_\alpha^+ + \hat{a}_\alpha)$ defines the photonic displacement coordinate for the αth mode, with creation(a^+) and annihilation(a) operators [35,36], and the commutation relation $[\hat{q}_\alpha, \hat{p}_{\alpha'}] = \imath\hbar\delta_{\alpha,\alpha'}$. The photonic displacement coordinate is directly proportional to the mode-projected electric displacement operator, $\hat{D}_\alpha = \epsilon_0\omega_\alpha\lambda_\alpha\hat{q}_\alpha$, while $\hat{p}_\alpha$ is proportional to the magnetic field [36,37]. The αth mode has frequency $\omega_\alpha = k_\alpha c = \alpha\pi c/V$, with k_α the wavevector and V the quantization volume. The electron–photon coupling strength is given by

$$\boldsymbol{\lambda}_\alpha = \sqrt{4\pi} S_\alpha(\mathbf{k}_\alpha \cdot \mathbf{X})\mathbf{e}_\alpha, \tag{3}$$

where S_α denotes the mode function, e.g. a sine-function for the case of a cubic cavity [36,39], $\mathbf{k}_\alpha$ the wave vector, and $\mathbf{X}$ the total dipole of the system. In particular, we emphasize at this point that the mode functions introduce a dependence of the coupling constants on the quantization volume of the electromagnetic field. By confining this volume, for example with an optical cavity, one can tune the interaction strength. Finally, we note that the sum in

equation (2) goes from 1 to $2N_p$, to take the two polarization possibilities of the electromagnetic field into account. The second term of equation (1) denotes the electronic Hamiltonian

$$\hat{H}_e(\underline{\underline{\mathbf{r}}}) = \sum_{i=1}^{N_e} \frac{\hat{\mathbf{p}}_i^2}{2m_e} + \frac{e^2}{4\pi\epsilon_0} \sum_{i>j}^{N_e} \frac{1}{|\mathbf{r}_i - \mathbf{r}_j|} = \hat{T}_e(\underline{\underline{\mathbf{r}}}) + \hat{V}_{ee}(\underline{\underline{\mathbf{r}}}) \,, \tag{4}$$

where m_e defines the electronic mass, $\hat{\mathbf{p}}_i$ the electronic momentum operator conjugate to $\hat{\mathbf{r}}_i$. The third term in equation (1) denotes the nuclear Hamiltonian

$$\hat{H}_n(\underline{\underline{\mathbf{R}}}) = \sum_{I=1}^{N_n} \frac{\hat{\mathbf{P}}_I^{\,2}}{2M_I} + \frac{e^2}{4\pi\epsilon_0} \sum_{i>j}^{N_n} \frac{Z_I Z_J}{|\mathbf{R}_I - \mathbf{R}_J|} \tag{5}$$

$$= \hat{T}_n(\underline{\underline{\mathbf{R}}}) + \hat{V}_{nn}(\underline{\underline{\mathbf{R}}}), \tag{6}$$

with analogous identifications to the electronic Hamiltonian and eZ_I here being the nuclear charge.

The remaining terms in equation (1) denote the couplings between the subsystems. The electron-nuclear coupling appears as the usual Coulombic interaction:

$$\hat{H}_{\text{en}} = -\sum_{i=1}^{N_e} \sum_{J=1}^{N_n} \frac{e^2 Z}{|\mathbf{r}_i - \mathbf{R}_J|} \tag{7}$$

the electron–photon coupling, in dipole approximation,

$$\hat{H}_{\text{ep}} = -\sum_{\alpha=1}^{2N_p} \omega_\alpha \hat{q}_\alpha \vec{\lambda}_\alpha \cdot \sum_{i=1}^{N_e} e\mathbf{r}_i, \tag{8}$$

(where e is the magnitude of the electronic charge) bilinearly couples the total electric dipole moment with the electric field operator for each mode of the photonic field. Similarly, the nuclear-photon coupling is

$$\hat{H}_{np} = \sum_{\alpha=1}^{2N_p} \omega_\alpha \hat{q}_\alpha \vec{\lambda}_\alpha \cdot \sum_{I=1}^{N_n} eZ_I \mathbf{R}_I. \tag{9}$$

Finally, H_{pen} represents the dipole self-energy of the matter in the radiation field:

$$\hat{H}_{\text{pen}} = \frac{1}{2} \sum_{\alpha=1}^{2N_p} \vec{\lambda}_\alpha \cdot \left(\sum_{I}^{N_n} Z_I \mathbf{R}_I - \sum_{i}^{N_e} \mathbf{r}_i \right)^2. \tag{10}$$

This self-energy term is essential for a mathematically well defined light-matter interaction. Without this term the Hamiltonian is not bound from below, and loses in addition translational invariance (in case of a vanishing external potential) [40].

The dynamics of such a coupled system is given by the solution of the time-dependent Schrödinger equation (TDSE)

$$\hat{H}\Psi(\underline{\underline{\mathbf{r}}}, \underline{\underline{\mathbf{R}}}, \underline{\underline{\mathbf{q}}}, t) = i\partial_t \Psi(\underline{\underline{\mathbf{r}}}, \underline{\underline{\mathbf{R}}}, \underline{\underline{\mathbf{q}}}, t), \tag{11}$$

where $\Psi(\underline{\underline{\mathbf{r}}}, \underline{\underline{\mathbf{R}}}, \underline{\underline{\mathbf{q}}}, t)$ is the full matter-photon wavefunction, that contains the complete information of the coupled system. However it is difficult to obtain an intuitive understanding and interpretation of such a coupled system from the high-dimensional $\Psi(\underline{\underline{\mathbf{r}}}, \underline{\underline{\mathbf{R}}}, \underline{\underline{\mathbf{q}}}, t)$, and moreover, we may not be interested in all the information as we might be interested in one of the subsystems. If one of these subsystems varies on a much slower time-scale than the others (in particular the nuclei), what is often done in coupled electron-nuclear systems is a Born–Oppenheimer (BO) adiabatic approximation where the faster time-scale subsystem (in particular the electrons) are assumed to instantaneously adjust to the positions of the nuclei, and hence if they begin in an eigenstate, they remain in an eigenstate parameterized by the nuclear coordinate. The eigenenergy maps out a BO potential energy surface (PES) which provides the potential for the nuclear dynamics. These potential-energy surfaces are clearly an approximation within the adiabatic ansatz, but in fact an *exact* PES can be defined quite generally without the need for any adiabatic approximation, which brings us to the main point of this paper. For the electron-nuclear problem, these arise from the exact factorization approach mentioned earlier in the introduction. In the next section we will extend the idea of the exact factorization for electron-nuclei systems to coupled photon-matter systems.

Before moving to this, we note that equation (1) is the most general form of Hamiltonian that we will consider in the present work. In later sections, in particular in the explicit examples, we will simplify to just a two-level electronic system interacting with the photonic field in a cavity. In that case, many of the terms in equation (1) are zero, and we simplify the remaining terms even further to a model Hamiltonian

$$\hat{H} = -\frac{\omega_0}{2}\hat{\sigma}_z + \sum_\alpha \left(-\frac{1}{2}\frac{\partial^2}{\partial q_\alpha^2} + \frac{1}{2}\omega_\alpha^2 q_\alpha^2 \right) + \sum_\alpha \omega_\alpha \lambda_\alpha \hat{q}_\alpha (d_{\text{eg}} \hat{\sigma_x}). \tag{12}$$

Here σ_i are the Pauli matrices. The first term is the two-level system that replaces the electronic Hamiltonian (including the dipole self-energy, which simplifies to a constant energy shift for a two-level system), where the energy-level difference is ω_0, and d_{eg}, appearing in the third term, is the dipole moment of the transition. The second term describes the free photon field, as in equation (2), while equation (8) reduces to the third term with λ_α as the coupling strength evaluated at the position of the atom in the cavity. The TDSE also simplifies, to

$$i\hbar\frac{\partial}{\partial t}\vec{\Psi}(\underline{\underline{\mathbf{q}}}, t) = \begin{pmatrix} -\frac{\omega_0}{2} + \hat{H}_p(\underline{\underline{\mathbf{q}}}) & \sum_\alpha \omega_\alpha \lambda_\alpha \hat{q}_\alpha d_{\text{eg}} \\ \sum_\alpha \omega_\alpha \lambda_\alpha \hat{q}_\alpha d_{\text{eg}} & \frac{\omega_0}{2} + \hat{H}_p(\underline{\underline{\mathbf{q}}}) \end{pmatrix} \vec{\Psi}(\underline{\underline{\mathbf{q}}}, t), \tag{13}$$

where we use the notation $\vec{\Psi}(\underline{\underline{\mathbf{q}}}, t)$ being a 2-vector defined at every $\underline{\underline{\mathbf{q}}}$ and t. A cartoon of the problem is given in Figure 1.

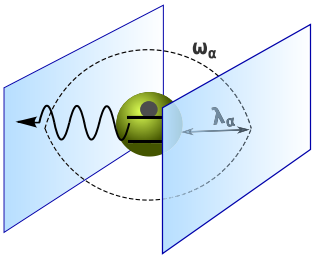

Fig. 1. Cavity-setup: particle (green) trapped in a cavity and coupled by coupling strength λ_α to the α photon mode with the photonic frequency ω_α, where $\alpha = \{1, 2, \ldots, 2n_p\}$.

2.2 Exact factorization approach

The exact factorization (EF) may be viewed as a reformulation of the quantum mechanics of interacting coupled systems where the wavefunction is factored into a marginal amplitude and a conditional amplitude [4–7,41]. With non-relativistic electron-nuclear systems in mind, the equations for these amplitudes were derived for Hamiltonians of the form

$$\hat{H} = \hat{T}_e + \hat{T}_n + \hat{V}, \tag{14}$$

where $\hat{V}$ is a scalar potential that includes coupling between the electrons and nuclei (usually Coulombic) and any externally applied fields. Here $\hat{T}_{e,n}$ are kinetic energy operators of the electronic and nuclear systems, just as in equations (4) and (6), that have the form of $-\sum_{i(I)} \nabla^2_{i(I)}/2m_{i(I)}$ (that is, no vector potential). The EF then proves that the exact full molecular wavefunction can be factored as

$$\Psi(\underline{\underline{\mathbf{r}}}, \underline{\underline{\mathbf{R}}}, t) = \chi(\underline{\underline{\mathbf{R}}}, t)\Phi_{\underline{\underline{\mathbf{R}}}}(\underline{\underline{\mathbf{r}}}, t)\,. \tag{15}$$

The equation for the nuclear amplitude χ has a TDSE form [5,6,42,43], equipped with a time-dependent scalar potential $\epsilon(\underline{\underline{\mathbf{R}}}, t)$ and a time-dependent vector potential $\mathbf{A}_I(\underline{\underline{\mathbf{R}}}, t)$ that include entirely the effects of coupling to the electronic system as well as external fields. The equation for the conditional electronic amplitude $\Phi_{\underline{\underline{\mathbf{R}}}}$ has a more complicated form, involving a coupling operator $\hat{U}_{\text{en}}$, that acts on the parametric dependence of $\Phi_{\underline{\underline{\mathbf{R}}}}$. The factorization is unique, up to a gauge-like transformation, provided $\Phi_{\underline{\underline{\mathbf{R}}}}$ satisfies the "partial normalization condition" (PNC), $\int d\underline{\underline{\mathbf{r}}} |\Phi_{\underline{\underline{\mathbf{R}}}}(\underline{\underline{\mathbf{r}}}, t)|^2 = 1$; under such a transformation, ϵ and $\mathbf{A}$ transform as scalar and vector potentials do in electrodynamics. The nuclear N_n-body probability density and current-density can be obtained in the usual way from the nuclear amplitude $\chi(\underline{\underline{\mathbf{R}}}, t)$, so in this sense, χ can be identified as the nuclear wavefunction of the system.

The form of equation (15) is similar to the BO approximation, however with the important difference that equation (15) is an *exact* representation of the wavefunction, not an approximation, and further that it is valid for time-dependent systems, with time-dependent external fields, as well. The BO approximation assumes that the electronic system remains always in the instantaneous ground (or eigen)-state associated with the nuclear configuration $\underline{\underline{\mathbf{R}}}$, and therefore misses all the physics associated with non-adiabatic effects, including wavepacket branching and decoherence. These effects are contained exactly in the coupling terms in the EF equations: the scalar and vector potentials and the coupling operator of the electronic equation. It is important to note that there is no assumption of different timescales in the EF approach, in contrast to the BO approximation.

As the scalar potential plays a role analogous to the BO PES, but now for the exact system, it is denoted the time-dependent potential energy surface (TDPES), while the vector potential (TDVP) is an exact time-dependent Berry connection. The gauge-freedom is a crucial part of the EF approach: in particular, whether a gauge exists in which the vector potential can be transformed into part of the TDPES has been explored in some works [44–47], especially since the common understanding is that Berry phases appear only out of an adiabatic separation of timescales, while the EF is exact and does not assume any such separation. Further, equally valid is the reverse factorization [8], $\Psi(\underline{\mathbf{r}}, \underline{\underline{\mathbf{R}}}, t) = \chi(\underline{\mathbf{r}}, t)\Phi_{\underline{\mathbf{r}}}(\underline{\underline{\mathbf{R}}}, t)$, which is particularly useful when one is interested in the electronic system, since in this factorization, the electronic system follows a TDSE in which the potentials can be analysed and interpreted.

2.3 Exact factorization approach for QED

Here, we extend the exact factorization to systems of coupled photons, electrons, and nuclei. Since all the kinetic operators in the Hamiltonian within the dipole approximation, equation (1), are of similar form to those that were considered in the original EF approach, equation (14), the mathematical structure of the equations and coupling terms will be similar when we make a factorization into two parts.

There are three possibilities for such a factorization, and we expect each to be useful in different contexts. One possibility, which is perhaps the most natural extension of the factorization of references [4–7,41], is to take the nuclear system as the marginal one,

$$\Psi(\underline{\underline{\mathbf{q}}}, \underline{\underline{\mathbf{r}}}, \underline{\underline{\mathbf{R}}}; t) = \chi(\underline{\underline{\mathbf{R}}}; t)\Phi_{\underline{\underline{\mathbf{R}}}}(\underline{\underline{\mathbf{q}}}, \underline{\underline{\mathbf{r}}}; t)\,, \tag{16}$$

with the PNC

$$\int d\underline{\underline{\mathbf{q}}} d\underline{\underline{\mathbf{r}}} |\Phi_{\underline{\underline{\mathbf{R}}}}(\underline{\underline{\mathbf{q}}}, \underline{\underline{\mathbf{r}}}; t)|^2 = 1 \tag{17}$$

for every nuclear configuration $\underline{\underline{\mathbf{R}}}$ at each time t. This would yield a TDSE for the nuclear system, much like in the original EF approach, but now the TDPES and TDVP includes not only the effects on the nuclei of coupling to the electrons, but also to the photons. This would be a particularly useful factorization for studying light-induced non-adiabatic chemical dynamics phenomena, when the quantum nature of light is expected to play a role. In fact, an approximation based on the normal BO approximation for the electron-ion dynamics has been used to study

the cavity-induced changes in the potential energy surfaces in the strong coupling regime [48]. This would be a particularly useful factorization for studying light-induced non-adiabatic phenomena, when the quantum nature of light is expected to play a role.

A second possibility is the natural extension of the reverse factorization [8], where the electronic system is the marginal amplitude

$$\Psi(\underline{\underline{\mathbf{q}}},\underline{\mathbf{r}},\underline{\underline{\mathbf{R}}};t)=\chi(\underline{\mathbf{r}};t)\Phi_{\underline{\mathbf{r}}}(\underline{\underline{\mathbf{q}}},\underline{\underline{\mathbf{R}}};t)\,, \tag{18}$$

with the PNC $\int d\underline{\underline{\mathbf{q}}}d\underline{\underline{\mathbf{R}}}|\Phi_{\underline{\mathbf{r}}}(\underline{\underline{\mathbf{q}}},\underline{\underline{\mathbf{R}}};t)|^2=1$, for all t and every electronic configuration $\underline{\mathbf{r}}$, which would yield a TDSE for electrons, with the e-TDPES and e-TDVP now incorporating the full effects on the electrons of coupling to the nuclei as well as the photons. This could be particularly useful for studying, for example, the impact of the vacuum field on electrical conductivity in a molecule or semiconductor.

This leaves the third possibility, where the photonic system is chosen as the marginal:

$$\Psi(\underline{\underline{\mathbf{q}}},\underline{\mathbf{r}},\underline{\underline{\mathbf{R}}};t)=\chi(\underline{\underline{\mathbf{q}}};t)\Phi_{\underline{\underline{\mathbf{q}}}}(\underline{\mathbf{r}},\underline{\underline{\mathbf{R}}};t)\,, \tag{19}$$

with the PNC

$$\int d\underline{\mathbf{r}}d\underline{\underline{\mathbf{R}}}|\Phi_{\underline{\underline{\mathbf{q}}}}(\underline{\mathbf{r}},\underline{\underline{\mathbf{R}}};t)|^2=1\,, \tag{20}$$

for each field-coordinate $\underline{\underline{\mathbf{q}}}$ and all times t. This is the factorization we will focus on in the present paper: it gives a TDSE for the photonic system, within which the scalar potential, which we call the q-TDPES, and vector potential, the q-TDVP, contain the feedback of the matter-system on the radiation field. In free space, the potential acting on the photons is quadratic as is evident from equation (2), however, in the presence of matter, the potential determining the photonic state deviates from its harmonic form due to interactions with matter. The cavity-BO approach introduced in reference [34] has demonstrated these deviations within the BO approximation. The EF approach now renders this concept exact, beyond any adiabatic assumptions.

The equations for each of these three factorizations follow from a straightforward generalization of the original EF equations, as the non-multiplicative operators (the kinetic operators) have the same form; hence the derivation proceeds quite analogously to that given in references [5,6,42]. In particular, for the factorization equation (19), we obtain

$$\left(\hat{H}_m(\underline{\mathbf{r}},\underline{\underline{\mathbf{R}}},\underline{\underline{\mathbf{q}}};t)-\epsilon(\underline{\underline{\mathbf{q}}};t)\right)\Phi_{\underline{\underline{\mathbf{q}}}}(\underline{\mathbf{r}},\underline{\underline{\mathbf{R}}};t)=i\partial_t\Phi_{\underline{\underline{\mathbf{q}}}}(\underline{\mathbf{r}},\underline{\underline{\mathbf{R}}};t), \tag{21}$$

$$\left(\sum_\alpha^{2n_p}\frac{1}{2}\left(i\frac{\partial}{\partial_{q_\alpha}}+A_\alpha(\underline{\underline{\mathbf{q}}};t)\right)^2+\epsilon(\underline{\underline{\mathbf{q}}};t)\right)\chi(\underline{\underline{\mathbf{q}}};t)=i\partial_t\chi(\underline{\underline{\mathbf{q}}};t), \tag{22}$$

where the matter Hamiltonian $\hat{H}_m$ is given by

$$\hat{H}_m(\underline{\mathbf{r}},\underline{\underline{\mathbf{R}}},\underline{\underline{\mathbf{q}}};t)=\hat{H}_{\mathrm{qBO}}+\hat{U}_{\mathrm{ep}} \tag{23}$$

with

$$\hat{H}_{\mathrm{qBO}}=\hat{H}_e+\hat{H}_n+\hat{H}_{\mathrm{en}}+\hat{H}_{\mathrm{pen}}+\hat{H}_{\mathrm{ep}}+\hat{H}_{np}+\frac{1}{2}\sum_{\alpha=1}^{2N_p}\omega_\alpha\hat{q}_\alpha^2 \tag{24}$$

defined in an analogous way to the BO Hamiltonian, but now for the photonic system. The electron–photon coupling potential $\hat{U}_{\mathrm{ep}}$ is given by

$$\hat{U}_{\mathrm{ep}}[\Phi_{\underline{\underline{\mathbf{q}}}},\chi]=\sum_\alpha^{2n_p}\left[\frac{(-i\partial_{q_\alpha}-A_\alpha(\underline{\underline{\mathbf{q}}};t))^2}{2}+\left(\frac{-i\partial_{q_\alpha}\chi(\underline{\underline{\mathbf{q}}};t)}{\chi(\underline{\underline{\mathbf{q}}};t)}+A_\alpha(\underline{\underline{\mathbf{q}}};t)\right)\left(-i\partial_{q_\alpha}-A_\alpha(\underline{\underline{\mathbf{q}}};t)\right)\right], \tag{25}$$

the q-TDPES by

$$\epsilon(\underline{\underline{\mathbf{q}}};t)=\int d\underline{\mathbf{r}}d\underline{\underline{\mathbf{R}}}\,\Phi^*_{\underline{\underline{\mathbf{q}}}}(\underline{\mathbf{r}},\underline{\underline{\mathbf{R}}};t)\left(\hat{H}_m(\underline{\mathbf{r}},\underline{\underline{\mathbf{R}}},\underline{\underline{\mathbf{q}}};t)-i\partial_t\right)\times\Phi_{\underline{\underline{\mathbf{q}}}}(\underline{\mathbf{r}},\underline{\underline{\mathbf{R}}};t) \tag{26}$$

and the q-TDVP by

$$A_\alpha(\underline{\underline{\mathbf{q}}};t)=-i\int d\underline{\mathbf{r}}d\underline{\underline{\mathbf{R}}}\,\Phi^*_{\underline{\underline{\mathbf{q}}}}(\underline{\mathbf{r}},\underline{\underline{\mathbf{R}}};t)\partial_{q_\alpha}\Phi_{\underline{\underline{\mathbf{q}}}}(\underline{\mathbf{r}},\underline{\underline{\mathbf{R}}};t)\,. \tag{27}$$

The factorization (19) is unique up to a gauge-like transformation, provided the PNC, equation (20) is satisfied. The gauge-like transformation has the structure of the usual one in electromagnetism, except here the scalar and vector potentials arise due to coupling, rather than due to external fields, and they are potentials on the photonic system, not on the matter system. The equations are form-invariant under the following transformation:

$$\begin{aligned}\Phi_{\underline{\underline{\mathbf{q}}}}(\underline{\mathbf{r}},\underline{\underline{\mathbf{R}}},t)&\to\Phi_{\underline{\underline{\mathbf{q}}}}(\underline{\mathbf{r}},\underline{\underline{\mathbf{R}}},t)\exp(i\theta(\underline{\underline{\mathbf{q}}},t))\\ \chi(\underline{\underline{\mathbf{q}}},t)&\to\chi(\underline{\underline{\mathbf{q}}},t)\exp(-i\theta(\underline{\underline{\mathbf{q}}},t))\\ A_\alpha(\underline{\underline{\mathbf{q}}};t)&\to A_\alpha(\underline{\underline{\mathbf{q}}};t)+\partial_\alpha\theta(\underline{\underline{\mathbf{q}}},t)\\ \epsilon(\underline{\underline{\mathbf{q}}};t)&\to\epsilon(\underline{\underline{\mathbf{q}}};t)+\partial_t\theta(\underline{\underline{\mathbf{q}}},t).\end{aligned} \tag{28}$$

Further, one can show that the displacement-field density represented by χ reproduces that of the full wavefunction, i.e.

$$|\chi(\underline{\underline{\mathbf{q}}};t)|^2=\int d\underline{\mathbf{r}}d\underline{\underline{\mathbf{R}}}|\Psi(\underline{\underline{\mathbf{q}}},\underline{\mathbf{r}},\underline{\underline{\mathbf{R}}};t)|^2\,, \tag{29}$$

and that the phase of χ together with the q-TDVP provide the displacement-field probability current in the natural way:

$$\mathrm{Im}\langle\Psi|\partial_\alpha\Psi\rangle = |\chi(\underline{\underline{\mathbf{q}}};t)|^2\mathbf{A}_\alpha(\underline{\underline{\mathbf{q}}};t) + \partial_\alpha S(\underline{\underline{\mathbf{q}}};t)\,, \tag{30}$$

where $\chi(\underline{\underline{\mathbf{q}}};t) = |\chi(\underline{\underline{\mathbf{q}}};t)|\exp(iS(\underline{\underline{\mathbf{q}}},t))$. This means that observables associated with multiplication by $\underline{\underline{\mathbf{q}}}$ can be obtained directly from $\chi(\underline{\underline{\mathbf{q}}},t)$, for example, the electric field

$$\mathbf{E}(\mathbf{r};t) = \sum_\alpha \omega_\alpha \boldsymbol{\lambda}_\alpha(\mathbf{r},t)\int d\underline{\underline{\mathbf{q}}}\, q_\alpha |\chi(\underline{\underline{\mathbf{q}}};t)|^2\,, \tag{31}$$

while the magnetic field is

$$\mathbf{B}(\mathbf{r};t) = \sum_\alpha \frac{c}{\omega_\alpha}\nabla\times\boldsymbol{\lambda}_\alpha(\mathbf{r},t)\int d\underline{\underline{\mathbf{q}}}|\chi(\underline{\underline{\mathbf{q}}};t)|^2 A_\alpha(\underline{\underline{\mathbf{q}}};t) + \partial_\alpha S(\underline{\underline{\mathbf{q}}};t). \tag{32}$$

2.4 Exact factorization for simplified model hamiltonian: two-level system in radiation field

For our exploration of the QED factorization in this paper, we will turn to the simplified model Hamiltonian of equation (12), where the matter system's Hamiltonian is a 2×2 matrix. First, it is useful to write equation (12) as

$$\hat{H} = -\sum_\alpha \frac{1}{2}\partial_{q_\alpha}^2 \mathbb{1}_2 + \hat{H}_{\mathrm{qBO}}\,, \text{ where} \tag{33}$$

$$\hat{H}_{\mathrm{qBO}} = -\frac{\omega_0}{2}\hat{\sigma}_z + \sum_\alpha \frac{1}{2}\omega_\alpha^2 q_\alpha^2 \mathbb{1}_2 + \sum_\alpha \omega_\alpha\lambda_\alpha\hat{q}_\alpha(d_{\mathrm{eg}}\hat{\sigma_x}). \tag{34}$$

Here $\hat{H}_{\mathrm{qBO}}$ is analogous to the BO Hamiltonian in the usual electron-nuclear case. We can define q-BO states as normalized eigenstates:

$$\hat{H}_{\mathrm{qBO}}\overrightarrow{\Phi}^{(1,2)}_{\underline{\underline{\mathbf{q}}}} = \epsilon^{(1,2)}_{\mathrm{qBO}}(\underline{\underline{\mathbf{q}}})\overrightarrow{\Phi}^{(1,2)}_{\underline{\underline{\mathbf{q}}}}, \tag{35}$$

with $\overrightarrow{\Phi}^{i,\dagger}_{\underline{\underline{\mathbf{q}}}}\cdot\overrightarrow{\Phi}^{j}_{\underline{\underline{\mathbf{q}}}} = \delta_{ij}$. and these can be used as a basis to expand the fully coupled wavefunction, i.e.

$$\overrightarrow{\Psi}(\underline{\underline{\mathbf{q}}},t) = \chi_1(\underline{\underline{\mathbf{q}}},t)\overrightarrow{\Phi}^{(1)}_{\underline{\underline{\mathbf{q}}}} + \chi_2(\underline{\underline{\mathbf{q}}},t)\overrightarrow{\Phi}^{(2)}_{\underline{\underline{\mathbf{q}}}}, \tag{36}$$

which would be analogous to the Born–Huang expansion but now for the cavity-matter system.

Now in the EF approach, the fully coupled wavefunction is instead factorized as a single product:

$$\overrightarrow{\Psi}(\underline{\underline{\mathbf{q}}},t) = \chi(\underline{\underline{\mathbf{q}}},t)\overrightarrow{\Phi}_{\underline{\underline{\mathbf{q}}}}(t), \tag{37}$$

where the PNC becomes

$$\overrightarrow{\Phi}^{\dagger}_{\underline{\underline{\mathbf{q}}}}(t)\cdot\overrightarrow{\Phi}_{\underline{\underline{\mathbf{q}}}}(t) = 1\,, \tag{38}$$

and holds for every $\underline{\underline{\mathbf{q}}}$ and each time t.

We note that there are two useful bases for this problem. One is obtained from diagonalizing the field-free two-level system, i.e. that defined by eigenvectors of the Pauli-σ_z matrix. The other basis is the q-BO basis, defined by the eigenvectors of $\hat{H}_{\mathrm{qBO}}$, as in equation (35).

The EF equations follow directly from equations (21)–(27) but with the much simplified $\hat{H}_{\mathrm{qBO}}$ above, and all integrals over $\underline{\mathbf{r}}$ and $\underline{\underline{\mathbf{R}}}$ replaced by 2×2 matrix-multiplication.

2.5 Photonic time-dependent potential energy surface

Unlike the original electron-nuclear factorization, the q-TDVP can always be chosen to be zero due to the one-dimensional nature of each photon-displacement mode. This means that one can always transform to a gauge in which the q-TDPES contains the *entire* effect of the coupling of the matter system on the radiation field, i.e. it is the only potential that is driving the photonic dynamics. For the matter system, both the q-TDPES and the photon-matter coupling operator incorporate the effect of the photonic system on the matter. In the original electron-nuclear factorization, the exact TDPES proved to be a powerful tool to analyze and interpret time-resolved dynamics of the system in cases ranging from dynamics of molecules in strong fields [5,6,8,49–52], to non-adiabatic proton-coupled electron-transfer [53–55], to nuclear-velocity perturbation theory [56,57] and dynamics through a conical intersection [58,59]. It provides an exact generalization of the adiabatic BO-PES.

In the present work, we will study the q-TDPES $\epsilon(\underline{\underline{\mathbf{q}}},t)$ of equation (26) for the case of the radiation field coupled to a two level-system, using the model Hamiltonian (12). Given a solution $\overrightarrow{\Psi}(\underline{\underline{\mathbf{q}}},t)$ for the coupled system, found from equation (13), we will extract the exact q-TDPES by inversion.

To do this, we first ensure that we work in the gauge where $A_\alpha = 0$. Similarly to previous work [6,54], this gauge can be fixed by choosing the phase $S(\underline{\underline{\mathbf{q}}},t)$ of the photonic wavefunction, $\chi(\underline{\underline{\mathbf{q}}},t) = |\chi(\underline{\underline{\mathbf{q}}},t)|\exp(i\tilde{S}(\underline{\underline{\mathbf{q}}},t))$, to satisfy

$$\partial_{q_\alpha}S(\underline{\underline{\mathbf{q}}},t) = \frac{\mathrm{Im}\left(\overrightarrow{\Psi}(\underline{\underline{\mathbf{q}}},t)\cdot\partial_{q_\alpha}\overrightarrow{\Psi}(\underline{\underline{\mathbf{q}}},t)\right)}{|\chi(\underline{\underline{\mathbf{q}}},t)|^2}. \tag{39}$$

So, from the given solution $\overrightarrow{\Psi}(\underline{\underline{\mathbf{q}}},t)$, we compute

$$\overrightarrow{\Phi}_{\underline{\underline{\mathbf{q}}}}(\underline{\mathbf{r}}) = \frac{\overrightarrow{\Psi}(\underline{\underline{\mathbf{q}}},t)}{|\chi(\underline{\underline{\mathbf{q}}},t)|e^{iS(\vec{q},t)}} \text{ with}$$
$$|\chi| = \sqrt{\overrightarrow{\Psi}^{\dagger}(\underline{\underline{\mathbf{q}}},t)\cdot\overrightarrow{\Psi}(\underline{\underline{\mathbf{q}}},t)} \tag{40}$$

Eur. Phys. J. B (2018) 91: 180

and insert into the q-TDPES

$$\begin{aligned}\epsilon(\underline{\underline{\mathbf{q}}},t) &= \overrightarrow{\Phi}^{\dagger}_{\underline{\underline{\mathbf{q}}}}(t)\cdot\hat{H}_{\mathrm{qBO}}\cdot\overrightarrow{\Phi}_{\underline{\underline{\mathbf{q}}}}(t)\\ &\quad+\sum_{\alpha}\frac{1}{2}|\partial_{\alpha}\overrightarrow{\Phi}_{\underline{\underline{\mathbf{q}}}}(t)|^2+\overrightarrow{\Phi}^{\dagger}_{\underline{\underline{\mathbf{q}}}}(t)\cdot(-i\partial_t\overrightarrow{\Phi}_{\underline{\underline{\mathbf{q}}}}(t))\\ &= \epsilon_{\mathrm{wBO}}(\underline{\underline{\mathbf{q}}},t)+\epsilon_{\mathrm{kin}}(\underline{\underline{\mathbf{q}}},t)+\epsilon_{\mathrm{GD}}(\underline{\underline{\mathbf{q}}},t)\,, \end{aligned}\tag{41}$$

where we have identified here the first term in equation (41) as ϵ_{wBO}, a "weighted q-BO" surface, weighted by the probabilities of being in the q-BO eigenstates: using the expansion equation (36),

$$\epsilon_{\mathrm{wBO}}=\frac{|\chi_1(\underline{\underline{\mathbf{q}}},t)|^2\epsilon^{(1)}_{\mathrm{qBO}}(\underline{\underline{\mathbf{q}}},t)+|\chi_2(\underline{\underline{\mathbf{q}}},t)|^2\epsilon^{(2)}_{\mathrm{qBO}}(\underline{\underline{\mathbf{q}}},t)}{|\chi(\underline{\underline{\mathbf{q}}},t)|^2}\,.\tag{42}$$

The second term arises from kinetic effects from the parametric dependence of the conditional matter wavefunction, hence we denote it as ϵ_{kin}, and it originates from the electron–photon coupling operator: in this gauge the only term that contributes to the electron–photon coupling operator expectation value is

$$\begin{aligned}\epsilon_{\mathrm{kin}}(\underline{\underline{\mathbf{q}}},t) &= \overrightarrow{\Phi}^{\dagger}_{\underline{\underline{\mathbf{q}}}}(t)\cdot\hat{U}_{\mathrm{ep}}\cdot\overrightarrow{\Phi}_{\underline{\underline{\mathbf{q}}}}(t)=-\frac{1}{2}\sum_{\alpha}^{2n_p}\overrightarrow{\Phi}^{\dagger}_{\underline{\underline{\mathbf{q}}}}(t)\cdot\partial^2_{\alpha}\overrightarrow{\Phi}_{\underline{\underline{\mathbf{q}}}}\\ &= \frac{1}{2}\sum_{\alpha}^{2n_p}|\partial_{\alpha}\Phi_{\underline{\underline{\mathbf{q}}}}|^2.\end{aligned}\tag{43}$$

Both ϵ_{wBO} and ϵ_{kin} are invariant under different gauge choices, while the last term in equation (41) is gauge-dependent, hence its name ϵ_{GD}.

3 Results and discussion

We will consider two extremes within the simplified model Hamiltonian equation (12). The first is the Wigner–Weisskopf limit where the two-level system is coupled to an infinite number of cavity modes. This is the classic model for spontaneous emission: an atom initially in an excited state in a vacuum decays to the ground-state by spontaneously emitting a photon. The second system we study is the two-level system coupled to a single resonant mode. The Hamiltonian is then the same as the Jaynes–Cummings one, but as we will begin with a photonic vacuum and excited atom, we will not see the famous collapses and revivals, but we will see Rabi oscillation type behavior for weak coupling. In both cases, our central question is what are the structures and features of the q-TDPES potential that drives the photonic system away from its vacuum state?

As initial condition, we take the photon modes in the vacuum state, and the two-level system in the excited state. For the single resonant mode case, we will compare the effect of starting in a fully factorized matter-photonic state with that of starting in a q-BO state. The fully factorized initial state would be the physical one when an excited atom is instantaneously brought into a closed cavity and just then its dynamics is studied, while the excited q-BO state results when there is initially an external dissipative coupling together with an applied resonant field to maintain the atom in that excited state before the dynamics is examined.

We notice that the dipole matrix element and coupling parameter appear only together as a product in this model equation (12), $d_{\mathrm{eg}}\lambda$. Physically, these are fixed by the problem at hand, specifically the volume of the cavity and the dipole coupling between the two levels in the atom, apart from fundamental constants. But here, in this model we choose them arbitrarily, and compare dynamics for different $d_{\mathrm{eg}}\lambda$ that range from relatively weak coupling to strong coupling.

3.1 Wigner–Weisskopf limit

We first consider the Wigner–Weisskopf limit, in which our two-level system is coupled to an infinite number of modes. In this limit, the accepted well-known approximate solution for the coupled system is known analytically, which makes the q-TDPES particularly straightforward to find. We begin by briefly reviewing this solution.

The solution for $\overrightarrow{\Psi}$ of the coupled problem can be found in the standard literature [60]. The initial state is taken to be a purely factorized state of the electron in the excited state and all photon modes in their ground states, i.e.

$$\overrightarrow{\Psi}(\underline{\underline{\mathbf{q}}},0)=\chi_0(\underline{\underline{\mathbf{q}}})\begin{pmatrix}1\\0\end{pmatrix},\tag{44}$$

where

$$\chi_0(\underline{\underline{\mathbf{q}}})=\prod_{\alpha}\left(\frac{\omega_{\alpha}}{\pi\hbar}\right)^{1/4}e^{-\omega_{\alpha}q^2_{\alpha}/2\hbar}\,,\tag{45}$$

which follows from the harmonic nature of the free photon field. The coupling in the off-diagonal elements of equation (12) then cause Ψ to evolve in time, as

$$\overrightarrow{\Psi}(\underline{\underline{\mathbf{q}}},t)=a(t)\chi_0(\underline{\underline{\mathbf{q}}})\begin{pmatrix}1\\0\end{pmatrix}+\sum_{\alpha}b_{\alpha}(t)\chi_{\alpha}(\underline{\underline{\mathbf{q}}})\begin{pmatrix}0\\1\end{pmatrix}\tag{46}$$

under the reasonable assumption that the coefficients of the two-photon and higher states are negligible. Here the one-photon states of the photonic system are

$$\chi_{\alpha}(\underline{\underline{\mathbf{q}}})=\sqrt{\frac{2\omega_{\alpha}}{\hbar}}q_{\alpha}\prod_{\beta}\left(\frac{\omega_{\beta}}{\pi\hbar}\right)^{1/4}e^{-\omega_{\beta}q^2_{\beta}/2\hbar}\,.\tag{47}$$

The coefficients $a(t)$ and $b_{\alpha}(t)$ can be found by substituting equation (46) into the TDSE equation (13). After making the Wigner–Weisskopf approximations (taking the continuum limit so $V\to\infty$, taking $a(t)$ to change with a rate much slower than the resonant frequency ω_0 and

performing a Markov rotating-wave approximation, and neglecting a divergent Lamb shift), we arrive at

$$a(t) = e^{-\frac{i\omega_0 t}{\hbar}} e^{-\frac{\Gamma t}{2}}, \tag{48}$$

$$b_\alpha(t) = e^{i\omega_\alpha} \frac{i g_\alpha (e^{i(\omega_\alpha - \omega_0)t - \Gamma t/2} - 1)}{i(\omega_\alpha - \omega_0) - \Gamma/2}, \tag{49}$$

where $g_\alpha = \sqrt{\frac{\pi\omega_\alpha}{2\hbar}} \lambda_\alpha d_{\text{eg}}$ and the decay (spontaneous emission rate), $\Gamma = (d_{\text{eg}}\lambda)^2 \omega_0^2 \frac{V}{\hbar c^3}$. The Wigner–Weisskopf solution is accurate for weak coupling, so that in this limit the solution also generates accurate q-TDPES.

With this Wigner–Weisskopf solution, we can then find the corresponding "exact" q-TDPES, equation (41), using equations (40) and (39). However, this yields an infinite dimensional surface, since $\underline{\underline{\mathbf{q}}} = (q_1..q_\alpha...q_\infty)$, which is challenging to visualize. Instead, we plot some one-dimensional cross-sections of the q-TDPES, along the ith mode, setting $q_{\alpha\neq i} = 0$. In the following, we use $\bar{q}$ to denote all modes not equal to q_i. We will abbreviate quantities such as $\epsilon(q_i, \bar{q} = 0, t)$ by $\epsilon(q_i, t)$, understood to be looking at the cross-section where the displacement-coordinate of all other modes is zero. We will choose two different modes to look along: one resonant with ω_0, and the other slightly off-resonant. With this choice of cross-sections through the origin of all modes but one, it can be shown that the phase of the nuclear wavefunction that satisfies the zero-q-TDVP condition, equation (27), $S(q_i, t) \equiv 0$. This leads to some simplification in the components of $\epsilon(q_i, t)$.

Before we discuss the q-TDPES, in Figure 2 we plot the autocorrelation function

$$A_\Phi(t) = \left| \int dq_i (\overrightarrow{\Phi}^\dagger(q_i; t=0) \cdot \overrightarrow{\Phi}(q_i; t)) \right|^2 \tag{50}$$

as this gives an indication of what time-scales to expect in the behavior of the q-TDPES $\epsilon(q_i, t)$ for different coupling strengths $d_{\text{eg}}\lambda = \{0.01, 0.1, 0.4\}$. In the upper panel, we have chosen to plot the q-TDPES along the mode of the radiation field that is resonant with the two-level system. In this case, the decay of the autocorrelation depends primarily on $(d_{\text{eg}}\lambda)^2$, through Γ, i.e. $A_\Phi(t) \propto e^{-\Gamma t}$, although there are some small polynomial corrections.

In the slightly off-resonant case, we have chosen $\omega_i = 0.41$ while $\omega_0 = 0.4$. In fact, we observe partial revivals in the autocorrelation function for very long times in the case of the weakest coupling shown ($d_{\text{eg}}\lambda = 0.01$), as shown in the inset, with the amplitude decreasing with each revival. However the initial decay follows a similar $d_{\text{eg}}\lambda$-scaling pattern to that of the on-resonant section. In either case, the dynamics of the decay is essentially the same for all coupling strengths, provided the time is scaled appropriately, and their q-TDPES's also map on to each other at the corresponding times. In the following then, we will focus on the case $d_{\text{eg}}\lambda = 0.01$, for both the cross-section taken along the on-resonant mode and the slightly off-resonant mode.

In Figures 3 and 4 we show the different components of the q-TDPES $\epsilon(q_i, t)$ for the different time snapshots

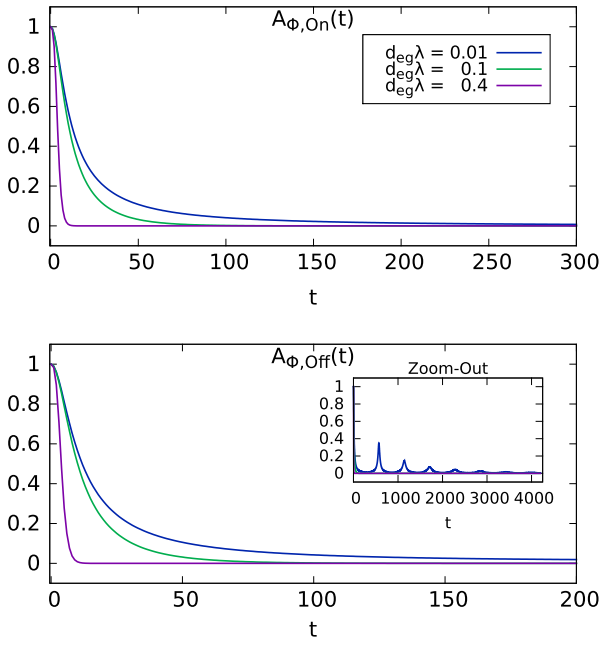

Fig. 2. The autocorrelation function $A_\Phi(t)$ where the different colors describe the different coupling strengths of the system. The upper panel shows the decay of this function when we choose to look on-resonance $\omega_i = \omega_0 = 0.4$. The lower panel illustrates the decay when looking along a slightly-off resonant mode $\omega_i = \omega_0 + 0.01$. The zoom-out shows the same off-resonance decay for a longer time.

indicated by the colored dots in the decay-plot in the top left panel, for the on-resonant and off-resonant sections respectively. The displacement-field density, $|\chi(q_i, t)|^2 = |\chi(q_i, \bar{q} = 0, t)|^2$ at these time-snapshots is shown in the top middle panel, and we observe the gradual evolution from the vacuum state towards the state with one photon during the decay. This is also seen in the conditional probability amplitudes shown in the top right panel, which we obtain from

$$|C^{1(2)}(q_i, t)|^2 = \overrightarrow{\Phi}^{(1(2))}_{q_i, \bar{q}=0} \cdot \overrightarrow{\Phi}_{q_i, \bar{q}=0}(t). \tag{51}$$

These are the coefficients of expansion of $\Phi_{q_i}(t)$ in the q-BO basis and are related to the coefficients in equation (36) via $C^j(q_i, t) = \chi_j(q_i, t)/\chi(q_i, t)$. $C^{(1)}(q_i, t)$ and $C^{(2)}(q_i, t)$ begin close to 0 and 1, respectively, as expected, and as the coupling kicks in and the atom decays, one might expect them to evolve to 1 and 0, respectively. This is in fact correct for almost all q_i, however non-uniformly in q_i. As expected from the nature of the bilinear coupling Hamiltonian equation (12), the conditional electronic amplitude associated with larger photonic displacements q_i couple more strongly than those associated with smaller ones, so the conditional amplitude on the upper surface falls away from 1 starting on the outer edges and then moving in. In fact, the conditional amplitude at $q = 0$ remains forever stubbornly at the upper surface, unaffected by the coupling to the field.

Eur. Phys. J. B (2018) 91: 180

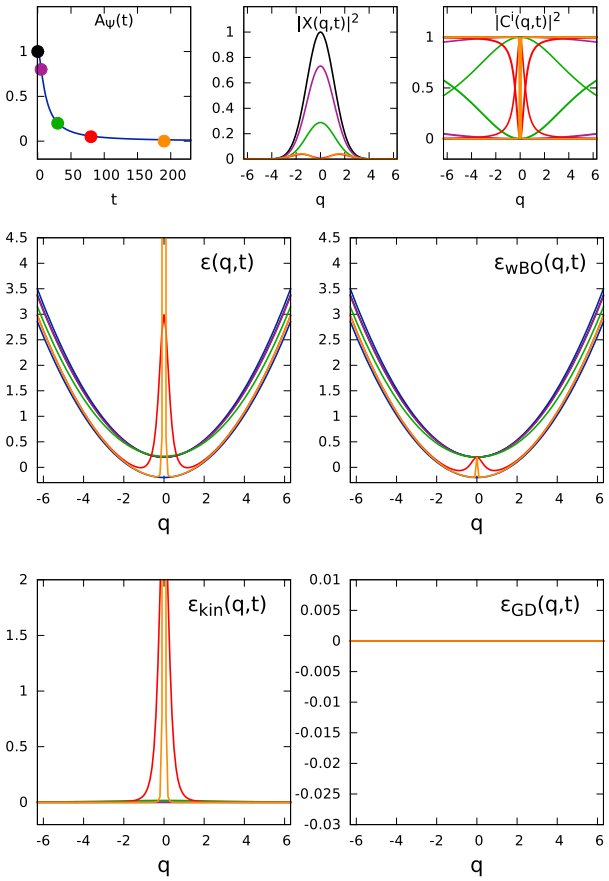

Fig. 3. Wigner–Weisskopf model, looking on-resonance $\omega_i = \omega_0$. The top left panel shows the decay $A_\Phi(t)$, where the different colored dots depict the times of the different time snapshots of the dynamics shown within this plot. The middle and right panels along the top show the photonic distribution $|\chi(q_i,t)|^2$ and each coefficient of the conditional electronic distribution $|C^{(1)}(q_i;t)|^2$ (dashed), $|C^{(2)}(q_i;t)|^2$ (solid) at the corresponding time snapshots. The middle and lower panels show the different components of the $\epsilon(q_i;t)$ as well as the full scalar potential at the given time snapshots. In the middle panels, the q-BO surfaces are shown in blue for reference.

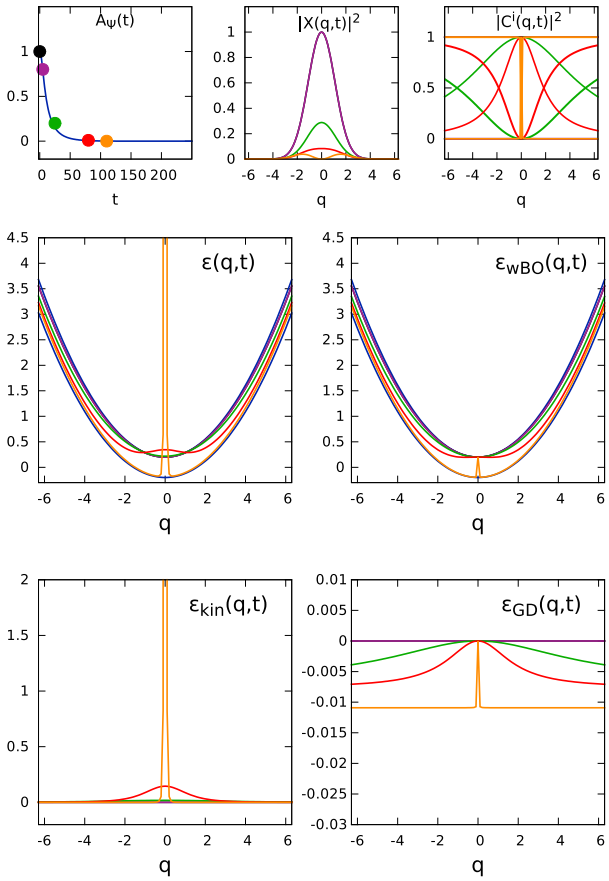

Fig. 4. As for Figure 3 but looking along the slightly-off resonant mode in the Wigner–Weisskopf model.

This non-uniformity is reflected in the q-TDPES $\epsilon(q_i,t)$, plotted in the middle panel, and leads to a strong deviation from the harmonic form it has in the absence of matter. The potential, driving the photonic motion, loses its harmonic form in the initial time steps as the decay begins, peeling away starting from the outer q_i. The potential nearer $q_i = 0$ remains harmonic for the initial stages, but as time goes on, more of the surface peels away from the upper surface, while a peak structure develops near $q_i = 0$ that gets increasingly localized and increasingly sharp as the atom decay process completes and the photon is fully emitted. It is this peak structure in the potential driving the photonic system that excites the system from the zero-photon state towards the one-photon state.

We turn now to the components of this exact surface. In the weighted BO surface, $\epsilon_{\mathrm{wBO}}(q_i,t)$ that is plotted in the middle right panel, we see the same peeling away from the outer edges, but sticking resolutely to the original upper surface at $q_i = 0$. As the decay occurs, $\epsilon_{\mathrm{wBO}}(q_i,t)$ gradually melts to the lower surface everywhere except for a shrinking region near the origin that sticks to the upper surface. The peak seen in the full q-TDPES on the other hand comes from $\epsilon_{\mathrm{kin}}(q_i,t)$, plotted in the lower left panel, which gets sharper and sharper as the photon is emitted. Mathematically, this structure follows from the change in the conditional-dependence of $\Phi_{\underline{\underline{\mathbf{q}}}}$ near $q_i = 0$, as the electronic state associated with $q_i = 0$ remains on the upper q-BO surface while away from $q = 0$, in a shrinking region, the electronic state is associated with the lower surface. This gets sharper as $\chi(q_i = 0,t)$ gets smaller and smaller there. One can show from the analytic solution, that, in the long-time limit, the surface at $q_i = 0$ grows exponentially with t at a rate determined by Γ, while for $q \neq 0$, $\epsilon_{\mathrm{kin}}(q_i \neq 0, t \to \infty) \to 0$.

These features of ϵ_{wBO} and ϵ_{kin} are very similar for both the cross-section that cuts along the resonant mode (Fig. 3) and the section that cuts along the slightly off-resonant (Fig. 4). The remaining component of the q-TDPES, ϵ_{GD} is much smaller than the other components, and has a different structure in the two cases. In fact, it is straightforward to show from the analytic solution that $\epsilon_{\mathrm{GD}}(q_i = 0,t)$ is independent of t, and that uniformly shifting $\epsilon_{\mathrm{GD}}(q_i,t)$ so that $\epsilon_{\mathrm{GD}}(q_i = 0,t) \equiv 0$ yields $\epsilon_{\mathrm{GD}}(q_i \neq 0, t \gg \Gamma) \to \omega_0 - \omega_i$ for q_i large. That is,

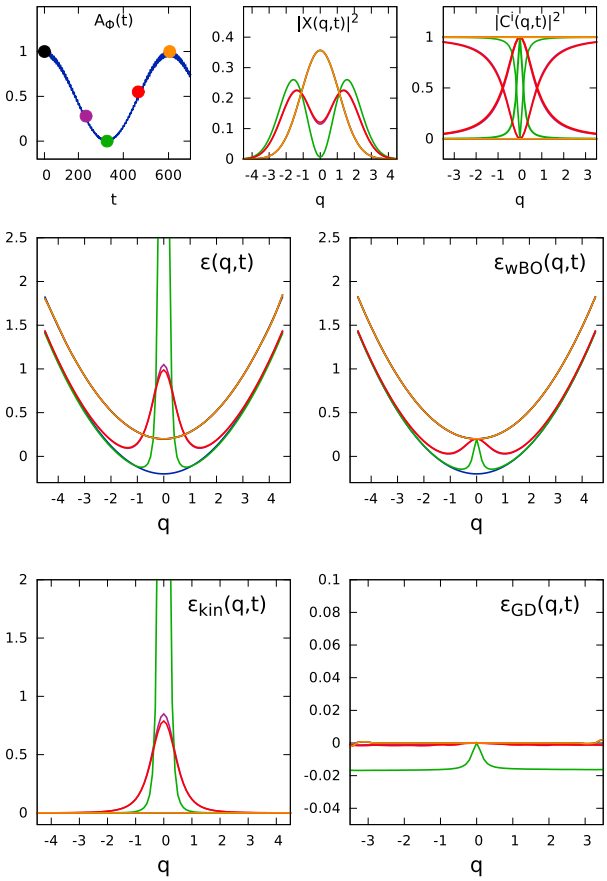

Fig. 5. The $\epsilon(q,t)$ for the excited BO initial state and coupling strength $d_{\rm eg}\lambda = 0.01$. The top left panel shows $A_\Phi(t)$, where the different colored dots depict the times of the dynamics within this plot. The top middle and right plots show the photonic distribution $|\chi(q,t)|^2$ and the electronic coefficients in the BO basis, $|C^{(1)}(q_i;t)|^2$ (dashed), $|C^{(2)}(q_i;t)|^2$ (solid), for the time snapshots shown. The middle and lower panel show the q-TDPES $\epsilon(q,t)$ and its decomposition into components for the given time snapshots. The q-BO surfaces are shown in the middle panel in blue for reference.

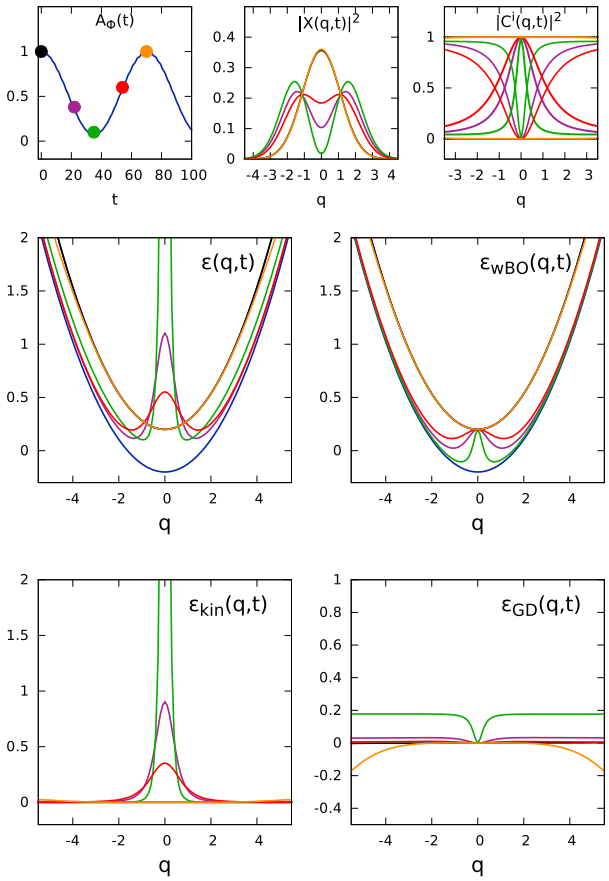

Fig. 6. As in Figure 5 but with coupling strength $d_{\rm eg}\lambda = 0.1$.

there is a symmetric step-like feature in $\epsilon_{\rm GD}$, of the size of the difference in the mode frequency of interest and the resonant mode, and as t gets larger, this feature sharpens.

Thus, we can see that in the Wigner–Weisskopf limit, the potential driving the photonic modes deviates significantly from its initial harmonic form during the decay, although once again becoming harmonic almost everywhere (except at $q = 0$) in the long-time limit. The atom-photon correlation is required to capture these effects, and if one wanted to model this exact q-TDPES, the conditional dependence of the electronic amplitude is crucial to include.

3.2 Two-level system coupled to a single resonant cavity photon mode

We now turn to the other limit, tuning the cavity so that there is just one mode that couples appreciably to the two-level atom, with a mode frequency that is resonant with the atomic energy difference.

The q-BO surfaces can be easily found by diagonalizing $H_{\rm qBO}$ of equation (34), keeping only one mode with $\omega_\alpha = \omega_0$ in the field:

$$\epsilon_{\rm qBO}(q) = \frac{1}{2}\omega_0^2 q^2 \mp \sqrt{\omega_0^2/4 + (d_{\rm eg}\lambda\omega_0)^2 q^2}. \qquad (52)$$

For couplings $\lambda d_{\rm eg} \ll 1/2$, the q-BO surfaces are approximately parallel and harmonic except at large q (see also Ref. [34]). So in this case if the initial photonic state is a vacuum, then the ensuing dynamics is driven by a largely harmonic potential, without much perturbation from the atom, except at larger q. Deviations from parallel harmonic surfaces, and hence non-q-BO behavior, occurs at larger q and as the coupling increases. We will investigate the q-TDPES driving the photonic dynamics for three different coupling strengths, ($d_{\rm eg}\lambda = \{0.01, 0.1, 0.4\}$) and will include a plot of the two q-BO surfaces with our results for comparison with the exact q-TDPES.

In Figures 5–7, we plot the exact q-TDPES for coupling strengths $d_{\rm eg}\lambda = 0.01, 0.1$ and 0.4, respectively, beginning with the atom in the excited q-BO level, multiplied by the photonic ground-state. On the upper panel (left) we plot the autocorrelation function

$$A_\Psi(t) = \left| \int dq \overrightarrow{\Psi}^\dagger(q,0) \cdot \overrightarrow{\Psi}(q,t) \right|^2 \qquad (53)$$

Eur. Phys. J. B (2018) 91: 180

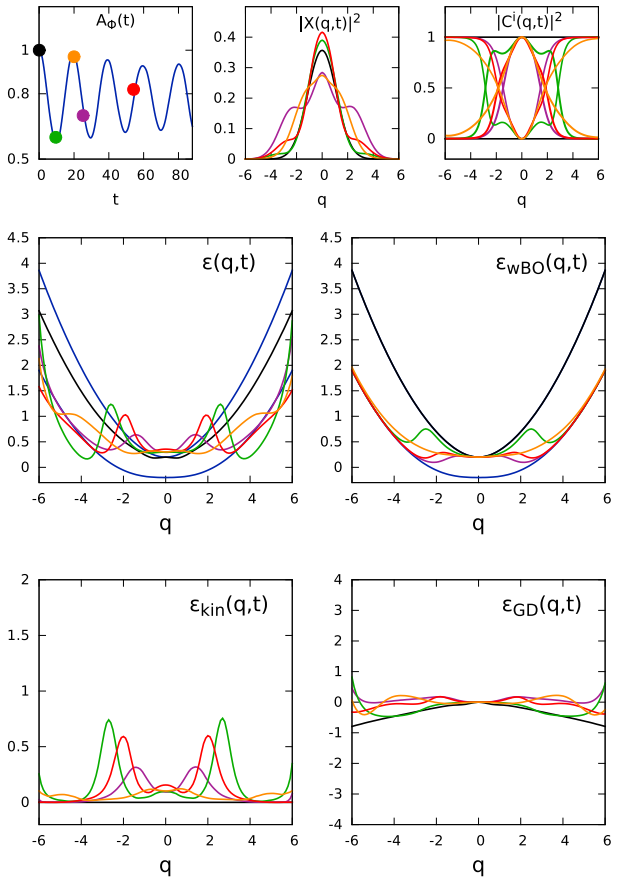

Fig. 7. As in Figure 5 but with coupling strength $d_{eg}\lambda = 0.4$.

to indicate the approximate periodicity of the system dynamics. Comparing $A_\Psi(t)$ in these three figures, we find a decrease of the approximate period with the increase of coupling strength until the periodicity breaks down for the strong coupling $d_{eg}\lambda = 0.4$. The weakest coupling strength we have chosen is on the borderline of being in the Rabi regime [61], while the strongest is far from it.

The photonic distribution (middle) and conditional electronic coefficients (right) are shown in the top panel of Figures 5–7. The initial coefficients are $C^{(1)}(q,0) = 1$ and $C^{(2)}(q,0) = 0$. After some time we see a transition of the electron from the excited state to the ground-state as indicated by these coefficients. We observe that the transfer begins earlier for higher values of q and then is followed by lower q-values, and again the conditional amplitude at $q = 0$ sticks to the upper surface at all times in all cases as there is no coupling for $q = 0$. The q-dependence of these coefficients has a significant role in shaping the structure of the q-TDPES that we will shortly discuss. At the same time, the probability of photon emission increases, as indicated by the morphing of the initial gaussian in $\chi(q,t)$ towards its first-excited profile. For the weakest coupling strength (Fig. 5), after a half period the system begins to move back approximately to its initial state, as the photon is reabsorbed and atom becomes excited again. For strong coupling $d_{eg}\lambda = 0.4$ (Fig. 7), the periodic character is lost and we find more wells and structure appearing in the displacement-field density profile. With such strong coupling the q-BO surfaces are quite distorted from a pure harmonic, as evident in the plot (blue lines in the middle panel), and the anharmonicity brings more frequencies into play. A one-photon state that is associated with the lower q-BO surface has a wider profile with density maxima further out than a one-photon state associated with the upper surface would have, for example. In fact the character of the coupled cavity-matter system becomes quite mixed, as is evident from the conditional electronic coefficients shown on the right, and as one goes along the photonic coordinate q one associates with different superpositions of the electronic states. This leads to interesting structure in the exact q-TDPES, that, when decomposed in terms of the q-BO surfaces, has components that vary a lot with q (i.e. not just approximately piecewise-in-q).

The q-TDPES for initial state prepared in the upper q-BO state begins with the weighted q-BO component, ϵ_{wBO} (middle right panel) on top of the upper q-BO surface as expected. For the weakest coupling, $d_{eg}\lambda = 0.01$, $\epsilon_{wBO}(q,t)$ then melts down to the lower surface over half a cycle, peeling away from the outer higher q-values first, in a similar way to what was seen in the Wigner–Weisskopf limit. This potential approaches the lower surface before returning back to the upper q-BO surface, but the region near $q = 0$ remains bound to the upper surface. The time-dependent double-well structure in the potential is again important in driving the photon emission. A similar trend is seen for the stronger coupling 0.1 in Figure 6, but for the strongest coupling $d_{eg}\lambda = 0.4$ of Figure 7, $\epsilon_{wBO}(q,t)$ shows a more complicated correlation in q, with structures mirroring those in the displacement-field density discussed above. As for the kinetic component, for the weaker couplings, a peak structure in $\epsilon_{kin}(q,t)$ (lower left panel) develops that grows and narrows during the photon emission stage, similar to what was seen in Wigner–Weisskopf, but this then reverses during the reabsorption here. Again for the stronger coupling, the structure is more complicated, mirroring the more complicated dynamics. The gauge-dependent part, ϵ_{GD} (lower right panel) is generally a smaller contribution to the total q-TDPES compared to the other components, but again we see step-like features for the weaker couplings, and more complicated dynamics for the strongest coupling.

The dynamics depends significantly on whether the initial state is the correlated q-BO state of Figures 5–7, or a fully factorized one, and now we turn to the surfaces, conditional probabilities, and displacement-field densities for the latter case, plotted in Figures 8–10. The initial coefficients were $C^{(1)}(q,0) = 1$ and $C^{(2)}(q,0) = 0$ when beginning in the q-BO states, but when beginning in the fully factorized state, these coefficients deviate from these uniform values, especially for larger q, with deviation increasing with the coupling strength. Although the photonic field still begins in the vacuum state, the electronic state is not purely in the upper q-BO surface; the electronic state associated with larger q already has some component in the ground-state. So at these larger values of q, the initial $\epsilon_{wBO}(q,0)$ surface dominates the q-TDPES and is anharmonic from the very start, lying intermediate between the upper and lower q-BO surface. In the weak

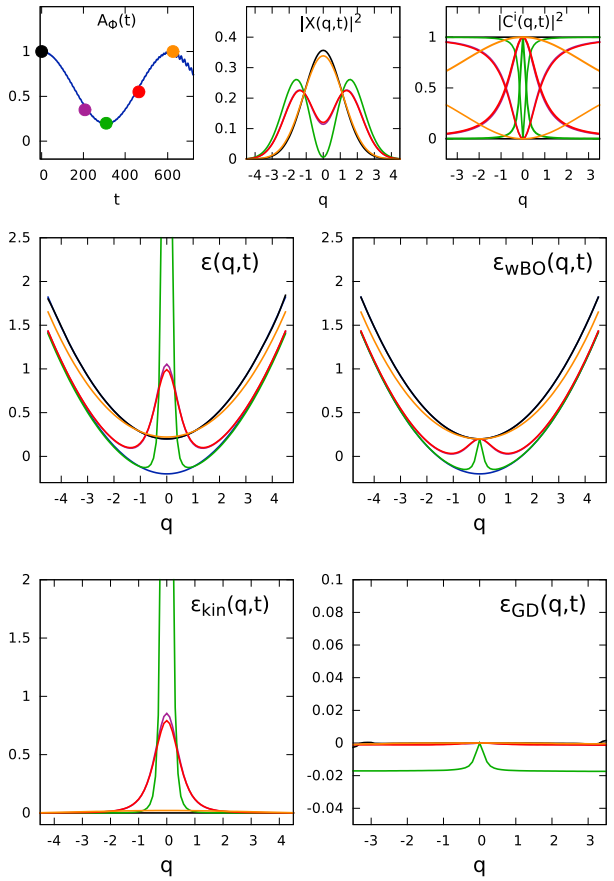

Fig. 8. As in Figure 5 with coupling strength $d_{\rm eg}\lambda = 0.01$ but with the initial purely factorized state.

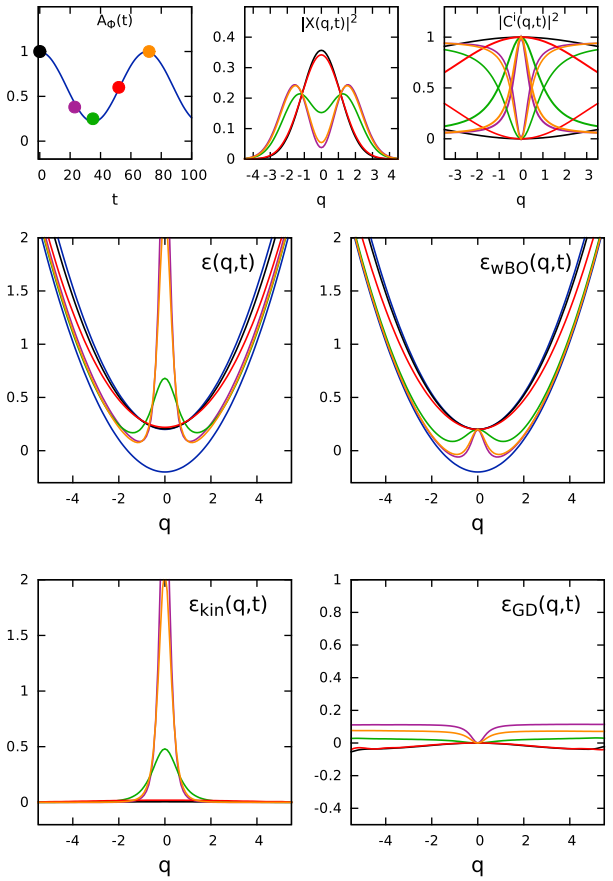

Fig. 9. As in Figure 6 with coupling strength $d_{\rm eg}\lambda = 0.1$ but with the initial purely factorized state.

coupling case, the differences are only large at values of q much larger than shown in the plot, and these are physically unimportant given there is very little photonic field probability there; hence Figures 5 and 8 are almost identical. For strong couplings, comparing Figures 7 and 10 show that the q-TDPES has a tamer structure for the fully-factorized initial state than for the correlated q-BO initial state, especially at larger q; this is likely because less energy is available at these larger q for the system to exchange between the atomic and photonic systems because the atomic state correlated with large q is not completely in its excited state initially.

To summarize: at time zero the exact q-TDPES starts on the upper q-BO-surface, which, depending on coupling strength and choice of initial state, ranges from lying directly on top of the upper q-BO surface (weaker coupling and with q-BO initial state), to in between the two q-BO surfaces with deviations from the upper being larger for larger q (stronger coupling, or fully factorized initial state). After some time the potential starts to melt down onto the lower BO-surface, first starting at higher q-values and then followed by lower q-values, with peak structures developing in the interior region. Around $q = 0$ the kinetic-component dominates, which leads to an increasing and after half a period decreasing peak. For stronger coupling we observe several peak features in the potential and significant deviations from the curvature of the q-BO surfaces throughout q small contribution below the lower BO-surface; the deviations at larger q arise from the gauge-dependent component.

4 Summary and outlook

We have introduced an extension of the exact–factorization approach, originally derived for coupled electron-nuclear systems, to light-matter systems in the non- relativistic limit within the dipole approximation. We have presented different possible choices for the factorization but in this work have focussed on the one where the marginal is chosen as the photonic system and the matter system is then conditionally-dependent on this. This choice is particularly relevant when one is primarily interested in the state of the radiation field since the exact factorization yields a time-dependent Schrödinger equation for the marginal, while the conditional is described by an equation with an unusual matter-photon coupling operator. The equation for the marginal is, in a sense, simpler than that in the electron-nuclear case, since the vector potential, q-TDVP, appearing in the equation can always be chosen to be zero, so only a scalar potential remains, the q-TDPES. We have studied the potential appearing in this equation in a gauge where the q-TDVP is zero, for a two-level system coupled to an infinite number of

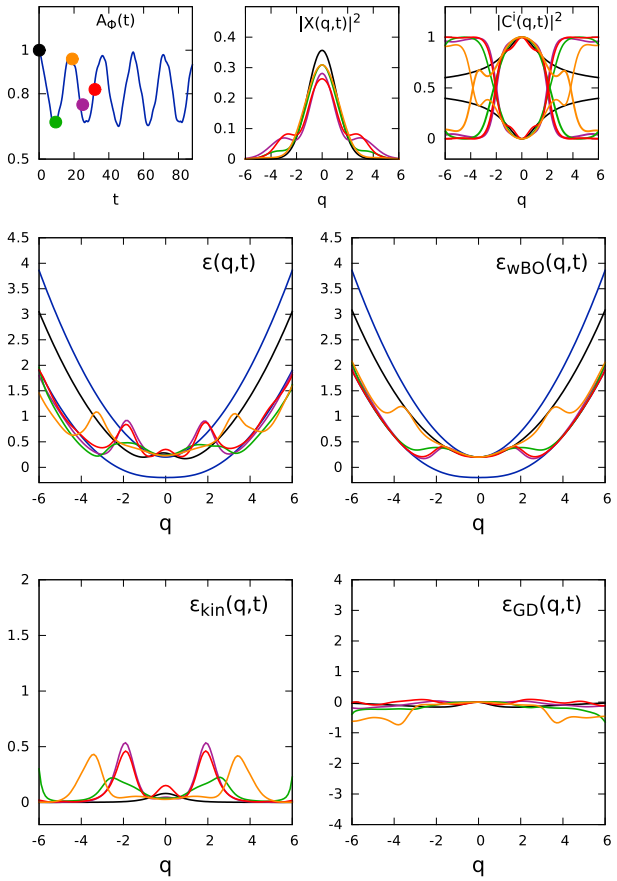

Fig. 10. As in Figure 7 with coupling strength $d_{eg}\lambda = 0.4$ but with the initial purely factorized state.

modes in the Wigner–Weisskopf approximation, and for a two-level system coupled to a single photonic field mode with a range of coupling strengths. In all cases we find a very interesting structure of the potential that drives the photonic dynamics, and in particular, large deviations from the harmonic form of the free-photon field. These deviations completely incorporate the effect of the matter system on the photonic dynamics. We also studied the effect of beginning in an initially purely factorized light-matter state, compared to a q-BO initial state, finding significant differences for larger coupling strengths in the ensuing dynamics, implying that in modelling these problems a careful consideration of the initial state is needed.

To use the exact factorization for realistic light-matter systems, approximations will be needed, since solving the exact factorization equations is at least as computationally expensive as solving the Schrödinger equation for the fully coupled system. The success of such an approximation depends on how well the q-TDPES is modelled. The components of the exact q-TDPES beyond the weighted BO depend significantly on the q-dependence of the conditional probability amplitude; approximations that neglect this dependence (Ehrenfest-like) will likely lead to errors in the dynamics. It has been shown recently that mixed quantum-classical trajectory methods that are derived from the exact factorization approach can correctly capture decoherence effects [62–64]. Since photons are intrinsically non-interacting and therefore even simpler to treat than nuclei, we expect in analogy to the electron-nuclear case that semiclassical trajectory methods derived from systematic and controlled approximations to the full exact factorization of the light-matter wavefunction will be able to capture decoherence effects beyond the Ehrenfest limit for light-matter coupling. This will be subject of future investigations.

We acknowledge financial support from the European Research Council(ERC-2015-AdG-694097) and European Union's H2020 programme under GA no.676580 (NOMAD) (NMH, HA, and AR). Financial support from the US National Science Foundation CHE-1566197 is also gratefully acknowledged (NTM). Open access funding provided by Max Planck Society.

Author contribution statement

All authors contributed to the design and implementation of the research, to the analysis of the results and to the writing of the manuscript.

References

1. E. Orgiu et al., Nat. Mater. **14**, 1123 (2015)
2. A. Csehi, G.J. Halász, L.S. Cederbaum, A. Vibók, J. Phys. Chem. Lett. **8**, 1624 (2017)
3. M. Gross, S. Haroche, Phys. Rep. **93**, 301 (1982)
4. N.I. Gidopoulos, E.K.U. Gross, Philos. Trans. R. Soc. Lond. A: Math., Phys. Eng. Sci. **372**, 2011 (2014)
5. A. Abedi, N.T. Maitra, E.K.U. Gross, Phys. Rev. Lett. **105**, 123002 (2010)
6. A. Abedi, N.T. Maitra, E.K.U. Gross, J. Chem. Phys. **137**, 22A530 (2012)
7. G. Hunter, Int. J. Quantum Chem. **9**, 237 (1975)
8. Y. Suzuki, A. Abedi, N.T. Maitra, K. Yamashita, E.K.U. Gross, Phys. Rev. A **89**, 040501(R) (2014)
9. A. Maser, B. Gmeiner, T. Utikal, S. Götzinger, V. Sandoghdar, Nat. Photonics **10**, 450 (2016)
10. C. Riek, D.V. Seletskiy, A.S. Moskalenko, J.F. Schmidt, P. Krauspe, S. Eckart, S. Eggert, G. Burkard, A. Leitenstorfer, Science **350**, 420 (2015)
11. A.S. Moskalenko, C. Riek, D.V. Seletskiy, G. Burkard, A. Leitenstorfer, Phys. Rev. Lett. **115**, 263601 (2015)
12. J. George, T. Chervy, A. Shalabney, E. Devaux, H. Hiura, C. Genet, T.W. Ebbesen, Phys. Rev. Lett. **117**, 153601 (2016)
13. T. Byrnes, N.Y. Kim, Y. Yamamoto, Nat. Phys. **10**, 803 (2014)
14. J. Kasprzak et al., Nature **443**, 409 (2006)
15. M.A. Sentef, M. Ruggenthaler, A. Rubio, arXiv:1802.09437 (2018)

16. S. Schmidt, Phys. Scr. **91**, 073006 (2016)
17. X. Zhong, T. Chervy, L. Zhang, A. Thomas, J. George, C. Genet, J. Hutchison, T.W. Ebbesen, Angew. Chem. Int. Ed. **56**, 9034 (2017)
18. D.M. Coles, Y. Yang, Y. Wang, R.T. Grant, R.A. Taylor, S.K. Saikin, A. Aspuru-Guzik, D.G. Lidzey, J.K.H. Tang, J.M. Smith, Nat. Commun. **5**, 5561 (2014)
19. J. Galego, F.J. Garcia-Vidal, J. Feist, Nat. Commun. **7**, 13841 EP (2016)
20. J. Flick, M. Ruggenthaler, H. Appel, A. Rubio, Proc. Natl. Acad. Sci. **114**, 3026 (2017)
21. T.W. Ebbesen, Acc. Chem. Res. **49**, 2403 (2016)
22. A. Thomas et al., Angew. Chem. **128**, 11634 (2016)
23. B. Barnes, F. García Vidal, J. Aizpurua, ACS Photonics **5**, 43 (2018)
24. F. Herrera, F.C. Spano, ACS Photonics **5**, 65 (2018)
25. J. Feist, J. Galego, F.J. Garcia-Vidal, ACS Photonics **5**, 205 (2018)
26. R.F. Ribeiro, L.A. Martínez-Martínez, M. Du, J. Campos-Gonzalez-Angulo, J. Yuen-Zhou, arXiv:1802.08681 (2018)
27. M. Ruggenthaler, N. Tancogne-Dejean, J. Flick, H. Appel, A. Rubio, Nat. Rev. Chem. **2**, 0118 (2018)
28. K.E. Dorfman, F. Schlawin, S. Mukamel, J. Phys. Chem. Lett. **5**, 2843 (2014)
29. K.E. Dorfman, F. Schlawin, S. Mukamel, Rev. Mod. Phys. **88**, 045008 (2016)
30. Z. Ficek, P.D. Drummond, Phys. Today **50**, 34 (1997)
31. D.N. Matsukevich, A. Kuzmich, Science **306**, 663 (2004)
32. E.J. Heller, J. Chem. Phys. **65**, 1289 (1976)
33. F.H. Faisal, *Theory of Multiphoton Processes* (Springer, Berlin, 1987)
34. J. Flick, H. Appel, M. Ruggenthaler, A. Rubio, J. Chem. Theory Comput. **13**, 1616 (2017)
35. I.V. Tokatly, Phys. Rev. Lett. **110**, 233001 (2013)
36. C. Pellegrini, J. Flick, I.V. Tokatly, H. Appel, A. Rubio, Phys. Rev. Lett. **115**, 093001 (2015)
37. J. Flick, M. Ruggenthaler, H. Appel, A. Rubio, Proc. Natl. Acad. Sci. **50**, 15285 (2015)
38. D.P. Craig, T. Thirunamachandran, *Molecular Quantum Electrodynamics: An Introduction to Radiation-molecule Interactions* (Dover Publications, INC., Mineola, New York, 1998)
39. M. Ruggenthaler, J. Flick, C. Pellegrini, H. Appel, I.V. Tokatly, A. Rubio, Phys. Rev. A **90**, 012508 (2014)
40. V. Rokaj, D.M. Welakuh, M. Ruggenthaler, A. Rubio, J. Phys. B: Atomic, Mol. Opt. Phys. **51**, 034005 (2017)
41. G. Hunter, Int. J. Quantum Chem. **19**, 755 (1981)
42. A. Abedi, N.T. Maitra, E.K.U. Gross, J. Chem. Phys. **139**, 087102 (2013)
43. J.L. Alonso, J. Clemente-Gallardo, P. Echenique-Robba, J.A. Jover-Galtier, J. Chem. Phys. **139**, 087101 (2013)
44. S.K. Min, A. Abedi, K.S. Kim, E.K.U. Gross, Phys. Rev. Lett. **113**, 263004 (2014)
45. R. Requist, F. Tandetzky, E.K.U. Gross, Phys. Rev. A **93**, 042108 (2016)
46. R. Requist, C.R. Proetto, E.K.U. Gross, Phys. Rev. A **96**, 062503 (2017)
47. Y.C. Chiang, S. Klaiman, F. Otto, L.S. Cederbaum, J. Chem. Phys. **140**, 054104 (2014)
48. J. Galego, F.J. Garcia-Vidal, J. Feist, Phys. Rev. X **5**, 041022 (2015)
49. Y. Suzuki, A. Abedi, N. Maitra, E.K.U. Gross, Phys. Chem. Chem. Phys. **17**, 29271 (2015)
50. E. Khosravi, A. Abedi, N.T. Maitra, Phys. Rev. Lett. **115**, 263002 (2015)
51. T. Fiedlschuster, J. Handt, E.K.U. Gross, R. Schmidt, Phys. Rev. A **95**, 063424 (2017)
52. A. Schild, E. Gross, Phys. Rev. Lett. **118**, 163202 (2017)
53. A. Abedi, F. Agostini, Y. Suzuki, E.K.U. Gross, Phys. Rev. Lett. **110**, 263001 (2013)
54. F. Agostini, A. Abedi, Y. Suzuki, S.K. Min, N.T. Maitra, E.K.U. Gross, J. Chem. Phys. **142**, 084303 (2015)
55. B.F.E. Curchod, F. Agostini, E.K.U. Gross, J. Chem. Phys. **145**, 034103 (2016)
56. A. Scherrer, F. Agostini, D. Sebastiani, E.K.U. Gross, R. Vuilleumier, Phys. Rev. X **7**, 031035 (2017)
57. A. Scherrer, F. Agostini, D. Sebastiani, E.K.U. Gross, R. Vuilleumier, J. Chem. Phys. **143**, 074106 (2015)
58. K. Hader, J. Albert, E.K.U. Gross, V. Engel, J. Chem. Phys. **146**, 074304 (2017)
59. B.F.E. Curchod, F. Agostini, J. Phys. Chem. Lett. **8**, 831 (2017)
60. M. Scully, A. Zubairy, *Quantum Optics* (Cambridge University Press, Cambridge, New York, 1997)
61. H.I. Yoo, J. Eberly, Phys. Rep. **118**, 239 (1985)
62. S.K. Min, F. Agostini, I. Tavernelli, E.K.U. Gross, J. Phys. Chem. Lett. **8**, 3048 (2017)
63. F. Agostini, S.K. Min, A. Abedi, E.K.U. Gross, J. Chem. Theory Comput. **12**, 2127 (2016)
64. S.K. Min, F. Agostini, E.K.U. Gross, Phys. Rev. Lett. **115**, 073001 (2015)

2.3 MIXED-QUANTUM CLASSICAL AND PERTURBATIVE METHODS FOR PHOTONS

"Benchmarking Semiclassical and Perturbative Methods for Real-time Simulations of Cavity-Bound Emission and Interference"

NM Hoffmann, C Schäfer, N Säkkinen, A Rubio, H Appel, A Kelly,

The Journal of Chemical Physics, (2019), 151 (24), 244113

MOTIVATION AND STATE OF THE ART Continuing our work of Sec. 2.1, the overall motivation for this work as well as the current state of the art research stays the same. However, based on the knowledge obtained from [O1], we now broaden our scope of investigation and target the question: How can we improve the results found within the MTEF, i.e. additionally capture interference effects and obtain quantitatively more accurate results, by going beyond the mean-field approach towards more advanced methods?

CONTRIBUTION AND MAIN FINDINGS In the present work we investigate the performance of a comprehensive class of MQC approaches for simulating spontaneous emission in an optical cavity, including the MTEF approach [15, 17–19], fewest switch surface hopping algorithm [29–34], fully linearized and partially linearized semiclassical dynamics techniques [20–26], and a selection of finite size corrected second Born BBGKY truncations [137–140]. More precisely, for all trajectory based methods the general extension to the photonic degrees of freedom is carried out analogously to [O1], i.e. Wigner sampling for the photons, while propagating the trajectories corresponding to the given either classical or now also semiclassical equations of motion. Considering the BBGKY we compare different restrictions and find that by restricting to the single electron subspace as well as enforcing at most a single photon in the cavity for the two level system, we obtain the best performance and therefore focus on those results in comparison with the classical and semiclassical approaches. Here, we find that with the exception of the fewest switch surface hopping all methods are able to capture quantum effects such as spontaneous emission and bound photon states and give a reasonable level of accuracy for the correlated light-matter dynamic. Additionally, although not fully accurate, the path integral methods are able to capture some level of interference effects.

OUTLOOK With respect to extrapolations towards realistic systems, we identify the MTEF approach as well as the path integral methods as the most promising

methods for applications along these lines. Furthermore, both methods exhibit similar convergence with respect to the trajectory numbers and allow a significant reduction of total run-time due to uncoupled trajectories during the time propagation. In contrast, a treatment of the photons within the fewest switch surface hopping approach would not be favourable due to its relatively poor performance, whereas BBGKY, although performing exceptionally well for the applied model systems, features a rather unfavourable high-order polynomial scaling, which restricts this method to comparable small systems. Therefore, following the outlook of Sec. 2.1, combining the *ab initio* light-matter coupling methodology introduced in [51] with either the MTEF or a path integral based methods could provide a computationally feasible way to simulate photon-field fluctuations and correlations in realistic three-dimensional systems.

The Journal of Chemical Physics ARTICLE scitation.org/journal/jcp

Benchmarking semiclassical and perturbative methods for real-time simulations of cavity-bound emission and interference

Cite as: J. Chem. Phys. 151, 244113 (2019); doi: 10.1063/1.5128076
Submitted: 16 September 2019 • Accepted: 29 November 2019 •
Published Online: 26 December 2019

Norah M. Hoffmann,[1,a),b)] Christian Schäfer,[1,a),c)] Niko Säkkinen,[1,d)] Angel Rubio,[1,e)] Heiko Appel,[1,f)] and Aaron Kelly[1,2,g)]

AFFILIATIONS

[1] Department of Physics, Max Planck Institute for the Structure and Dynamics of Matter and Center for Free-Electron Laser Science, 22761 Hamburg, Germany
[2] Department of Chemistry, Dalhousie University, Halifax, Nova Scotia B3H 4R2, Canada

[a)] **Contributions:** N. M. Hoffmann and C. Schäfer contributed equally to this work.
[b)] **Electronic mail:** norah-magdalena.hoffmann@mpsd.mpg.de
[c)] **Electronic mail:** christian.schaefer@mpsd.mpg.de
[d)] **Electronic mail:** nsakkinen@gmail.com
[e)] **Electronic mail:** angel.rubio@mpsd.mpg.de
[f)] **Electronic mail:** heiko.appel@mpsd.mpg.de
[g)] **Electronic mail:** aaron.kelly@dal.ca

ABSTRACT

We benchmark a selection of semiclassical and perturbative dynamics techniques by investigating the correlated evolution of a cavity-bound atomic system to assess their applicability to study problems involving strong light-matter interactions in quantum cavities. The model system of interest features spontaneous emission, interference, and strong coupling behavior and necessitates the consideration of vacuum fluctuations and correlated light-matter dynamics. We compare a selection of approximate dynamics approaches including fewest switches surface hopping (FSSH), multitrajectory Ehrenfest dynamics, linearized semiclassical dynamics, and partially linearized semiclassical dynamics. Furthermore, investigating self-consistent perturbative methods, we apply the Bogoliubov-Born-Green-Kirkwood-Yvon hierarchy in the second Born approximation. With the exception of fewest switches surface hopping, all methods provide a reasonable level of accuracy for the correlated light-matter dynamics, with most methods lacking the capacity to fully capture interference effects.

I. INTRODUCTION

Profound changes in the properties of cavity-bound molecular systems can be achieved in regimes where the quantum nature of light becomes important. A few notable examples are the change in conductivity in semiconductors due to vacuum field hybridization,[1] the appearance of mixed states due to strong coupling,[2,3] and multiple Rabi splittings caused by ultrastrong vibrational coupling.[4] Although the forefront of the rapidly expanding domain of cavity-modified chemistry has been strongly driven by experiments, theoretical investigations have offered complementary insights into the various possibilities opening up with this new field of research.[5–16]

Describing chemical processes that are strongly correlated with quantum light[17–19] requires an accurate and flexible, furthermore computationally efficient, treatment of the light-matter interactions. Thus, in order to meet the demand of developing an *ab initio* theoretical description of cavity modified chemical systems, extensions to the traditional theoretical toolkits for quantum optics and quantum chemistry are required. In this paper, we focus on

The Journal of Chemical Physics ARTICLE scitation.org/journal/jcp

semiclassical dynamics methods, which due to the simplicity, efficiency, and especially scalability, present an interesting alternative or extension to existing quantum electrodynamical wavefunction[20–23] and density-functional (QEDFT) based approaches.[15,24–26]

The semiclassical concept has the advantage of providing an intuitive qualitative understanding of the dynamics through trajectories in phase space. Furthermore, many semiclassical methods do not exhibit an exponential scaling of the computational effort with system size or simulation time. However, these methods can fail to quantitatively, and sometimes even qualitatively, describe all of the relevant physical features in a variety of nonadiabatic reactive scattering and excited state relaxation processes, such as nuclear interference and detailed balance.[27,28] Hence, benchmark tests of these approaches are needed in this particular regime of the problem in order to be able to verify their viability. In order to address some of these challenges, we have recently shown the potential of the Multitrajectory Ehrenfest (MTEF) method to capture the correlated dynamics of a one-dimensional QED cavity-setup with a two-level atomic system coupled to a large set of cavity photon-modes.[29] Furthermore, we note that in contrast to recent work of Subotnik and co-workers, who investigated light-matter interaction with an adjusted Ehrenfest theory based method to simulate spontaneous emission of classical light,[30–32] we focus on the description of quantized light fields.

Here, we broaden our scope by investigating the performance of a comprehensive class of approximate quantum dynamics methods for simulating spontaneous emission in an optical cavity, including Ehrenfest mean-field theory,[33,34] Tully's surface hopping algorithm,[35] fully linearized[36] and partially linearized[37,38] semiclassical dynamics techniques, and a selection of approximate closures for the quantum mechanical Bogoliubov-Born-Green-Kirkwood-Yvon (BBGKY) hierarchy. Through benchmark comparisons with exact numerical results, we assess the accuracy and efficiency of each method and highlight the possibilities and theoretical challenges involved with extending these approaches toward realistic systems.

The remainder of this work is divided into four sections: Section II gives a short overview of general quantum mechanical light-matter interactions and a brief introduction of the class of model systems used in this study. Section III contains a short introduction to each of the selected dynamics methods that we consider in this work. In Sec. IV, we report the results of our benchmark tests of the performance of these techniques in describing spontaneous emission, stimulated absorption, and strongly correlated light-matter dynamics. In Sec. V, we offer some conclusions and outlooks.

II. ELECTRON-PHOTON CORRELATED SYSTEMS

The total Hamiltonian for a coupled light-matter system can be written as follows:

$$\hat{H} = \hat{H}_A + \hat{H}_F + \hat{H}_{AF}. \tag{1}$$

The first term, $\hat{H}_A$, is the matter Hamiltonian, which may be generally expressed in the spectral representation as follows:

$$\hat{H}_A = \sum_k \varepsilon_k |k\rangle\langle k|.$$

Here, $\{\varepsilon_k, |k\rangle\}$ are the energies and stationary states of the electron-nuclei system in the absence of coupling to the cavity. The second term is the Hamiltonian of the uncoupled cavity field $\hat{H}_F$,

$$\hat{H}_F = \frac{1}{2}\sum_{\alpha=1}^{2N}\left(\hat{P}_\alpha^2 + \omega_\alpha^2 \hat{Q}_\alpha^2\right). \tag{2}$$

The photon-field operators, $\hat{Q}_\alpha$ and $\hat{P}_\alpha$, obey the canonical commutation relation, $[\hat{Q}_\alpha, \hat{P}_{\alpha'}] = \imath\hbar\delta_{\alpha,\alpha'}$, and can be expressed using creation and annihilation operators for each mode of the cavity field,

$$\hat{Q}_\alpha = \sqrt{\frac{\hbar}{2\omega_\alpha}}(\hat{a}_\alpha^\dagger + \hat{a}_\alpha), \quad \hat{P}_\alpha = i\sqrt{\frac{\hbar\omega_\alpha}{2}}(\hat{a}_\alpha^\dagger - \hat{a}_\alpha),$$

where $\hat{a}_\alpha^\dagger$ and $\hat{a}_\alpha$ denote the usual photon creation and annihilation operators for photon mode α. The coordinatelike operators, $\hat{Q}_\alpha$, are directly proportional to the electric displacement operator, while the conjugate momentalike operators, $\hat{P}_\alpha$, are related to the magnetic field.[25,39,40] The upper limit of the sum in Eq. (2) is $2N$, as there are (in principle) two independent polarization degrees of freedom for each photon mode; however in the 1D cavity models presented here only a single polarization will be considered.

The final term in Eq. (1) represents the coupling between the electron-nuclei system and the cavity field. In Coulomb gauge, and the dipole approximation,[15,39] this term can be written as follows:

$$\hat{H}_{AF} = \sum_{\alpha=1}^{2N}\left(\omega_\alpha \hat{Q}_\alpha(\lambda_\alpha \cdot \hat{\mu}) + \frac{1}{2}(\lambda_\alpha \cdot \hat{\mu})^2\right), \tag{3}$$

where we denote $\hat{\mu}$ as the electronic plus nuclear dipole moment and λ_α as the matter-photon coupling vector.[15,24,41] The featured methodologies can be generically applied to arbitrary complex matter systems.

With the demand for exact reference solutions, as part of the benchmarking procedure, we are forced to restrict the Hilbert-space of interest. Focusing on the evolution of the photonic degrees of freedom, we restrict the matter part to a highly simplified few-level atomic system trapped in a cavity[14,29,42] as depicted in Fig. 1. The fundamental limitations of the few-level approximation have been presented in a variety of recent publications.[16,23,26,43,44] While

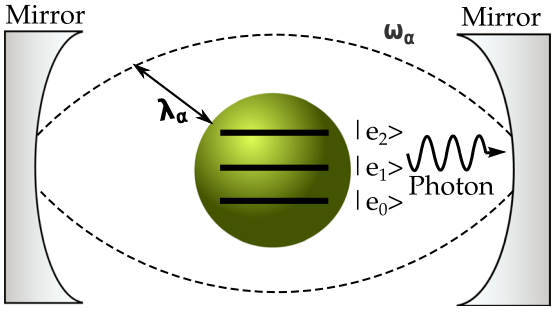

FIG. 1. Cavity-setup: Few-level approximated atomic system (green) trapped in a cavity and coupled by coupling strength λ_α to 400 photon modes with their photonic frequency ω_α, where $\alpha = \{1, 2, \ldots, 400\}$.

The Journal of Chemical Physics ARTICLE scitation.org/journal/jcp

this approximation results in a strongly simplified problem, it has the advantage that exact numerical results, although nontrivial to obtain, are still achievable with a reasonable computational effort. In the case of a two-level approximation of the matter system, the quadratic term $(\lambda_\alpha \cdot \hat{\mu})^2$ simply results in a constant energy shift and hence can be discarded.[23] For simplicity, we also neglect this term in the case of the three level model system, to remain consistent across setups and previous publications.[14,29,42,78] However, the quadratic term is generally important to consider as it stems from a proper definition of field observables, renders the system stable, and is essential to retain gauge and translational invariance. Applications to realistic systems should of course consider this term; for a detailed discussion of this topic, one may refer to Ref. 44, for example.

In the case of a two-level atomic system, this corresponds to a special case of the spin-boson model. With the position of the atom fixed at $r_A = \frac{L}{2}$ in this study, half of the $2N$ cavity modes decouple from the atomic system by symmetry. We adopt the same parameters as in Refs. 14 and 45, which are based on a 1D Hydrogen atom with a soft Coulomb potential (in atomic units): $\{\varepsilon_1, \varepsilon_2\} = \{-0.6738, -0.2798\}$, $\lambda_\alpha(\frac{L}{2}) = 0.0103 \cdot (-1)^\alpha$, $L = 2.362 \cdot 10^5$, and $\mu_{12} = 1.034$.

For the three-level atom, we adopt all the same parameters for the field and the atom-field coupling as for the two-level case. The atomic energies for the three level model are $\{\varepsilon_1, \varepsilon_2, \varepsilon_3\} = \{-0.6738, -0.2798, -0.1547\}$, and as before the numerical parameters are based on the 1D soft-Coulomb hydrogen atom. The dipole moment operator only couples adjacent states such that the only nonzero matrix elements are $\{\mu_{12}, \mu_{23}\} = \{1.034, -2.536\}$ and their conjugates.

Furthermore, with $\frac{g_{2,1}}{\varepsilon_2-\varepsilon_1} = 1.2 \cdot 10^{-2}$ for the two-level system and $\frac{g_{3,2}}{\varepsilon_3-\varepsilon_2} = 2.1 \cdot 10^{-2}$ for the three-level system, where $g_{i,j} = \mu_{k,l}\sqrt{\frac{\varepsilon_i-\varepsilon_j}{2}}\lambda$ is the coupling strength for the resonant mode, our system is beyond common perturbative approaches most illustratively indicated by the appearances of a bound photon peak in the intensity as consequence of counter-rotating components. Cavity losses are not considered at this point but could be included in future developments.

III. METHODS

A. Multitrajectory methods

In this section, we briefly review a selection of semiclassical dynamics methods that are based on ensembles of independent trajectories. These methods have been introduced traditionally to study electron-nuclear systems, and they typically involve the use of the Wigner representation for the non-subsystem degrees of freedom. In this work, we extend the application of these methods to treat coupled quantum mechanical light-matter systems, in which the degrees of freedom of the photon field will be partially Wigner transformed. The structural similarity allows for the trivial inclusion of nuclear degrees of freedom. The general expression for the average value of any observable, $\langle B(t)\rangle$, in the partial Wigner representation can be written as follows:

$$\begin{aligned}\langle B(t)\rangle &= \mathrm{Tr}_A \int dX \hat{B}_W(X,t)\hat{\rho}_W(X,t=0),\\ &= \sum_{\lambda\lambda'} \int dX B_W^{\lambda\lambda'}(X,t)\rho_W^{\lambda'\lambda}(X),\end{aligned}$$

where the subscript W denotes the partial Wigner transform over the photonic degrees of freedom, which are represented on the continuous phase space $X = (R, P)$. The partial Wigner transforms for an arbitrary operator $\hat{B}$ and the density matrix $\hat{\rho}$ are defined as follows:[46]

$$\begin{aligned}\hat{B}_W(R,P) &= \int dZ e^{iP\cdot Z}\left\langle R - \frac{Z}{2}|\hat{B}|R + \frac{Z}{2}\right\rangle,\\ \hat{\rho}_W(R,P) &= \frac{1}{(2\pi\hbar)^{2N}}\int dZ e^{iP\cdot Z}\left\langle R - \frac{Z}{2}|\hat{\rho}|R + \frac{Z}{2}\right\rangle.\end{aligned}$$

Thus, in order to assemble the average value a multitrajectory method may be employed, which is essentially a hybrid Monte Carlo molecular dynamics method in which initial conditions are sampled from the initial Wigner distribution, and then an ensemble of molecular dynamics trajectories is used to evaluate the time-evolution of the property of interest.

1. Ehrenfest mean-field theory

The Ehrenfest equations of motion may be derived by assuming that the total density can be written as an uncorrelated product of the atomic and field reduced densities at all times, and then taking the appropriate classical limit,[33,34] or by starting with the quantum-classical Liouville equation (QCLE), which is formally exact for the class of systems studied here,[47] and then making the uncorrelated approximation, i.e.,

$$\hat{\rho}_W(X,t) = \hat{\rho}_A(t)\rho_{F,W}(X,t),$$

where the reduced density matrix of the atomic system is as follows:

$$\hat{\rho}_A(t) = \mathrm{Tr}_F\left(\hat{\rho}_W(X,t)\right) = \int dX \hat{\rho}_W(X,t),$$

and the Wigner function of the cavity field is $\rho_{F,W}(X,t) = Tr_A(\hat{\rho}_W(X,t))$. The Ehrenfest mean-field equations of motion for the atomic system are as follows:

$$\partial_t\hat{\rho}_A(t) = -i\left[\hat{H}_A + \hat{H}_{AF,W}(X(t)), \hat{\rho}_A(t)\right],$$

where $\hat{H}_{AF,W}$ denotes the Wigner transform of the bilinear coupling and $\hat{H}_A$ the atomic Hamiltonian. The evolution of the Wigner function of the photon field can be represented as a statistical ensemble of independent trajectories with $\mathcal{N}$ being the ensemble size, where we select uniform weights $w^j = 1/\mathcal{N}$,

$$\rho_{F,W}(X,t) = \frac{1}{\mathcal{N}}\sum_{j=1}^{\mathcal{N}}\delta(X - X^j(t)),$$

that evolve according to Hamilton's equations of motion,

$$\frac{dQ_\alpha}{dt} = \frac{\partial H_{F,W}^{Eff}}{\partial P_\alpha}, \quad \frac{dP_\alpha}{dt} = -\frac{\partial H_{F,W}^{Eff}}{\partial Q_\alpha}.$$

The mean field photonic Hamiltonian is as follows:

$$H_{F,W}^{Eff} = \frac{1}{2}\sum_\alpha\left(P_\alpha^2 + \omega_\alpha^2 Q_\alpha^2 + 2\omega_\alpha\lambda_\alpha Q_\alpha\mu(t)\right),$$

where $\mu(t) = \mathrm{Tr}_A(\hat{\rho}_A(0)\hat{\mu}(t))$.

The Journal of Chemical Physics ARTICLE scitation.org/journal/jcp

2. Fewest switches surface-hopping

In the following, we outline the fewest switches surface hopping (FSSH) method for the electron-photon coupled system. FSSH allows feedback between the classical and quantum subsystems, which, however, requires the photons to always propagate on a particular electronic adiabatic state, with hops between adiabatic surfaces.[48–51]

Considering the mode displacement moving along some classical trajectory $R(t) = \{R_{\alpha=1}(t), \ldots, R_{2N}(t)\}$, the effective electronic Hamiltonian,

$$\hat{H}^{el}[R(t)] = \hat{H}_A + \hat{H}_{AF}[R(t)] + \frac{1}{2}\sum_{\alpha=1}^{2N}\omega_\alpha^2 R_\alpha(t)^2,$$

then becomes parametrically dependent on time through the photonic trajectory. Expanding the electronic wavefunction in the adiabatic basis yields the following:

$$\Psi(r,R,t) = \sum_i c_i(t)\phi_i(r,R(t)),$$

where r denotes the collection of all electronic degrees of freedom and $c_i(t)$ are time-dependent complex expansion coefficients. Assuming the photonic motion with the momentum $P(t)$ to be classical, the equation of motion is given by the following equation:

$$\begin{aligned}\partial_t\rho_{ij} = &-i\sum_k\left(H_{ik}^{el}[R(t)]\rho_{kj} - \rho_{ik}H_{kj}^{el}[R(t)]\right)\\ &- P(t)\cdot\sum_k\left(\mathbf{d}_{ik}^{\alpha}[R(t)]\rho_{kj} - \rho_{ik}\mathbf{d}_{kj}^{\alpha}[R(t)]\right),\end{aligned}$$

with the photon mode α and $\rho_{ij} = c_i(t)c_j^*(t)$ being the corresponding electronic density matrix. Furthermore, the movement of the photon is given by moving along a single potential energy surface except for some instantaneous switches. The probability for those switches, jumping from the current state i to another state j, is defined by the following:

$$g_{ij} = \frac{b_{ij}\Delta t}{\rho_{ii}},$$

where Δt is a time interval from t to $t + \Delta t$ and $b_{ij} = -2\mathrm{Re}(\rho_{ij}P(t)\cdot\mathbf{d}_{ij})$, with $\mathbf{d}_{ij} = \langle\phi_i(r,R(t))|\partial_R\phi_j(r,R(t))\rangle$ being the nonadiabatic coupling vector.

a. Semiclassical mapping methods. Here, we briefly sketch two semiclassical methods that are based on the mapping representation. These approaches can be rigorously derived from the path-integral formulation of the dynamics, or, for example, using the quantum-classical Liouville equation (QCLE).[38] Originally, however, the linearized semiclassical (LSC) approach has been developed through a stationary-phase approximation to the full path-integral, and subsequently applying a linearization approximation to the resulting subsystem propagator.[36]

With the intention of providing only the essential information about these techniques, we will briefly introduce the representation in a mapping basis and then simply give the expressions for the corresponding equations of motion and expectation values. The interested reader may refer to specific literature (e.g., Refs. 27, 37, 38, and 52–55 for example) for further information and technical details.

In order to achieve a classical-like description of the quantum subsystem, the Meyer-Miller-Stock-Thoss mapping representation[52,53] is used. Each subsystem state $|\lambda\rangle$ is represented by a mapping state $|m_\lambda\rangle$, that is, an eigenfunction of a system of N fictitious harmonic oscillators, that have occupation numbers which are constrained to be 0 or 1: $|\lambda\rangle \to |m_\lambda\rangle = |0_1, \ldots, 1_\lambda, \ldots 0_N\rangle$.

3. Linearized semiclassical dynamics

In the LSC method, the mapping version of an operator on the subsystem Hilbert space, $\hat{B}_m(X)$, is defined such that its matrix elements are equivalent to those of the corresponding operator, $\hat{B}_W(X)$. For example, the mapping Hamiltonian can be written as follows:[55]

$$\hat{B}_m(X) = \sum_{\lambda\lambda'} B_W^{\lambda\lambda'}(X)\hat{a}_\lambda^\dagger\hat{a}_{\lambda'},$$

where the creation and annihilation operators on the subsystem mapping states, $\hat{a}_\lambda^\dagger$ and $\hat{a}_\lambda$, satisfy the usual bosonic commutation relation $[\hat{a}_\lambda, \hat{a}_{\lambda'}^\dagger] = \delta_{\lambda\lambda'}$. Completing the Wigner transform over the subsystem, the mapping Hamiltonian can be written as a function of continuous phase space variables $(X, x) = (R, P, r, p)$,

$$B_m(X) = \sum_{\lambda\lambda'} B_W^{\lambda\lambda'}(X)(r_\lambda r_{\lambda'} + p_\lambda p_{\lambda'} - \delta_{\lambda\lambda'}).$$

The LSC time-evolution of an arbitrary operator in the mapping representation, $B_m(X)$, can be written as a classical-like dynamics in the extended Wigner-mapping phase space,

$$\frac{\partial}{\partial t}B_m(X,x,t) = \left\{H_m(X,x), B_m(X,x,t)\right\}_{X,x}.$$

Due to the Poisson bracket structure of this equation, the density can be obtained from the evolution of an ensemble of independent trajectories, $\rho_m(X,t) = \mathcal{N}^{-1}\sum_{i=1}^{\mathcal{N}}\delta(X - X_i(t))$, where $X_i(t) = (R_i(t), P_i(t))$ are given by the solutions of the following set of ordinary differential equations:[56]

$$\frac{dr_\lambda}{dt} = \frac{\partial H_m}{\partial p_\lambda}, \qquad \frac{dp_\lambda}{dt} = -\frac{\partial H_m}{\partial r_\lambda},$$
$$\frac{dR}{dt} = \frac{\partial H_m}{\partial P}, \qquad \frac{dP}{dt} = -\frac{\partial H_m}{\partial R}.$$

4. Partially linearized quantum-Classical dynamics

A less severe approximation to the QCLE[37,57] uses a partially linearized approximation to the equations of motion for the coupled system, using the mapping representation for the forward and backward time-propagators separately. This doubles the number of mapping variables used to describe each subsystem state but yields an efficient approximate solution to the QCLE in this forward-backward mapping form. This forward-backward trajectory solution (FBTS) describes a classical-like dynamics in the extended phase space of the environmental and the mapping variables that represent the subsystem degrees of freedom. The effective Hamiltonian function that generates the FBTS evolution is as follows:

The Journal of Chemical Physics ARTICLE scitation.org/journal/jcp

$$H_e(X,x,x') = \frac{1}{2}(H_m(X,x) + H_m(X,x')),$$

where $(X, x, x') = (R, P, r, r', p, p')$.

The continuous trajectories that define the FBTS solution to the quantum-classical Liouville equation can be represented by the following Hamiltonian equations of motion:[58]

$$\begin{aligned}
\frac{dr_\mu}{dt} &= \frac{\partial H_e(X,x)}{\partial p_\mu}, & \frac{dp_\mu}{dt} &= -\frac{\partial H_m(X,x)}{\partial r_\mu},\\
\frac{dr'_\mu}{dt} &= \frac{\partial H_m(X,x')}{\partial p'_\mu}, & \frac{dp'_\mu}{dt} &= -\frac{\partial H_m(X,x')}{\partial r'_\mu},\\
\frac{dR}{dt} &= \frac{P}{M}, & \frac{dP}{dt} &= -\frac{\partial H_e(X,x,x')}{\partial R}.
\end{aligned}$$

In the FBTS simulation algorithm, the matrix elements of the operator $\hat{B}_W(t)$ are approximated using the following expression:

$$\begin{aligned}
B_W^{\lambda\lambda'}(X,t) = \sum_{\mu\mu} \int dx dx' \phi(x)\phi(x')(r_\lambda + ip_\lambda)(r'_\lambda - ip'_\lambda)\\
\times B_W^{\mu\mu'}(X_t)(r_\mu(t) + ip_\mu(t))(r'_{\mu'}(t) - ip'_{\mu'}(t)),
\end{aligned}$$

where $\phi(x) = (\pi)^{-2N} e^{-\sum_\mu (r_\mu^2 + p_\mu^2)}$ are normalized Gaussian distribution functions, and evaluation of the integrals over the time-independent $\phi(x)$ functions is carried out by Monte Carlo sampling.

B. Quantum BBGKY-Hierarchy

In the following, we briefly describe the quantum mechanical BBGKY-hierarchy, which is an exact reformulation of many-body quantum dynamics. As such it can capture quantum interference and fluctuations. In practice, some approximate closures for the hierarchy have to be employed to reduce the computational cost of this approach. For a system of interacting fermions and bosons according to Eq. (3), where we focus on the explicit Pauli-spin representation of the 2-level system, i.e.,

$$\begin{aligned}
\hat{H} &= -\frac{\Delta\varepsilon}{2}\hat{\sigma}_z + \frac{1}{2}\sum_{\alpha=1}^{2N}\left(\hat{P}_\alpha^2 + \omega_\alpha^2\hat{Q}_\alpha^2\right) + \hat{E}(r_A)\hat{\sigma}_x,\\
\hat{E}(r_A) &= \sum_{\alpha=1}^{2N}\mu_{12}\omega_\alpha\lambda_\alpha(r_A)\hat{Q}_\alpha,
\end{aligned} \tag{4}$$

with $\Delta\varepsilon = \varepsilon_2 - \varepsilon_1$, the underlying equations of motion, known as the quantum BBGKY-hierarchy[59–61] follow from the Heisenberg equations of motion for the Hamiltonian. Consistent with previous publications,[64] we introduce the short-hand notation $\hat{X}_{1\alpha} \equiv \hat{Q}_\alpha$, $\hat{X}_{2\alpha} \equiv \hat{P}_\alpha$ such that the correlation functions are given by the following:

$$\begin{aligned}
\Lambda_{i\alpha,j\beta} &\equiv \langle \hat{X}_{i\alpha}\hat{X}_{j\beta}\rangle - X_{i\alpha}X_{j\beta},\\
\Lambda_{\varepsilon;j\alpha} &\equiv \langle \hat{X}_{j\alpha}\hat{\sigma}_\varepsilon\rangle - X_{j\alpha}\sigma_\varepsilon,
\end{aligned}$$

with $i, j \in \{1, 2\}$, $\varepsilon \in \{x, y, z\}$, and we chose to suppress the time-arguments for brevity. In this work, we truncate the infinite hierarchy of equations of motion at the doublets level for the correlation functions,[63] resulting in an approximation conventionally referred to as the second Born approximation.[64,65] This extends the Hartree-Fock-type approximation as presented in Refs. 14 and 25 to the next higher consistent approximation level of the hierarchy. With $\mathbf{X} \equiv (Q_{\alpha=1}, \ldots, Q_{\alpha=(2N)}, P_{\alpha=1}, \ldots, P_{\alpha=(2N)})^T = (X_{11}, \ldots, X_{1(2N)}, X_{21}, \ldots, X_{2(2N)})^T$ the normal coordinate averages satisfy

$$\dot{\mathbf{X}} = \{\mathbf{X}, H_{\mathrm{cl}}(\sigma_x, \mathbf{X})\},$$

where $\{\cdot,\cdot\}$ denotes the canonical Poisson bracket. Furthermore, H_{cl} defines the classical Hamiltonian function, i.e., providing the classical equivalent to Eq. (4) $\hat{B} \to \langle B\rangle$. The spin-projection averages in turn obey the following equations:

$$\begin{aligned}
\dot{\sigma}_z &= 2E(r_A)\sigma_y + 2\boldsymbol{\lambda}_{\mathrm{eff}}^T \cdot \boldsymbol{\Lambda}_y,\\
\dot{\sigma}_y &= -\Delta\varepsilon\sigma_x - 2E(r_A)\sigma_z - 2\boldsymbol{\lambda}_{\mathrm{eff}}^T \cdot \boldsymbol{\Lambda}_z,\\
\dot{\sigma}_x &= \Delta\varepsilon\sigma_y,
\end{aligned}$$

where $\boldsymbol{\lambda}_{\mathrm{eff}} \equiv (\omega_1\lambda_1(r_A)\mu_{12}, \ldots, \omega_M\lambda_{(2N)}(r_A)\mu_{12})^T$ represents the effective light-matter coupling. Moreover, we introduced the vector notation $\boldsymbol{\Lambda}_\varepsilon \equiv (\Lambda_{\varepsilon;11}, \ldots, \Lambda_{\varepsilon;1(2N)}, \Lambda_{\varepsilon;21}, \ldots, \Lambda_{\varepsilon;2(2N)})^T$ for the correlation functions. The dynamics of the correlation functions are determined by

$$\begin{aligned}
\dot{\boldsymbol{\Lambda}}_z &= \{\boldsymbol{\Lambda}_z, H_{\mathrm{cl}}(-\imath\sigma_y - \sigma_x\sigma_z, \boldsymbol{\Lambda}_z)\} + 2E\boldsymbol{\Lambda}_y + 2\sigma_y\boldsymbol{\Lambda} \cdot \boldsymbol{\lambda}_{\mathrm{eff}}(r_A),\\
\dot{\boldsymbol{\Lambda}}_y &= \{\boldsymbol{\Lambda}_y, H_{\mathrm{cl}}(-\imath\sigma_z - \sigma_y\sigma_x, -\boldsymbol{\Lambda}_y)\} - \Delta\varepsilon\boldsymbol{\Lambda}_x + 2E\boldsymbol{\Lambda}_z\\
&\quad + 2\sigma_z\boldsymbol{\Lambda} \cdot \boldsymbol{\lambda}_{\mathrm{eff}}(r_A),\\
\dot{\boldsymbol{\Lambda}}_x &= \{\boldsymbol{\Lambda}_x, H_{\mathrm{cl}}(1 - \sigma_x^2, \boldsymbol{\Lambda}_x)\} - \Delta\varepsilon\boldsymbol{\Lambda}_y,
\end{aligned}$$

where the matrix $\boldsymbol{\Lambda}$ with the elements $\Lambda_{i\alpha,j\beta}$ is the covariance matrix satisfying the following equation:

$$\dot{\boldsymbol{\Lambda}} = \boldsymbol{J} \cdot \boldsymbol{\Omega} \cdot \boldsymbol{\Lambda} - \boldsymbol{\Lambda} \cdot \boldsymbol{\Omega} \cdot \boldsymbol{J} - \boldsymbol{\lambda}_{\mathrm{eff}} \cdot \boldsymbol{\Lambda}_x^T - \boldsymbol{\Lambda}_x \cdot \boldsymbol{\lambda}_{\mathrm{eff}}^T.$$

Here, $\boldsymbol{J}$ is the standard symplectic matrix

$$\boldsymbol{J} = \begin{pmatrix} 0 & 1 & 0 & \\ -1 & 0 & 1 & \ldots \\ 0 & -1 & 0 & \\ & \ldots & & \end{pmatrix}$$

and $\boldsymbol{\Omega}$ denotes a matrix such that $\Omega_{1\alpha,1\alpha} = \omega_\alpha^2$, $\Omega_{2\alpha,2\alpha} = 1$, and otherwise zero.

Evolving the covariance matrix in time allows the field fluctuations to dynamically respond to the polarizable matter. Deriving the equation of motions from the many-body perturbation hierarchy sets an implicit condition on the dynamic fluctuations as the 2-particle reduced density matrix has to be identically zero to guarantee that only a single electron is acting in our system. In Sec. IV A 1, we will show that enforcing this condition cures almost completely all nonphysical negative intensities that arise otherwise and overall improves the performance of the second Born approximation considerably.

C. Configuration Interaction expansion

To obtain accurate reference solutions, considered as exact benchmarks for this low dimensional model, we truncate the Configuration Interaction (CI) expansion such that we allow at most two

The Journal of Chemical Physics ARTICLE scitation.org/journal/jcp

photons per mode, featuring 400 modes, while retaining the full two and three state representation for the atomic system,

$$|\Psi(t)\rangle = \sum_k c_{k,0}(t)|k\rangle \otimes |0\rangle + \sum_k \sum_{n_1}^{2N} c_{k,n_1}(t)|k\rangle \otimes \hat{a}^\dagger_{n_1}|0\rangle + \sum_k \sum_{n_1,n_2}^{2N^2+N} c_{k,n_1,n_2}(t)|k\rangle \otimes \hat{a}^\dagger_{n_1}\hat{a}^\dagger_{n_2}|0\rangle. \quad (5)$$

In line with the nature of CI expansions, the numerical cost exponentially grows when increasing the number of allowed photonic excitations. When exploiting the bosonic symmetry of the photons in total $1 + 2N + 2N(2N - 1)/2$ photon basis functions span the zero-photon (vacuum), one-photon (1pt), and two-photon (2pt) space. Combined with the low-dimensional matter system featuring the eigenstates $|k\rangle$, it is computationally nontrivial but feasible to propagate this CI expanded wavefunction using the Lanczos algorithm.[66,67] We ensured that the above (vacuum + 1pt + 2pt) CI basis is sufficient for the observables and parameters studied in this work.[79] Although spontaneous decay from the 2-level atomic system will lead to at most a single observable photon, the photonic fluctuations can reach the 2pt state space which results in the possibility to bind photon intensity at the atomic position (see Fig. 6).

IV. RESULTS AND DISCUSSION

As in earlier work,[29] we note that the Wick normal ordered form for operators (denoted $:\hat{B}:$ for some operator $\hat{B}$) is used when calculating average values in this study. The reason for using the normal ordered form, in practice, is to remove the typically non-measurable[68,69] effect of vacuum fluctuations from the results, which ensures that both $\langle E\rangle = 0$ and $\langle I\rangle = 0$, irrespective of the number of photon modes in the cavity field, when the field is in the vacuum state. In order to guarantee a distinct spatial resolution for the dynamics of the photonic wave-packet in the cavity and to ensure the inclusion of all possible inference effects we use 400 photon modes to represent the cavity field that is coupled to a two or three energy-level atomic system in all calculations shown below. We choose the atom to be initially in the highest excited state and the cavity field in the vacuum state at zero temperature. For our benchmark numerical treatment, we solved the time-dependent Schrödinger equation by using a truncated Configuration Interaction expansion as introduced in Sec. III C. The atomic population operator is given by $\hat{\sigma}_i(t) = |c_i(t)|^2$, where $c_i(t)$ denotes the time-dependent CI coefficient for the corresponding atomic energy level. Furthermore, we define the normal-ordered electric field intensity operator as follows:

$$:\hat{I}(r,t):=:\hat{E}^2(r,t):= 2\sum_{\alpha=1}^{2N}\omega_\alpha\zeta^2_\alpha(r)\hat{Q}^2_\alpha(t) - \sum_{\alpha=1}^{2N}\zeta^2_\alpha(r),$$

with

$$\zeta_\alpha(r) = \sqrt{\frac{\omega_\alpha}{\varepsilon_0 L}}\sin\left(\frac{\alpha\pi}{L}r\right).$$

A. 2-Level atom: One-photon emission process

In Fig. 2, we show a schematic sketch of the propagating photon-field intensity along the axis of the cavity for four different time snap-shots. As the spontaneous emission process evolves, a photon wave-packet with a sharp front is emitted from the atom [e.g., panel (a) of Fig. 2] and travels toward the boundaries [e.g., panel (b) of Fig. 2] where it is reflected, and then travels back to the atom [e.g., panel (c) of Fig. 2]. The emitted photon is then absorbed and re-emitted by the atom, which results in the emergence of interference phenomena in the electric field. This produces a photonic wave-packet with a more complex shape [e.g., panel (d) of Fig. 2]. In Figs. 3 and 4, we plot this spontaneous emission process for the different methods compared to the exact result (black dashed line). Here, we observe that the essential differences among the methods are (i) determining the correct amplitude of the wave-packet, (ii) capturing the re-emission interference pattern, and (iii) resembling the bound photon at the atomic position.

1. Finite size corrections to the BBGKY hierarchy

By partially summing the infinite series of perturbative diagrams that arise as a consequence of the Heisenberg equation of motion using Hamiltonian (4), we intrinsically introduce spurious interaction between physically nonexistent particles as we consider that more diagrams than particles are present in the physical system. This is a well-known subject of interest in electronic structure theory.[70–76] Specifically for our problem, this can result in such fundamental violations as producing negative atomic state occupations or photon field intensities (see Fig. 3). Enforcing the correct fermionic truncation of the many-body hierarchy acts to cure most of the nonphysical features that appear, i.e., negative intensities after the re-emission and strong oscillations around the exact solution. This restriction to the single electron subspace (1efsc) is performed by enforcing that the two-particle reduced density matrix be identically zero, $\rho^{(2)}_{ijkl} = 0$. For one-body reduced density-matrices $\rho^{(1)}_{ij}$, the cluster expansion on the exchange-only level $\rho^{(2)}_{ijkl} \approx \rho^{(1)}_{il}\rho^{(1)}_{jk} - \rho^{(1)}_{ik}\rho^{(1)}_{jl}$ guarantees this if $\rho^{(1)}_{ij}$ is idempotent.

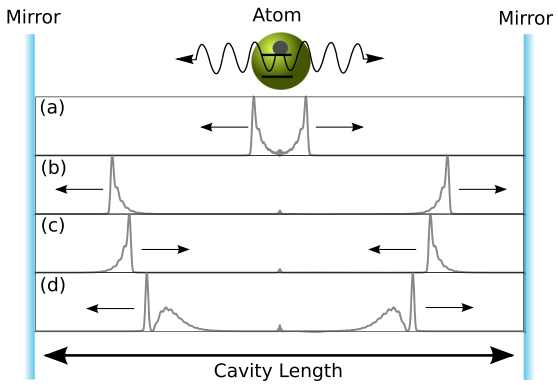

FIG. 2. A schematic sketch of the photon-field intensity propagating through the cavity for four time snap-shots: (a) t = 100 a.u., (b) t = 600 a.u., (c) t = 1200 a.u., and (d) t = 2100 a.u.

The Journal of Chemical Physics ARTICLE scitation.org/journal/jcp

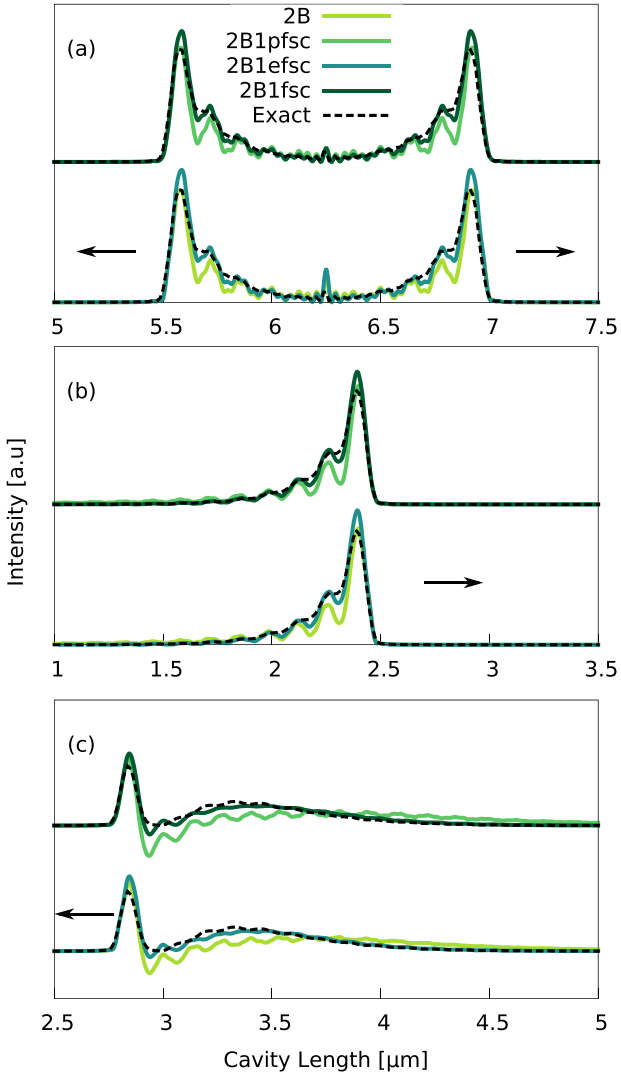

FIG. 3. Intensity of the emitted (normal-ordered) photon field using different finite-size corrections at three different time snapshots: (a) t = 100 a.u., (b) t = 1200 a.u., and (c) t = 2100 a.u.; no correction, single-photon correction (1pfsc), single-electron correction (1efsc), and single-photon and single-electron correction (1fsc) for the BBGKY hierarchy within the second Born approximation. The arrow indicates the direction of the wave-packet.

A further correction is possible in the photonic subspace, i.e., enforcing at most a single photon in the cavity for the two-level system (1pfsc). This is achieved by substituting higher correlation matrices with lower order expansions such that the equation of motion does not connect to higher excitations and corrects the bound photon intensity to excellent accuracy. Employing both restrictions at the same time (1fsc) leads to the overall best performance, and we focus on those results in Sec. IV. For multiple electrons and photonic excitations, such corrections will become less relevant and less straightforward to apply.

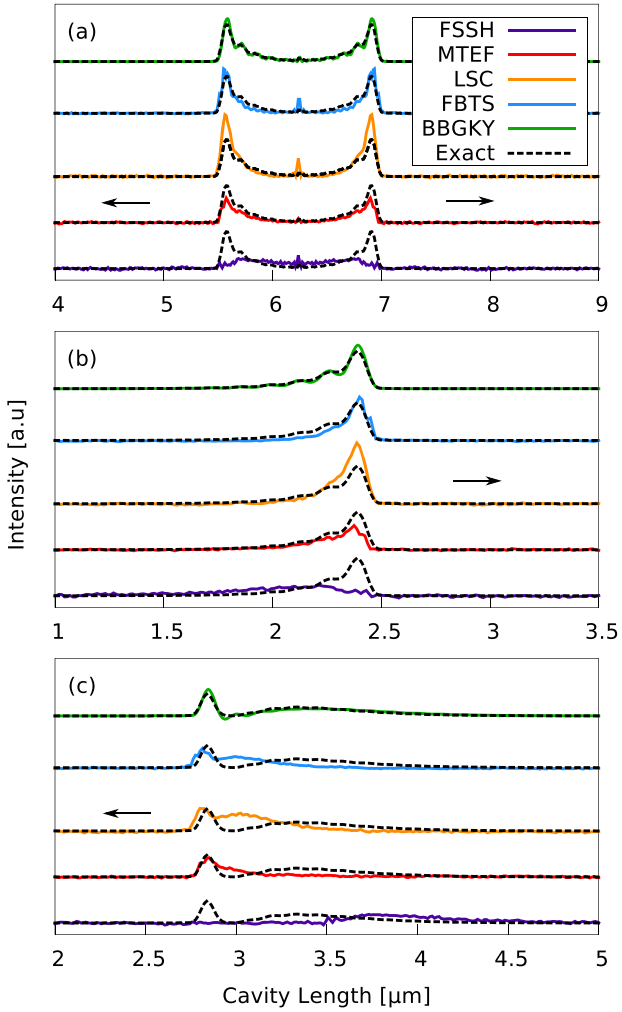

FIG. 4. Time-evolution of the average field intensity for the one-photon emission process, at three different time snapshots: (a) t = 100 a.u., (b) t = 1200 a.u., and (c) t = 2100 a.u. Exact solution (black-dashed), FSSH (purple), MTEF (red), LSC (orange), FBTS (blue), and (1fsc) BBGKY (green). The arrow indicates the direction of the wave-packet.

2. Trajectory-based semiclassical methods

To perform numerical simulations using the semiclassical dynamics methods, we first employ Monte Carlo sampling from the Wigner transform of the initial density operator of the photon field, $\hat{\rho}_{F,W}(X,0)$, to generate an ensemble of initial conditions for the trajectory ensemble $(Q_\alpha^j(0), P_\alpha^j(0))$. The Wigner transform of the zero temperature vacuum state is given by the following:

$$\rho_{F,W}(X,0) = \prod_{\alpha=1}^{2N} \frac{1}{\pi} \exp\left[-\frac{P_\alpha^2}{\omega_\alpha} - \omega_\alpha Q_\alpha^2\right].$$

We then evolve each initial condition independently according to the corresponding equations of motion to produce a trajectory. Average values are then constructed by summing over the entire

The Journal of Chemical Physics ARTICLE scitation.org/journal/jcp

trajectory ensemble and normalizing the result with respect to $\mathcal{N}$, the total number of trajectories. We use an ensemble of $\mathcal{N} = 10^5$ independent trajectories for the MTEF, FSSH, LSC, and FBTS calculations, sampled from the Wigner transform of the initial field density operator. This level of sampling is sufficient to converge the atomic observables to graphical accuracy, while the field intensity would require a slightly larger trajectory ensemble for graphical convergence.

In order to illustrate the comparison more accurately, a zoom-in of Fig. 4 is depicted in Figs. 5 and 7 in the same coloring. We find that the shapes of the (2B-1fsc) BBGKY-method and the FBTS-method nicely agree with the exact wave-packet shape for time 100 a.u., while the MTEF and LSC simulations are qualitatively accurate but miss the correct wave-packet amplitude. We find that FSSH performs rather poorly, as it fails to capture the qualitative structure of the outgoing wave-packet. Furthermore, we observe at time 2100 a.u. that the FSSH-method has broken down completely as it fails to reproduce the wave-packet structure in addition to exhibiting a time-delay. As a consequence of the *ad hoc* nature of the FSSH approach, we do not have a controlled and well-defined error term, and it is nontrivial to obtain an educated guess for the failure of this approach. Considering the other trajectory-based methods, we find that MTEF is not able to reproduce the photon re-emission due to the lack of capturing interferences within mean-field methods. On the other hand, FBTS and LSC predict a substantial amount of interference in the form of a second maximum, however shifted to earlier times in relation to the exact solution. As seen previously, the corrected second Born truncation of the BBGKY hierarchy is in very good agreement with the exact simulation; nevertheless, it still develops very small unphysical negative intensity values in between the first and second wave-packet maxima.

All methods are capable of describing the remaining intensity at the atomic position. This intensity corresponds to the bound photon intensity, which emerges from beyond rotating-wave approximation (RWA) effects. More precisely, in Fig. 6, we show the photon field intensity for the exact reference solution calculated in four

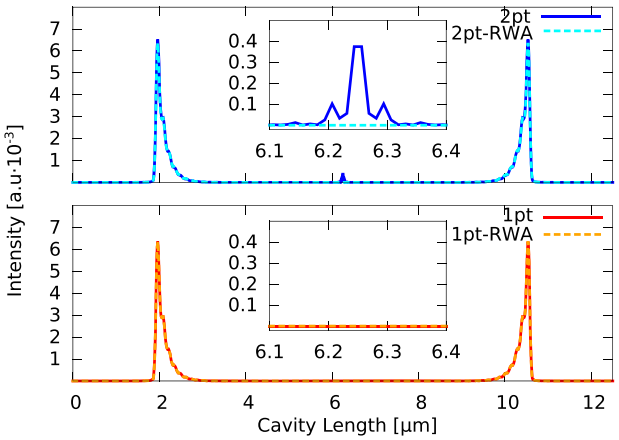

FIG. 6. Photon field intensity for the exact reference solution at time 600 a.u. for blue: including two-photon states (2pt) and no RWA, cyan: including two-photon states (2pt) with RWA, red: including only one-photon states (1pt) and no RWA, and orange: including only one-photon states (1pt) with RWA.

different ways according to Eq. (5). First including all two-photon states (2pt) without RWA (blue) and then performing the same calculation within RWA (cyan). Here, we find that using the RWA erases the bound photon state. Furthermore, we find that only including the one-photon states (1pt) is also not sufficient to capture this higher-order effect, as in both cases without RWA (red) and with RWA (orange) no bound photon is observed. Therefore, those results show that all methods are indeed capable of describing effects beyond the perturbative regime such as bound photon states. In Fig. 7, we depict this signature feature of the bound photon state for time 1200 a.u.. Here, we find that BBGKY and MTEF perform best, as FBTS, LSC, and FSSH overestimate the amplitude for the remaining intensity. Without single photon correction, the BBGKY amplitude is comparable to that of FBTS, i.e., finite size corrections in both, fermionic and photonic subspace, are important to obtain excellent results.

In Fig. 8, we plot the atomic adiabatic state population in the same color code as in Fig. 4. Here, BBGKY leads to excellent accuracy while among the trajectory methods LSC performs best. The initial decay, which is connected to the shape of the wavefront, is,

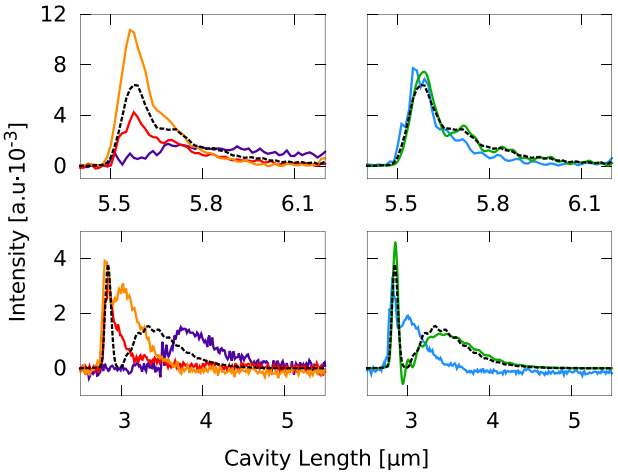

FIG. 5. Zoom-in onto the wavefronts of Fig. 4 (same color code) at time t = 100 a.u. (upper panels) and t = 2100 a.u. (lower panels).

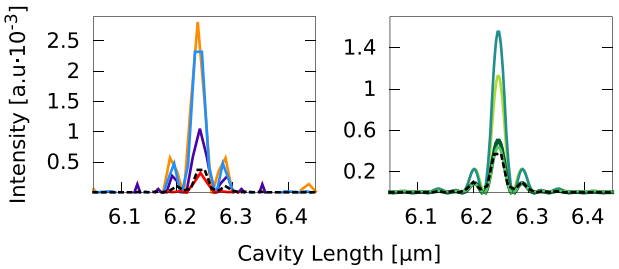

FIG. 7. Left: Zoom-in on the bound photon state of Fig. 4 (same color code). Right: Zoom-in on the bound photon state of Fig. 3 (same color code).

The Journal of Chemical Physics ARTICLE scitation.org/journal/jcp

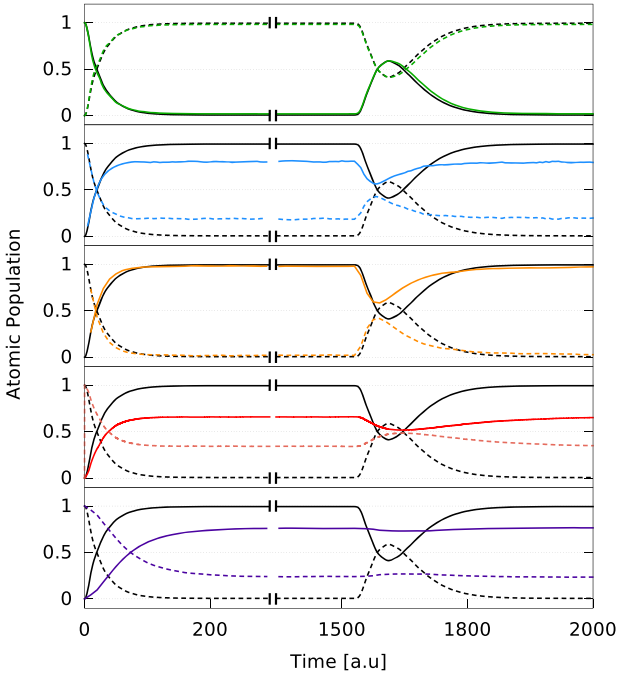

FIG. 8. Time-evolution of the atomic state population in the same color code as Fig. 4. The solid lines represent the atomic ground state, and the dashed lines represent the excited state.

however, superior in FBTS with the drawback of an incomplete de-excitation. While MTEF is capable of qualitatively describing the process, it fails on quantitative scales and even worse is FSSH which not even qualitatively resembles the process.

B. 3-Level atom: Two-photon emission process

Let us turn our attention to the slightly more complex three-level system where we focus on the most promising approaches with respect to extrapolations toward realistic systems in mind. We thus exclude FSSH due to its relatively poor performance and BBGKY due to its high computational effort, which we will later discuss in more detail.

In Fig. 9, we show the intensity of the cavity field during the two-photon emission process for MTEF, LSC, and FBTS compared to the exact solution. Furthermore, in order to allow a more quantitative and accurate comparison, a zoom-in of Fig. 9 is depicted in the same color-code in Figs. 10 and 11. Here, similar dynamics are observed compared to the two-level case. However, due to the additional intermediate atomic state, we now observe a double-peak feature in the emitted photonic wave-packet. This feature corresponds to the emission of two photons, as the excited atom initially decays to the first excited state emitting one photon and then further relaxes to the ground state, emitting a second photon. We find in accordance with the two-level case that the shape of the FBTS-method is in a good agreement with the exact wave-packet shape for time 100 a.u., while the MTEF and LSC-simulation are qualitatively in line, but underestimate the wave-packet amplitude. Furthermore,

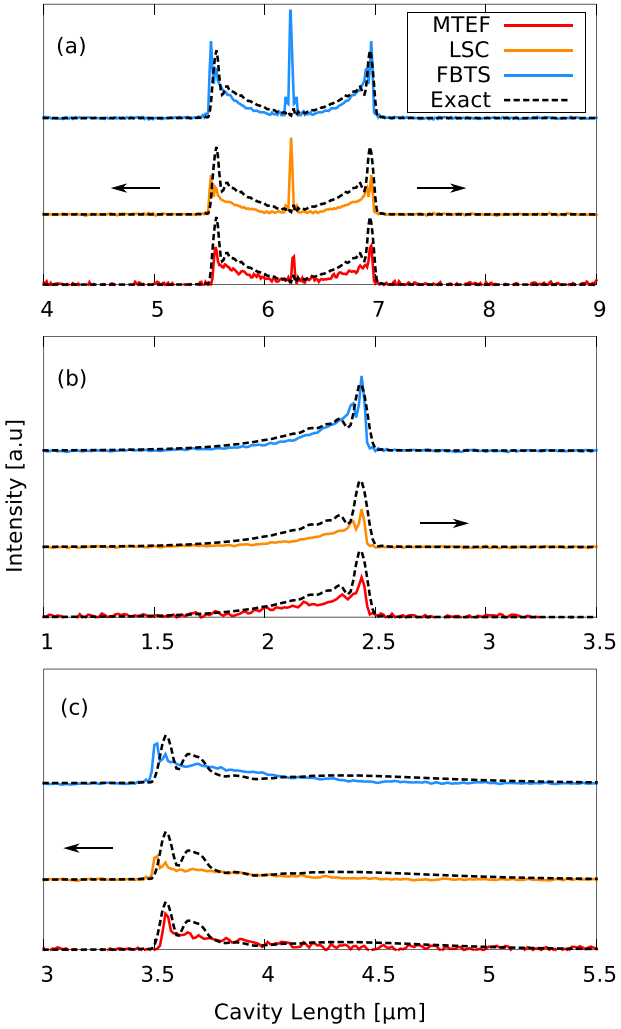

FIG. 9. Time-evolution of the average field intensity for the two-photon emission process, at three different time snapshots: (a) t = 100 a.u., (b) t = 1200 a.u., and (c) t = 2100 a.u. Exact solution (black-dashed), MTEF (red), LSC (orange), and FBTS (blue). Please note that in this plot, the amplitude of the bound photon state for the FBTS simulation is reduced in order to improve the illustration of the results. Explicit quantitative results for the bound photon state can be found in Fig. 11. The arrow indicates the direction of the wave-packet.

we observe that at time 2100 a.u., none of the methods sufficiently captures the complex re-emission structure while overestimating the bound photon peak in Fig. 11.

In Fig. 12, we show the time evolution of the atomic state populations. As before, the emitted photonic wave-packet moves through the cavity, is reflected at the mirrors, and returns to the atom. The first and second excited states are then repopulated due to stimulated absorption. A second spontaneous emission process ensues, and the emitted field again takes on a more complex profile due to interference. While MTEF features the pronounced incomplete emission, LSC and especially FBTS quite accurately capture the short-time decay dynamics. Each method provides a qualitative indication of

The Journal of Chemical Physics ARTICLE scitation.org/journal/jcp

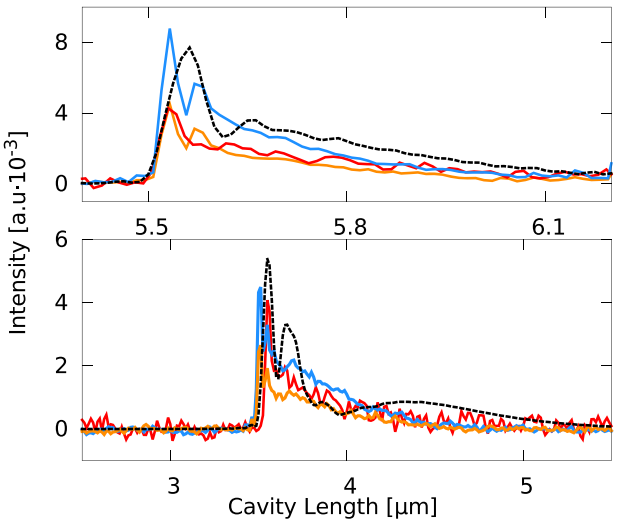

FIG. 10. A zoom-in onto the wavefronts of Fig. 9 (same color code) for time t = 100 a.u. (upper panel) and t = 2100 a.u. (lower panel).

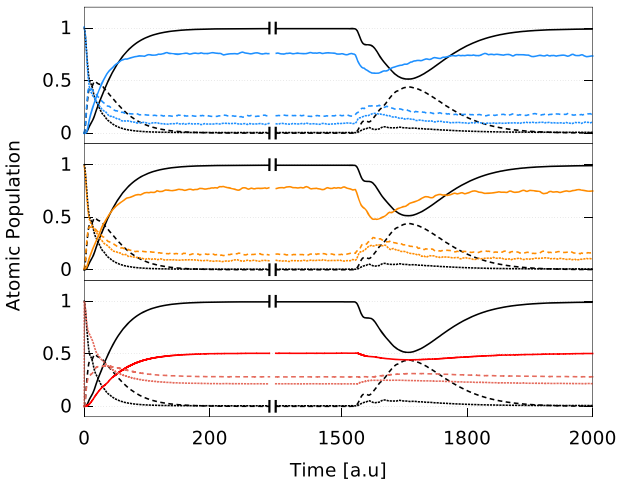

FIG. 12. Time-evolution of the atomic state population in the same color-code as Fig. 9. The solid lines represent the atomic ground state, the dashed lines represent the first excited state, and the dotted lines represent the second excited state.

the reabsorption and consecutive emission with LSC and FBTS performing clearly superior, suffering from a diminished incomplete (de-)excitation in relation to MTEF.

C. Computational effort and scaling

Regarding the BBGKY-method, the computational cost for this specific model is similar to the exact time-propagation for a two-photon subspace. This makes BBGKY, also in relation to the highly accurate results it provides, the most rigorous method for the model when considering the finite size corrections. Depending on the selected approximation and numerical details such as sparsity, it, however, features a rather unfavorable high-order polynomial scaling which restricts this method to comparably small systems.

In terms of the other semiclassical approaches, we have found that different numbers of trajectories are needed to converge different observables to the same statistical accuracy. In particular, for subsystem observables like the atomic populations, the FSSH and MTEF data are relatively well converged with 10^3–10^4 trajectories, while LSC and FBTS require 10^4–10^5. However, for observables related to the photon field, such as the intensity, the observable remains rather noisy for all the trajectory-based simulation methods with 10^5 trajectories.

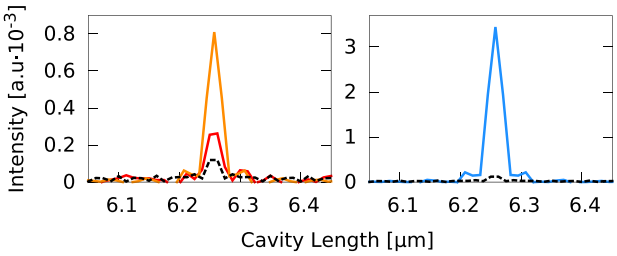

FIG. 11. A zoom-in on the bound photon state of Fig. 9 (same color code).

As all the independent trajectory based methods employ a Monte Carlo sampling procedure, their statistical error is proportional to the inverse square-root of the number of trajectories in the ensemble. However, as shown in this work, we have observed that more trajectories are required to converge photon-field (environmental) quantities compared to atomic (subsystem) quantities to within the same relative error. Furthermore, as the trajectories are not coupled during their time evolution, the corresponding algorithms can be implemented in a highly parallel manner to reduce the total run-time.

V. CONCLUSION

In this work, we have adapted and benchmarked a variety of approximate quantum dynamics methods, i.e., multitrajectory Ehrenfest (MTEF), linearized, and partially linearized semiclassical mapping (LSC and FBTS) methods, Tully's fewest switches surface hopping (FSSH), as well as a set of finite size corrected second Born BBGKY truncations, to treat correlated electron-photon systems. We have applied these methods to model QED cavity bound atomic systems in order to simulate the one and two photon spontaneous emission and interference processes and to analyze the performance of these approaches.

Consistently for the one- and two-photon emission processes, we find that MTEF, LSC, and FBTS are able to qualitatively characterize the correct dynamics. The initial spontaneous emission, the associated atomic occupations, and the emitted photon wave-packet improve from qualitative agreement within MTEF, to slightly better agreement while overestimating the decay-rate in LSC, to almost quantitative agreement using FBTS. However, these methods perform poorly when interference patterns emerge in the reabsorbed and re-emitted photonic wave-packet; MTEF totally fails to capture

The Journal of Chemical Physics ARTICLE scitation.org/journal/jcp

any of the interference effects associated with the excitation and re-emission processes, while LSC and FBTS qualitatively recover some of the characteristics of the outgoing intensity. The FSSH-method in contrast is not capable of properly resembling the wavefront of the photonic wave-packet, and, furthermore, exhibits an incorrect time delay in the re-emitted wave-packet. Consequentially, this technique performs rather poorly compared to the other trajectory based methods. It is possible, however, that improved versions of this algorithm may offer improvement over these initial results. The self-consistent perturbative expansion form of the BBGKY-hierarchy behaves exceptionally well when restricted to the physical subspace although some unphysical effects such as negative photon intensities can result. Finally, all methods investigated here can, in fact, capture the bound photonic state. Here, MTEF and BBGKY present the best performance while LSC and FBTS consistently overestimate the amplitude of this feature.

For the two-photon emission process, we focused on the most promising approaches considering the balance between performance and computational scalability. Here, we find in accordance with the two-level system that MTEF, LSC, and FBTS are able to qualitatively characterize the correct dynamics of this process; however, they suffer from quantitative drawbacks, especially pronounced for interference features.

Moreover, as experimental advances drive the need for realistic *ab initio* descriptions of light-matter coupled systems, trajectory-based quantum-classical algorithms emerge as a promising route towards treating more complex and realistic systems, more precisely extending to molecular systems beyond the few-level description and incorporating nuclear dynamics. In particular, combining the *ab initio* light-matter coupling methodology recently presented by Jestädt *et al.*[77] with the multitrajectory approach could provide a computationally feasible way to simulate photon-field fluctuations and correlations in realistic three-dimensional systems, and work along these lines is already in progress.

ACKNOWLEDGMENTS

We would like to thank J. Flick and N. T. Maitra for insightful discussions and acknowledge financial support from the European Research Council (Grant No. ERC-2015-AdG-694097). A.K. acknowledges support from the National Sciences and Engineering Research Council (NSERC) of Canada.

REFERENCES

[1] E. Orgiu, J. George, J. A. Hutchison, E. Devaux, J. F. Dayen, B. Doudin, F. Stellacci, C. Genet, J. Schachenmayer, C. Genes, G. Pupillo, P. Samori, and T. W. Ebbesen, "Conductivity in organic semiconductors hybridized with the vacuum field," Nat. Mater. **14**(11), 1123–1129 (2015).

[2] R. Chikkaraddy, B. de Nijs, F. Benz, S. J. Barrow, O. A. Scherman, E. Rosta, A. Demetriadou, P. Fox, O. Hess, and J. J. Baumberg, "Single-molecule strong coupling at room temperature in plasmonic nanocavities," Nature **535**(7610), 127–130 (2016).

[3] S. R. Casey and J. R. Sparks, "Vibrational strong coupling of organometallic complexes," J. Phys. Chem. C **120**(49), 28138–28143 (2016).

[4] J. George, T. Chervy, A. Shalabney, E. Devaux, H. Hiura, C. Genet, and T. W. Ebbesen, "Multiple Rabi splittings under ultrastrong vibrational coupling," Phys. Rev. Lett. **117**, 153601 (2016).

[5] J. Feist, J. Galego, and F. J. Garcia-Vidal, "Polaritonic chemistry with organic molecules," ACS Photonics **5**(1), 205–216 (2018).

[6] R. F. Ribeiro, L. A. Martínez-Martínez, M. Du, J. Campos-Gonzalez-Angulo, and J. Yuen-Zhou, "Polariton chemistry: Controlling molecular dynamics with optical cavities," Chem. Sci. **9**, 6325–6339 (2018).

[7] J. Flick, N. Rivera, and P. Narang, "Strong light-matter coupling in quantum chemistry and quantum photonics," Nanophotonics **7**(9), 1479–1501 (2018).

[8] J. del Pino, F. A. Y. N. Schröder, A. W. Chin, J. Feist, and F. J. Garcia-Vidal, "Tensor network simulation of non-Markovian dynamics in organic polaritons," Phys. Rev. Lett. **121**, 227401 (2018).

[9] M. Reitz, C. Sommer, and C. Genes, "Langevin approach to quantum optics with molecules," Phys. Rev. Lett. **122**, 203602 (2019).

[10] L. A. Martínez-Martínez, E. Eizner, S. Kena-Cohen, and J. Yuen-Zhou, "Triplet harvesting in the polaritonic regime: A variational polaron approach," J. Chem. Phys. **151**(5), 054106 (2019).

[11] J. Feist and F. J. Garcia-Vidal, "Extraordinary exciton conductance induced by strong coupling," Phys. Rev. Lett. **114**, 196402 (2015).

[12] J. Schachenmayer, C. Genes, E. Tignone, and P. Guido, "Cavity-enhanced transport of excitons," Phys. Rev. Lett. **114**, 196403 (2015).

[13] M. Cirio, S. De Liberato, N. Lambert, and F. Nori, "Ground state electroluminescence," Phys. Rev. Lett. **116**, 113601 (2016).

[14] J. Flick, M. Ruggenthaler, H. Appel, and A. Rubio, "Atoms and molecules in cavities, from weak to strong coupling in quantum-electrodynamics (QED) chemistry," Proc. Natl. Acad. Sci. U. S. A. **114**(12), 3026–3034 (2017).

[15] M. Ruggenthaler, N. Tancogne-Dejean, J. Flick, H. Appel, and A. Rubio, "From a quantum-electrodynamical light–matter description to novel spectroscopies," Nat. Rev. Chem. **2**(3), 0118 (2018).

[16] C. Schäfer, M. Ruggenthaler, H. Appel, and A. Rubio, "Modification of excitation and charge transfer in cavity quantum-electrodynamical chemistry," Proc. Natl. Acad. Sci. U. S. A. **116**(11), 4883–4892 (2019).

[17] A. Thomas, J. George, A. Shalabney, M. Dryzhakov, S. J. Varma, J. Moran, T. Chervy, X. Zhong, E. Devaux, C. Genet, J. A. Hutchison, and T. W. Ebbesen, "Ground-state chemical reactivity under vibrational coupling to the vacuum electromagnetic field," Angew. Chem., Int. Ed. **55**(38), 11462–11466 (2016).

[18] H. Hiura, A. Shalabney, and J. George, "Cavity Catalysis–Accelerating Reactions under Vibrational Strong Coupling," Angewandte Chemie International Edition (Wiley online, 2019).

[19] A. Thomas, L. Lethuillier-Karl, K. Nagarajan, R. M. A. Vergauwe, J. George, T. Chervy, A. Shalabney, E. Devaux, C. Genet, J. Moran *et al.*, "Tilting a ground-state reactivity landscape by vibrational strong coupling," Science **363**(6427), 615–619 (2019).

[20] J. Galego, F. J. Garcia-Vidal, and J. Feist, "Cavity-induced modifications of molecular structure in the strong-coupling regime," Phys. Rev. X **5**, 041022 (2015).

[21] J. Flick, H. Appel, M. Ruggenthaler, and A. Rubio, "Cavity Born-Oppenheimer approximation for correlated electron-nuclear-photon systems," J. Chem. Theory Comput. **13**(4), 1616–1625 (2017).

[22] H. Ling Luk, J. Feist, J. J. Toppari, and G. Groenhof, "Multiscale molecular dynamics simulations of polaritonic chemistry," J. Chem. Theory Comput. **13**(9), 4324–4335 (2017).

[23] C. Schäfer, M. Ruggenthaler, and A. Rubio, "*Ab initio* nonrelativistic quantum electrodynamics: Bridging quantum chemistry and quantum optics from weak to strong coupling," Phys. Rev. A **98**(4), 043801 (2018).

[24] M. Ruggenthaler, J. Flick, C. Pellegrini, H. Appel, I. V. Tokatly, and A. Rubio, "Quantum-electrodynamical density-functional theory: Bridging quantum optics and electronic-structure theory," Phys. Rev. A **90**, 012508 (2014).

[25] C. Pellegrini, J. Flick, I. V. Tokatly, H. Appel, and A. Rubio, "Optimized effective potential for quantum electrodynamical time-dependent density functional theory," Phys. Rev. Lett. **115**, 093001 (2015).

[26] J. Flick, C. Schäfer, M. Ruggenthaler, H. Appel, and A. Rubio, "*Ab-initio* optimized effective potentials for real molecules in optical cavities: Photon contributions to the molecular ground state," ACS Photonics **5**, 992 (2018).

[27] W. H. Miller, "The semiclassical initial value representation: A potentially practical way for adding quantum effects to classical molecular dynamics simulations," J. Phys. Chem. A **105**(13), 2942–2955 (2001).

[28] A. Kelly, A. M. Montoya-Castillo, L. Wang, and T. E. Markland, "Generalized quantum master equations in and out of equilibrium: When can one win?," J. Chem. Phys. **144**, 184105 (2016).

The Journal of Chemical Physics ARTICLE scitation.org/journal/jcp

[29]N. M. Hoffmann, C. Schäfer, A. Rubio, A. Kelly, and H. Appel, "Capturing vacuum fluctuations and photon correlations in cavity quantum electrodynamics with multi-trajectory Ehrenfest dynamics," Phys. Rev. A **99**(6), 063819 (2019).
[30]H.-T. Chen, T. E. Li, M. Sukharev, A. Nitzan, and J. E. Subotnik, "Ehrenfest+R dynamics. II. A semiclassical QED framework for Raman scattering," J. Chem. Phys. **150**(4), 044103 (2019).
[31]H.-T. Chen, T. E. Li, M. Sukharev, A. Nitzan, and J. E. Subotnik, "Ehrenfest+R dynamics. I. A mixed quantum-classical electrodynamics simulation of spontaneous emission," J. Chem. Phys. **150**(4), 044102 (2019).
[32]T. E. Li, A. Nitzan, M. Sukharev, T. Martinez, H.-T. Chen, and J. E. Subotnik, "Mixed quantum-classical electrodynamics: Understanding spontaneous decay and zero-point energy," Phys. Rev. A **97**, 032105 (2018).
[33]P. Ehrenfest, Z. Phys. A **45**(7-8), 455 (1927).
[34]A. D. McLachlan, Mol. Phys. **8**, 39 (1964).
[35]J. C. Tully, "Molecular dynamics with electronic transitions," J. Chem. Phys. **93**(2), 1061–1071 (1990).
[36]H. Wang, X. Sun, and W. H. Miller, "Semiclassical approximations for the calculation of thermal rate constants for chemical reactions in complex molecular systems," J. Chem. Phys. **108**(23), 9726–9736 (1998).
[37]C.-Y. Hsieh and R. Kapral, "Nonadiabatic dynamics in open quantum-classical systems: Forward-backward trajectory solution," J. Chem. Phys. **137**(22), 22A507 (2012).
[38]C.-Y. Hsieh and R. Kapral, "Analysis of the forward-backward trajectory solution for the mixed quantum-classical Liouville equation," J. Chem. Phys. **138**(13), 134110 (2013).
[39]D. P. Craig and T. Thirunamachandran, *Molecular Quantum Electrodynamics: An Introduction to Radiation-Molecule Interactions* (Dover Publications, 1998).
[40]J. Flick, M. Ruggenthaler, H. Appel, and R. Angel, "Kohn-Sham approach to quantum electrodynamical density-functional theory: Exact time-dependent effective potentials in real space," Proc. Natl. Acad. Sci. U. S. A. **112**, 15285 (2015).
[41]I. V. Tokatly, "Time-dependent density functional theory for many-electron systems interacting with cavity photons," Phys. Rev. Lett. **110**, 233001 (2013).
[42]V. Bužek, G. Drobný, M. G. Kim, M. Havukainen, and P. L. Knight, "Numerical simulations of atomic decay in cavities and material media," Phys. Rev. A **60**, 582–592 (1999).
[43]D. De Bernardis, P. Pilar, T. Jaako, S. De Liberato, and P. Rabl, "Breakdown of gauge invariance in ultrastrong-coupling cavity QED," Phys. Rev. A **98**(5), 053819 (2018).
[44]C. Schäfer, M. Ruggenthaler, V. Rokaj, and A. Rubio, "Relevance of the quadratic diamagnetic and self-polarization terms in cavity quantum electrodynamics" e-print arXiv:1911.08427 (2019).
[45]Q. Su and J. H. Eberly, "Model atom for multiphoton physics," Phys. Rev. A **44**, 5997–6008 (1991).
[46]M. Hillery, R. F. O'Connell, M. O. Scully, and E. P. Wigner, Phys. Rep. **106**, 121 (1984).
[47]R. Grunwald, A. Kelly, and R. Kapral, *Quantum Dynamics in Almost Classical Environments* (Springer Berlin Heidelberg, Berlin, Heidelberg, 2009), pp. 383–413.
[48]J. C. Tully and R. K. Preston, "Trajectory surface hopping approach to nonadiabatic molecular collisions: The reaction of H^+ with D_2," J. Chem. Phys. **55**(2), 562–572 (1971).
[49]J. E. Subotnik and N. Shenvi, "A new approach to decoherence and momentum rescaling in the surface hopping algorithm," J. Chem. Phys. **134**(2), 024105 (2011).
[50]E. R. Bittner and P. J. Rossky, "Quantum decoherence in mixed quantum-classical systems: Nonadiabatic processes," J. Chem. Phys. **103**(18), 8130–8143 (1995).
[51]O. V. Prezhdo and P. J. Rossky, "Evaluation of quantum transition rates from quantum-classical molecular dynamics simulations," J. Chem. Phys. **107**(15), 5863–5878 (1997).
[52]H.-D. Meyer and W. H. Miller, "A classical analog for electronic degrees of freedom in nonadiabatic collision processes," J. Chem. Phys. **70**(7), 3214–3223 (1979).
[53]G. Stock and M. Thoss, "Semiclassical description of nonadiabatic quantum dynamics," Phys. Rev. Lett. **78**(4), 578–581 (1997).
[54]G. Stock and M. Thoss, "Classical description of nonadiabatic quantum dynamics," Adv. Chem. Phys. **131**, 243–376 (2005).
[55]H. Kim, A. Nassimi, and R. Kapral, "Quantum-classical Liouville dynamics in the mapping basis," J. Chem. Phys. **129**(8), 084102 (2008).
[56]A. Nassimi, S. Bonella, and R. Kapral, "Analysis of the quantum-classical Liouville equation in the mapping basis," J. Chem. Phys. **133**(13), 134115 (2010).
[57]P. Huo and D. F. Coker, "Communication: Partial linearized density matrix dynamics for dissipative, non-adiabatic quantum evolution," J. Chem. Phys. **135**(20), 201101 (2011).
[58]A. Kelly, R. van Zon, J. Schofield, and R. Kapral, "Mapping quantum-classical Liouville equation: Projectors and trajectories," J. Chem. Phys. **136**(8), 084101 (2012).
[59]W. Shun-jin and W. Cassing, "Explicit treatment of N-body correlations within a density-matrix formalism," Ann. Phys. **159**(2), 328–350 (1985).
[60]J. Fricke, "Transport equations including many-particle correlations for an arbitrary quantum system: A general formalism," Ann. Phys. **252**(2), 479–498 (1996).
[61]M. Bonitz, *Quantum Kinetic Theory*, 2nd ed. (Springer International Publishing Switzerland, 2016).
[62]N. Säkkinen, Y. Peng, H. Appel, and R. van Leeuwen, "Many-body Green's function theory for electron-phonon interactions: The Kadanoff-Baym approach to spectral properties of the Holstein dimer," J. Chem. Phys. **143**(23), 234102 (2015).
[63]W. Hoyer, M. Kira, and S. W. Koch, *Cluster Expansion in Semiconductor Quantum Optics* (Springer Berlin Heidelberg, Berlin, Heidelberg, 2004), pp. 309–335.
[64]R. Zimmermann and J. Wauer, "Non-Markovian relaxation in semiconductors: An exactly soluble model," J. Lumin. **58**(1), 271–274 (1994).
[65]H. Lohmeyer, V. M. Axt, and T. Kuhn, "Electron-phonon quantum kinetics beyond the second-order Born approximation," AIP Conf. Proc. **772**(1), 907–908 (2005).
[66]T. J. Park and J. C. Light, "Unitary quantum time evolution by iterative Lanczos reduction," J. Chem. Phys. **85**(10), 5870–5876 (1986).
[67]J. Flick, "Exact nonadiabatic many-body dynamics: Electron-phonon coupling in photoelectron spectroscopy and light-matter interactions in quantum electrodynamical density-functional theory," Ph.D. thesis, Humboldt-Universität zu Berlin, Berlin, 2016.
[68]C. Riek, D. V. Seletskiy, A. S. Moskalenko, J. F. Schmidt, P. Krauspe, S. Eckart, S. Eggert, G. Burkard, and A. Leitenstorfer, "Direct sampling of electric-field vacuum fluctuations," Science **350**(6259), 420–423 (2015).
[69]I.-C. Benea-Chelmus, F. F. Settembrini, G. Scalari, and J. Faist, "Electric field correlation measurements on the electromagnetic vacuum state," Nature **568**(7751), 202 (2019).
[70]D. Kremp, M. Bonitz, W. D. Kraeft, and M. Schlanges, "Non-Markovian Boltzmann equation," Ann. Phys. **258**(2), 320–359 (1997).
[71]M. P. von Friesen, C. Verdozzi, and C.-O. Almbladh, "Successes and failures of Kadanoff-Baym dynamics in Hubbard nanoclusters," Phys. Rev. Lett. **103**(17), 176404 (2009).
[72]C. Verdozzi, D. Karlsson, M. P. von Friesen, C.-O. Almbladh, and U. von Barth, "Some open questions in TDDFT: Clues from lattice models and Kadanoff–Baym dynamics," Chem. Phys. **391**(1), 37–49 (2011).
[73]G. Stefanucci and R. van Leeuwen, *Nonequilibrium Many-Body Theory of Quantum Systems: A Modern Introduction* (Cambridge University Press, 2013).
[74]M. Florian, C. Gies, J. Frank, H. A. M. Leymann, and J. Wiersig, "Equation-of-motion technique for finite-size quantum-dot systems: Cluster expansion method," Phys. Rev. B **87**(16), 165306 (2013).
[75]H. A. M. Leymann, A. Foerster, and J. Wiersig, "Expectation value based equation-of-motion approach for open quantum systems: A general formalism," Phys. Rev. B **89**(8), 085308 (2014).
[76]M. Richter, A. Carmele, A. Sitek, and A. Knorr, "Few-photon model of the optical emission of semiconductor quantum dots," Phys. Rev. Lett. **103**(8), 087407 (2009).
[77]R. Jestädt, M. Ruggenthaler, M. J. T. Oliveira, A. Rubio, and H. Appel, "Real-time solutions of coupled Ehrenfest-Maxwell-Pauli-Kohn-Sham equations:

The Journal of Chemical Physics ARTICLE scitation.org/journal/jcp

Fundamentals, implementation, and nano-optical applications," preprint arXiv:1812.05049 (2018).

[78] We have verified that in the parameter regimes studied in this work including the quadratic term into adjusted eigenstates, according to the Hamiltonian $\acute{H}_A + \sum_{\alpha=1}^{2N} \frac{1}{2}(\lambda_\alpha \cdot \hat{\boldsymbol{\mu}})^2$, has no qualitative influence on the time-evolution of the observables associated with the cavity-bound emission process.

[79] As the exponential scaling permits the inclusion of higher photon states for the given model, we ensured convergence investigating a related 3-level system based on a screened Hydrogen atom with 1/10 of the atomic binding potential coupled to the 100 lowest harmonics of the former cavity. Including the three-photon states resulted in marginal numerical changes such that we deem the selected two-photon states sufficient for the investigated model.

3

ELECTRON-NUCLEI-PHOTON CORRELATED SYSTEMS

3.1 TIME-DEPENDENT POTENTIAL ENERGY SURFACE FOR MOLECULES IN CAVITIES

"Exact Potential Energy Surface for Molecules in Cavities"

L Lacombe, NM Hoffmann, NT Maitra

Physical Review Letters (2019), 123 (8), 083201

MOTIVATION Continuing the work of Sec. 2.2 the overall question stays the same, i.e. can we find a Schrödinger equation for one of the subsystems alone, such that the solution yields the wavefunction of that subsystem and the potential appearing in the equation incorporate the couplings to the other subsystems as well as to any externally applied fields. However, within this work, we are now interested in the nuclear subsystem under the influence of both the electronic and the photonic subsystems.

STATE OF THE ART It has been shown that the cavity clearly modifies the potential that the matter evolves in [70, 122, 141–143], and various constructs have been put forward complementary to the BO surfaces that have proved valuable for understanding cavity-free dynamics. In particular, polaritonic surfaces that arise from diagonalizing the electron-photon Hamiltonian parametrized by nuclear coordinates have been instructive in interpreting some of the novel phenomena [107, 115, 144]. Another construct are the cavity-BO surfaces where the photonic displacement field and nuclear coordinates are treated on the same footing [70, 82]. Furthermore, going beyond using the surfaces for qualitative interpretation, and implementing them in dynamics schemes, couplings between the surfaces must be included [108, 122], as well as nonadiabatic effects arising from photon-matter coupling interplay with electron-nuclear couplings. The EF approach bypasses these questions, while also shedding light on them, as a single TDPES replaces the manifold of static surfaces and represents the exact potential that the nuclear wave packet evolves in, which exactly contains the effects of coupling to the electrons and photons.

CONTRIBUTION AND MAIN FINDINGS In this work, we extend the EF approach to light-matter interactions so that $\Psi(\mathbf{q}, \mathbf{r}, \mathbf{R}, t) = \chi(\mathbf{R}, t)\Phi_{\mathbf{R}}(\mathbf{q}, \mathbf{r}, t)$ yields a time-dependent Schrödinger equation for the nuclear system, parametrically depending on both the electronic $\mathbf{r}$ and the photonic $\mathbf{q}$ subsystem. We find and

analyze the exact TDPES driving the proton motion for a model of cavity-induced suppression of PCET. Additionally, we show how its features directly correlate to the proton dynamics and we discuss cavity modifications of its structure responsible for the suppression. The results highlight the interplay between nonadiabatic effects from coupling to photons and coupling to electrons. Furthermore, we find, that the polaritonic surfaces, although providing a useful backdrop, are not able to predict dynamics or mechanisms without considering their couplings to each other in a dynamics scheme [122, 141]. Therefore, care is needed with such dynamics schemes, due to the propensity of near crossings caused by both electron-nuclear and matter-photon couplings.

OUTLOOK For mixed quantum-classical methods, which would be required for many-molecule systems [108, 145], overcoherence in surface-hopping methods is likely to be problematic. Instead, following the outlook of Sec. 2.2, this work shows the promise of rigorously based mixed quantum-classical approximations for cavity-QED, based on, for example, generalizations of the schemes of [37–39], that have been successful for cavity-free nonadiabatic dynamics

SUPPLEMENTARY MATERIAL In the supplementary material to this paper we provide more details on the full exact factorization equations and their form within the applied model system. We furthermore provide more numerical details and three movies[1] corresponding to the discussed results in the paper.

1 Movies: https://journals.aps.org/prl/supplemental/10.1103/PhysRevLett.123.083201

PHYSICAL REVIEW LETTERS **123,** 083201 (2019)

Exact Potential Energy Surface for Molecules in Cavities

Lionel Lacombe,[1] Norah M. Hoffmann,[2,1] and Neepa T. Maitra[1,3]
[1]*Department of Physics and Astronomy, Hunter College of the City University of New York, 695 Park Avenue, New York, New York 10065, USA*
[2]*Max Planck Institute for the Structure and Dynamics of Matter and Center for Free-Electron Laser Science and Department of Physics, Luruper Chaussee 149, 22761 Hamburg, Germany*
[3]*Physics Program and Chemistry Program, Graduate Center of the City University of New York, New York 10016, USA*

(Received 31 May 2019; published 22 August 2019)

We find and analyze the exact time-dependent potential energy surface driving the proton motion for a model of cavity-induced suppression of proton-coupled electron transfer. We show how, in contrast to the polaritonic surfaces, its features directly correlate to the proton dynamics and we discuss cavity modifications of its structure responsible for the suppression. The results highlight the interplay between nonadiabatic effects from coupling to photons and coupling to electrons and suggest caution is needed when applying traditional dynamics methods based on polaritonic surfaces.

DOI: 10.1103/PhysRevLett.123.083201

Impressive experimental advances [1–5] have led to a rekindling of interest in cavity quantum electrodynamics. Rapidly expanding applications to molecules and nanostructures require going beyond the simplest few-level-single-mode models explored in the early days of quantum mechanics, with the interplay of coupled electronic, nuclear, and photonic excitations revealing a plethora of new phenomena, from enhanced conductivity and superconductivity to photochemical suppression of chemical reactions to superradiance; see, e.g., Refs. [6–12]. There is the possibility to manipulate matter with cavity parameters providing tunable dials for photochemical control of reactions, replacing shaped laser pulses as photonic reagents [1,13,14]. The hope is to attain strong light-matter coupling and control without large power sources, reducing unintended byproducts such as multiphoton absorption and ionization channels.

The cavity clearly modifies the potential that the matter evolves in, and various constructs have been put forward to serve in lieu of the Born-Oppenheimer (BO) surfaces that have proved so instrumental for understanding cavity-free dynamics. In particular, "polaritonic surfaces" that arise from diagonalizing the electron-photon Hamiltonian parametrized by nuclear coordinates have been instructive in interpreting some of the novel phenomena mentioned above [15–19]. Another construct is the "cavity-BO surfaces" where the photonic displacement field and nuclear coordinates are treated on the same footing [7,20]. A complete dynamical picture of how the electrons and photons influence the nuclear dynamics can only be obtained when several of such surfaces in the chosen manifold together with their couplings are considered: typically, at a given time, the nuclear wave packet locally straddles several surfaces or has distinct parts associated with different surfaces. Going beyond using the surfaces for qualitative interpretation, and implementing them in dynamics schemes, couplings between the surfaces must be included [8,21], and nonadiabatic effects arising from photon-matter coupling interplay with electron-nuclear couplings. Practical necessity calls for approximations which work best when this choice of surfaces in some sense represents a "zeroth-order" picture. The situation somewhat mirrors that for a molecule driven by classical light, where, for example, in surface-hopping schemes sometimes Floquet states (which are the classical-light analogues to the polaritonic surfaces) work best [22,23], while in other cases quasistatic (a.k.a. instantaneous BO) states are argued to be more appropriate [24,25].

The exact factorization approach (EFA) bypasses these questions while also shedding light on them. Originally presented for coupled electron-nuclear systems, a single time-dependent potential energy surface (TDPES) replaces the manifold of static surfaces and represents the exact potential that the nuclear wave packet evolves in, which exactly contains the effects of coupling to the electrons [26,27]. Generalizations of EFA have been made to include photons [28,29]. Explicit examples of how coupling to photons affects features of the potential driving an electron are given in Ref. [29], while Ref. [28] finds the exact photon-matter coupling-induced corrections to the potential driving the photons. So far, how the presence of the cavity modifies the potential driving the nuclei has not been explored. In this Letter, we find the exact cavity-modified TDPES for a model that demonstrates suppression of photo-induced proton-coupled electron transfer (PCET), a key process in energy conversion in biological and chemical systems. In contrast to polaritonic surfaces, its features alone indicate the suppression phenomenon, and it

provides the exact, unambiguous force on the nuclei to be used in mixed quantum-classical methods.

The minimal model of Refs. [30–32] has been remarkably instructive for studying nonadiabatic effects in cavity-free PCET [31–34]. The Hamiltonian involves one electron and one proton moving between two fixed ions separated by L in one dimension

$$\hat{H}_m = \hat{T}_n + \hat{H}_{\mathrm{BO}} = \hat{T}_n + \hat{T}_e + \hat{V}_m, \tag{1}$$

where $\hat{T}_n = -(1/2M)(\partial^2/\partial R^2)$, $\hat{T}_e = -\frac{1}{2}(\partial^2/\partial r^2)$, and

$$\hat{V}_m = \sum_{\sigma=\pm 1}\left(\frac{1}{|R+\frac{\sigma L}{2}|} - \frac{\mathrm{erf}(\frac{|r+\frac{\sigma L}{2}|}{a_\sigma})}{|r+\frac{\sigma L}{2}|}\right) - \frac{\mathrm{erf}(\frac{|R-r|}{a_f})}{|R-r|}, \tag{2}$$

where we chose $L = 19.0$ a.u., $a_{+1} = 3.1$ a.u., $a_{-1} = 4.0$ a.u., $a_f = 5.0$ a.u., and proton mass $M = 1836$ a.u. Atomic units ($\hbar = e^2 = m_e = 1$) are used throughout. Changing these parameters changes the strength of the electron-nuclear couplings and eigenstates; a closely related model [31,32] was used to study sequential versus concerted PCET mechanisms in solvents, while a two-dimensional version was used to model a conical intersection [35].

The top panel in Fig. 1 shows the BO surfaces for the cavity-free system. Considering an initial sudden vertical electronic excitation out of the ground-state donor well on the left to the first excited BO state, the nuclear wave packet slides down the surface and splits soon after encountering the avoided crossing (see the figures shortly and movie in the Supplemental Material [36]). The part of the nuclear wave packet evolving on the lower surface then becomes associated with an electron transfer as evident from comparing the conditional BO electronic wave functions shown in the insets in Fig. 1. To investigate how placing the molecule in a cavity affects the PCET, we consider the nonrelativistic photon-matter Hamiltonian in the dipole approximation in the Coulomb gauge [19,20,28,37,38]

$$\hat{H} = \hat{H}_m + \hat{H}_p + \hat{V}_{pm} + \hat{V}_{\mathrm{dipSE}}, \tag{3}$$

where, for a single cavity mode of frequency ω_α,

$$\hat{H}_p(q) = \frac{1}{2}(\hat{p}_\alpha^2 + \omega_\alpha^2\hat{q}_\alpha^2) \quad \text{and} \quad \hat{V}_{pm} = \omega_\alpha\lambda_\alpha\hat{q}_\alpha(R-r), \tag{4}$$

where $\hat{q}_\alpha = \sqrt{1/2\omega_\alpha}(\hat{a}_\alpha^\dagger + \hat{a}_\alpha)$ is the photonic displacement-field coordinate, related to the electric displacement operator, while $\hat{p}_\alpha$ is proportional to the magnetic field. The coupling strength $\lambda_\alpha = \lambda$ generally depends on the mode function of the cavity, but here we take it constant, assuming that the cavity is much longer than the spatial range of the molecular dynamics. The dipole self-energy

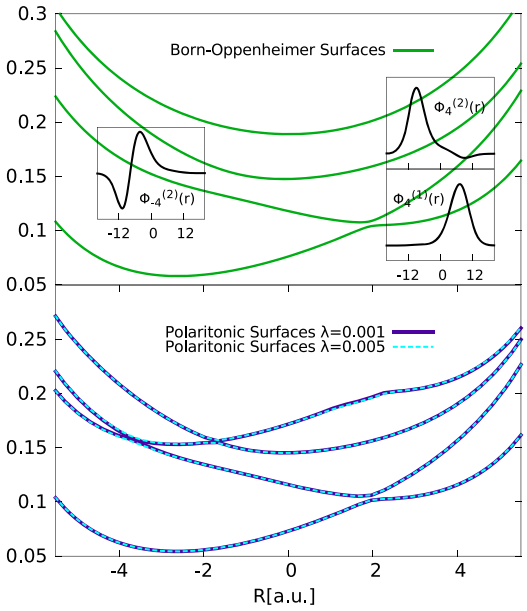

FIG. 1. Upper panel: the lowest BO surfaces for the PCET model. The initial conditional electronic wave function associated with the initial excitation on the donor side is shown in the inset on the left, showing localization of the electron at negative r values, while those associated with the BO surfaces after a proton transfer are shown on the right. The latter show that on the second surface the electron is localized at negative r values, while on the lower surface the electron becomes localized at positive r. Lower panel: the polaritonic surfaces, for coupling strengths indicated.

$\hat{V}_{\mathrm{dipSE}} = \frac{1}{2}[\lambda_\alpha(R-r)]^2$ has a negligible effect in all cases studied. Polaritonic surfaces, defined by the eigenvalues of $\hat{H} - \hat{T}_n$, are shown in the lower panel of Fig. 1 for $\omega_\alpha = 0.1$ a.u. and $\lambda = 0.005$ a.u. and 0.001 a.u. Immediately evident is the increased number of avoided crossings compared to the BO surfaces, as nonadiabatic effects from photon-matter and electron-nuclear couplings come into play.

Turning to the dynamics, the lower part of the upper six panels in Fig. 2 shows time snapshots of the nuclear density (red) resulting from the initial wave function, $\Psi(r, q, R, 0) = \mathcal{N}e^{-[(R+4)^2/2.85]}\Phi_R^{\mathrm{BO},(2)}(r)\xi^{(0)}(q)$, where $\xi^{(0)}(q) = (\omega_\alpha/\pi)^{1/4}e^{-\omega_\alpha q^2/2}$ is the zero-photon state in the cavity. The figure and movie in the Supplemental Material [36] demonstrate cavity-induced suppression of PCET: significantly less proton density moves to the right compared to the cavity-free case (black), and while the electron transfers in concert with the proton transfer in cavity-free dynamics (see black dipoles in the lowest right panel), it is partially suppressed when the molecule is placed in the cavity with $\lambda = 0.005$ a.u. The snapshots show that part of the wave packet becomes trapped on the left, reducing the nuclear dipole moment and consequently reducing the electron transfer.

Attempting to understand the suppression from the shape of the polaritonic surfaces (Fig. 1) alone is impossible: one

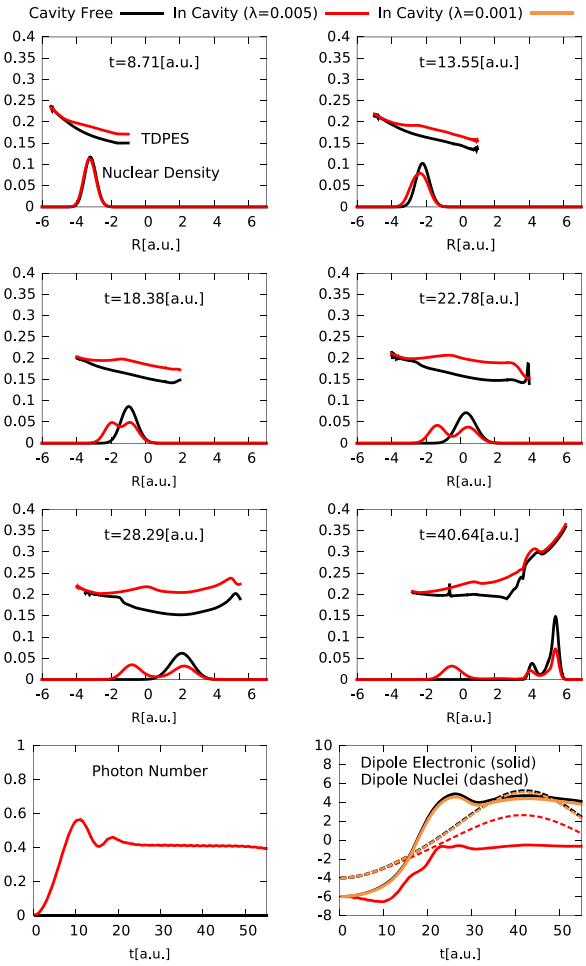

FIG. 2. Snapshots of the nuclear density (scaled by 0.1) and exact TDPES for dynamics inside (red) and outside (black) the cavity. The lowest panels show the electronic and nuclear dipole moments and the photon number over time. Cavity-induced suppression of PCET is evident in the red density as part of the nuclear wave packet becomes trapped on the left, consistent with the structure of the TDPES (see text).

might be tempted to attribute the partial trapping of the density to the barrier in the third polaritonic surface at around $R \approx -2$ a.u.; however not only does the trapped density evolve past this point, but also the barrier is present in the weaker coupling $\lambda = 0.001$ a.u. case which shows negligible suppression as indicated by the orange dipole shown in the lowest panel of Fig. 2 and movie in the Supplemental Material [36]. Instead, as we shortly discuss, the structure of the exact TDPES shown in Fig. 2 directly correlates with the dynamics.

The TDPES is a fundamental construct arising from the EFA [26,27]. When extended to systems of coupled electrons, nuclei, and photons [28,29], EFA factorizes the complete wave function into a nuclear wave function $\chi(R,t)$ and a conditional electron-photon wave function $\Phi_R(r,q,t)$, $\Psi(r,q,R,t) = \chi(R,t)\Phi_R(r,q,t)$, in which the exact equation for the marginal $\chi(R,t)$ is Schrödinger,

$$\{-[\nabla + A(R,t)]^2/2M + \epsilon(R,t)\}\chi(R,t) = i\partial_t\chi(R,t), \quad (5)$$

(written here for one nuclear coordinate), with a scalar potential, the TDPES $\epsilon(R,t)$, and a vector potential $A(R,t)$, both of which depend on $\Phi_R(r,q,t)$. The time evolution for the latter is more complicated [39], with a $\chi(R,t)$-dependent non-Hermitian operator that operates on the R dependence of $\Phi_R(r,q,t)$. The exact equations are provided in the Supplemental Material [36]. The roles of the nuclei, electrons, and photons can be permuted in EFA such that the subsystem of most interest is chosen for the marginal factor χ since this satisfies the Schrödinger equation [28], e.g., choosing the photonic system as the marginal, Ref. [28] found distortions of the exact potential driving the photonic field away from harmonic due to photon-matter coupling.

The factorization of Ψ is unique up to an (R,t)-dependent phase-factor multiplying $\chi(R,t)$ with its inverse multiplying $\Phi_R(r,q,t)$; this in turn transforms the potentials, and for one nuclear dimension, a gauge can always be found in which $A(R,t)$ is zero. Then, the only potential driving the nuclei is $\epsilon(R,t)$ and, for the cavity-enclosed PCET model, is shown in the time snapshots of Fig. 2. Comparing with the cavity-free TDPES, the structures that lead to the partial trapping of the nuclear density, and the subsequent partial PCET suppression, are clearly seen. At early times, the slope of the TDPES is smaller compared to the cavity-free case, even sloping upward in the trailing part of wave packet, therefore slowing down and spreading out the wave packet compared to the cavity-free case (up to $t = 13.55$ a.u.). A gentle step develops, lowering the potential on the left of the wave packet, which begins to split the wave packet in two parts ($t = 18.38$ a.u.): one associated with TDPES turning downward and forming a well to the left and the other turning downward to the right, further enhancing the splitting. The nuclear wave packet on the left becomes trapped in the well, and eventually oscillates in it, unable to reach the region of electron-nuclear nonadiabatic coupling that leads to the electron transfer. In contrast, the nuclear wave packet on the right continues moving to the right ($t = 22.78$, 28.29 a.u.), where it later splits and behaves similarly to the cavity-free dynamics but scaled down since some density was lost in the trapped region on the left ($t = 40.64$ a.u.).

The shape of the TDPES therefore directly reflects the proton's dynamics. To understand the physical mechanisms yielding its shape, we consider the TDPES against the backdrop of polaritonic surfaces. First, we decompose the surface into weighted polaritonic (wpol), kinetic (kin), and gauge-dependent (GD) components that arise from the form of the EFA [27,28] (see the Supplemental Material [36]),

$$\epsilon(R,t) = \epsilon_{\mathrm{wpol}}(R,t) + \epsilon_{\mathrm{kin}}(R,t) + \epsilon_{\mathrm{GD}}(R,t), \quad (6)$$

$$\epsilon_{\mathrm{wpol}}(R,t) = \langle\Phi_R|\hat{H}_{\mathrm{BO}} + \hat{H}_p + \hat{V}_{pm}|\Phi_R\rangle_{r,q}, \quad (7)$$

PHYSICAL REVIEW LETTERS **123,** 083201 (2019)

$$\epsilon_{\mathrm{kin}}(R,t) = \langle \Phi_R | - \nabla_R^2 \Phi_R \rangle_{r,q} / 2M, \tag{8}$$

$$\epsilon_{\mathrm{GD}}(R,t) = \langle \Phi_R | - i\partial_t \Phi_R \rangle_{r,q}. \tag{9}$$

In Fig. 3, we plot $\epsilon_{\mathrm{wpol}}(R,t)$ and $\epsilon_{\mathrm{GD}}(R,t)$ against the backdrop of the static polaritonic surfaces; ϵ_{kin} remains negligible throughout, due to the $1/M$ prefactor. At early times we observe that ϵ_{wpol} on the left lies intermediate between the second and third polaritonic surfaces, acquiring a mixed character, while on the right adheres to the second surface. Looking at the middle row, this behavior resolves into the left part of the nuclear wave packet being correlated with the third polaritonic surface, while the right correlates with the second: this piecewise behavior illustrates matter-photon correlation, with the left part correlated with photon emission accompanying an electronic transition to the lower BO surface (see also Fig. 4 shortly), while the right part of the nuclear wave packet is correlated with a zero-photon electronically excited state. The step in ϵ_{wpol} that bridges the two polaritonic surfaces after the photon-emission event is analogous to that found in earlier work between BO surfaces [33] and between Floquet surfaces [23], which polaritonic surfaces reduce to in the classical-light limit [40]. Also analogous is that ϵ_{GD} displays a countering step [34], that adjusts the energy locally in the nuclear system to account for the different energies of the electron-photon system associated with the different characters on the left and right. It is important to note that the suppression mechanism sets in during the stage when the surface has mixed character, before the piecewise-shifted character of ϵ_{GD} sets in. This is also well before part of the wave packet encounters the avoided crossing associated with strong electron-nuclear coupling around $R \approx 2$ a.u. (see also the BO surfaces Fig. 1), which is where the nuclear wave packet splits again with the part moving to the lowest surface associated with the electron transfer. At the final time shown we see three parts to the nuclear wave packet: the left part trapped in the left well associated with a one-photon BO ground state, and two lobes on the right, with the extreme right associated with PCET on the BO ground state, and the other with the excited BO state, both with zero photons. The ϵ_{wpol} component of the TDPES directly reflects this matter-polariton correlation, while ϵ_{GD} adjusts the local energy in a piecewise manner.

To further clarify the dynamics in the conditional variables q and r, Fig. 4 shows the n photon resolved nuclear density, defined as

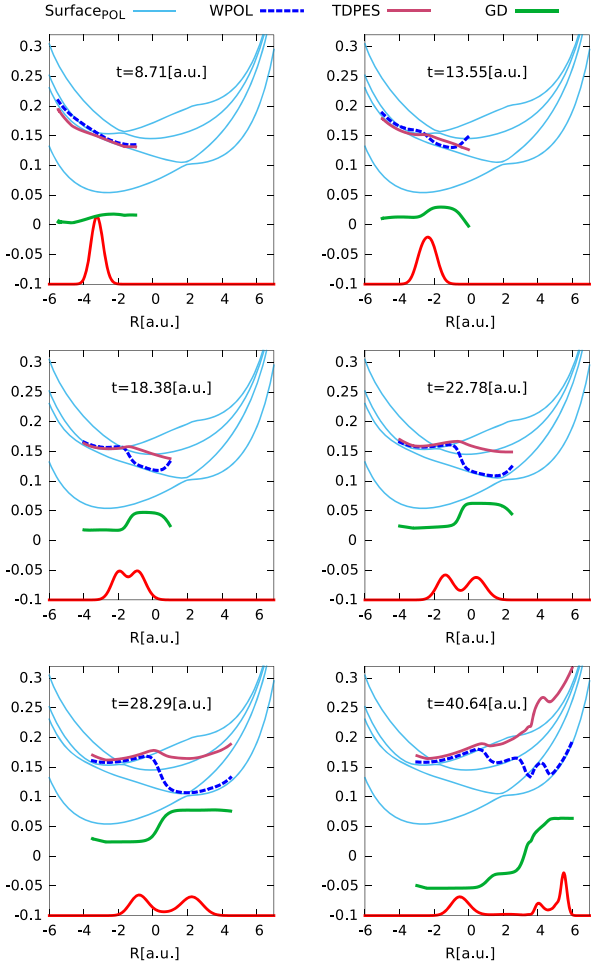

FIG. 3. Snapshots of the nuclear density and the components of the TDPES for dynamics in the cavity, $\lambda = 0.005$, $\omega_\alpha = 0.1$. The thin lines represent the polaritonic surfaces.

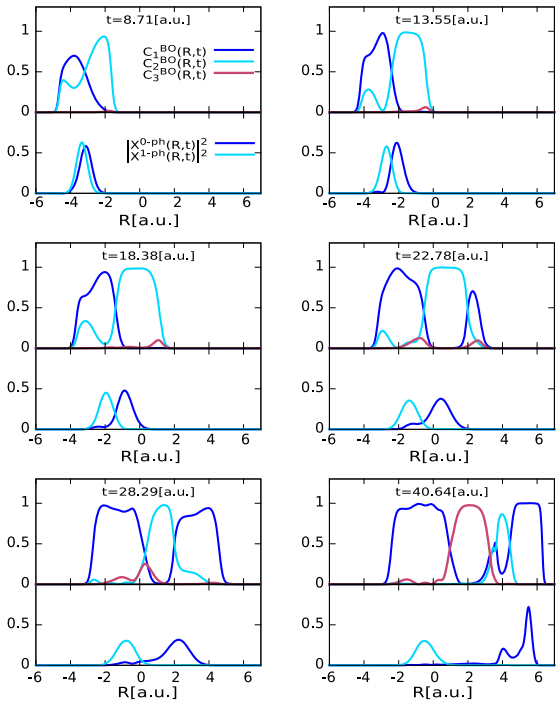

FIG. 4. Snapshots of the zero- and one-photon resolved nuclear densities of Eq. (10) (lower panel), along with the BO coefficients of Eq. (11) (upper panel).

$$|\chi^{n-ph}(R,t)|^2 = |\langle \xi_n|\Psi(t)\rangle_{r,q}|^2, \tag{10}$$

where $\xi_n(q)$ are the harmonic oscillator eigenstates of H_p, and the BO coefficients, defined as

$$C_i^{\mathrm{BO}}(R,t) = |\langle \Phi_R^{\mathrm{BO},i}|\Psi(t)\rangle_{r,q}|^2/|\chi(R,t)|^2. \tag{11}$$

These measures clearly show the nuclear-photon and nuclear-electron correlations throughout the evolution (see also movie in the Supplemental Material [36]). At early times there is mixed character of the electron-photon state, with both zero-photon and one-photon contributions associated with the nuclear density at a given R, and fractional BO coefficients contributing with occupation even in the third BO state. At later times local regions of the nuclear density become correlated with different electronic and photonic characters.

In conclusion, we analyzed the structure of the TDPES for a model of PCET and have shown how its features predict the cavity-induced suppression. While polaritonic surfaces provide a useful backdrop, they are not able to predict dynamics or mechanisms without considering their couplings to each other in dynamics [8,9], and care is needed with such dynamics schemes, due to the propensity of near crossings caused by both electron-nuclear and matter-photon couplings. For mixed quantum-classical methods, which would be required for many-molecule systems [21,41], overcoherence in surface-hopping methods is likely to be quite problematic. Instead, this work shows the promise of rigorously based mixed quantum-classical approximations for cavity-qed, based on, for example, generalizations of the schemes of Refs. [42–49], that have been successful for cavity-free nonadiabatic dynamics.

Financial support from the U.S. National Science Foundation CHE-1566197 (L. L.) and the Department of Energy, Office of Basic Energy Sciences, Division of Chemical Sciences, Geosciences and Biosciences under Award No. DE-SC0015344 (N. T. M) is gratefully acknowledged. N. M. H. gratefully acknowledges funding from the Max-Planck Institute for the Structure and Dynamics of Matter, and an IMPRS fellowship.

[1] T. W. Ebbesen, Acc. Chem. Res. **49**, 2403 (2016).
[2] B. Barnes, F. García Vidal, and J. Aizpurua, ACS Photonics **5**, 1 (2018).
[3] P. Vasa and C. Lienau, ACS Photonics **5**, 2 (2018).
[4] D. G. Baranov, M. Wersäll, J. Cuadra, T. J. Antosiewicz, and T. Shegai, ACS Photonics **5**, 24 (2018).
[5] J. T. Hugall, A. Singh, and N. F. van Hulst, ACS Photonics **5**, 43 (2018).
[6] E. Orgiu, J. George, J. A. Hutchison, E. Devaux, J. F. Dayen, B. Doudin, F. Stellacci, C. Genet, J. Schachenmayer, C. Genes, G. Pupillo, P. Samori, and T. W. Ebbesen, Nat. Mater. **14**, 1123 (2015).
[7] J. Flick, M. Ruggenthaler, H. Appel, and A. Rubio, Proc. Natl. Acad. Sci. U.S.A. **114**, 3026 (2017).
[8] M. Kowalewski, K. Bennett, and S. Mukamel, J. Phys. Chem. Lett. **7**, 2050 (2016).
[9] M. Kowalewski and S. Mukamel, Proc. Natl. Acad. Sci. U.S.A. **114**, 3278 (2017).
[10] F. Herrera and F. C. Spano, Phys. Rev. Lett. **116**, 238301 (2016).
[11] G. Mazza and A. Georges, Phys. Rev. Lett. **122**, 017401 (2019).
[12] M. A. Sentef, M. Ruggenthaler, and A. Rubio, Sci. Adv. **4**, eaau6969 (2018).
[13] R. F. Ribeiro, L. A. Martinez-Martinez, M. Du, J. Campos-Gonzalez-Angulo, and J. Yuen-Zhou, Chem. Sci. **9**, 6325 (2018).
[14] A. Csehi, A. Halasz, G. J. Vibok, and M. Kowalewski, arXiv:1904.12693.
[15] J. Galego, F. J. Garcia-Vidal, and J. Feist, Phys. Rev. X **5**, 041022 (2015).
[16] J. Galego, F. J. Garcia-Vidal, and J. Feist, Nat. Commun. **7**, 13841 (2016).
[17] J. Feist, J. Galego, and F. J. Garcia-Vidal, ACS Photonics **5**, 205 (2018).
[18] C. Schäfer, M. Ruggenthaler, H. Appel, and A. Rubio, Proc. Natl. Acad. Sci. U.S.A. **116**, 4883 (2019).
[19] M. Ruggenthaler, N. Tancogne-Dejean, J. Flick, H. Appel, and A. Rubio, Nat. Rev. Chem. **2**, 0118 (2018).
[20] J. Flick, H. Appel, M. Ruggenthaler, and A. Rubio, J. Chem. Theory Comput. **13**, 1616 (2017).
[21] H. L. Luk, J. Feist, J. J. Toppari, and G. Groenhof, J. Chem. Theory Comput. **13**, 4324 (2017).
[22] M. Fischer, U. Lorenz, B. Schmidt, and R. Schmidt, Phys. Rev. A **84**, 033422 (2011).
[23] T. Fiedlschuster, J. Handt, E. K. U. Gross, and R. Schmidt, Phys. Rev. A **95**, 063424 (2017).
[24] M. Thachuk, M. Y. Ivanov, and D. M. Wardlaw, J. Chem. Phys. **105**, 4094 (1996).
[25] Y. Sato, H. Kono, S. Koseki, and Y. Fujimura, J. Am. Chem. Soc. **125**, 8019 (2003).
[26] A. Abedi, N. T. Maitra, and E. K. U. Gross, Phys. Rev. Lett. **105**, 123002 (2010).
[27] A. Abedi, N. T. Maitra, and E. K. U. Gross, J. Chem. Phys. **137**, 22A530 (2012).
[28] N. M. Hoffmann, H. Appel, A. Rubio, and N. T. Maitra, Eur. Phys. J. B **91**, 180 (2018).
[29] A. Abedi, E. Khosravi, and I. V. Tokatly, Eur. Phys. J. B **91**, 194 (2018).
[30] S. Shin and H. Metiu, J. Chem. Phys. **102**, 9285 (1995).
[31] J.-Y. Fang and S. Hammes-Schiffer, J. Chem. Phys. **106**, 8442 (1997).
[32] J.-Y. Fang and S. Hammes-Schiffer, J. Chem. Phys. **107**, 5727 (1997).
[33] A. Abedi, F. Agostini, Y. Suzuki, and E. K. U. Gross, Phys. Rev. Lett. **110**, 263001 (2013).
[34] F. Agostini, A. Abedi, Y. Suzuki, S. K. Min, N. T. Maitra, and E. K. U. Gross, J. Chem. Phys. **142**, 084303 (2015).
[35] S. K. Min, A. Abedi, K. S. Kim, and E. K. U. Gross, Phys. Rev. Lett. **113**, 263004 (2014).

[36] See Supplemental Material at http://link.aps.org/supplemental/10.1103/PhysRevLett.123.083201 for a brief presentation of the exact factorization equations we use here, the values of numerical parameters used in the calculations, and three movies as described in the text to support the figures shown.
[37] I. V. Tokatly, Phys. Rev. Lett. **110**, 233001 (2013).
[38] M. Ruggenthaler, J. Flick, C. Pellegrini, H. Appel, I. V. Tokatly, and A. Rubio, Phys. Rev. A **90**, 012508 (2014).
[39] G. H. Gossel, L. Lacombe, and N. T. Maitra, J. Chem. Phys. **150**, 154112 (2019).
[40] S. Guérin, F. Monti, J.-M. Dupont, and H. R. Jauslin, J. Phys. A **30**, 7193 (1997).
[41] B. Mignolet and B. F. E. Curchod, J. Phys. Chem. A **123**, 3582 (2019).
[42] F. Agostini, S. K. Min, A. Abedi, and E. K. U. Gross, J. Chem. Theory Comput. **12**, 2127 (2016).
[43] S. K. Min, F. Agostini, and E. K. U. Gross, Phys. Rev. Lett. **115**, 073001 (2015).
[44] S. K. Min, F. Agostini, I. Tavernelli, and E. K. U. Gross, J. Phys. Chem. Lett. **8**, 3048 (2017).
[45] F. Agostini and B. F. E. Curchod, Comput. Mol. Sci. **9**, e1417 (2019).
[46] G. H. Gossel, F. Agostini, and N. T. Maitra, J. Chem. Theory Comput. **14**, 4513 (2018).
[47] J.-K. Ha, I. S. Lee, and S. K. Min, J. Phys. Chem. Lett. **9**, 1097 (2018).
[48] M. Filatov, M. Paolino, S. K. Min, and C. H. Choi, Chem. Commun. **55**, 5247 (2019).
[49] M. Filatov, S. K. Min, and C. H. Choi, Phys. Chem. Chem. Phys. **21**, 2489 (2019).

Supplementary Material for "Exact Potential Energy Surface for Molecules in Cavities"

Lionel Lacombe
Department of Physics and Astronomy, Hunter College of the City University of New York, 695 Park Avenue, New York, New York 10065, USA

Norah M. Hoffman
Max Planck Institute for the Structure and Dynamics of Matter and Center for Free-Electron Laser Science and Department of Physics, Luruper Chaussee 149, 22761 Hamburg, Germany and
Department of Physics and Astronomy, Hunter College of the City University of New York, 695 Park Avenue, New York, New York 10065, USA

Neepa T. Maitra
Department of Physics and Astronomy, Hunter College of the City University of New York, 695 Park Avenue, New York, New York 10065, USA and
Physics Program and Chemistry Program, Graduate Center of the City University of New York, New York, USA

(Dated: May 30, 2019)

I. EXACT FACTORIZATION EQUATIONS

The full equations of the EF factorization we use here are based on the generalization given in Ref. [1] of the original time-dependent EF equations of Ref. [2, 3]. These are based on the factorization

$$\Psi(\underline{\underline{r}},\underline{\underline{q}},\underline{\underline{R}},t)=\chi(\underline{\underline{R}},t)\Phi_{\underline{\underline{R}}}(\underline{\underline{r}},\underline{\underline{q}},t) \tag{1}$$

where $\underline{\underline{r}},\underline{\underline{q}},\underline{\underline{R}}$ represent all electronic-, photonic displacement-field mode-, and nuclear- coordinates, respectively, and the partial normalization condition

$$\int|\Phi_{\underline{\underline{R}}}(\underline{\underline{r}},\underline{\underline{q}},t)|^2 d\underline{\underline{r}}d\underline{\underline{q}}=1 \tag{2}$$

is satisfied. The marginal and conditional parts each satisfy the following coupled equations of motion:

$$\left(\hat{H}_{\rm BO}+\hat{H}_p+\hat{V}_{pm}+\hat{V}_{\rm dipSE}+\hat{U}_{\rm ep-n}-\epsilon(\underline{\underline{R}},t)\right)\Phi_{\underline{\underline{R}}}(\underline{\underline{r}},\underline{\underline{q}},t)=i\partial_t\Phi_{\underline{\underline{R}}}(\underline{\underline{r}},\underline{\underline{q}},t) \tag{3}$$

$$\left(\sum_{J=1}^{N_n}(-i\nabla_J+\mathbf{A}_J(\underline{\underline{R}},t))^2/2M_J+\epsilon(\underline{\underline{R}},t)\right)\chi(\underline{\underline{R}},t)=i\partial_t\chi(\underline{\underline{R}},t) \tag{4}$$

with

$$\hat{U}_{ep-n}=\sum_{J=1}^{N_n}\frac{1}{M_J}\left(\frac{(-i\nabla_J-\mathbf{A}_J(\underline{\underline{R}},t))^2}{2}+\left(\frac{-i\nabla_J\chi(\underline{\underline{R}},t)}{\chi(\underline{\underline{R}},t)}+\mathbf{A}_J(\underline{\underline{R}},t)\right)\cdot\left(-i\nabla_J-\mathbf{A}_J(\underline{\underline{R}},t)\right)\right) \tag{5}$$

$$\epsilon(\underline{\underline{R}},t)=\langle\Phi_{\underline{\underline{R}}}|\hat{H}_{\rm BO}+\hat{H}_p+\hat{V}_{pm}+\hat{V}_{\rm dipSE}+\hat{U}_{\rm ep-n}-i\partial_t|\Phi_{\underline{\underline{R}}}\rangle_{\underline{\underline{r}},\underline{\underline{q}}} \tag{6}$$

$$\mathbf{A}_J(\underline{\underline{R}},t)=\langle\Phi_{\underline{\underline{R}}}|-i\nabla_J\Phi_{\underline{\underline{R}}}\rangle_{\underline{\underline{r}},\underline{\underline{q}}} \tag{7}$$

and all other terms in Eqs. 3 and 4 are given in the main text for the one-dimensional model we studied. The notation $\langle...\rangle_{\underline{\underline{r}},\underline{\underline{q}}}$ indicates an integral over all photonic displacement-field and electronic coordinates only.

The marginal part, $\chi(\underline{\underline{R}},t)$ is a nuclear wavefunction in the sense that it reproduces the exact nuclear density and exact nuclear current-density of the exact full photon-matter wavefunction. The equations 3–7 are form-invariant under the phase-transformation $\Phi_{\underline{\underline{r}},\underline{\underline{q}}}(\underline{\underline{R}},t)\rightarrow\Phi_{\underline{\underline{r}},\underline{\underline{q}}}(\underline{\underline{R}},t)e^{i\theta(\underline{\underline{R}},t)}$, $\chi(\underline{\underline{R}},t)\rightarrow\chi(\underline{\underline{R}},t)e^{-i\theta(\underline{\underline{R}},t)}$ with the potentials undergoing the gauge-like transformation $\mathbf{A}_J(\underline{\underline{R}},t)\rightarrow\mathbf{A}_J(\underline{\underline{R}},t)+\nabla_J\theta(\underline{\underline{R}},t)$, $\epsilon(\underline{\underline{R}},t)\rightarrow\epsilon(\underline{\underline{R}},t)+\partial_t\theta(\underline{\underline{R}},t)$, and the factorization Eq. 1 is unique up to such a transformation.

The model we studied has a one-dimensional nuclear coordinate so a gauge can always be found in which the vector potential $\mathbf{A}(\underline{\underline{R}},t)$ is zero. This is the gauge we chose in our calculations. The equations then simplify in the sense, for example, that there is only one potential, the scalar $\epsilon(\underline{\underline{R}},t)$ appearing in the nuclear equation, and the scalar potential can then be written as three terms, as prescribed in Eqs. (6)–(9) of the main paper.

In practise, we obtained the potential energy surface $\epsilon(\underline{\underline{R}},t)$ by inversion [3]. That is, we first solved the time-dependent Schrödinger equation for $\Psi(r,q,R,t)$ on a three-dimensional grid, and extracted $\chi(R,t)=|\chi(R,t)|e^{iS(R,t)}$ using

$$|\chi(R,t)|=\sqrt{\int dqdr|\Psi(r,q,R,t)|^2} \tag{8}$$

and

$$S(R,t)=\int^R\left(\frac{\mathrm{Im}\int drdq\,\Psi(r,q,R',t)\frac{d\Psi(r,q,R',t)}{dR'}}{|\chi(R',t)|^2}\right)dR' \tag{9}$$

Then we found $\Phi_{r,q}(R,t)=\Psi(r,q,R,t)/\chi(R,t)$ enabling us to evaluate the matrix elements involved for $\epsilon(R,t)$ (Eqs.(6) – (9) of the main text).

II. NUMERICAL DETAILS

In our calculations, we used 192, 96, 1280 points on a grid of size ±120.20 a.u., ±80 a.u., ±9.5 a.u., for the electronic, photonic or nuclear calculation respectively. We also used a time-step of 0.1 a.u.

III. MOVIES

We provide three movies:

(i) **movieCpl0p005** shows the dynamics for the case where the resonant frequency of the cavity is $\omega_\alpha = 0.1$au and the coupling strength is $\lambda = 0.005$ in red, compared to the cavity-free dynamics in black.

Top left: exact TDPES, shown against the background of polaritonic surfaces in blue and green, and the nuclear density, scaled by 0.1 and shifted down, is shown in the lower part of all plots in the first row.
Top middle: weighted polaritonic component of the exact TDPES $\epsilon_{\rm wpol}(R,t)$.
Right middle: gauge-dependent component of the exact TDPES $\epsilon_{\rm GD}(R,t)$.
Lower left: BO coefficients $C_i(R,t)$ as defined in Eq. (11) of the main text as a function of time
Lower middle: number of photons emitted as a function of time
Lower right: electronic (solid) and nuclear (dashed) dipole moments as a function of time.

(ii) **movieCpl0p001** as above but for coupling strength $\lambda = 0.001$.

(iii) **movieCpl0p005phdenCBO** shows the n-photon resolved densities and BO-coefficients for the $\omega_\alpha = 0.1$ and $\lambda = 0.005$ case as compared with the cavity-free case.
Top left panel: the total nuclear density (as a reference)
Top right panel: the 0-photon resolved density
Middle left: the 1-photon resolved density
Middle right: the 2-photon resolved density
Lower left: the BO coefficients in the cavity
Lower right: the BO-coefficients for the cavity-free case.

---

[1] N. M. Hoffmann, H. Appel, A. Rubio, and N. T. Maitra, The European Physical Journal B **91**, 180 (2018).
[2] A. Abedi, N. T. Maitra, and E. K. U. Gross, Phys. Rev. Lett. **105**, 123002 (2010).
[3] A. Abedi, N. T. Maitra, and E. K. U. Gross, J. Chem. Phys. **137**, 22A530 (2012).

3.2 POLARITONIC CHEMISTRY VIA MULTI-TRAJECTORY EHRENFEST

"Effect of Many Modes on Self-Polarization and Photochemical Suppression in Cavities"

NM Hoffmann, L Lacombe, A Rubio, NT Maitra

ArXiv (2020), arXiv preprint: *arXiv: 2001.07330*

MOTIVATION Continuing our work of Sec. 2.1 and Sec. 3.2, the overall motivation for this work as well as the current state of the art research stays the same. However, based on the knowledge obtained from [O1, O3], we now broaden our scope by investigating a full molecular system, i.e. electron-nuclei-photon correlated system and investigate the performance of the MTEF[1] approach within the cavity-induced suppression of the PCET investigated in [O4]. With the ability to go beyond single photon-mode calculations via the MTEF approach, we further target the so far unexplored question: How does including many cavity-modes affect the cavity-modified phenomena?

STATE OF THE ART Apart from a handful of exceptions [70, 146–149] the simulations of cavity-modified chemistry largely involve coupling to only one (resonant) photon mode, and the vast majority uses simple model systems for the matter part. The modeling of realistic cavity set-ups requires coupling to multiple photon modes that are resonant in the cavity even if they are not resonant with matter degrees of freedom and, further, the description should account for losses at the cavity boundaries. Some strategies have been put forward to treat quantized field modes in the presence of dispersive and absorbing materials [150–154] and theories have been developed to treat many modes and many matter degrees of freedom [56, 70, 79, 80, 146–149, 155]. So far unexplored, however, is a demonstration of how the cavity-modified electronic-nuclear dynamics that were simulated using a single loss-less mode change as one increases the number of photon modes. Nonetheless, in order to calculate such high-dimensional systems, i.e. molecules coupled to multiple photon modes requires accurate and computationally efficient approximations.

CONTRIBUTION AND MAIN FINDINGS To this end, we extend the MTEF approach to polaritonic chemistry, i.e. coupled electron-nuclear-photon dynamics,

1 In order to avoid confusion for future publications with potential combinations of the MTEF approach and the EF approach, the acronym MTEF has been changed to MTE in this paper.

focusing on the effect that including many photon modes has on the process of cavity-induced suppression of PCET. To validate the MTEF treatment of photons, we first study the single-mode case, for which exact results can be computed, finding that MTEF performs well but tends to underestimate the photon emission and cavity-induced effects. We explain this by using the EF approach [O2]. Treating the nuclei classically as well gives reasonable averaged dipoles and photon numbers, but a poor nuclear density, as expected. Turning to multi-mode dynamics computed from MTEF for photons, we find that the effect of multiple cavity photon modes on the reaction dynamics can be dramatically different than when only a single mode is accounted for. More precisely, as the number of cavity modes increases (without changing the coupling strength), the suppression of both proton transfer and electron transfer significantly increases, the electronic character becomes more mixed throughout, the photon number begins to increase, and the photon frequency acquires a small but growing Lamb-like shift. This suggests that single-mode simulations tend to underestimate the cavity-induced effects on dynamics in realistic cavities. The self-polarization term [71, 83, 84] in the Hamiltonian that is often neglected in the literature, has an increasingly crucial impact on the dynamics, and we introduce the concept of spBO surfaces as an instructive tool for analysis of chemical processes mediated by cavity-coupling.

OUTLOOK Analogously to the outlook discussed in Secs. 2.1 and 3.2, to obtain a practical approach for realistic systems we further need an approximate treatment of the matter part. From the electronic side TDDFT would be a natural choice, while a practical treatment of nuclei calls for a classical treatment such as Ehrenfest or surface-hopping in some basis. However, the increase of crossings the more photon-modes are accounted for suggests that simple surface-hopping treatments based on BO (or spBO) surfaces should be used with much caution and that decoherence-corrections should be applied, for example those generalized from the EF approach, to the electron-nuclear problem [37–39, 156–158]. Furthermore, we note that the findings in this work are general in that the increasing importance of self-polarization with more photon modes is expected to hold for the description and control of cavity-driven physical processes of molecules, nanostructures and solids embedded in cavities in general. These findings could yield a new way to control and change chemical reactions via the self-polarization without the need to explicitly change the light-matter coupling strength itself.

SUPPLEMENTARY MATERIAL In the supplementary material to this paper provides three movies[2] corresponding to the discussed results in the paper.

2 Movies: https://github.com/nhoffma5/Effect_of_Many_Modes_Supplementary

Effect of Many Modes on Self-Polarization and Photochemical Suppression in Cavities

Norah M. Hoffmann,[1,2,*] Lionel Lacombe,[1,†] Angel Rubio,[2,3,4,‡] and Neepa T. Maitra[1,§]

[1]*Department of Physics, Rutgers University at Newark, Newark, NJ 07102, USA*
[2]*Max Planck Institute for the Structure and Dynamics of Matter and Center for Free-Electron Laser Science and Department of Physics, Luruper Chaussee 149, 22761 Hamburg, Germany*
[3]*Center for Computational Quantum Physics, Flatiron Institute, 162 5th Avenue, New York, NY 10010, USA*
[4]*Nano-Bio Spectroscopy Group and ETSF, Universidad del Pas Vasco, 20018 San Sebastian, Spain*

(Dated: January 22, 2020)

The standard description of cavity-modified molecular reactions typically involves a single (resonant) mode, while in reality the quantum cavity supports a range of photon modes. Here we demonstrate that as more photon modes are included, physico-chemical phenomena can dramatically change, as illustrated by the cavity-induced suppression of the important and ubiquitous process of proton-coupled electron-transfer. Using a multi-trajectory Ehrenfest treatment for the photon-modes, we find that self-polarization effects become essential, and we introduce the concept of self-polarization-modified Born-Oppenheimer surfaces as a new construct to analyze dynamics. As the number of cavity photon modes increases, the interplay between photon emission and absorption inside the increasingly wide bands of these surfaces, together with their deviations from the cavity-free Born-Oppenheimer surfaces, leads to enhanced suppression. The present findings are general and will have implications for the description and control of cavity-driven physical processes of molecules, nanostructures and solids embedded in cavities.

The interaction between photons and quantum systems is the foundation of a wide spectrum of phenomena, with applications in a range of fields. One rapidly-expanding domain is cavity-modified chemistry, by which we mean here nuclear dynamics concomitant with electron dynamics when coupled to confined quantized photon modes [1–4]. The idea is to harness strong light-matter coupling to enhance or quench chemical reactions, manipulate conical intersections, selectively break or form bonds, control energy, charge, spin, or heat transfer, and reduce dissipation to the environment, for example. This forefront has has been strongly driven by experiments [2, 5–11], with theoretical investigations revealing complementary insights [4, 12–31]. However, apart from a handful of exceptions [32–38] the simulations of cavity-modified chemistry largely involve coupling to only one (resonant) photon mode, and the vast majority uses simple model systems for the matter part. The modeling of realistic cavity set-ups requires coupling to multiple photon modes that are resonant in the cavity even if they are not resonant with matter degrees of freedom, and further, the description should account for losses at the cavity boundaries. Some strategies have been put forward to treat quantized field modes in the presence of dispersive and absorbing materials [39–43] and theories have been developed to treat many modes and many matter degrees of freedom [14, 27, 30, 32, 34–38, 44]. So far unexplored however is a demonstration of how the cavity-modified electronic-nuclear dynamics that were simulated using a single loss-less mode change as one increases the number of photon modes.

Molecules coupled to multiple photon modes represent high-dimensional systems for which accurate and computationally efficient approximations beyond model systems are needed. To this end, the Multi-Trajectory Ehrenfest (MTE) approach for light-matter interaction has been recently introduced [33, 34], and benchmarked for two- or three-level electronic systems in a cavity. Wigner-sampling the initial photonic state to properly account for the vacuum-fluctuations of the photonic field while using mean-field trajectories for its propagation, this method is able to capture quantum effects such as spontaneous-emission, bound photon states and second order photon-field correlations [33, 34]. In particular, as the trajectories are not coupled during their time-evolution the algorithm is highly parallelizable. Therefore, due to the simplicity, efficiency, and especially scalability the MTE approach for photons emerges as an interesting alternative or extension to other multi-mode treatments [27, 30, 32, 34, 36, 37, 42, 44]. [1]

In this work, we extend the MTE approach to cavity-modified chemistry, and observe for the first time (to our knowledge) the effect that accounting for many photon modes has on coupled electron-ion dynamics. We focus on the process of polaritonic suppression of an important and ubiquitous process in chemistry and biology, the proton-coupled electron transfer [45], finding

* norah.magdalena.hoffmann@mpsd.mpg.de
† liolacombe@gmail.com
‡ angel.rubio@mpsd.mpg.de
§ neepa.maitra@rutgers.edu

[1] This includes Quantum-Electrodynamical Density Functional Theory (QEDFT) [4, 27, 30, 44], which is an exact non-relativistic generalization of time-dependent density functional theory that dresses electronic states with photons and allows to retain the electronic properties of real materials in a computationally efficient way.

the electron-nuclear dynamics significantly depends on the number of modes, as sketched in Fig. 1. We neglect (for now) any effects from cavity losses so we can isolate effects purely from having many modes in the cavity rather than a single mode. To validate the MTE treatment of photons, we first study the single-mode case for which exact results can be computed, finding that MTE performs well but tends to underestimate the photon emission and cavity-induced effects. We explain why using the exact factorization approach [46]. Treating also the nuclei classically gives reasonable averaged dipoles, and photon numbers, but a poor nuclear density, as expected. Turning to multi-mode dynamics computed from MTE, we find that as the number of cavity modes increases (without changing the coupling strength), the suppression of both proton transfer and electron transfer significantly increases, the electronic character becomes more mixed throughout, the photon number begins to increase, and the photon frequency acquires a small but growing Lamb-like shift. This suggests that single-mode simulations tend to underestimate the cavity-induced effects on dynamics in realistic cavities. The self-polarization term [19, 47, 48] in the Hamiltonian that is often neglected in the literature, has an increasingly crucial impact on the dynamics, and we introduce the concept of self-polarization-modified Born-Oppenheimer (spBO) surfaces as an instructive tool for analysis of chemical processes mediated by cavity-coupling.

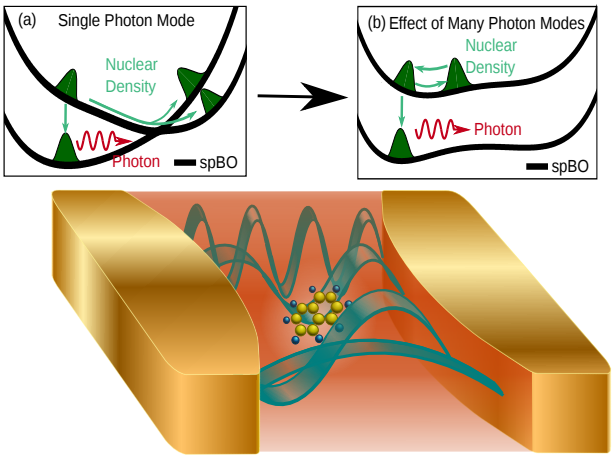

FIG. 1. An exemplary sketch of a molecule coupled to many photon modes. (a) Sketches the spBO surfaces and the corresponding nuclear dynamics for a coupling to a single photon mode. (b) Depicts the effect of many photon modes on the spBO surfaces and the corresponding complete photochemical suppression of the proton-coupled electron transfer.

RESULTS

A. Self-Polarization-Modified BO Surfaces

Potential energy surfaces play a paramount role in analyzing coupled electron-dynamics: we have Born-Oppenheimer (BO) surfaces for cavity-free dynamics, Floquet [49, 50] or quasistatic [51, 52] surfaces for molecules in strong fields, cavity-BO [18] or polaritonic surfaces [13] for molecules in cavities and the exact-factorization based time-dependent potential energy surface [45, 53, 54] for all cases that yields a complete single-surface picture. The surfaces so far explored for molecules in cavities have largely neglected the self-polarization term, which is typically indeed negligible for single-mode cavities except at ultra-strong coupling strengths [19]; its importance in obtaining a consistent ground-state and maintaining gauge-invariance has also been emphasized [47, 48]. In the multi-mode case however, there is a sum over modes in this term that can become as important as the other terms in the Hamiltonian, and, as we shall see below, it cannot be neglected, especially becoming relevant for large mode-numbers, contributing forces on the nuclei as the total dipole evolves in time. Therefore, to analyze the dynamics, we define self-polarization-modified Born-Oppenheimer (spBO) surfaces $\epsilon^{\rm SP}_{\rm BO}(R)$, as eigenvalues of the spBO Hamiltonian, where $H^{\rm SP}_{\rm BO}$ defines the traditional BO-Hamiltonian plus the self-polarization term (see Methods for details): $\hat{H}^{\rm SP}_{\rm BO}\Phi^{\rm SP}_{R,\rm BO} = \epsilon^{\rm SP}_{\rm BO}(R)\Phi^{\rm SP}_{R,\rm BO}$.

Further, we define 1-photon-spBO surfaces by simply shifting the spBO surfaces uniformly by the energy of one photon, $\hbar\omega_\alpha$. These can be viewed as approximate (self-polarization modified) polaritonic surfaces, becoming identical to them in the limit of zero coupling. For small non-zero coupling the polaritonic surfaces, defined as eigenvalues of $\hat{H} - \hat{T}_n$, where $\hat{T}_n$ denotes the nuclear kinetic term, resemble the n-photon-spBO surfaces when they are well-separated from each other, but when they become close, the crossings become avoided crossings.

The top middle panel of Fig. 2 shows the spBO surfaces (pink) for the case of a single photon mode at frequency $\omega_\alpha = 0.1$ a.u. coupled to our molecule, along with the 1-photon-spBO surfaces (black). Our model molecule consists of one electronic and one nuclear degree of freedom, with the Hamiltonian given in the Methods section, and we truncate the electronic Hilbert space to the lowest two BO-surfaces throughout this paper. For one mode at the coupling strength of $\lambda = 0.005$ a.u. (see Methods) the spBO surfaces coincide with the BO surface, i.e. the self-polarization energy is negligible [45].

As the number of cavity modes grows, the spBO surfaces begin to strongly deviate from the BO surfaces. We consider cavities with resonant modes at frequencies $\omega_\alpha = 0.1 + \frac{\alpha\pi c}{\mathcal{L}}$ with $\alpha = \{-\frac{\mathcal{M}}{2}\cdots\frac{\mathcal{M}}{2}\}$ with $\mathcal{M}$ the number of modes ranging from 0 (single mode), to $10, 40, 200, 440$ and $\mathcal{L} = 50\mu m$ is the cavity-length. The black curves in the top panel of Fig. 3 indicate the corresponding spBO surfaces, and clearly show an in-

creasing departure from the BO surfaces as the number of photon modes increases. Given that the landscape of such surfaces provides valuable intuition about the nuclear wavepacket dynamics, with their gradients supplying forces, this suggests an important role of the self-polarization term in the dynamics of the nuclear wavepacket, as we will see shortly.

With more modes, the 1-photon-spBO surfaces begin to form a quasi-continuum: band-like structures indicated by the shaded colors in the top row of Fig. 3. The shading actually represents parallel surfaces separated by the mode-spacing 0.00045 a.u. (We note that, as a function of cavity-length, the mode-spacing decreases, approaching the continuum limit as $\mathcal{L}$ approaches infinity, however the coupling strength λ_α also decreases, vanishing in the infinite-$\mathcal{L}$ limit such that the free BO surfaces are recovered). The 1-photon ground-spBO band and 1-photon excited-spBO band show growing width and increasing overlap as the number of photon modes increases, suggesting a nuclear wavepacket will encounter an increasing number of avoided crossings between ground- and excited- polaritonic states as it evolves. Note that as lower frequencies are included in the band, n-photon-spBO ($n \geq 2$) states will overlap with the 1-photon-spBO band. For simplicity however we will still refer to these as simply 1-photon-spBO bands with the understanding that they may include some 2-photon and higher-photon-number states for low frequencies. We return to the implications of the spBO bands later in the discussion of the multi-mode cases.

B. Single-Mode Benchmark

First we consider the single-mode case for which we are able to compare the MTE method (see Methods for details) to numerically exact results[2]. The central photon frequency of 0.1 a.u. is chosen to coincide with the BO energy difference at $R = -4$ a.u., which is where we launch an initial Gaussian nuclear wavepacket on the excited BO surface. We take the initial state as a simple factorized product of the photonic vacuum state $\xi_0(q)$ for each mode, the excited BO state, and the nuclear Gaussian wavepacket: $\Psi(r, R, \underline{q}, 0) = \mathcal{N} e^{-[(R+4)^2/2.85]} \Phi^{\mathrm{BO}}_{R,2}(r)\xi_0(\underline{q})$, where $\underline{q}$ denotes the vector of photonic displacement-field coordinates.

The top panel of Fig. 2 shows the electronic wavefunctions at $R = -4$ a.u. (left) and $R = 4$ a.u. (right) in the cavity-free case, showing that the transition of the initial wavepacket to the lower BO surface through non-adiabatic coupling near the avoided crossing results in an electron transfer. Hence the molecule models proton-coupled electron transfer. Ref. [45] found that this proton-coupled electron transfer is suppressed when the molecule is placed in a single-mode cavity resonant with the initial energy difference between the BO surfaces.

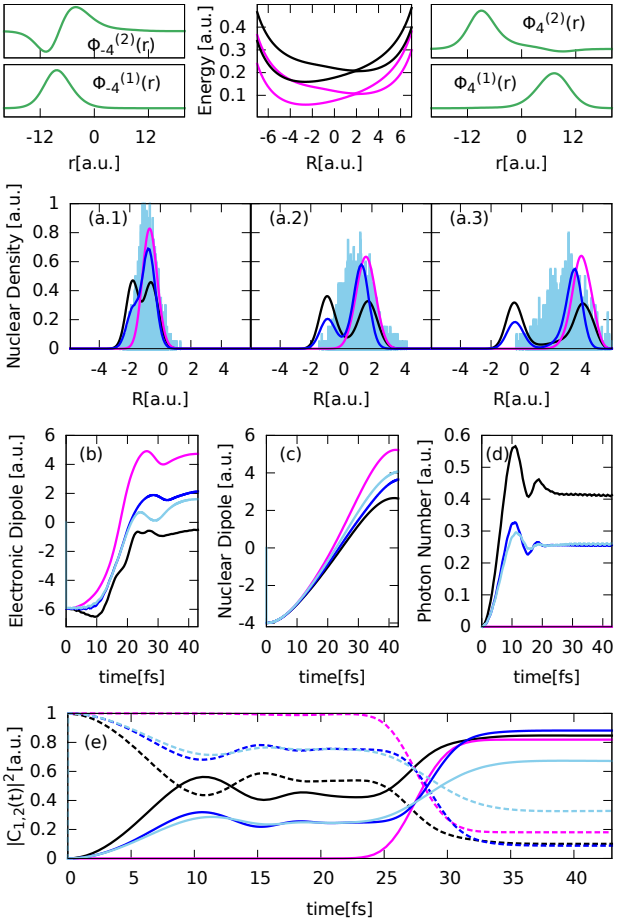

FIG. 2. Single-Mode Case: The top panel shows the ground (lower) and excited (upper) BO wavefunctions at $R = -4$ a.u. (left) and at $R = 4$ a.u. (right) and the spBO surfaces (pink) and one-photon spBO surfaces (black). The second panel depicts the nuclear density for cavity-free (pink), full quantum treatment (black), MTE treatment of the photons only (blue) and MTE treatment of both photons and nuclei (light blue) at time snapshots $t = 22$ fs (a.1) ,$t = 30$ fs (a.2) and $t = 38$ fs (a.3). The third panel shows the electronic (b) and nuclear (c) dipole and the photon number (d). The lowest panel depicts the BO occupations, $|C_{1,2}(t)|^2$.

The second row of Fig. 2 shows the dynamics of the nuclear wavepacket (see also supplementary materials, movie 1) for the exact cavity-free case (pink), exact single-mode case (black), MTE for photons (blue) and MTE for both photons and nuclei (light blue). As discussed in Ref. [45], the exact dynamics in the cavity shows suppression of proton-coupled electron transfer (compare pink and black dipoles in third panel), due to

[2] We note that the two-mode case can also be solved exactly numerically, but the single-mode comparison here already illustrates the main points.

photon emission at early times (black line in panel (d)) yielding a partially trapped nuclear wavepacket, leading to less density propagating to the avoided crossing to make the transition to the lower BO surface. The BO-populations in the lowest panel (e) show the initial partial drop to the ground-state surface associated with the photon emission.

Both MTE approaches are able to approximately capture the cavity-induced suppression of the proton-coupled electron transfer, as indicated by the blue and light-blue dipoles and photon-number in panels (b–d), and approximate the BO occupations in panel (e) reasonably well. However both approaches somewhat underestimate the suppression; the photon emission is underestimated by about a third, as is the suppression of the electronic dipole transfer, for example. To understand why, we compare the potentials the MTE photons experience to the exact potential acting on the photons as defined by the exact factorization approach, which was presented in Ref. [46]. In this approach, the total wavefunction of a system of coupled subsystems is factorized into a single product of a marginal factor and a conditional factor, and the equation for the marginal satisfies a Schrödinger equation with potentials that exactly contain the coupling effects to the other subsystem. When the photonic system is chosen as the marginal, one obtains then the exact potential driving the photons, and this was found for the case of an excited two-level system in a single resonant mode cavity in Ref. [46]. It was shown that the potential develops a barrier for small q-values while bending away from an upper harmonic surface to a lower one at large q, creating a wider and unharmonic well. This leads then to a photonic displacement-field density with a wider profile in q than would be obtained via the uniform average of harmonic potentials that underlie the MTE dynamics, i.e. MTE gives lower probabilities for larger electric-field values, hence a smaller photon-number and less suppression compared to the exact.

An additional treatment of the nuclei within MTE yields a spreading of the nuclear wave packet instead of a real splitting (Fig. 2(a.3)), a well-known problem of Ehrenfest-nuclei. This error is less evident in averaged quantities such as dipoles and BO coefficients.

Having now understood the limitations of MTE, we now apply the MTE framework for photons to the multi-mode case.

C. MTE Dynamics for Multi-Mode Cases

The top panel of Fig. 3 shows the ground and excited 1-photon spBO bands. As we observed earlier, including more photon modes has two effects on the spBO surfaces. First, the self-polarization morphs them away from the cavity-free BO surfaces, increasing their separation, and what was a narrow avoided crossing in the cavity-free case shifts leftward in R with increased

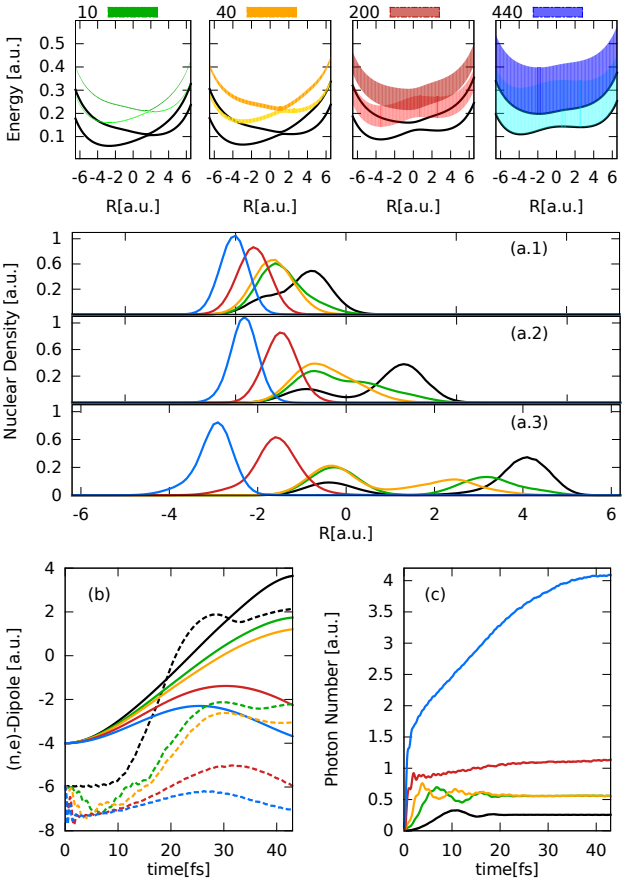

FIG. 3. The ground- and excited 1-photon spBO bands, representing surfaces separated by 0.00045 a.u. (see text) for 10 modes (green), 40 modes (orange), 200 modes (red) and 440 modes (blue). The middle panel depicts the nuclear density at time snap shots $t = 22$fs (a.1), $t = 30$fs (a.2) and $t = 41$fs (a.3) in the same color code along with the single mode case computed within MTE-for-photons (black). The lowest panel shows the electronic and nuclear dipole (b) and the photon number (c).

separation. Second, the 1-photon ground and excited spBO bands both broaden with increasing number of crossings with the 0-photon spBO surfaces and with each other in the regions of overlap. As the gradient of these surfaces and the couplings between them are considerably altered, we expect significant differences in the nuclear dynamics when going from the single-mode case to the many-mode case. Indeed, this is reflected in the middle panel of Fig. 3 which shows the nuclear wavepacket at time snapshots 22 fs (a.1), 30 fs (a.2), 41 fs (a.3) and in the lower panel, showing the electronic (dashed) and nuclear (solid) dipoles (panel (b)) and photon number (panel (c)). The corresponding R-resolved BO-occupations of the ground-BO electronic state divided by the nuclear density, $|c_1(R,t)|^2$ (as defined in Methods), shown in Fig.4(a), and the R-averaged occupations $|C_{1,2}(t)|^2$ over time plotted in Fig.4(b) also show

significant mode-number dependence (A movie is also provided in supplementary materials, movie 2).

Going from a single-mode (black in Fig. 2) to 10-modes (green), the spBO surfaces are only slightly distorted from the BO surfaces, but there is an enhancement of the suppression, since the 1-photon ground-spBO band contains 10 surfaces each with slightly shifted crossings with the 0-photon excited spBO surface on which the wavepacket is initially; these crossings become avoided crossings once the matter-photon coupling is accounted for, i.e. in the polaritonic surfaces. This enhances the probability of photon emission (panel (c)) into the narrow band of cavity-modes. This is reflected also in the narrow frequency band of panel (a) in Fig. 5 which provides a spectral decomposition of the occupied photon modes as a function of time. The increased photon emission corresponds to a larger portion of the nuclear wavepacket (panels (a) of Fig. 3) being trapped in the ground electronic state to the left of the avoided crossing than in the single-mode case, while the right-going part continues on the upper electronic-surface. Still, as there is only little distortion of the spBO surfaces, these two branches of nuclear wavepacket follow closely the two branches of the single-mode dynamics. A larger trapped portion of the wavepacket clearly leads to a smaller nuclear dipole moment at larger times but also a smaller electron transfer: the final electron transfer is largely due to the splitting at the electron-nuclear avoided crossing at around $R = 2$ a.u. to which less nuclear density has reached. The R-resolved BO-occupation of the ground-BO state in Fig.4(a) show that the electronic character throughout the nuclear wavepacket is similar to the single-mode case, especially after the initial interaction region, which is maybe less obvious to discern from the R-averaged occupations in Fig. 4(b) that gives the overall picture from the electronic side over time.

Turning now to the 40-mode case (orange), the distortion of the spBO states from the BO increases, with the avoided crossing shifting a little leftward and widening slightly. Although the overall dynamics follow the 10-mode case closely, the now broadened one-photon bands lead to more and faster initial photon emission compared to the 10-mode case (Fig. 3(c)) , which is also reflected in the more mixed character of the R-resolved BO ground-state population at early times (orange in panel (a.1) in Fig. 4). The combined effects of increased early transitions to the electronic ground spBO state and a slightly less sharp electron-nuclear non-adiabatic region, leads to a little more of the nuclear wavepacket being trapped on the left side of the avoided crossing and a reduced electron-transfer, as shown by the electronic and nuclear dipoles and the BO-occupations. A notable difference between the 10- and 40-mode cases is in the spectral decomposition of the occupied photon modes in Fig. 5(b), where a small Lamb-like shift is evident [55] with the center of the dominant band slightly shifting from 0.1 a.u. to 0.102 a.u..

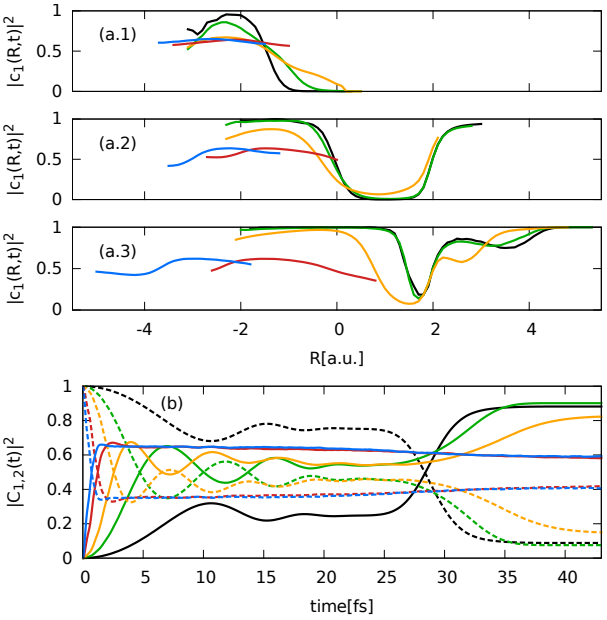

FIG. 4. Groundstate BO-surface population (a) at time snap shots $t = 22$ fs (1), $t = 30$ fs (2) and $t = 41$ fs (3) over R and the averaged population over time (c) in the same color code as Fig.4.

It is important to note that the calculated photon number reflects both a propagating photon (photon emission) as well as a quasi-bound photon component; the latter arises from dressed photon-matter eigenstates where pure BO states get coupled through the counter rotating-wave terms and molecular dipole terms in the Hamiltonian, and, as perturbation theory suggests, grows as the number of photon modes increases. The photon number $\langle \sum_\alpha a_\alpha^\dagger a_\alpha \rangle$ that we plot in Fig. 4 and its spectrally-resolved version in Fig. 5 do not distinguish these.

In the 200-mode case (red), the self-polarization term distorts the spBO surfaces significantly and shifts the electron-nuclear non-adiabatic region to be centered near $R = 0$ a.u.. This shift and widening weakens the non-adiabatic coupling at the electron-nuclear avoided crossing significantly, which suggests that the population transfer from the upper to the lower BO state at this crossing would be much reduced, which is in fact the case (see the very gentle slope in panel Fig. 4(a.3)). However, there is actually very little nuclear density reaching this crossing due to the extended overlap of the excited spBO surface and the 1-photon ground spBO band. As a result the photon number rapidly increases from the beginning and almost immediately there is a mixed electronic character throughout the nuclear density, as reflected in Figs. 3(c) and 4(a). The flatter slope of the excited spBO surface together with the increased population in the lower spBO surface (Fig. 4.a), greatly slows the nuclear density down compared to the fewer-

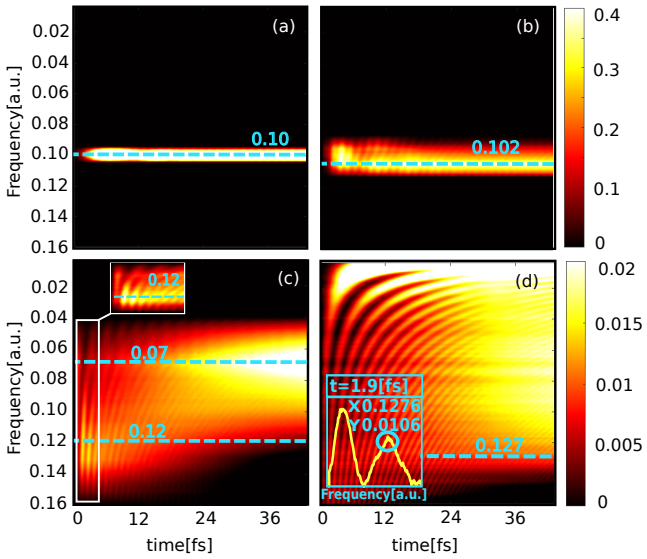

FIG. 5. Photon-mode occupation for 10 (a), 40 (b), 200 (c) and 440 (d) modes. The dashed blue lines denotes the resonant frequency $\omega = 0.1$ at initial $R = -4$ as well as the Lamb-like shift. The inset in panel (d) depicts a cut through the heat map at initial time $t = 1.9$ fs..

mode cases, and results in a significantly increased suppression of both the proton and electron transfer, as evident from panels (a) and (b) in Fig. 3. The photon number continues to grow slightly throughout the evolution. This can also be seen in the spectral decomposition in Fig. 5(c), where for initial times we find a wide band with dominant occupation around a frequency of 0.12 a.u. (inset), which represents the initial spBO energy-difference (0.1 a.u.) with a small Lamb-like shift. As time evolves we see a continual re-absorption and re-emission (yielding the slight constant increase of the photon number) into a wider band building around 0.07 a.u.. Since the energy-difference between the spBO surfaces near the turning point of the nuclear dipole $R \approx -1$ a.u. is about 0.05a.u., this frequency can be interpreted as the central frequency of transition between the excited and ground spBO surfaces in the region where the nuclear wavepacket is moving the slowest with the Lamb-like shift again on the order of 0.02a.u..

The 440-mode case (blue) leads to an even stronger suppression of proton-coupled electron transfer. The key feature causing this is the strong deviation of the excited spBO surface such that its gradient slopes back to the left soon after the initial nuclear wavepacket slides down from its initial position at $R = -4$ a.u., in contrast to the cavity-free excited BO surface. The overlap of the extensively broadened $1(n)$-photon-excited- and $1(n)$-ground-bands increases significantly creating a near-continuum of avoided crossings. The 0-photon surfaces are everywhere surrounded by near-lying n-photon surfaces with the upper parts of both bands now reaching up into higher energies and the lowest part of the 1-photon ground-state band reaching the fundamental cavity mode of frequency $\pi c/\mathcal{L}$. Compared to the 200-mode case, even less density reaches the region of closest approach of the two (0-photon) spBO surfaces, which is now even wider. The slopes of bands results in an even slower nuclear dynamics, with the nuclear and electronic dipole returning to their initial positions after only a small excursion away, as evident in Fig. 3. By including the lowest allowable cavity modes, we find a significant increase of the photon number due to the population of low frequency photons. This can be seen in spectral decomposition in Fig.5(d), as we find bright bands rapidly developing at lower frequencies. As expected, we find a larger Lamb-like shift at 0.1276 a.u. at initial times (inset, a cut through the heat map at $t = 1.9$ fs). However, due to the densely-spaced $0, 1, 2$...-photon surfaces we observe a quite fast re-absorption and re-emission of photons into a broad band yielding the larger constant increase of the photon number.

Finally, to emphasize the importance of the self-polarization term on the dynamics, in Fig. 6 we compare the results of the MTE dynamics on the electronic and nuclear dipoles and photon number when this term is neglected (dashed) or included (solid) for 10, 40, 200 and 440 modes. Here we find only small differences for the 10 mode case, however, as anticipated from the discussion above, including more photon modes leads to larger differences in the dynamics. More precisely, the very initial photon emission remains the same with and without self-polarization. However, as more photon modes are accounted for, there are larger deviations as time evolves, especially for the 440 mode case, which yields quantitative deviations up to a factor of 2. The differences in the dynamics are distinct for the electronic and nuclear dipole, where already for the 10 mode case deviations up to 0.3 a.u. (electronic) and 0.2 a.u. (nuclear) are found at later times. The error in neglecting self-polarization becomes especially significant for the 200- and 440-mode cases, where there is qualitatively different behavior in the nuclear dipole. In the 200-mode case, the differences reach 5.8 a.u. for nuclear dipole and 1.8 a.u. for electronic dipole. Indeed, neglecting the self-polarization term leads to an increase of the proton transfer compared to the single-mode case, in contrast to the increased suppression observed when including the self-polarization. Therefore, neglecting the self-polarization term for many photon modes does not only change the quantitative results dramatically, but can also result in overall different physical effects. The nuclear and electronic wavepackets in the 440-mode case becomes delocalized over the entire region, so plotting simply the dipole, an averaged quantity, appears to give more agreement with the self-polarization-neglected dynamics, when in fact the wavepackets look completely different (see also supplementary material, compare movie 2. and 3.).

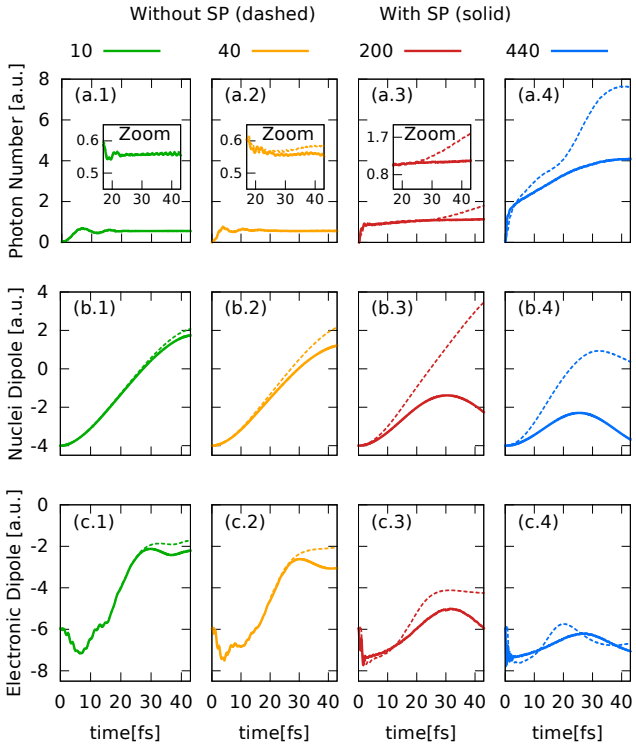

FIG. 6. Difference of the photon number (upper panel), nuclear dipole (middle panel) and electronic dipole (lower panel) without self-polarization term (dashed) and with self-polarization term (solid) in the same color code as Fig.4

I. DISCUSSION AND OUTLOOK

Our results suggest that the effect of multiple cavity-modes on the reaction dynamics can be dramatically different than when only a single mode is accounted for. This is particularly true when there are cavity-modes resonant with the matter system. In particular, for the model of cavity-induced suppression of proton-coupled electron transfer investigated here, we find an overall increase of the suppression the more photon modes are accounted for. Two mechanisms are fundamentally responsible for the difference: First, the self-polarization term grows in significance with more modes with the effect that self-polarization-modified BO surfaces are distorted significantly away from their cavity-free shape. Polaritonic surfaces, eigenvalues of $H - T_n$, should include the explicit matter-photon coupling on top of these spBO surfaces. Second, the n-photon-spBO bands become wider and increasingly overlapping, yielding a very mixed electronic character and continual exchange between surfaces. These new dressed potential energy surfaces provide a useful backdrop to analyze the dynamics, and will form a useful tool in analyzing the different surfaces put forward to study coupled photon-matter systems, for example the polaritonic surfaces, and especially the time-dependent potential energy surface arising from the exact factorization as this single surface alone provides a complete picture of the dynamics.

The MTE treatment of the photons appears to be a promising route towards treating realistic light-matter correlated systems. In particular, this method is able to capture quantum effects such as cavity-induced suppression of proton-coupled electron transfer, yet overcomes the exponential scaling problem with the number of quantized cavity modes. However, a practical approach for realistic systems will further need an approximate treatment of the matter part. From the electronic side TDDFT would be a natural choice, while a practical treatment of nuclei calls for a classical treatment such as Ehrenfest or surface-hopping in some basis. However, the multiple-crossings inside the n-photon spBO bands suggest that simple surface-hopping treatments based on spBO surfaces should be used with much caution and that decoherence-corrections should be applied, for example those generalized from the exact factorization approach to the electron-nuclear problem [56, 57]. Further, the MTE approach could provide a way to accurately approximate the light-matter interaction part of the QEDFT xc functional [4, 27, 30, 44].

Finally, we note that the present findings are general in that the increasing importance of self-polarization with more photon modes is expected to hold for the description and control of cavity-driven physical processes of molecules, nanostructures and solids embedded in cavities in general. These findings could yield a new way to control and change chemical reactions via the self-polarization without the need to explicitly change the light-matter coupling strength itself.

II. METHODS

A. Hamiltonian

Here we consider the non-relativistic photon-matter Hamiltonian in the dipole approximation in the Coulomb gauge as [4, 18, 30, 46, 58]

$$\hat{H} = \hat{H}_m^{\mathrm{SP}} + \hat{H}_p + \hat{V}_{pm} \,, \tag{1}$$

with the Hamiltonian for the matter in the cavity as

$$\hat{H}_m^{\mathrm{SP}} = \hat{T}_n + \hat{H}_{\mathrm{BO}}^{\mathrm{SP}} \text{ where } \hat{H}_{\mathrm{BO}}^{\mathrm{SP}} = \hat{T}_e + \hat{V}_m + \hat{V}^{\mathrm{SP}} \,. \tag{2}$$

Our model is in one dimension, with one electronic coordinate r and one nuclear coordinate R, where the nuclear and electronic kinetic terms $\hat{T}_n = -\frac{1}{2M}\frac{\partial^2}{\partial R^2}$, $\hat{T}_e = -\frac{1}{2}\frac{\partial^2}{\partial r^2}$, while $\hat{H}_{\mathrm{BO}}^{\mathrm{SP}}$ denotes the spBO Hamiltonian, defined by adding the self-polarization term,

$$\hat{V}^{\mathrm{SP}} = \frac{1}{2}\sum_{\alpha}^{\mathcal{M}} \lambda_\alpha^2 (Z\hat{R} - \hat{r})^2 \,, \tag{3}$$

to the usual BO Hamiltonian. The self-polarization term depends only on matter-operators but scales with the sum over modes of the squares of the photon-matter coupling parameters λ_α; a thorough discussion of this term can be found in Ref. [19, 47, 48]. Atomic units, in which $\hbar = e^2 = m_e = 1$, are used here and throughout. The photon Hamiltonian and photon-matter coupling read as follows

$$\hat{H}_p(q) = \frac{1}{2}\sum_{\alpha}^{\mathcal{M}} \left(\hat{p}_\alpha^2 + \omega_\alpha^2 \hat{q}_\alpha^2\right) \tag{4}$$

$$\hat{V}_{pm} = \sum_{\alpha}^{\mathcal{M}} \omega_\alpha \lambda_\alpha \hat{q}_\alpha \left(Z\hat{R} - \hat{r}\right) , \tag{5}$$

where α denotes the photon modes, $\hat{q}_\alpha = \sum_\alpha \sqrt{\frac{1}{2\omega_\alpha}}(\hat{a}_\alpha^\dagger + \hat{a}_\alpha)$ is the photonic displacement-field coordinate, related to the electric displacement operator, while $\hat{p}_\alpha$ is proportional to the magnetic field. We choose the matter-photon coupling strength through the 1D mode function $\lambda_\alpha = \sqrt{\frac{2}{\mathcal{L}\epsilon_0}}\sin(k_\alpha X)$ where $\mathcal{L}$ denotes the length of the cavity and $k_\alpha = \alpha\pi/\mathcal{L}$ the wave vector, and X the total dipole. Here we take $X = \mathcal{L}/2$, assuming that the molecule is placed at the center of the cavity, and that $\mathcal{L} = 50\mu m$ is much longer than the spatial range of the molecular dynamics.

In our particular model the matter potential $\hat{V}_m$ is given by the 1D Shin-Metiu model [59–61], which consists of a single electron and proton ($Z = 1$ above), which can move between two fixed ions separated by a distance L in one-dimension. This model has been studied extensively for both adiabatic and nonadiabatic effects in cavity-free [60–63] and in-cavity cases [18, 45, 64]. The Shin-Metiu potential is:

$$\hat{V}_m = \sum_{\sigma=\pm1}\left(\frac{1}{|R+\frac{\sigma L}{2}|} - \frac{\mathrm{erf}\left(\frac{|r+\frac{\sigma L}{2}|}{a_\sigma}\right)}{|r+\frac{\sigma L}{2}|}\right) - \frac{\mathrm{erf}\left(\frac{|R-r|}{a_f}\right)}{|R-r|} \tag{6}$$

We choose here $L = 19.0$ a.u., $a_+ = 3.1$ a.u., $a_- = 4.0$ a.u., $a_f = 5.0$ a.u., and the proton mass $M = 1836$ a.u.; with these parameters, the phenomenon of proton-coupled electron transfer occurs after electronic excitation out of the ground-state of a model molecular dimer [45].

B. MTE Treatment of Photonic System

A computationally feasible treatment of coupled electron-ion-photon dynamics in a multi-mode cavity calls for approximations. Here we have one electronic and one nuclear degree of freedom but up to 440 photon modes, so we use MTE for the photons, coupled to the molecule treated quantum mechanically. As mentioned above we take the initial state as a simple factorized product of the photonic vacuum state $\xi_0(\underline{q})$ for each mode, the excited BO state, and the nuclear Gaussian wavepacket. More precisely, for the MTE for photons we sample the initial photonic vacuum state from the Wigner distribution given by: $\xi_0(q,p) = \prod_\alpha \frac{1}{\pi} e^{\left[-\frac{p_\alpha^2}{\omega_\alpha} - \omega_\alpha q_\alpha^2\right]}$. Furthermore, with two electronic surfaces, the equations of motion are as follows, for the lth trajectory:

$$\ddot{q}_\alpha{}^l(t) = -\omega_\alpha^2 q_\alpha{}^l - \omega_\alpha\lambda_\alpha(Z\langle R\rangle^l - \langle r\rangle^l), \tag{7}$$

$$i\partial_t \begin{pmatrix} C_1(R,t) \\ C_2(R,t)\end{pmatrix} = \begin{pmatrix} h_{11} & h_{12} \\ h_{21} & h_{22}\end{pmatrix}\begin{pmatrix} C_1(R,t) \\ C_2(R,t)\end{pmatrix}, \tag{8}$$

with the diagonal matrix elements

$$h_{ii} = \epsilon_{\mathrm{BO}}^i(R) - \frac{1}{2M}\partial_R^2 + \sum_\alpha \Big(\lambda_\alpha\omega_\alpha q_\alpha^l(ZR - r_{ii}(R)) + \frac{\lambda_\alpha^2}{2}\cdot((ZR)^2 - 2ZRr_{ii}(R) + r_{ii}^{(2)})\Big) \tag{9}$$

and for $i \neq j$,

$$h_{ij} = -\frac{1}{M}d_{ij}(R)\partial_R - \frac{d_{ij}^{(2)}(R)}{2M} - \sum_\alpha \lambda_\alpha\omega_\alpha q_\alpha^l r_{ij}(R) + \sum_\alpha\left(\frac{\lambda_\alpha^2}{2}\cdot\left(-2ZRr_{ij}(R) + r_{ij}^{(2)}(R)\right)\right) \tag{10}$$

Here the non-adiabatic coupling terms are $d_{ij}(R) = \langle\Phi_{R,i}^{\mathrm{BO}}|\partial_R\Phi_{R,j}^{\mathrm{BO}}\rangle$, $d_{ij}^{(2)}(R) = \langle\Phi_{R,i}^{\mathrm{BO}}|\partial_R^2\Phi_{R,j}^{\mathrm{BO}}\rangle$, and the transition dipole and quadrupole terms $r_{ij}^{(n)} = \langle\Phi_{R,i}^{\mathrm{BO}}|\hat{r}^n|\Phi_{R,j}^{\mathrm{BO}}\rangle$. The coefficients $C_i(R,t)$ are the expansion coefficients of the electron-nuclear wavefunction in the BO basis: $\Psi(r,R,t) = \sum_{i=1,2} C_i(R,t)\Phi_{R,i}^{\mathrm{BO}}(r)$. Subsequently the R-resolved and R-averaged BO-populations are defined as $|c_{1,2}(R,t)|^2 = |C_{1,2}(R,t)|^2/|\chi(R,t)|^2$ and $|C_{1,2}(t)|^2 = \int dR|C_{1,2}(R,t)|^2$ respectively. In the single-mode case we also present the results for when the proton is also treated by MTE with the nuclear trajectory satisfying $M\ddot{R}^l(t) = -\langle\partial_R\epsilon_{\mathrm{BO}}(R^l)\rangle - \sum_\alpha \omega_\alpha\lambda_\alpha q_\alpha^l - \sum_\alpha\left(\lambda_\alpha^2 Z(Z\langle R\rangle^l - \langle r\rangle^l)\right)$. For the photonic system, 10,000 trajectories were enough for convergence for all cases except the 440-mode case which required 50,000 trajectories (the results shown used 100,000 trajectories in all cases).

Data Availability

The data that support the findings of this work are available from the corresponding authors on reasonable request.

ACKNOWLEDGMENTS

We would like to thank Johannes Feist for insightful discussions. Financial support from the US National

Science Foundation CHE-1940333 (NM) and the Department of Energy, Office of Basic Energy Sciences, Division of Chemical Sciences, Geosciences and Biosciences under Award de-sc0020044 (LL) are gratefully acknowledged. NMH gratefully acknowledges an IMPRS fellowship. This work was also supported by the European Research Council (ERC-2015-AdG694097), the Cluster of Excellence (AIM), Grupos Consolidados (IT1249-19) and SFB925 "Light induced dynamics and control of correlated quantum systems. The Flatiron Institute is a division of the Simons Foundation.

AUTHOR CONTRIBUTIONS

All authors contributed to the conception of the research. NT.M. supervised the work. NM.H. performed the MTE calculations. L.L. performed the exact reference calculations. A.R. proposed the idea of treating photon modes with MTE for this problem. All authors analysed the results and contributed to the writing of the manuscript.

COMPETING INTERESTS

The authors declare no competing interests.

[1] T. W. Ebbesen, Accounts of chemical research **49**, 2403 (2016).
[2] J. George, T. Chervy, A. Shalabney, E. Devaux, H. Hiura, C. Genet, and T. W. Ebbesen, Phys. Rev. Lett. **117**, 153601 (2016).
[3] H. Hiura, A. Shalabney, and J. George, ChemRxiv (2018).
[4] M. Ruggenthaler, N. Tancogne-Dejean, J. Flick, H. Appel, and A. Rubio, Nature Reviews Chemistry **2**, 0118 (2018).
[5] C. Riek, D. V. Seletskiy, A. S. Moskalenko, J. F. Schmidt, P. Krauspe, S. Eckart, S. Eggert, G. Burkard, and A. Leitenstorfer, Science **350**, 420 (2015).
[6] A. S. Moskalenko, C. Riek, D. V. Seletskiy, G. Burkard, and A. Leitenstorfer, Phys. Rev. Lett. **115**, 263601 (2015).
[7] T. Byrnes, N. Y. Kim, and Y. Yamamoto, Nature Physics **10**, 803 (2014).
[8] J. Kasprzak, M. Richard, S. Kundermann, A. Baas, P. Jeambrun, J. Keeling, F. Marchetti, M. Szymańska, R. Andre, J. Staehli, *et al.*, Nature **443**, 409 (2006).
[9] S. Schmidt, Physica Scripta **91**, 073006 (2016).
[10] A. Thomas, E. Devaux, K. Nagarajan, T. Chervy, M. Seidel, D. Hagenmüller, S. Schütz, J. Schachenmayer, C. Genet, G. Pupillo, *et al.*, arXiv preprint arXiv:1911.01459 (2019).
[11] A. Thomas, L. Lethuillier-Karl, K. Nagarajan, R. M. Vergauwe, J. George, T. Chervy, A. Shalabney, E. Devaux, C. Genet, J. Moran, *et al.*, Science **363**, 615 (2019).
[12] J. Feist and F. J. Garcia-Vidal, Phys. Rev. Lett. **114**, 196402 (2015).
[13] J. Galego, F. J. Garcia-Vidal, and J. Feist, Phys. Rev. X **5**, 041022 (2015).
[14] J. Flick, M. Ruggenthaler, H. Appel, and A. Rubio, Proceedings of the National Academy of Sciences **112**, 15285 (2015).
[15] J. Galego, F. J. Garcia-Vidal, and J. Feist, Nature Communications **7**, 13841 EP (2016).
[16] J. Schachenmayer, C. Genes, E. Tignone, and G. Pupillo, Phys. Rev. Lett. **114**, 196403 (2015).
[17] M. Cirio, S. De Liberato, N. Lambert, and F. Nori, Phys. Rev. Lett. **116**, 113601 (2016).
[18] J. Flick, H. Appel, M. Ruggenthaler, and A. Rubio, Journal of Chemical Theory and Computation **13**, 1616 (2017), pMID: 28277664.
[19] C. Schäfer, M. Ruggenthaler, H. Appel, and A. Rubio, Proceedings of the National Academy of Sciences **116**, 4883 (2019).
[20] R. F. Ribeiro, L. A. Martínez-Martínez, M. Du, J. Campos-Gonzalez-Angulo, and J. Yuen-Zhou, Chem. Sci. **9**, 6325 (2018).
[21] M. Kowalewski, K. Bennett, and S. Mukamel, The Journal of Physical Chemistry Letters **7**, 2050 (2016).
[22] J. F. Triana, D. PelÃ¡ez, and J. L. Sanz-Vicario, The Journal of Physical Chemistry A **122**, 2266 (2018), pMID: 29338227.
[23] T. Szidarovszky, G. J. Halász, A. G. Császár, L. S. Cederbaum, and A. Vibók, The Journal of Physical Chemistry Letters **9**, 6215 (2018).
[24] G. Groenhof and J. J. Toppari, The Journal of Physical Chemistry Letters **9**, 4848 (2018), pMID: 30085671.
[25] H. L. Luk, J. Feist, J. J. Toppari, and G. Groenhof, Journal of Chemical Theory and Computation **13**, 4324 (2017), pMID: 28749690.
[26] O. Vendrell, Chemical Physics **509**, 55 (2018).
[27] J. Flick, C. Schäfer, M. Ruggenthaler, H. Appel, and A. Rubio, ACS Photonics **5**, 992 (2018).
[28] J. F. Triana, D. Peláez, and J. L. Sanz-Vicario, The Journal of Physical Chemistry A **122**, 2266 (2018).
[29] J. Flick, *Exact nonadiabatic many-body dynamics: Electron-phonon coupling in photoelectron spectroscopy and light-matter interactions in quantum electrodynamical density-functional theory*, Ph.D. thesis, Humboldt-Universität zu Berlin Berlin (2016).
[30] M. Ruggenthaler, J. Flick, C. Pellegrini, H. Appel, I. V. Tokatly, and A. Rubio, Phys. Rev. A **90**, 012508 (2014).
[31] C. Schäfer, M. Ruggenthaler, and A. Rubio, Physical Review A **98**, 043801 (2018).
[32] M. Sánchez-Barquilla, R. Silva, and J. Feist, (2019), arXiv:1911.07037.
[33] N. M. Hoffmann, C. Schäfer, A. Rubio, A. Kelly, and H. Appel, Phys. Rev. A **99**, 063819 (2019).
[34] N. M. Hoffmann, C. Schäfer, N. Säkkinen, A. Rubio, H. Appel, and A. Kelly, The Journal of Chemical Physics **151**, 244113 (2019).
[35] J. Flick, M. Ruggenthaler, H. Appel, and A. Rubio, Proceedings of the National Academy of Sciences **114**, 3026 (2017).
[36] J. del Pino, F. A. Y. N. Schröder, A. W. Chin, J. Feist, and F. J. Garcia-Vidal, Phys. Rev. Lett. **121**, 227401 (2018).

[37] S. Franke, S. Hughes, M. K. Dezfouli, P. T. Kristensen, K. Busch, A. Knorr, and M. Richter, Phys. Rev. Lett. **122**, 213901 (2019).
[38] J. Flick, D. M. Welakuh, M. Ruggenthaler, H. Appel, and A. Rubio, ACS photonics **6**, 2757 (2019).
[39] B. Huttner and S. M. Barnett, Phys. Rev. A **46**, 4306 (1992).
[40] S. Y. Buhmann, *Dispersion forces I: Macroscopic quantum electrodynamics and ground-state Casimir, Casimir–Polder and van der Waals Forces*, Vol. 247 (Springer, 2013).
[41] S. Buhmann, *Dispersion Forces II: Many-Body Effects, Excited Atoms, Finite Temperature and Quantum Friction*, Vol. 248 (Springer, 2013).
[42] S. Y. Buhmann and D.-G. Welsch, Physical Review A **77**, 012110 (2008).
[43] S. Scheel and S. Buhmann, Acta Physica Slovaca. Reviews and Tutorials **58**, 675 (2008).
[44] C. Pellegrini, J. Flick, I. V. Tokatly, H. Appel, and A. Rubio, Phys. Rev. Lett. **115**, 093001 (2015).
[45] L. Lacombe, N. M. Hoffmann, and N. T. Maitra, Phys. Rev. Lett. **123**, 083201 (2019).
[46] N. M. Hoffmann, H. Appel, A. Rubio, and N. T. Maitra, The European Physical Journal B **91**, 180 (2018).
[47] C. Schäfer, M. Ruggenthaler, V. Rokaj, and A. Rubio, arXiv preprint (2019), arXiv::1911.08427.
[48] V. Rokaj, D. M. Welakuh, M. Ruggenthaler, and A. Rubio, Journal of Physics B: Atomic, Molecular and Optical Physics **51**, 034005 (2018).
[49] H. Sambe, Phys. Rev. A **7**, 2203 (1973).
[50] T. Fiedlschuster, J. Handt, and R. Schmidt, Phys. Rev. A **93**, 053409 (2016).
[51] M. Thachuk, M. Y. Ivanov, and D. M. Wardlaw, The Journal of Chemical Physics **105**, 4094 (1996).
[52] Y. Sato, H. Kono, S. Koseki, and Y. Fujimura, Journal of the American Chemical Society **125**, 8019 (2003).
[53] A. Abedi, N. T. Maitra, and E. K. Gross, Physical Review Letters **105**, 123002 (2010).
[54] A. Abedi, N. T. Maitra, and E. Gross, The Journal of Chemical Physics **137**, 22A530 (2012).
[55] H. A. Bethe, Physical Review **72**, 339 (1947).
[56] S. K. Min, F. Agostini, and E. K. U. Gross, Phys. Rev. Lett. **115**, 073001 (2015).
[57] J.-K. Ha, I. S. Lee, and S. K. Min, The Journal of Physical Chemistry Letters **9**, 1097 (2018), pMID: 29439572, https://doi.org/10.1021/acs.jpclett.8b00060.
[58] I. V. Tokatly, Phys. Rev. Lett. **110**, 233001 (2013).
[59] S. Shin and H. Metiu, The Journal of Chemical Physics **102**, 9285 (1995).
[60] J.-Y. Fang and S. Hammes-Schiffer, The Journal of Chemical Physics **106**, 8442 (1997).
[61] J.-Y. Fang and S. Hammes-Schiffer, The Journal of Chemical Physics **107**, 5727 (1997).
[62] A. Abedi, F. Agostini, Y. Suzuki, and E. K. U. Gross, Phys. Rev. Lett. **110**, 263001 (2013).
[63] F. Agostini, A. Abedi, Y. Suzuki, S. K. Min, N. T. Maitra, and E. K. U. Gross, J. Chem. Phys. **142**, 084303 (2015).
[64] J. Galego, C. Climent, F. J. Garcia-Vidal, and J. Feist, Phys. Rev. X **9**, 021057 (2019).

Supplementary Material for "Effect of Many Modes on Self-Polarization and Photochemical Suppression in Cavities"

Norah M. Hoffmann*
Max Planck Institute for the Structure and Dynamics of Matter and Center for Free-Electron Laser Science and Department of Physics, Luruper Chaussee 149, 22761 Hamburg, Germany and
Department of Physics, Rutgers University at Newark, Newark, NJ 07102, USA

Lionel Lacombe†
Department of Physics, Rutgers University at Newark, Newark, NJ 07102, USA

Angel Rubio‡
Max Planck Institute for the Structure and Dynamics of Matter and Center for Free-Electron Laser Science and Department of Physics, Luruper Chaussee 149, 22761 Hamburg, Germany
Center for Computational Quantum Physics, Flatiron Institute, 162 5th Avenue, New York, NY 10010, USA and
Nano-Bio Spectroscopy Group and ETSF, Universidad del Pas Vasco, 20018 San Sebastian, Spain

Neepa T. Maitra§
Department of Physics, Rutgers University at Newark, Newark, NJ 07102, USA
(Dated: January 20, 2020)

* norah.magdalena.hoffmann@mpsd.mpg.de
† liolacombe@gmail.com
‡ angel.rubio@mpsd.mpg.de
§ neepa.maitra@rutgers.edu

I. MOVIES

We provide three movies:

1. **MovieSingleMode.mp4** shows the nuclear dynamics for the cavity free case (pink) and for a coupling to one resonant photon mode with coupling strength $\lambda = 0.005$ and resonant frequency 0.1 for the full quantum solution (black), quantum nuclei with MTE treatment for the photons (blue) and MTE treatment for nuclei and photos (light blue) in comparison. The surfaces represent the BO surfaces (pink) and spBO surfaces (black) with the coupling to the one resonant photon mode. This movie corresponds to the results given in Fig.2 in the paper.

2. **MovieMultiModeWithSP.mp4** shows the spBO surfaces (upper pannel), the nuclear density (second panel), the R-resolved BO-population (third and last panel) over time. Here we treat the photons with the MTE-approach, the matter part quantum mechanically and all simulations include the self-polarization term. As in (1.) we choose the coupling strength to be $\lambda = 0.005$ for all cases and compare the dynamics of the cavity free case (pink), the coupling to a single resonant mode (black) and the coupling to 10- (green), 40- (orange), 200- (red), 440- (blue) photon modes. This movie corresponds to Fig.3 and Fig.4 in the paper.

3. **MovieMultiMode.mp4** shows the same calculations, dynamics and comparison as (2.), however now without taking the self-polarization into account and the upper panel now shows the BO-surfaces. This movie gives more details for the discussion of Fig.6.

Part III

CONCLUSION AND OUTLOOK

4

SUMMARY, CONCLUSION AND OUTLOOK

In this thesis we introduced an extension of MQC methods and the EF approach, traditionally developed to electron-nuclear systems, to the photonic degrees of freedom in order to pave the way to full *ab initio* and computational feasible descriptions of quantum effects in correlated light-matter systems within cavity quantum electrodynamics. To guarantee a proper benchmarking, we first investigate both methods within electron-photon correlated systems and then extended both approaches to the full electron-photon-nuclei system. For the MQC methods we identified a particularly promising route towards treating complex realistic light-matter correlated systems. Furthermore, we gained a fundamental understanding of the results found in the MQC approach by investigating the TDPES within the EF approach.

More precisely, considering the electron-photon correlated system we first adapted the MTEF method, where we investigated a two and three-level cavity-bound atomic system coupled to 400 photon modes. Here we analyzed the performance of the MTEF method by properly accounting for the quantum statistics of the vacuum field, while using mean field trajectories to describe the time-evolution compared to the exact quantum solution within the spontaneous-emission process. We found that, although having some quantitative drawbacks, MTEF is indeed able to qualitatively characterize quantum effects such as one and two photon spontaneous-emission, polariton peaks, and second-order correlation functions. Furthermore, it is implied that classical Wigner dynamics for the free photonic field, i.e. harmonic oscillators up to a linear coupling, yield exact results. But, although accurate, the results found within the MTEF approach were not exact. In order to investigate this, we analyzed the photonic TDPES driving the electronic motion within the EF approach for the same model system coupled to either one or infinite photon modes (Wigner-Weisskopf approximation). Here, we found interesting structures of the potential driving the dynamics and, in particular, large deviations from the harmonic form of the free-photon field. These deviations completely incorporate the effect of the matter system on the photonic dynamics and, thus, corroborated the accurate, but inexact, results found within the classical Wigner approach. Therefore, in order to then improve the results found within the MTEF approach we benchmarked a selection of MQC and semiclassial methods such as MTEF, path integral methods, and fewest switch surface hopping, as well as perturbative methods within the same model system, i.e. a cavity-bound two and three-level atomic system coupled to 400 photon modes. Here we found that, with the exception of the fewest switch surface hopping method, all MQC methods performed well and were able to capture quantum effects such as bound photon states and spontaneous emission. Additionally, the path-integral methods were also able to qualitatively capture some level of interference effects, which were only seen as broadening of the

wave packet within the MTEF method. Considering the perturbative methods, i.e. the BBGKY hierarchy in the second Born approximation, we found that this method performed exceptionally well, yet inherits an exponential scaling with the increase of the degrees of freedom and therefore, in contrast to the MQC methods, is not feasible for realistic systems.

To enable the treatment of more realistic systems and as a natural extension to the work within the electron-correlated systems, we then extended the MTEF approach and the EF approach to the full electron-photon-nuclear system. Here, we first investigated the exact TDPES driving the proton motion for a cavity induced suppression of PCET within the EF approach. We analyzed its features and showed that the TDPES, indeed, can predict the correct dynamics of the cavity induced suppression of PCET. Furthermore, by investigating the proton dynamics on the back-drop of the polaritonic surfaces, we found that polaritonic surfaces, conventionally used in polaritonic chemistry, are themselves not able to predict the dynamics or mechanisms without considering how they couple to each other. Finally, we then analyzed and simulated cavity-modified reactions within the MTEF approach, i.e. cavity induced suppression of PCET. We carefully benchmarked our approach by step-wise increasing the MTEF-treatment, where we first treated electrons and nuclei quantum mechanically and the photonic degrees of freedom classically and then extended to a MTEF treatment for both the photons and nuclei. We compared this benchmarking to the exact quantum solution for a model of cavity induced PCET coupled to a single photon mode. We found that MTEF is, indeed, able to describe the suppression of PCET, but tends to underestimate these results, which we explained in detail by referring to the findings within the TDPES for photons. With the exact reference solution out of reach, we then coupled the matter system to up to 440 photon modes. Here, we found that as more photon modes are included, cavity-modified phenomena can significantly change and the self-polarization, which is often neglected, has an increasingly crucial impact on the dynamics and even more so presents a potential new tool to control and change chemical reactions. To this end, we introduce the concept of spBO surfaces as an instructive tool for analysis.

In summary, methods based on classical and semiclassical Wigner dynamics performed very well for light-matter correlated systems and emerge as a promising route towards realistic systems, as they are able to capture quantum effects, yet do not inherent the exponential scaling. Especially, as the trajectories are not coupled during their time evolution, the corresponding algorithms can be implemented in a highly parallel manner to reduce the total run-time. Additionally, we note that the conventional harmonic-oscillator picture for photons does not hold within the investigated systems, as, due to the nonlinear coupling of matter and light, the photonic potential driving the electronic motion deviates strongly from being harmonic. Furthermore, considering the potential driving the proton motion, caution is needed when applying MQC on the conventionally used polaritonic surfaces and we suggest using PES beyond the adiabtic approximation, e.g. TDPES, within the EF approach. However, as the presented work just started to explore the MQC methods and EF approach within the area of cavity quantum electrodynamics, there is still a lot of work to be done and open questions to be

answered. We address these questions and possible next steps in the following paragraph.

OPEN QUESTIONS AND OUTLOOK With the exciting findings in the MQC methods and the EF approach in mind, we conclude this thesis with some open questions and possible next steps within this framework. Here, all open questions and future steps are related to the goal to enable a full *ab initio* realistic description of processes and dynamics within cavity QED.

1. *More realistic cavities*: In all our calculations presented above we assume a perfect cavity. However, reality does not have the perfect cavity and requires taking losses into account. Furthermore, in order to mimic a real experiment, an external light field is required to prepare the initial states of the matter, i.e. excited state. Moreover, considering the measurement of the observables, one would need to consider that all observables such as intensities, photon number and correlation are measured outside of the cavity. Therefore, future steps include, adding external light fields for initial state preparation, including losses in the calculations and extracting the observables outside of the cavity.

2. *Excited state sampling*: This is related to the preparation of the initial state of the matter. Here, one could also imagine a single-photon source to act as an external laser, which opens up the new applications such as quantum sensing and secure quantum communication [159, 160]. In these cases, a sampling beyond the vacuum state in the MQC methods is needed, which can lead to unphysical negative pockets in the Wigner transform for the photons. However, similar attempts of excited state sampling are already known from electron-nuclear systems, where a sampling of the nuclei beyond zero Kelvin is required [161–164]. Therefore, future steps include, exploring the exited state sampling for photons in order to mimic external single-photon sources.

3. *Reduction of Trajectories*: All results for the MQC methods presented in this thesis usually require $10^4 - 10^6$ trajectories to converge. However, considering more complex and realistic systems such as three-dimensional cavites, a smaller number of required trajectories would reduce the computational cost tremendously. Therefore, another future step also includes investigating enhanced sampling techniques in order to obtain same-level results with fewer trajectories.

4. *The way to three dimensions*: Finally, the most important next step is the extension of our methods beyond model systems to full *ab initio* three-dimensional calculations. Thus, as we investigated two methodologies throughout this thesis, i.e. MQC methods and EF approach, there are two possible paths forward:

    a) One the one hand, we explored the extension of the EF approach, where the photonic degrees of freedom are directly included within

the exact TDPES. Thus, one could now run trajectory-based methods on these TDPES. Therefore, one possible future step could be to develop rigorous mixed quantum-classical approximations for cavity quantum electrodynamics based on generalizations of the coupled-trajectory scheme of [37–39], which already has been proven to be successful for cavity-free non-adiabatic dynamics.

b) On the other hand, which is the most natural extension to the work presented within this thesis, is to extend the MQC methods themselves. More precisely, in order to go beyond model systems, one could couple the presented MQC approach to *ab initio* electronic structure calculations such as TDDFT. In particular, as the equations of motion for the photonic system presented in this work can be seen as a one-dimensional Maxwell's equation, one possible route, especially for the MTEF, is the combination with the recently presented work in [51]. This work presents an *ab initio* light-matter coupling methodology, which treats coupled classical light, electrons, and nuclei by solving the Ehrenfest-Maxwell-Pauli-Kohn-Sham equations in quantum electrodynamics and is ideally suited for applications in nano-optics and nano-plasmonics. Therefore, combining the MTEF approach presented in this thesis with the algorithm developed in [51] allows a fully quantized treatment of electrons, photons, and nuclei in realistic systems. However, note that within this algorithm one also needs to extend the Ehrenfest treatment of the nuclei to more sophisticated approaches, as, within molecular systems coupled to multiple photon modes, an Ehrenfest-like treatment for the nuclei is not favourable due to the larger number of avoided crossings. Therefore, future steps include combining and extending the methodology of [51] with the multi-trajectory approach presented in this thesis, which provides a computationally feasible route towards simulating photon-field fluctuations and correlations in realistic three-dimensional systems.

In conclusion, MQC methods for photons emerge as a very promising route towards treating realistic light-matter systems within cavity QED. Especially, considering the increasing need for well-scaling methods [165], this approach could be of great interest for the quantum chemistry as well as quantum optics community. Therefore, with this work being on the interface of quantum chemistry and quantum optics, we hope to have added some bricks to the bridge between these two fields and look forward to add many more in order to enable new physics in the exciting and fast emerging field of cavity QED.

BIBLIOGRAPHY

[1] James Clerk Maxwell. "A dynamical theory of the electromagnetic field." In: *Philosophical transactions of the Royal Society of London* 155 (1865), pp. 459–512. DOI: 10.1098/rstl.1865.0008.

[2] Nobel Lectures in Physics, ed. *Nobel Lectures Physics 1901-1921*. 1901-1921. World Scientific Publishing, 1998.

[3] Nobel Lectures in Physics, ed. *Nobel Lectures in Physics*. 1922-1941. World Scientific Publishing, 1998.

[4] Erwin Schrödinger. "An undulatory theory of the mechanics of atoms and molecules." In: *Physical Review* 28.6 (1926), p. 1049. DOI: 10.1103/PhysRev.28.1049.

[5] David J Griffiths and Darrell F Schroeter. *Introduction to quantum mechanics*. Cambridge University Press, 2018.

[6] Miguel AL Marques, Neepa T Maitra, Fernando MS Nogueira, Eberhard KU Gross, and Angel Rubio. *Fundamentals of time-dependent density functional theory*. Vol. 837. Springer Science & Business Media, 2012. DOI: 10.1007/978-3-642-23518-4.

[7] W. Kohn. "Nobel Lecture: Electronic structure of matter—wave functions and density functionals." In: *Rev. Mod. Phys.* 71 (5 Oct. 1999), pp. 1253–1266. DOI: 10.1103/RevModPhys.71.1253.

[8] Pierre Hohenberg and Walter Kohn. "Inhomogeneous electron gas." In: *Physical Review* 136.3B (1964), B864. DOI: 10.1103/PhysRev.136.B864.

[9] Erich Runge and Eberhard KU Gross. "Density-functional theory for time-dependent systems." In: *Physical Review Letters* 52.12 (1984), p. 997. DOI: 10.1103/PhysRevLett.52.997.

[10] Oktay Sinanoğlu. "Many-electron theory of atoms and molecules. i. shells, electron pairs vs many-electron correlations." In: *The Journal of Chemical Physics* 36.3 (1962), pp. 706–717. DOI: 10.1063/1.1732596.

[11] M Peter Nightingale and Cyrus J Umrigar. *Quantum Monte Carlo methods in physics and chemistry*. 525. Springer Science & Business Media, 1998. ISBN: 0792355520.

[12] M.P. Allen and D.J. Tildesley. *Computer simulation of liquids*. Oxford Science Publ. Clarendon Press, 1989. ISBN: 9780198556459.

[13] Richard Car and Mark Parrinello. "Unified approach for molecular dynamics and density-functional theory." In: *Physical Review Letters* 55.22 (1985), p. 2471. DOI: 10.1103/PhysRevLett.55.2471.

[14] Max Born and Robert Oppenheimer. "Zur quantentheorie der molekeln." In: *Annalen der Physik* 389.20 (1927), pp. 457–484. DOI: 10.1002/andp.19273892002.

[15] JohnáC Tully. "Mixed quantum–classical dynamics." In: *Faraday Discussions* 110 (1998), pp. 407–419. DOI: 10.1039/A801824C.

[16] Raymond Kapral and Giovanni Ciccotti. "Mixed Quantum-Classical Dynamics." In: *The Journal of Chemical Physics* 110.18 (1999), pp. 8919–8929. DOI: 10.1063/1.478811.

[17] Paul Ehrenfest. "Bemerkung über die angenäherte Gültigkeit der klassischen Mechanik innerhalb der Quantenmechanik." In: *Zeitschrift für Physik A Hadrons and Nuclei* 45.7 (1927), pp. 455–457.

[18] AD McLachlan. "A variational solution of the time-dependent Schrödinger equation." In: *Molecular Physics* 8.1 (1964), pp. 39–44. DOI: 10.1080/00268976400100041.

[19] Nancy Makri and William H Miller. "Time-dependent self-consistent field (TDSCF) approximation for a reaction coordinate coupled to a harmonic bath: single and multiple configuration treatments." In: *The Journal of Chemical Physics* 87.10 (1987), pp. 5781–5787. DOI: 10.1063/1.453501.

[20] Hans-Dieter Meyer and William H Miller. "A classical analog for electronic degrees of freedom in nonadiabatic collision processes." In: *The Journal of Chemical Physics* 70.7 (1979), pp. 3214–3223. DOI: 10.1063/1.437910.

[21] William H Miller. "The semiclassical initial value representation: A potentially practical way for adding quantum effects to classical molecular dynamics simulations." In: *The Journal of Physical Chemistry A* 105.13 (2001), pp. 2942–2955. DOI: 10.1021/jp003712k.

[22] Gerhard Stock and Michael Thoss. "Classical description of nonadiabatic quantum dynamics." In: *Advances in Chemical Physics* 131 (2005), pp. 243–376. DOI: 10.1002/0471739464.ch5.

[23] Hyojoon Kim, Ali Nassimi, and Raymond Kapral. "Quantum-classical Liouville dynamics in the mapping basis." In: *The Journal of Chemical Physics* 129.8 (2008), p. 084102. DOI: 10.1063/1.2971041.

[24] Chang-Yu Hsieh and Raymond Kapral. "Nonadiabatic dynamics in open quantum-classical systems: Forward-backward trajectory solution." In: *The Journal of Chemical Physics* 137.22 (2012), 22A507. DOI: 10.1063/1.4736841.

[25] Chang-Yu Hsieh and Raymond Kapral. "Analysis of the forward-backward trajectory solution for the mixed quantum-classical Liouville equation." In: *The Journal of Chemical Physics* 138.13 (2013), p. 134110. DOI: 10.1063/1.4798221.

[26] Haobin Wang, Xiong Sun, and William H Miller. "Semiclassical approximations for the calculation of thermal rate constants for chemical reactions in complex molecular systems." In: *The Journal of Chemical Physics* 108.23 (1998), pp. 9726–9736. DOI: 10.1063/1.476447.

[27] Shunsuke A Sato, Aaron Kelly, and Angel Rubio. "Coupled forward-backward trajectory approach for nonequilibrium electron-ion dynamics." In: *Physical Review B* 97.13 (2018), p. 134308. DOI: 10.1103/PhysRevB.97.134308.

[28] Aaron Kelly and Thomas E Markland. "Efficient and accurate surface hopping for long time nonadiabatic quantum dynamics." In: *The Journal of Chemical Physics* 139.1 (2013), p. 014104. DOI: 10.1063/1.4812355.

[29] John C Tully. "Molecular dynamics with electronic transitions." In: *The Journal of Chemical Physics* 93.2 (1990), pp. 1061–1071. DOI: 10.1063/1.459170.

[30] John C Tully and Richard K Preston. "Trajectory surface hopping approach to nonadiabatic molecular collisions: the reaction of H+ with D2." In: *The Journal of Chemical Physics* 55.2 (1971), pp. 562–572. DOI: 10.1063/1.1675788.

[31] Joseph E Subotnik and Neil Shenvi. "A new approach to decoherence and momentum rescaling in the surface hopping algorithm." In: *The Journal of chemical physics* 134.2 (2011), p. 024105. DOI: 10.1063/1.3506779.

[32] Philip Shushkov, Richard Li, and John C Tully. "Ring polymer molecular dynamics with surface hopping." In: *The Journal of Chemical Physics* 137.22 (2012), 22A549. DOI: 10.1063/1.4766449.

[33] Eric R Bittner and Peter J Rossky. "Quantum decoherence in mixed quantum-classical systems: Nonadiabatic processes." In: *The Journal of Chemical Physics* 103.18 (1995), pp. 8130–8143. DOI: 10.1063/1.470177.

[34] Oleg V Prezhdo and Peter J Rossky. "Evaluation of quantum transition rates from quantum-classical molecular dynamics simulations." In: *The Journal of Chemical Physics* 107.15 (1997), pp. 5863–5878. DOI: 10.1063/1.474312.

[35] Ali Abedi, Neepa T Maitra, and Eberhard KU Gross. "Exact factorization of the time-dependent electron-nuclear wave function." In: *Physical Review Letters* 105.12 (2010), p. 123002. DOI: 10.1103/PhysRevLett.105.123002.

[36] Ali Abedi, Neepa T Maitra, and EKU Gross. "Correlated electron-nuclear dynamics: Exact factorization of the molecular wavefunction." In: *The Journal of Chemical Physics* 137.22 (2012), 22A530. DOI: 10.1063/1.4745836.

[37] Federica Agostini, Seung Kyu Min, Ali Abedi, and EKU Gross. "Quantum-classical nonadiabatic dynamics: Coupled-vs independent-trajectory methods." In: *Journal of Chemical Theory and Computation* 12.5 (2016), pp. 2127–2143. DOI: 10.1021/acs.jctc.5b01180.

[38] Seung Kyu Min, Federica Agostini, and Eberhard KU Gross. "Coupled-trajectory quantum-classical approach to electronic decoherence in nonadiabatic processes." In: *Physical Review letters* 115.7 (2015), p. 073001. DOI: 10.1103/PhysRevLett.115.073001.

[39] Seung Kyu Min, Federica Agostini, Ivano Tavernelli, and Eberhard KU Gross. "Ab initio nonadiabatic dynamics with coupled trajectories: A rigorous approach to quantum (de) coherence." In: *The Journal of Physical Chemistry Letters* 8.13 (2017), pp. 3048–3055. DOI: 10.1021/acs.jpclett.7b01249.

[40] Andreas Maser, Benjamin Gmeiner, Tobias Utikal, Stephan Götzinger, and Vahid Sandoghdar. "Few-photon coherent nonlinear optics with a single molecule." In: *Nature Photonics* 10.7 (2016), p. 450. DOI: 10.1038/nphoton.2016.63.

[41] Claudius Riek, DV Seletskiy, Andrey S Moskalenko, JF Schmidt, Philipp Krauspe, Sebastian Eckart, Stefan Eggert, Guido Burkard, and Alfred Leitenstorfer. "Direct sampling of electric-field vacuum fluctuations." In: *Science* 350.6259 (2015), pp. 420–423. DOI: 10.1126/science.aac9788.

[42] Andrey S Moskalenko, Claudius Riek, Denis V Seletskiy, Guido Burkard, and Alfred Leitenstorfer. "Paraxial theory of direct electro-optic sampling of the quantum vacuum." In: *Physical Review Letters* 115.26 (2015), p. 263601. DOI: 10.1103/PhysRevLett.115.263601.

[43] Jino George, Thibault Chervy, Atef Shalabney, Eloıse Devaux, Hidefumi Hiura, Cyriaque Genet, and Thomas W Ebbesen. "Multiple Rabi splittings under ultrastrong vibrational coupling." In: *Physical Review Letters* 117.15 (2016), p. 153601. DOI: 10.1103/PhysRevLett.117.153601.

[44] Tim Byrnes, Na Young Kim, and Yoshihisa Yamamoto. "Exciton–polariton condensates." In: *Nature Physics* 10.11 (2014), pp. 803–813. DOI: 10.1038/nphys3143.

[45] Jacek Kasprzak, M Richard, S Kundermann, A Baas, P Jeambrun, JMJ Keeling, FM Marchetti, MH Szymańska, R André, JL Staehli, et al. "Bose–Einstein condensation of exciton polaritons." In: *Nature* 443.7110 (2006), p. 409. DOI: 10.1038/nature05131.

[46] Christian Schäfer, Michael Ruggenthaler, and Angel Rubio. "Ab initio nonrelativistic quantum electrodynamics: Bridging quantum chemistry and quantum optics from weak to strong coupling." In: *Physical Review A* 98.4 (2018), p. 043801. DOI: 10.1103/PhysRevA.98.043801.

[47] Sebastian Schmidt. "Frustrated polaritons." In: *Physica Scripta* 91.7 (2016), p. 073006. DOI: 10.1088/0031-8949/91/7/073006.

[48] John David Jackson. *Classical electrodynamics*. 1999.

[49] Ludwig Silberstein. "Elektromagnetische grundgleichungen in bivektorieller behandlung." In: *Annalen der Physik* 327.3 (1907), pp. 579–586. DOI: 10.1002/andp.19073270313.

[50] Iwo Bialynicki-Birula and Zofia Bialynicka-Birula. "The role of the Riemann–Silberstein vector in classical and quantum theories of electromagnetism." In: *Journal of Physics A: Mathematical and Theoretical* 46.5 (2013), p. 053001. DOI: 10.1088/1751-8113/46/15/159501.

[51] René Jestädt, Michael Ruggenthaler, Micael JT Oliveira, Angel Rubio, and Heiko Appel. "Real-time solutions of coupled Ehrenfest-Maxwell-Pauli-Kohn-Sham equations: fundamentals, implementation, and nano-optical applications." In: *arXiv* (2018). arXiv: 1812.05049.

[52] Christopher Gerry, Peter Knight, and Peter L Knight. *Introductory quantum optics*. Cambridge university press, 2005.

[53] David Parker Craig and Thiru Thirunamachandran. *Molecular quantum electrodynamics: an introduction to radiation-molecule interactions*. Courier Corporation, 1998.

[54] Herbert Walther, Benjamin TH Varcoe, Berthold-Georg Englert, and Thomas Becker. "Cavity quantum electrodynamics." In: *Reports on Progress in Physics* 69.5 (2006), p. 1325. DOI: 10.1088/0034-4885/69/5/r02.

[55] Johannes Flick. "Exact nonadiabatic many-body dynamics: Electron-phonon coupling in photoelectron spectroscopy and light-matter interactions in quantum electrodynamical density-functional theory." PhD thesis. Humboldt-Universität zu Berlin Berlin, 2016.

[56] Michael Ruggenthaler, Johannes Flick, Camilla Pellegrini, Heiko Appel, Ilya V Tokatly, and Angel Rubio. "Quantum-electrodynamical density-functional theory: Bridging quantum optics and electronic-structure theory." In: *Physical Review A* 90.1 (2014), p. 012508. DOI: 10.1103/PhysRevA.90.012508.

[57] Yoshihiro Akahane, Takashi Asano, Bong-Shik Song, and Susumu Noda. "High-Q photonic nanocavity in a two-dimensional photonic crystal." In: *nature* 425.6961 (2003), p. 944. DOI: 10.1038/nature02063.

[58] Dirk Englund, Andrei Faraon, Ilya Fushman, Nick Stoltz, Pierre Petroff, and Jelena Vučković. "Controlling cavity reflectivity with a single quantum dot." In: *Nature* 450.7171 (2007), p. 857. DOI: 10.1038/nature06234.

[59] J Pelal Reithmaier, G Sęk, A Löffler, C Hofmann, S Kuhn, S Reitzenstein, LV Keldysh, VD Kulakovskii, TL Reinecke, and A Forchel. "Strong coupling in a single quantum dot–semiconductor microcavity system." In: *Nature* 432.7014 (2004), p. 197. DOI: 10.1038/nature02969.

[60] JL Jewell, SL McCall, Yong-Hee Lee, Axel Scherer, AC Gossard, and JH English. "Lasing characteristics of GaAs microresonators." In: *Applied Physics Letters* 54.15 (1989), pp. 1400–1402. DOI: 10.1063/1.100679.

[61] Salvatore Savasta, Rosalba Saija, Alessandro Ridolfo, Omar Di Stefano, Paolo Denti, and Ferdinando Borghese. "Nanopolaritons: vacuum Rabi splitting with a single quantum dot in the center of a dimer nanoantenna." In: *ACS Nano* 4.11 (2010), pp. 6369–6376. DOI: 10.1021/nn100585h.

[62] Xue-Wen Chen, Vahid Sandoghdar, and Mario Agio. "Coherent interaction of light with a metallic structure coupled to a single quantum emitter: from superabsorption to cloaking." In: *Physical Review Letters* 110.15 (2013), p. 153605. DOI: 10.1103/PhysRevLett.110.153605.

[63] Gülis Zengin, Martin Wersäll, Sara Nilsson, Tomasz J Antosiewicz, Mikael Käll, and Timur Shegai. "Realizing strong light-matter interactions between single-nanoparticle plasmons and molecular excitons at ambient conditions." In: *Physical Review Letters* 114.15 (2015), p. 157401. DOI: 10.1103/PhysRevLett.114.157401.

[64] Frédéric Peyskens, Darrick Chang, and Dirk Englund. "Integrated nanoplasmonic quantum interfaces for room-temperature single-photon sources." In: *Physical Review B* 96.23 (2017), p. 235151. DOI: 10.1103/PhysRevB.96.235151.

[65] R Sáez-Blázquez, Johannes Feist, FJ Garcıa-Vidal, and AI Fernández - Domınguez. "Photon statistics in collective strong coupling: Nanocavities and microcavities." In: *Physical Review A* 98.1 (2018), p. 013839. DOI: 10.1103/PhysRevA.98.013839.

[66] Denis G Baranov, Martin Wersäll, Jorge Cuadra, Tomasz J Antosiewicz, and Timur Shegai. "Novel nanostructures and materials for strong light–matter interactions." In: *ACS Photonics* 5.1 (2017), pp. 24–42. DOI: 10.1021/acsphotonics.7b00674.

[67] Johannes Feist and Francisco J Garcia-Vidal. "Extraordinary exciton conductance induced by strong coupling." In: *Physical Review Letters* 114.19 (2015), p. 196402. DOI: 10.1103/PhysRevLett.114.196402.

[68] Johannes Schachenmayer, Claudiu Genes, Edoardo Tignone, and Guido Pupillo. "Cavity-enhanced transport of excitons." In: *Physical Review Letters* 114.19 (2015), p. 196403. DOI: 10.1103/PhysRevLett.114.196403.

[69] Mauro Cirio, Simone De Liberato, Neill Lambert, and Franco Nori. "Ground state electroluminescence." In: *Physical Review Letters* 116.11 (2016), p. 113601. DOI: 10.1103/PhysRevLett.116.113601.

[70] Johannes Flick, Michael Ruggenthaler, Heiko Appel, and Angel Rubio. "Atoms and molecules in cavities, from weak to strong coupling in quantum-electrodynamics (QED) chemistry." In: *Proceedings of the National Academy of Sciences* 114.12 (2017), pp. 3026–3034. DOI: 10.1073/pnas.1615509114.

[71] Christian Schäfer, Michael Ruggenthaler, Heiko Appel, and Angel Rubio. "Modification of excitation and charge transfer in cavity quantum-electrodynamical chemistry." In: *Proceedings of the National Academy of Sciences* 116.11 (2019), pp. 4883–4892. DOI: 10.1073/pnas.1814178116.

[72] Anoop Thomas, Jino George, Atef Shalabney, Marian Dryzhakov, Sreejith J Varma, Joseph Moran, Thibault Chervy, Xiaolan Zhong, Eloıse Devaux, Cyriaque Genet, et al. "Ground-State Chemical Reactivity under Vibrational Coupling to the Vacuum Electromagnetic Field." In: *Angewandte Chemie International Edition* 55.38 (2016), pp. 11462–11466. DOI: 10.1002/anie.201605504.

[73] Hidefumi Hiura, Atef Shalabney, and Jino George. "Cavity Catalysis–Accelerating Reactions under Vibrational Strong Coupling–." In: *Preprint at ChemRxiv* (2018).

[74] Anoop Thomas, Lucas Lethuillier-Karl, Kalaivanan Nagarajan, Robrecht MA Vergauwe, Jino George, Thibault Chervy, Atef Shalabney, Eloıse Devaux, Cyriaque Genet, Joseph Moran, et al. "Tilting a ground-state reactivity landscape by vibrational strong coupling." In: *Science* 363.6427 (2019), pp. 615–619. DOI: 10.1126/science.aau7742.

[75] Michael Ruggenthaler, Nicolas Tancogne-Dejean, Johannes Flick, Heiko Appel, and Angel Rubio. "From a quantum-electrodynamical light–matter description to novel spectroscopies." In: *Nature Reviews Chemistry* 2.3 (2018), p. 0118. DOI: 10.1038/s41570-018-0118.

[76] Walter Greiner and Joachim Reinhardt. *Field quantization*. Springer Science & Business Media, 2013.

[77] Hans A Bethe. "The electromagnetic shift of energy levels." In: *Physical Review* 72.4 (1947), p. 339. DOI: 10.1103/PhysRev.72.339.

[78] Ilya V Tokatly. "Time-dependent density functional theory for many-electron systems interacting with cavity photons." In: *Physical Review Letters* 110.23 (2013), p. 233001. DOI: 10.1103/PhysRevLett.110.233001.

[79] Camilla Pellegrini, Johannes Flick, Ilya V Tokatly, Heiko Appel, and Angel Rubio. "Optimized effective potential for quantum electrodynamical time-dependent density functional theory." In: *Physical Review Letters* 115.9 (2015), p. 093001. DOI: 10.1103/PhysRevLett.115.093001.

[80] Johannes Flick, Michael Ruggenthaler, Heiko Appel, and Angel Rubio. "Kohn–Sham approach to quantum electrodynamical density-functional theory: Exact time-dependent effective potentials in real space." In: *Proceedings of the National Academy of Sciences* 112.50 (2015), pp. 15285–15290. DOI: 10.1073/pnas.1518224112.

[81] Farhad HM Faisal. *Theory of Multiphoton Processes*. Springer Science & Business Media, 1987.

[82] Johannes Flick, Heiko Appel, Michael Ruggenthaler, and Angel Rubio. "Cavity Born–Oppenheimer approximation for correlated electron–nuclear-photon systems." In: *Journal of Chemical Theory and Computation* 13.4 (2017), pp. 1616–1625. DOI: 10.1021/acs.jctc.6b01126.

[83] Vasil Rokaj, Davis M Welakuh, Michael Ruggenthaler, and Angel Rubio. "Light–matter interaction in the long-wavelength limit: No ground-state without dipole self-energy." In: *Journal of Physics B: Atomic, Molecular and Optical Physics* 51.3 (2018), p. 034005. DOI: 10.1088/1361-6455/aa9c99.

[84] Christian Schäfer, Michael Ruggenthaler, Vasil Rokaj, and Angel Rubio. "Relevance of the quadratic diamagnetic and self-polarization terms in cavity quantum electrodynamics." In: (2019). arXiv: 1911.08427.

[85] Seokmin Shin and Horia Metiu. "Nonadiabatic effects on the charge transfer rate constant: A numerical study of a simple model system." In: *The Journal of Chemical Physics* 102.23 (1995), pp. 9285–9295. DOI: 10.1063/1.468795.

[86] V Bužek, G Drobnỳ, Min Gyu Kim, M Havukainen, and PL Knight. "Numerical simulations of atomic decay in cavities and material media." In: *Physical Review A* 60.1 (1999), p. 582. DOI: 10.1103/PhysRevA.60.582.

[87] Jian-Yun Fang and Sharon Hammes-Schiffer. "Proton-coupled electron transfer reactions in solution: molecular dynamics with quantum transitions for model systems." In: *The Journal of Chemical Physics* 106.20 (1997), pp. 8442–8454. DOI: 10.1063/1.473903.

[88] Jian-Yun Fang and Sharon Hammes-Schiffer. "Excited state dynamics with nonadiabatic transitions for model photoinduced proton-coupled electron transfer reactions." In: *The Journal of Chemical Physics* 107.15 (1997), pp. 5727–5739. DOI: 10.1063/1.474333.

[89] Ali Abedi, Federica Agostini, Yasumitsu Suzuki, and EKU Gross. "Dynamical steps that bridge piecewise adiabatic shapes in the exact time-dependent potential energy surface." In: *Physical Review Letters* 110.26 (2013), p. 263001. DOI: 10.1103/PhysRevLett.110.263001.

[90] Federica Agostini, Ali Abedi, Yasumitsu Suzuki, Seung Kyu Min, Neepa T Maitra, and EKU Gross. "The exact forces on classical nuclei in non-adiabatic charge transfer." In: *The Journal of Chemical Physics* 142.8 (2015), p. 084303. DOI: 10.1063/1.4908133.

[91] Javier Galego, Clàudia Climent, Francisco J Garcia-Vidal, and Johannes Feist. "Cavity Casimir-Polder Forces and Their Effects in Ground-State Chemical Reactivity." In: *Physical Review X* 9.2 (2019), p. 021057. DOI: 10.1103/PhysRevX.9.021057.

[92] MOSM Hillery, Robert F O'Connell, Marlan O Scully, and Eugene P Wigner. "Distribution functions in physics: fundamentals." In: *Physics reports* 106.3 (1984), pp. 121–167. DOI: 10.1007/978-3-642-59033-7_28.

[93] Eugene P Wigner. "On the quantum correction for thermodynamic equilibrium." In: *Part I: Physical Chemistry. Part II: Solid State Physics*. Springer, 1997, pp. 110–120. DOI: 10.1103/PhysRev.40.749.

[94] José E Moyal. "Quantum mechanics as a statistical theory." In: 45.1 (1949), pp. 99–124. DOI: 10.1017/S0305004100000487.

[95] James T Hynes, JM Deutch, Chin Hsien Wang, and Irwin Oppenheim. "Quantum Corrections to Time Correlation Functions." In: *The Journal of Chemical Physics* 48.7 (1968), pp. 3085–3091. DOI: 10.1063/1.1669577.

[96] Hai-Woong Lee. "Theory and application of the quantum phase-space distribution functions." In: *Physics Reports* 259.3 (1995), pp. 147–211. DOI: 10.1016/0370-1573(95)00007-4.

[97] Richard A Campos. "Correlation coefficient for incompatible observables of the quantum harmonic oscillator." In: *American Journal of Physics* 66.8 (1998), pp. 712–718. DOI: 10.1119/1.18937.

[98] Daniel F Styer, Miranda S Balkin, Kathryn M Becker, Matthew R Burns, Christopher E Dudley, Scott T Forth, Jeremy S Gaumer, Mark A Kramer, David C Oertel, Leonard H Park, et al. "Nine formulations of quantum mechanics." In: *American Journal of Physics* 70.3 (2002), pp. 288–297. DOI: 10.1119/1.1445404.

[99] M Belloni, MA Doncheski, and Richard Wallace Robinett. "Wigner quasi-probability distribution for the infinite square well: Energy eigenstates and time-dependent wave packets." In: *American journal of physics* 72.9 (2004), pp. 1183–1192. DOI: 10.1119/1.1767100.

[100] William B Case. "Wigner functions and Weyl transforms for pedestrians." In: *American Journal of Physics* 76.10 (2008), pp. 937–946. DOI: 10.1119/1.2957889.

[101] Hermann Weyl. "Quantenmechanik und gruppentheorie." In: *Zeitschrift für Physik* 46.1-2 (1927), pp. 1–46. DOI: 10.1007/BF02055756.

[102] Neal H McCoy. "On the function in quantum mechanics which corresponds to a given function in classical mechanics." In: *Proceedings of the National Academy of Sciences of the United States of America* 18.11 (1932), p. 674. DOI: 10.1073/pnas.18.11.674.

[103] Pawel Blasiak, Andrzej Horzela, Karol A Penson, Allan I Solomon, and Gerard HE Duchamp. "Combinatorics and Boson normal ordering: A gentle introduction." In: *American Journal of Physics* 75.7 (2007), pp. 639–646. DOI: 10.1119/1.2723799.

[104] Claudius Riek, DV Seletskiy, Andrey S Moskalenko, JF Schmidt, Philipp Krauspe, Sebastian Eckart, Stefan Eggert, Guido Burkard, and Alfred Leitenstorfer. "Direct sampling of electric-field vacuum fluctuations." In: *Science* 350.6259 (2015), pp. 420–423. DOI: 10.1126/science.aac9788.

[105] Ileana-Cristina Benea-Chelmus, Francesca Fabiana Settembrini, Giacomo Scalari, and Jérôme Faist. "Electric field correlation measurements on the electromagnetic vacuum state." In: *Nature* 568.7751 (2019), p. 202. DOI: 10.1038/s41586-019-1083-9.

[106] Roy J Glauber. "Photon correlations." In: *Physical Review Letters* 10.3 (1963), p. 84. DOI: 10.1103/PhysRevLett.10.84.

[107] Javier Galego, Francisco J Garcia-Vidal, and Johannes Feist. "Suppressing photochemical reactions with quantized light fields." In: *Nature Communications* 7 (2016), p. 13841. DOI: 10.1038/ncomms13841.

[108] Hoi Ling Luk, Johannes Feist, J Jussi Toppari, and Gerrit Groenhof. "Multiscale molecular dynamics simulations of polaritonic chemistry." In: *Journal of Chemical Theory and Computation* 13.9 (2017), pp. 4324–4335. DOI: 10.1021/acs.jctc.7b00388.

[109] Geoffrey Hunter. "Conditional probability amplitudes in wave mechanics." In: *International Journal of Quantum Chemistry* 9.2 (1975), pp. 237–242. DOI: 10.1002/qua.560090205.

[110] Nikitas I Gidopoulos and EKU Gross. "Electronic non-adiabatic states: towards a density functional theory beyond the Born–Oppenheimer approximation." In: *Philosophical Transactions of the Royal Society A: Mathematical, Physical and Engineering Sciences* 372.2011 (2014), p. 20130059. DOI: 10.1098/rsta.2013.0059.

[111] Ali Abedi, Neepa T Maitra, and EKU Gross. "Response to "Comment on 'Correlated electron-nuclear dynamics: Exact factorization of the molecular wavefunction"'[J. Chem. Phys. 139, 087101 (2013)]." In: *The Journal of Chemical Physics* 139.8 (2013), p. 087101. DOI: 10.1063/1.4818523.

[112] José Luis Alonso, Jesús Clemente-Gallardo, P Echenique-Robba, and Jorge Alberto Jover-Galtier. "Comment on "Correlated electron-nuclear dynamics: Exact factorization of the molecular wavefunction"[J. Chem. Phys. 137, 22A530 (2012)]." In: *The Journal of Chemical Physics* 139.8 (2013), p. 087101. DOI: 10.1063/1.4818521.

[113] Guillermo Albareda, Aaron Kelly, and Angel Rubio. "Nonadiabatic quantum dynamics without potential energy surfaces." In: *Physical Review Materials* 3.2 (2019), p. 023803. DOI: 10.1103/PhysRevMaterials.3.023803.

[114] Christian Schäfer, Michael Ruggenthaler, and Angel Rubio. "Ab initio nonrelativistic quantum electrodynamics: Bridging quantum chemistry and quantum optics from weak to strong coupling." In: *Physical Review A* 98.4 (2018), p. 043801. DOI: 10.1103/PhysRevA.98.043801.

[115] Javier Galego, Francisco J Garcia-Vidal, and Johannes Feist. "Cavity-induced modifications of molecular structure in the strong-coupling regime." In: *Physical Review X* 5.4 (2015), p. 041022. DOI: 10.1103/PhysRevX.5.041022.

[116] Yasumitsu Suzuki, Ali Abedi, Neepa T Maitra, Koichi Yamashita, and EKU Gross. "Electronic Schrödinger equation with nonclassical nuclei." In: *Physical Review A* 89.4 (2014), p. 040501. DOI: 10.1103/PhysRevA.89.040501.

[117] Alberto Castro, Heiko Appel, Micael Oliveira, Carlo A Rozzi, Xavier Andrade, Florian Lorenzen, Miguel AL Marques, EKU Gross, and Angel Rubio. "octopus: a tool for the application of time-dependent density functional theory." In: *Physica Status Solidi (b)* 243.11 (2006), pp. 2465–2488. DOI: 10.1002/pssb.200642067. URL: https://gitlab.com/octopus-code/octopus.

[118] Eric J Heller. "Wigner phase space method: Analysis for semiclassical applications." In: *The Journal of Chemical Physics* 65.4 (1976), pp. 1289–1298. DOI: 10.1063/1.433238.

[119] Javier Galego, Francisco J Garcia-Vidal, and Johannes Feist. "Many-molecule reaction triggered by a single photon in polaritonic chemistry." In: *Physical Review Letters* 119.13 (2017), p. 136001. DOI: 10.1103/PhysRevLett.119.136001.

[120] Arkajit Mandal and Pengfei Huo. "Investigate New Reactivities Enabled by Polariton Photochemistry." In: 10.18 (2019), pp. 5519–5529. DOI: 10.1021/acs.jpclett.9b01599.

[121] Raphael F Ribeiro, Luis A Martınez-Martınez, Matthew Du, Jorge Campos-Gonzalez-Angulo, and Joel Yuen-Zhou. "Polariton chemistry: controlling molecular dynamics with optical cavities." In: *Chemical science* 9.30 (2018), pp. 6325–6339. DOI: 10.1039/C8SC01043A.

[122] Markus Kowalewski, Kochise Bennett, and Shaul Mukamel. "Cavity femtochemistry: Manipulating nonadiabatic dynamics at avoided crossings." In: *The Journal of Physical Chemistry Letters* 7.11 (2016), pp. 2050–2054. DOI: 10.1021/acs.jpclett.6b00864.

[123] Johan F Triana, Daniel Peláez, and José Luis Sanz-Vicario. "Entangled Photonic-Nuclear Molecular Dynamics of LiF in Quantum Optical Cavities." In: *The Journal of Physical Chemistry A* 122.8 (2018), pp. 2266–2278. DOI: 10.1021/acs.jpca.7b11833.

[124] Tamás Szidarovszky, Gábor J Halász, Attila G Császár, Lorenz S Cederbaum, and Ágnes Vibók. "Conical intersections induced by quantum light: field-dressed spectra from the weak to the ultrastrong coupling regimes." In: *The Journal of Physical Chemistry Letters* 9.21 (2018), pp. 6215–6223. DOI: 10.1021/acs.jpclett.8b02609.

[125] Gerrit Groenhof and J Jussi Toppari. "Coherent light harvesting through strong coupling to confined light." In: *The Journal of Physical Chemistry Letters* 9.17 (2018), pp. 4848–4851. DOI: 10.1021/acs.jpclett.8b02032.

[126] Oriol Vendrell. "Coherent dynamics in cavity femtochemistry: application of the multi-configuration time-dependent Hartree method." In: *Chemical Physics* 509 (2018), pp. 55–65. DOI: 10.1016/j.chemphys.2018.02.008.

[127] Daniele De Bernardis, Philipp Pilar, Tuomas Jaako, Simone De Liberato, and Peter Rabl. "Breakdown of gauge invariance in ultrastrong-coupling cavity QED." In: *Physical Review A* 98.5 (2018), p. 053819. DOI: 10.1103/PhysRevA.98.053819.

[128] András Vukics and Peter Domokos. "Adequacy of the Dicke model in cavity QED: A counter-no-go statement." In: *Physical Review A* 86.5 (2012), p. 053807. DOI: 10.1103/PhysRevA.86.053807.

[129] Johannes Flick and Prineha Narang. "Cavity-Correlated Electron-Nuclear Dynamics from First Principles." In: *Physical Review Letters* 121.11 (2018), p. 113002. DOI: 10.1103/PhysRevLett.121.113002.

[130] Kieron Burke. "Perspective on density functional theory." In: *The Journal of Chemical Physics* 136.15 (2012), p. 150901. DOI: 10.1063/1.4704546.

[131] Neepa T Maitra. "Perspective: Fundamental Aspects of Time-Dependent Density Functional Theory." In: *The Journal of Chemical Physics* 144.22 (2016), p. 220901. DOI: 10.1063/1.4953039.

[132] Hsing-Ta Chen, Tao E Li, Maxim Sukharev, Abraham Nitzan, and Joseph E Subotnik. "Ehrenfest+ R dynamics. II. A semiclassical QED framework for Raman scattering." In: *The Journal of Chemical Physics* 150.4 (2019), p. 044103. DOI: 10.1063/1.5057366.

[133] Hsing-Ta Chen, Tao E Li, Maxim Sukharev, Abraham Nitzan, and Joseph E Subotnik. "Ehrenfest+ R dynamics. I. A mixed quantum–classical electrodynamics simulation of spontaneous emission." In: *The Journal of Chemical Physics* 150.4 (2019), p. 044102. DOI: 10.1063/1.5057365.

[134] Tao E Li, Abraham Nitzan, Maxim Sukharev, Todd Martinez, Hsing-Ta Chen, and Joseph E Subotnik. "Mixed quantum-classical electrodynamics: Understanding spontaneous decay and zero-point energy." In: *Physical Review A* 97.3 (2018), p. 032105. DOI: 10.1103/PhysRevA.97.032105.

[135] Tao E Li, Hsing-Ta Chen, Abraham Nitzan, and Joseph E Subotnik. "Quasiclassical Modeling of Cavity Quantum Electrodynamics." In: *arXiv preprint* (2019). arXiv: 1910.02299.

[136] Gerhard Stock and Michael Thoss. "Semiclassical description of nonadiabatic quantum dynamics." In: *Physical Review Letters* 78.4 (1997), p. 578. DOI: 10.1103/PhysRevLett.78.578.

[137] Wang Shun-Jin and W Cassing. "Explicit treatment of N-body correlations within a density-matrix formalism." In: *Annals of Physics* 159.2 (1985), pp. 328–350. DOI: 10.1016/0003-4916(85)90116-2.

[138] Jens Fricke. "Transport equations including many-particle correlations for an arbitrary quantum system: A general formalism." In: *Annals of Physics* 252.2 (1996), pp. 479–498. DOI: 10.1006/aphy.1996.0142.

[139] M Bonitz. *Quantum Kinetic Theory*. Second Edition. Springer International Publishing Switzerland, 2016.

[140] Niko Säkkinen, Yang Peng, Heiko Appel, and Robert van Leeuwen. "Many-body Green's function theory for electron-phonon interactions: Ground state properties of the Holstein dimer." In: *The Journal of Chemical Physics* 143.23 (2015), p. 234101. DOI: 10.1063/1.4936142.

[141] Markus Kowalewski and Shaul Mukamel. "Manipulating molecules with quantum light." In: *Proceedings of the National Academy of Sciences* 114.13 (2017), pp. 3278–3280. ISSN: 0027-8424. eprint: https://www.pnas.org/content/114/13/3278.full.pdf.

[142] Felipe Herrera and Frank C. Spano. "Cavity-Controlled Chemistry in Molecular Ensembles." In: *Physical Review Letters* 116 (2016), p. 238301. DOI: 10.1103/PhysRevLett.116.238301.

[143] András Csehi, Ágnes Vibók, Gábor J Halász, and Markus Kowalewski. "Quantum control with quantum light of molecular nonadiabaticity." In: *Physical Review A* 100.5 (2019), p. 053421. DOI: 10.1103/PhysRevA.100.053421.

[144] Johannes Feist, Javier Galego, and Francisco J. Garcia-Vidal. "Polaritonic Chemistry with Organic Molecules." In: *ACS Photonics* 5.1 (2018), pp. 205–216. DOI: 10.1021/acsphotonics.7b00680.

[145] Benoit Mignolet and Basile FE Curchod. "Excited-State Molecular Dynamics Triggered by Light Pulses—Ab Initio Multiple Spawning vs Trajectory Surface Hopping." In: *The Journal of Physical Chemistry A* 123.16 (2019), pp. 3582–3591. DOI: 10.1021/acs.jpca.9b00940.

[146] M Sánchez-Barquilla, REF Silva, and J Feist. "Cumulant expansion for the treatment of light-matter interactions in arbitrary material structures." In: (2019). arXiv: 1911.07037.

[147] Javier del Pino, Florian AYN Schröder, Alex W Chin, Johannes Feist, and Francisco J Garcia-Vidal. "Tensor network simulation of non-Markovian dynamics in organic polaritons." In: *Physical review letters* 121.22 (2018), p. 227401. DOI: 10.1103/PhysRevLett.121.227401.

[148] Sebastian Franke, Stephen Hughes, Mohsen Kamandar Dezfouli, Philip Trøst Kristensen, Kurt Busch, Andreas Knorr, and Marten Richter. "Quantization of quasinormal modes for open cavities and plasmonic cavity quantum electrodynamics." In: *Physical review letters* 122.21 (2019), 2139 bibrangedash 01. DOI: 10.1103/PhysRevLett.122.213901.

[149] Johannes Flick, Davis M Welakuh, Michael Ruggenthaler, Heiko Appel, and Angel Rubio. "Light–Matter Response in Nonrelativistic Quantum Electrodynamics." In: *ACS photonics* 6.11 (2019), pp. 2757–2778. DOI: 10.1021/acsphotonics.9b00768.

[150] Bruno Huttner and Stephen M Barnett. "Quantization of the electromagnetic field in dielectrics." In: *Physical Review A* 46.7 (1992), p. 4306. DOI: 10.1103/PhysRevA.46.4306.

[151] Stefan Yoshi Buhmann. *Dispersion forces I: Macroscopic quantum electrodynamics and ground-state Casimir, Casimir–Polder and van der Waals Forces*. Vol. 247. Springer, 2013.

[152] Stefan Buhmann. *Dispersion Forces II: Many-Body Effects, Excited Atoms, Finite Temperature and Quantum Friction*. Vol. 248. Springer, 2013.

[153] Stefan Yoshi Buhmann and Dirk-Gunnar Welsch. "Casimir-Polder forces on excited atoms in the strong atom-field coupling regime." In: *Physical Review A* 77.1 (2008), p. 012110. DOI: 10.1103/PhysRevA.77.012110.

[154] Stefan Scheel and Stefan Buhmann. "Macroscopic quantum electrodynamics-concepts and applications." In: *Acta Physica Slovaca. Reviews and Tutorials* 58.5 (2008), pp. 675–809. arXiv: 0902.3586.

[155] Johannes Flick, Christian Schäfer, Michael Ruggenthaler, Heiko Appel, and Angel Rubio. "Ab initio optimized effective potentials for real molecules in optical cavities: photon contributions to the molecular ground state." In: *ACS photonics* 5.3 (2018), pp. 992–1005. DOI: 10.1021/acsphotonics.7b01279.

[156] Jong-Kwon Ha, In Seong Lee, and Seung Kyu Min. "Surface hopping dynamics beyond nonadiabatic couplings for quantum coherence." In: *The Journal of Physical Chemistry Letters* 9.5 (2018), pp. 1097–1104. DOI: 10.1021/acs.jpclett.8b00060.

[157] Michael Filatov, Marco Paolino, Seung Kyu Min, and Cheol Ho Choi. "Design and photoisomerization dynamics of a new family of synthetic 2-stroke light driven molecular rotary motors." In: *Chemical Communications* 55.36 (2019), pp. 5247–5250. DOI: 10.1039/C9CC01955C.

[158] Michael Filatov, Seung Kyu Min, and Cheol Ho Choi. "Theoretical modelling of the dynamics of primary photoprocess of cyclopropanone." In: *Physical Chemistry Chemical Physics* 21.5 (2019), pp. 2489–2498. DOI: 10.1039/C8CP07104G.

[159] Fabian Ripka, Harald Kübler, Robert Löw, and Tilman Pfau. "A Room-Temperature Single-Photon Source Based on Strongly Interacting Rydberg atoms." In: *Science* 362.6413 (2018), pp. 446–449. DOI: 10.1126/science.aau1949.

[160] YO Dudin and A Kuzmich. "Strongly interacting Rydberg excitations of a cold atomic gas." In: *Science* 336.6083 (2012), pp. 887–889. DOI: 10.1126/science.1217901.

[161] J Patrick Zobel, Juan J Nogueira, and Leticia González. "Finite-temperature Wigner phase-space sampling and temperature effects on the excited-state dynamics of 2-nitronaphthalene." In: *Physical Chemistry Chemical Physics* (2019). DOI: 10.1039/C8CP03273D.

[162] Roland Mitrić, Michael Hartmann, B Stanca, V Bonačić-Koutecký, and P Fantucci. "Ab Initio Adiabatic Dynamics Combined with Wigner Distribution Approach to Femtosecond Pump- Probe Negative Ion to Neutral to Positive Ion (NeNePo) Spectroscopy of Ag2Au, Ag4, and Au4 Clusters." In: *The Journal of Physical Chemistry A* 105.39 (2001), pp. 8892–8905. DOI: 10.1021/jp011759f.

[163] Vlasta Bonačić-Koutecký and Roland Mitrić. "Theoretical exploration of ultrafast dynamics in atomic clusters: Analysis and control." In: *Chemical Reviews* 105.1 (2005), pp. 11–66. DOI: 10.1021/cr0206925.

[164] Merle IS Röhr, Roland Mitrić, and Jens Petersen. "Vibrationally resolved optical spectra and ultrafast electronic relaxation dynamics of diamantane." In: *Physical Chemistry Chemical Physics* 18.12 (2016), pp. 8701–8709. DOI: 10.1039/C6CP00137H.

[165] Bill Barnes, Francisco García Vidal, and Javier Aizpurua. "Special Issue on "Strong Coupling of Molecules to Cavities"." In: (2018). DOI: 10.1021/acsphotonics.7b01609.

LIST OF FIGURES

ACRONYMS

BBGKY	Bogoliubov-Born-Green-Kirkwood-Yvon
BO	Born-Oppenheimer
DFT	Density Functional Theory
EF	Exact Factorization
MQC	Mixed-Quantum Classical
MTEF	Multi-Trajectory Ehrenfest
PCET	Proton-Coupled Electron Transfer
PES	Potential Energy Surface
PNC	Partial Normalization Condition
spBO	self-polarization-modified Born-Oppenheimer
TDDFT	Time-Dependent Density Functional Theory
TDPES	Time-Dependent Potential Energy Surface
QED	Quantum Electrodynamics
QEDFT	Quantum Electrodynamical Density Functional Theory

LIST OF TALKS, POSTERS, AWARDS AND SCHOLARSHIPS

LIST OF TALKS PRESENTED AT CONFERENCES

(1) **ACS National Meeting**
Orlando (USA), March 2019, Contributed

(2) **Scientific Advisory Board Meeting**
Hamburg (Germany), January 2019, Invited

(3) **ACS National Meeting**
Boston (USA), August 2018, Contributed

(4) **Young Researcher's Meeting**
Hamburg (Germany), June 2018, Contributed

(5) **APS March Meeting**
Los Angeles (USA), March 2018, Contributed

(6) **Summer School: Electronic Structure and Dynamics**
Telluride (USA), July 2017, Contributed

(7) **DPG-Frühjahrstagung**
Mainz (Germany), March 2017 Contributed

(8) **Physikerinnen Tagung der DPG**
Hamburg (Germany), November 2016, Contributed

(9) **Summer School: Time-Dependent Density-Functional Theory**
Benasque (Spain), September 2016, Poster-Prize Talk

(10) **Young Researcher's Meeting**
London (United Kingdom), July 2016, Contributed

LIST OF POSTERS PRESENTED AT CONFERENCES

(1) **Summer School: Time-Dependent Density-Functional Theory**
Benasque (Spain), September 2016, Contributed

LIST OF AWARDS AND SCHOLARSHIPS

(1) **IMPRS Scholarship**
International Max Plank Research School for Ultrafast Imaging and Structural Dynamics, Hamburg (Germany), Since 2017

(2) **Pedro-Pascual Poster-Prize**
Summer School, Time-Dependent Density-Functional Theory: Prospects and Applications, Benasque (Spain)

COLLABORATIONS AND PERSONAL CONTRIBUTIONS

This cumulative thesis comprises the work presented in publications [O1]–[O5] in collaboration with A Rubio, NT Maitra, H Appel, A Kelly, L Lacombe, N Säkkinen and C Schäfer. All authors that contributed to a publication are indicated on its title page and below. The order reflects each author's contribution in terms of conception, design, drafting and substantively revising the work, as well as the analysis and interpretation of data, and numerical simulations and has been agreed upon by all authors prior to publication. The detailed contributions of the author of this thesis, Norah M Hoffmann (NM H.), are as follows:

[O1] *NM Hoffmann, C Schäfer, A Rubio, A Kelly, H Appel*
Role: Main Author; NM H. performed implementations, numerical simulations, analysis, and writing of the manuscript.

[O2] *NM Hoffmann, H Appel, A Rubio, NT Maitra*
Role: Main Author; NM H. performed implementations, numerical simulations, analysis, and writing of the manuscript.

[O3] *NM Hoffmann, C Schäfer, N Säkkinen, A Rubio, H Appel, A Kelly*
Role: Main Author; NM H. performed partial implementations and numerical simulations (Ehrenfest Mean Field and Exact Simulations). Further, NM.H performed analysis, and writing of the manuscript.

[O4] *L Lacombe, NM Hoffmann, NT Maitra*
Role: Contributing Author; NM H. performed numerical simulations and contributed to analysis, and writing of the manuscript.

[O5] *NM Hoffmann, L Lacombe, A Rubio, NT Maitra*
Role: Main Author; NM H. initiated the work and performed implementations, numerical simulations, analysis, and writing of the manuscript.

ACKNOWLEDGMENTS

This thesis would have not been possible without the help of many people.

First and foremost I would like to thank my supervisor Angel Rubio for his great support, encouragement and for giving me the opportunity to work on my PhD at the Max-Planck Institute. Thank you for being so amazingly open minded with all my crazy plans and ideas and thank you so much for making my research stay in New York possible!

I would like to thank my supervisor at the University of Hamburg, Ludwig Mathey, for accepting me as a PhD student and for agreeing to review my thesis.

I dearly and from the bottom of my heart want to thank Neepa T. Maitra for being the best PhD supervisor I could have ever asked for. Thank you for all the laughs, countless discussions, great support, amazing advise and thank you for being patient when I got careless with the analytics for 100th time. Thank you for being such an amazing role-model and I am very grateful to have learned from all your knowledge and experience. Thank you, Neepa!

This work would not have been possible without the tremendous support and amazing ideas of my supervisor Heiko Appel. Thank you for all the fruitful discussions, many Skype-calls and your incredible help developing my code on countless train-rides between Berlin and Hamburg. Thank you, Heiko!

I sincerely want to thank Aaron Kelly for the fruitful collaboration, his support and many discussions. Furthermore, special thanks go to my Trajectory-team partner Christian Schäfer. Thank you for all the great team-work and very helpful discussions. Can't belief we made it! Especially I want to thank Lionel Lacombe, for being the best, smartest and most french office colleague and collaborator. Merci beaucoup! I also want to thank Michele Pavanello, for his kind hospitality during my stay at Rutgers University, Patricia Vindel-Zandbergen for her support in fancy molecule-painting, Henning Glawe for is constant IT-support and Johannes Flick and Johannes Feist for the insightful discussions.

I would like to to thank Julia Quante and Neda Lotfionran from IMPRS for their support throughout my PhD. I also want to thank the administration of the MPSD for all their help with my Dienstreiseanträgen. I especially want to thank Kathja Schroeder and Patricia Rihs for always answering my thousand phone calls and all the help with the German as well as American bureaucracy.

All this would not have been possible without the tremendous support of my friends and family. Special thanks you go to Gratenzwerg, Siggi, Bobsman and BinSa. And there are no words that could possibly express how grateful I am to have the support of the best family one could have ever asked for. Thank you Mama, Papa and Lolli for all your support, love and endless telephone sessions. I never could have done it without you. You mean the world to me!

And thank you Robertinio for all your love and support!

DECLARATION

Hiermit versichere ich an Eides statt, die vorliegende Dissertationsschrift selbst verfasst und keine anderen als die angegebenen Hilfsmittel und Quellen benutzt zu haben. Die eingereichte schriftliche Fassung entspricht der auf dem elektronischen Speichermedium. Die Dissertation wurde in der vorgelegten oder einer ähnlichen Form nicht schon einmal in einem früheren Promotionsverfahren angenommen oder als ungenügend beurteilt.

Hamburg, June 3, 2020

Norah M. Hoffmann